Ecdysone steroid hormone remote controls epithelial expansion and cancer progression in the *Drosophila* intestine

Inaugural-Dissertation

zur Erlangung des Doktorgrades
der Mathematisch-Naturwissenschaftlichen Fakultät
der Heinrich-Heine-Universität Düsseldorf

vorgelegt von

Lisa Zipper
aus Aachen

Düsseldorf, August 2025

aus dem Institut für Genetik

der Heinrich-Heine-Universität Düsseldorf

Gedruckt mit der Genehmigung der

Mathematisch-Naturwissenschaftlichen Fakultät der

Heinrich-Heine-Universität Düsseldorf

Berichterstatter:

1. Prof. Dr. Thomas Klein

2. Prof. Dr. Hermann Aberle

Tag der mündlichen Prüfung: 22.07.25

Table of Contents

1 Introduction

The transition from unicellular to multicellular organisms involved the evolution of higher organized cells into specialized tissues and organs with distinct functions. To ensure the accurate development of these functions, distant organs must communicate with each other. Additional requirements for inter-organ communication emerge post-development when an organism adapts to external conditions, such as the female body adjusting to shifts in metabolic demands during the production of offspring.

1.1 Physiological adaptations during pregnancy and lactation

Female reproduction is energetically costly and relies on several adaptations of the mother's body to ensure proper development of the offspring. These physiological changes influence the mother's metabolism by affecting insulin regulation and glucose homeostasis (Bailey & Ahmed-Sorour, 1980; Costrini & Kalkhoff, 1971), lipid handling (Tiano & Mauvais-Jarvis, 2012), and appetite regulation (Fungfuang *et al*, 2013; Stelmańska & Sucajtys-Szulc, 2014) to meet the increased energy demands during pregnancy. To further support metabolic adaptations and enhance nutrient absorption, the maternal intestine proportionally increases in size (Hammond, 1997; Speakman, 2008).

In rats, the expansion of intestinal mass is facilitated by both hyperplastic and hypertrophic changes. The epithelium of the small intestine shows more numerous and larger cells (Cairnie & Bentley, 1967). Interestingly, increases in intestinal mass during lactation are tightly correlated with the number of pups, as a larger number of pups comes along with higher energy demands that need to be covered by the mother (Hammond, 1997). These correlated adaptations, connecting specific energy demands determined by litter size to the extent of intestinal expansion, underline a precise regulation mediated by inter-organ communication and systemic signals. However, the exact systemic signals driving

pregnancy-related intestinal remodelling and the mechanisms by which they control intestinal size in mammals remain unknown.

Following pregnancy and lactation, when energy demands diminish, the pregnancy-related intestinal enlargement and increased nutrient absorption often contribute to weight gain, especially following multiple pregnancies (Casirola & Ferraris, 2003; Scholl *et al*, 1995), and in obese women (Hytten, 1991). Postpartum weight retention is a significant concern, as obesity is a health condition that elevates the risk of various diseases, including metabolic disorders like diabetes and certain types of cancer (Haslam & James, 2005; James *et al*, 2004). It is thus important to identify the signals and molecular mechanisms regulating intestinal size adaptations as it would allow to prevent or treat pregnancy-related intestinal hypertrophy.

1.2 Steroid hormones as mediators of inter-organ communication

Hormones are systemic signals, which play a crucial role in inter-organ communication, as they allow a rapid and coordinated response throughout the entire organism by simultaneously targeting multiple organs. They are secreted by endocrine cells and transported via the circulation system to reach target cells in organs at distant body sites.

Growing evidence suggests that hormones derive from nutritional compounds. Sex steroids, a subclass of steroid hormones, are derived from cholesterol, which is directly influenced by diet (Laudet & Markov, 2018). Many hormones like sex steroids are regulating reproduction and are thought to be derived from signalling pathways controlling reproduction in response to nutritional conditions (Della Torre *et al*, 2014). Interestingly the chemical structures of mammalian steroid hormones and plant-growth hormones is conserved suggesting that biochemical molecules existed prior to the separation of the plant and animal kingdoms even before either group became multicellular (Kushiro *et al*, 2003), highlighting the importance of hormone-driven inter-organ communication in the evolution of multicellular organisms. Once a hormone reached its target cell it is recognized by a specific receptor. These hormone receptors are

absent in unicellular eukaryotes like *Saccharomyces cerevisiae* and must have evolved later simultaneously with multicellularity (Clarke & Berg, 1998).

The mammalian sex steroids, including oestrogens, progesterone and androgens are well known for their regulatory role in sexual differentiation, secondary sex characteristics, sexual behaviours and reproduction. In addition, oestrogen and progesterone levels are altered throughout pregnancy (Soldin *et al*, 2005) and associated with pregnancy-related adaptations in the female body (Moya *et al*, 2014), suggesting they may also play a role in regulating intestinal re-sizing.

1.3 The controversial role of steroid hormones in colorectal tumours

1.3.1 Indications of protective roles for oestrogens in colorectal cancer

Besides their roles in physiology, sex steroids, especially oestrogens are extensively discussed in relation to diseases such as cancer. Numerous colorectal cancer (CRC) studies have in common, that they report a lower incidence in women across all age groups, regardless of other CRC-related risk factors (Siegel & Jemal, 2011; Siegel *et al*, 2017). Furthermore, premenopausal women with metastatic CRC have a higher overall survival compared to men (Hendifar *et al*, 2009). As these sex specific differences in CRC incidence and progression cannot be explained by differences in well-known cancer-related risk factors such as smoking or consumption of alcohol, the implication of sex hormones is strongly suggested. Further supported by the fact that postmenopausal women using hormone replacement therapy have a reduced risk of developing CRC (Calle *et al*, 1995; Chute *et al*, 1991; de Verdier & London, 1992; Wu *et al*, 1987). Indeed, functional studies in mouse models with colon adenomas have demonstrated that ovariectomy, which leads to a reduction in oestrogen synthesis, resulted in a 77% increase in intestinal adenomas. Conversely, treatment with the oestrogen 17β-estradiol in ovariectomized mice reduced adenoma development (Weyant *et al*, 2001).

1.3.2 Indications of detrimental roles for oestrogens in colorectal cancer

In contrast to the protective role of oestrogens on the formation of colon adenomas observed in mice models, other studies suggest a detrimental role for oestrogens in CRC incidence. Nuns as a nullipara group of the female population are thought to be longer exposed to oestrogens compared to other female cohorts due to missing disruptions of their menstrual cycles. A study performed in 1969 by the national cancer institute revealed that nuns show an elevated risk of developing colon cancer (Fraumeni *et al*, 1969). In line with this, long-term hormonal changes upon pregnancy relate to lower risk of developing colon cancers (McMichael & Potter, 1980; Weiss *et al*, 1981).

The proposed roles of oestrogens in CRC progression emphasize the need to uncover the molecular mechanisms that regulate ISC proliferation and tumour growth downstream of the hormone. Model organisms such as the fruit fly *Drosophila melanogaster* are utilized to investigate these mechanisms.

1.4 Steroid hormones as mediators of inter-organ communication in *Drosophila*

1.4.1 Systemic roles of steroidal ecdysone hormone in *Drosophila*

Steroid hormones and their roles in inter-organ communication are not restricted to mammals but also found in arthropods like the fruit fly *Drosophila melanogaster*. In insects the steroidal ecdysone hormone (E) with its active form 20 hydroxy ecdysone (20HE) is the functional equivalent to mammalian oestrogen and is able to activate expression of human oestrogen responsive genes (Aranda & Pascual, 2001; Martinez *et al*, 1991; Oberdörster *et al*, 2001).

The major role for 20HE in *Drosophila* is the initiation of larval molting and pupariation. The progression of these processes are driven by pulses of 20HE, which is produced in the endocrine prothoracic gland and released into the circulating haemolymph (Gilbert & Warren, 2005; Huang *et al*, 2008; Riddiford, 1993). On the other hand systemic juvenile

hormone (JH) from the corpus allatum prevents metamorphosis in developing larvae thereby antagonizing 20HE signalling (Riddiford, 1994).

1.4.2 Steroid hormone-induced physiological adaptations upon mating

After pupariation and full development, 20HE is produced in the germarial cells of adult ovaries and plays a role in maintaining germline stem cells (GSC) (Ables *et al*, 2015; Ables & Drummond-Barbosa, 2010; König *et al*, 2011; Morris & Spradling, 2012; Uryu *et al*, 2015). Mating triggers male-derived sex peptides (SP) to stimulate 20HE synthesis in the ovaries. Released 20HE then activates ecdysone signalling in the ovarian niche cells directly via its receptor, thus stimulating GSC proliferation and lipid accumulation (Ameku & Niwa, 2016) (Fig.1).

Additionally, it was shown that 20HE functions similarly to oestrogen in regulating whole-animal lipid metabolism and feeding rates in mated female flies (Sieber & Spradling, 2015) (Fig.1). Consequently, like human sex steroids *Drosophila* 20HE is involved in regulating reproduction and mating induced adaptations of the female metabolism.

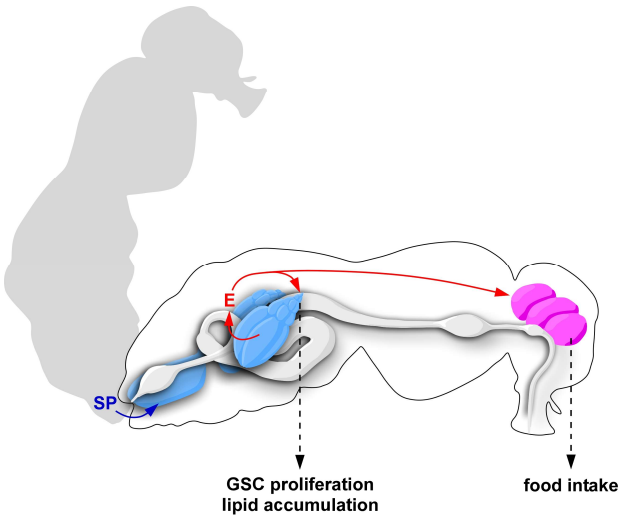

Fig.1: Ecdysone steroid hormone-induced adaptations upon mating.

Male-derived sex peptide (SP) induces synthesis and release of ecdysone (E) in ovaries. Circulating E reaches the GSC and remote organs like the brain. In GSC E induces proliferation and lipid accumulation. Whereas via the brain food intake is regulated.

1.5 *Drosophila melanogaster* as an established model for investigations in physiology and pathology of the intestine

1.5.1 Similarities between the *Drosophila* midgut and the mammalian small intestine

The functional and cellular similarities between the mammalian small intestine and the *Drosophila* midgut establish the fly's digestive tract as a valuable model for studying intestinal homeostasis. Primary functions of both organs are the digestion and absorption of nutrients and water, as well as excretion. In both systems, the mammalian small intestine and the *Drosophila* midgut, these functions are fulfilled by a monolayered epithelium.

In the mammalian small intestine, the epithelium forms elongated domains towards the lumen, called villi, and invaginated domains, called crypts. ISC reside at the bottom of the crypt and divide to self-renew and to give rise to another population of ISC located at position +4 (+4 ISC), secretory cells including paneth cells (PC) and enteroendocrine cells (EE) (Banjac *et al*, 2025), and progenitor cells called transit amplifying (TA) cells. PC are located in between the ISC and provide signalling molecules that sustain stem cell fate. EE are involved in regulating digestion by releasing various peptide hormones. TA cells in turn proliferate and differentiate into absorptive enterocytes (EC) as they move to the top towards the villus (Krausova & Korinek, 2014; Kretzschmar & Clevers, 2017; Schepers & Clevers, 2012) (Fig.2 top).

Almost two decades ago two labs independently discovered that the adult *Drosophila* midgut is constantly renewed by adult intestinal stem cells (ISC) as well (Micchelli & Perrimon, 2006; Ohlstein & Spradling, 2006). As in the mammalian counterpart, *Drosophila* ISC are located basally and divide symmetrically to renew the stem cell pool, or asymmetrically into one new ISC and either an EC precursor, called enteroblast (EB), or an enteroendocrine cell precursor (EEP). These precursor cells in turn differentiate into absorptive EC and secretory EE, respectively (Chen *et al*, 2018; Micchelli & Perrimon, 2006; Ohlstein & Spradling, 2006, 2007) (Fig.2 bottom).

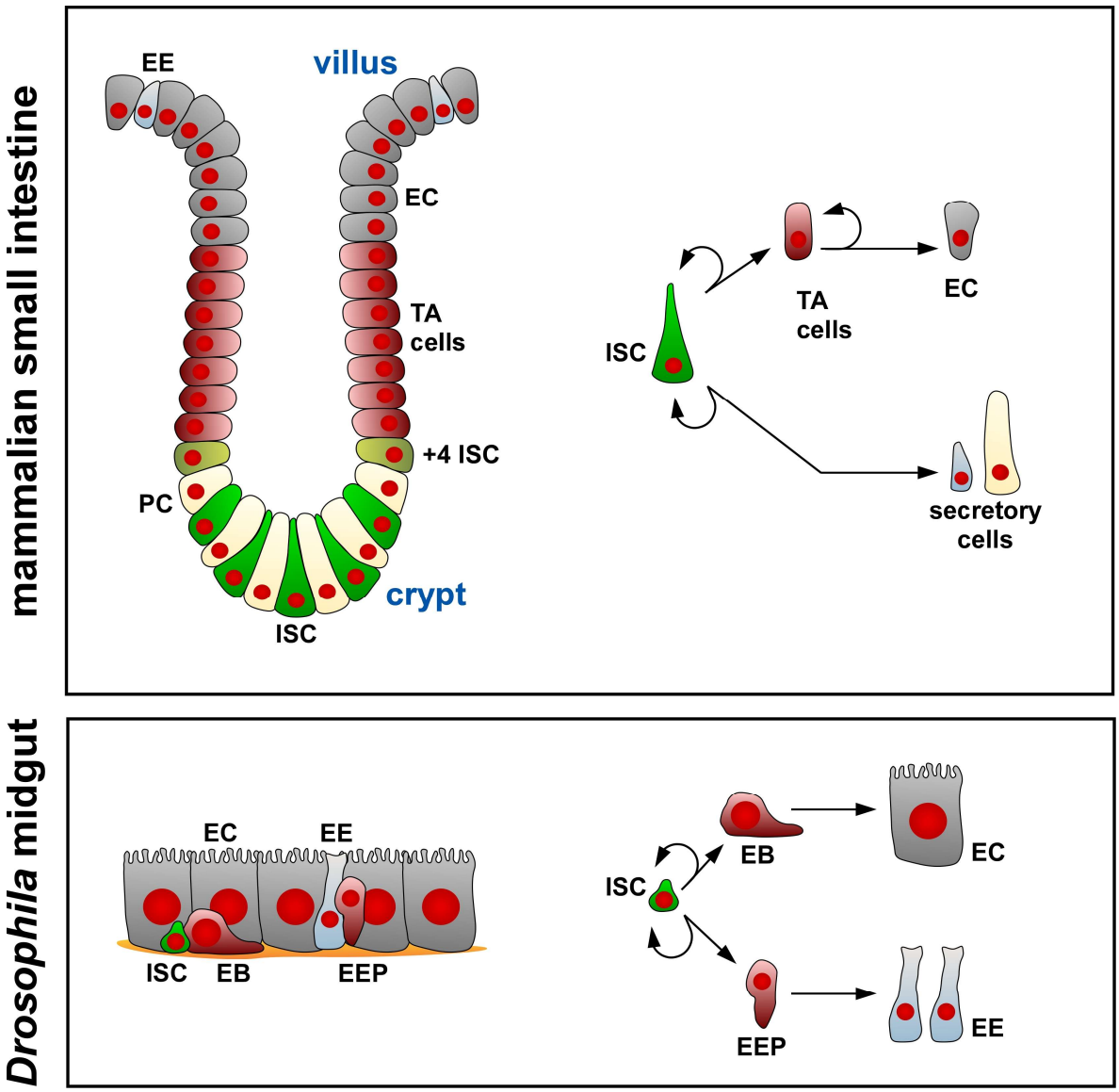

Fig.2: Schematic comparing cellular composition of the mammalian small intestine and the *Drosophila* midgut.

(Top) The mammalian small intestine is made of a monolayered epithelium which forms elongated domains towards the lumen, called villi, and invaginated domains, called crypts. Intestinal stem cells (ISC) reside at the bottom of the crypt interspersed by paneth cells (PC) which comprise the stem cell niche by expressing signalling molecules that sustain stem cell fate in ISC. Another group of ISC is located just above the PC at position +4 (+4 ISC), which are characterized by expression of different markers. ISC divide asymmetrically to self-renew and give rise to transit amplifying (TA) cells. Furthermore, ISC differentiate directly into secretory cells including PC and enteroendocrine cells (EE). TA cells proliferate and differentiate into absorptive enterocytes (EC) as they move to the top towards the villus. (Bottom) In the *Drosophila* midgut epithelium ISC are located basally at the basal membrane. ISC divide asymmetrically to self-renew and give rise to progenitor cells comprising enteroblasts (EB) and EE. These progenitor cells in turn differentiate into absorptive EC and EE, respectively.

Besides the described similarities in functionality and cellular composition, the *Drosophila* midgut cell lineage is regulated by similar local signalling pathways as its mammalian counterpart. In mammals intestinal homeostasis depends on Wnt/Wg signalling. Inactivation of Wnt/Wg signalling induces differentiation and blocks ISC proliferation (Fevr *et al*, 2007; van Es *et al*, 2012). Conversely, aberrant activation of Wnt/Wg signalling leads to the formation of colon adenomas and is associated with CRC being the most frequently altered signalling pathway in CRC patients (Bangi *et al*, 2016; Groden *et al*, 1991; Muzny *et al*, 2012; Wood *et al*, 2007). Similarly, in the *Drosophila* midgut, the expression of a temperature-sensitive mutant allele of the Wnt/Wg ligand Wingless (Wg) diminishes the ISC pool (Lin *et al*, 2008), and conversely overexpression of Wg induces ISC proliferation (Cordero *et al*, 2012a; Lin *et al.*, 2008; Singh *et al*, 2019). However, the precise source of Wg and its role in regulating *Drosophila* midgut homeostasis remain debated, as knocking down Wg in ISC/EB and visceral muscle cells does not reduce ISC numbers (Cordero *et al*, 2012b) and inactivating Wnt/Wg pathway components only has a mild effect on ISC proliferation(Lin *et al.*, 2008).

1.5.2 'ReDDM'-tracing as genetic tool to investigate re-sizing of the *Drosophila* midgut

There is a wide range of genetic tools for investigating intestinal homeostasis in adult *Drosophila*, including 'ReDDM'-tracing (Repressible Dual Differential stability cell Marker). 'ReDDM' consists of two UAS-driven fluorophores with different half-lifes: An *UAS-CD8::GFP* with short half-life which is labelling the membranes of cells with active Gal4 expression, whereas *UAS-H2B::RFP* has a longer half-life and is not restricted to the nuclei of cells with active Gal4, but also persists in the progeny of cells which once had active Gal4. Additionally, an ubiquitously expressed temperature-sensitive Gal80 repressor (*tub-Gal80^{ts}*) allows temporal expression control of the fluorophores. The 'ReDDM'-tracing system is complemented by a Gal4-driver and can also be used for expression of further UAS-driven transgenes. Using an *escargot-Gal4* (*esg-Gal4*) driver, UAS-driven expression of fluorophores and transgenes is specifically induced in ISC/EB, labelling these cells with

CD8::GFP and H2B::RFP. Whereas their progeny, epithelial EC and EE, are labelled with H2B::RFP only (Antonello *et al*, 2015). With its tracing capability, 'ReDDM' is an excellent genetic tool for studying physiological adaptations to pregnancy in female *Drosophila*. It labels intestinal progenitor cells and enables the tracking of newly produced epithelial cells, facilitating the study of hyperplastic intestinal growth (Antonello *et al.*, 2015).

1.5.3 Pregnancy induced re-sizing of the *Drosophila* intestine

The cellular composition and functionality of the *Drosophila* midgut are comparable to those of the mammalian small intestine, and resizing of the digestive tract during offspring production has also been observed in the fruit fly (Reiff *et al*, 2015). Upon mating male-derived SP stimulate the synthesis of endocrine JH in the corpus allatum and synthesis of E in the ovaries, resulting in higher hormone levels in the circulating haemolymph (Ameku & Niwa, 2016; Reiff *et al.*, 2015). JH from the haemolymph is involved in sustaining ovarian maturation and thus egg production (Flatt *et al*, 2005) (Fig.3A). Additionally, by using 'ReDDM'-tracing it was shown that JH also reaches and affects the posterior midgut. In ISC, JH induces proliferation through its receptors Methoprene-tolerant (Met) and Germ cell-expressed bHLH-PAS (Gce), acting through their target Kr transcription factor homolog 1 (Kr-h1) (Fig.3B). Furthermore, JH stimulates lipid metabolism in EC via the *Drosophila* homologue of the mammalian family of sterol regulatory element-binding proteins (SREBP) (Fig.3B). Together the adaptations of ISC proliferation and lipid metabolism ensure an increased nutrient uptake to match higher energy demands during egg production (Reiff *et al.*, 2015).

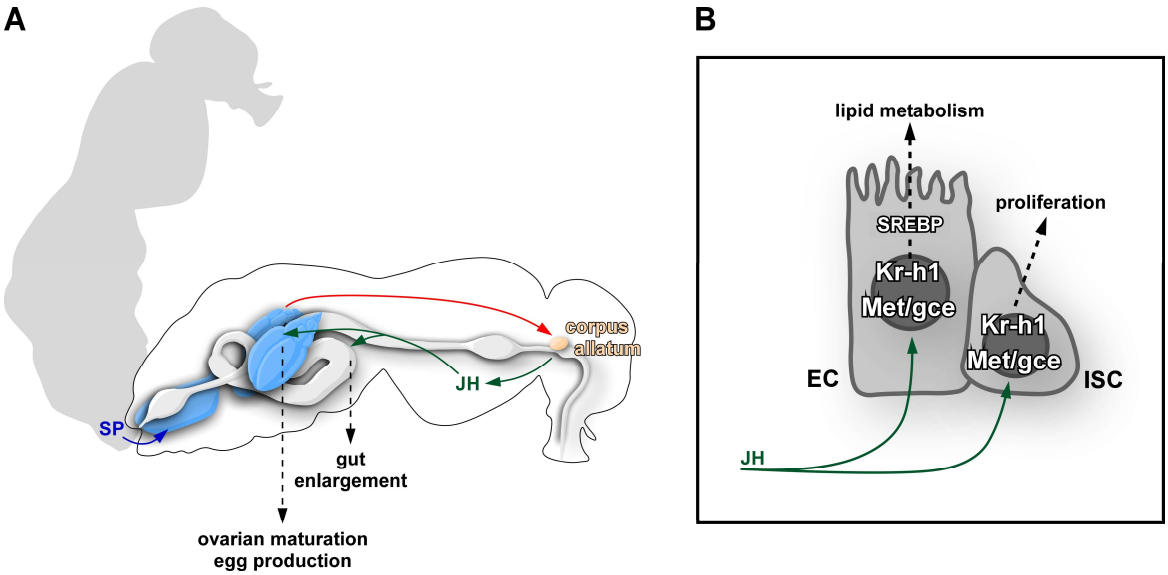

Fig.3: Hormone-induced re-sizing of the midgut in mated female *Drosophila*.

(A) Upon mating male-derived sex peptides (SP) stimulate the synthesis of juvenile hormone (JH) in the corpus allatum. JH is released into the haemolymph and reaches remote organs like the ovaries and midgut. In ovaries JH sustains maturation and in turn stimulates egg production. In the midgut JH regulates expansion of the intestinal epithelium to increase nutrient uptake. (B) In detail JH stimulates the *Drosophila* homologue of the mammalian family of sterol regulatory element-binding proteins (SREBP) and in turn lipid metabolism in EC via its receptors Methoprene tolerant (Met) and germ cell-expressed bHLH-PAS (gce) and their target Kr transcription factor homolog 1 (Kr-h1). Whereas in ISC, JH via Met/gce and Kr-h1 stimulates proliferation to increase the number of cells and sequentially intestinal size.

1.5.4 *Drosophila* as a model for investigating intestinal tumours

Besides genetic tools like 'ReDDM'-tracing *Drosophila* is also used for drug screenings in diseases such as inflammatory bowel disease or CRC (Bangi *et al*, 2019; Bangi *et al.*, 2016; Martorell *et al*, 2014; Xiu *et al*, 2022). Fly models mimicking CRC are constantly improved with additional new insights into CRC progression and developing toolkits like CRISPR/Cas (Clustered Regularly Interspaced Short Palindromic Repeats/CRISPR-associated Protein) (Jinek *et al*, 2012). Existing and future *Drosophila* CRC models can additionally be combined with 'ReDDM'-tracing to further disentangle the heterogeneity of tumours by differentially labelling ISC/EB and their progeny. Furthermore, with the help of *Drosophila*

CRC models the roles of steroid hormones on tumour initiation and progression can be analysed to unravel the proposed controversial roles of oestrogens in CRC.

1.6 Aims of this thesis

1.6.1 A possible role for systemic ecdysone in regulating mating-induced adaptations of the *Drosophila* midgut

The endocrine *Drosophila* JH was already shown to be implicated in physiological size adaptations of the female intestine in mated flies (Reiff *et al.*, 2015). During larval development and metamorphosis JH acts in concert with steroidal 20HE (Truman & Riddiford, 2002). An involvement of 20HE in regulating reproduction and mating induced adaptations of the female metabolism has been demonstrated previously (Carney & Bender, 2000; Kozlova & Thummel, 2000). However, it remained unknown if 20HE also has a role in mediating intestinal re-sizing. Investigating a possible role of 20HE in intestinal size adaptations is of particular interest, because 20HE serves as the functional equivalent of mammalian oestrogens (Aranda & Pascual, 2001; Martinez *et al.*, 1991; Oberdörster *et al.*, 2001), enabling the application of insights gained from the role of 20HE in intestinal re-sizing to potential implications of mammalian oestrogens in similar processes. Paper I addresses the following questions:

Is 20HE also involved in regulating mating-induced re-sizing of the female *Drosophila* midgut?

Which local factors downstream of 20HE are involved in mediating adaptations in the remote midgut?

Are the roles of JH and 20HE signalling in mating-induced re-sizing of the female midgut antagonizing as shown for *Drosophila* development?

How is 20HE signalling affecting the initiation and progression of benign ISC-tumours?

1.6.2 Generation of novel avatar flies mimicking CRC

Additional to investigations of 20HE in physiological conditions and benign ISC-tumours used in Paper I, the hormone's role in CRC progression should be analysed. The generation and establishment of novel CRC avatar flies is part of Paper II. CRISPR/Cas9 is used and combined with 'ReDDM'-tracing to create novel fly avatars that mimic CRC from human patients (Jinek *et al.*, 2012; Port & Bullock, 2016; Port *et al*, 2014; Port *et al*, 2015). This approach uses CRISPR/Cas9 to induce mutations in key tumour suppressor genes involved in the most frequently altered signalling pathways in CRC, including Adenomatous polyposis coli (Apc), Tumor protein p53 (p53), Medea (med), and Phosphatase and tensin homolog (pten), alongside the expression of oncogenic Ras^{G12V}. Insights gained from manipulating systemic 20HE signalling in CRC avatar flies could provide a deeper understanding of the contrasting effects of steroidal oestrogens on CRC development and progression.

1.6.3 Identification of factors linking systemic ecdysone with local signals in the remote intestine

Additional objectives of this thesis delve deeper into exploring how endocrine hormonal signals are converted into local signals that regulate ISC proliferation and differentiation. In developmental studies on *Drosophila* wing imaginal discs it was previously shown that 20HE controls proliferation via its translation into local signals regulating cell cycle progression (D'Avino & Thummel, 1998; Mitchell *et al*, 2008; Mitchell *et al*, 2013). A zinc finger transcription factor, namely Crooked legs (Crol), was shown to be induced by systemic 20HE and to directly regulate expression of the Wnt/Wg ligand Wingless (Wg) and the cell cycle regulator and CDC25-orthologue String (Stg) (D'Avino & Thummel, 1998; Mitchell *et al.*, 2008; Mitchell *et al.*, 2013). It would thus be interesting to investigate whether the same link of systemic 20HE and local signals by Crol can be found in the adult *Drosophila* midgut as well. Paper III focuses on answering the following questions:

> Is Crol also expressed in adult *Drosophila* midgut cells and regulated by 20HE signalling? What are its functions within different cell types?

Are Wg and Stg also regulated by Crol within the midgut cells?

How is Crol affecting the initiation and progression of benign ISC tumours when expressed within the tumour or within the tumour microenvironment? How is Crol affecting tumour progression in CRC avatar flies?

Does Crol relay endocrine regulation of mating-induced increase in intestinal size?

To investigate the non-autonomous regulation of ISC behaviour by Crol in EC, a new binary expression system is developed. This system enables labelling of ISC and tracing of their progeny with simultaneous and independent manipulation of EC. Additionally, when combined with N-RNAi to induce benign ISC-tumours, this system enables the investigation of Crol's non-autonomous roles in tumour initiation and progression.

2 Paper

This chapter has been published in identical form:

Paper I: **Zipper L**, Jassmann D, Burgmer S, Görlich B, Reiff, T. (2020) Ecdysone steroid hormone remote controls intestinal stem cell fate decisions via the PPARγ-homolog Eip75B in *Drosophila*. ***eLife*** 9:e55795. https://doi.org/10.7554/eLife.55795

Lisa Zipper contributed to this work by:

- **Performing and analysing** all *in vivo* experiments except for:
  - esg^{ReDDM} specific *EcR* and sole *Eip75B* manipulations performed by Bastian Görlich und Denise Jassmann
  - esg^{ReDDM} comparison of VF and MF performed by Denise Jassmann
  - Pioglitazone feeding experiment performed by Sofie Burgmer
  - N-tumour experiments performed by Denise Jassmann

Paper II: **Zipper L**, Batchu S, Kaya NH, Antonello ZA, Reiff T. (2022) The MicroRNA *miR-277* Controls Physiology and Pathology of the Adult *Drosophila* Midgut by Regulating the Expression of Fatty Acid β-Oxidation-Related Genes in Intestinal Stem Cells. ***Metabolites*** *12*, 315. https://doi.org/10.3390/metabo12040315

Lisa Zipper contributed to this work by:

- **Developing** the cloning strategy of the multiplex guide-RNA array for the CRC model
- **Performing and analysing** all *in vivo* experiments except for:
  - Expression analysis of miR277 performed by Tobias Reiff
  - Molecular cloning of the CRC model performed by Nida Hatice Kaya
- Creating figures for **visualization** of *in vivo* data
- **Writing** parts of the original draft and rebuttal letter

Paper III: **Zipper L**, Corominas-Murtra B & Reiff T. (2025) Steroid hormone-induced wingless ligands tune female intestinal size in *Drosophila*. ***Nat Commun*** 16, 436. https://doi.org/10.1038/s41467-024-55664-2

Lisa Zipper contributed to this work by:

- **Planning and conceptualisation** of the research
- **Performing and analysing** all *in vivo* experiments
- Creating all figures for **visualization** of the data except for:
  - Figures Fig.S8-Fig.S11 created by Bernat Corominas Murtra
- **Writing** parts of the original draft and rebuttal letter

2.1 Paper I: Ecdysone steroid hormone remote controls intestinal stem cell fate decisions via the *PPARγ*-homolog *Eip75B* in *Drosophila*

eLife RESEARCH ARTICLE

Ecdysone steroid hormone remote controls intestinal stem cell fate decisions via the *PPARγ*-homolog *Eip75B* in *Drosophila*

Lisa Zipper, Denise Jassmann, Sofie Burgmer, Bastian Görlich, Tobias Reiff*

Institute of Genetics, Heinrich-Heine-University, Düsseldorf, Germany

Abstract Developmental studies revealed fundamental principles on how organ size and function is achieved, but less is known about organ adaptation to new physiological demands. In fruit flies, juvenile hormone (JH) induces intestinal stem cell (ISC) driven absorptive epithelial expansion balancing energy uptake with increased energy demands of pregnancy. Here, we show 20-Hydroxy-Ecdysone (20HE)-signaling controlling organ homeostasis with physiological and pathological implications. Upon mating, 20HE titer in ovaries and hemolymph are increased and act on nearby midgut progenitors inducing *Ecdysone-induced-protein-75B* (*Eip75B*). Strikingly, the *PPARγ*-homologue *Eip75B* drives ISC daughter cells towards absorptive enterocyte lineage ensuring epithelial growth. To our knowledge, this is the first time a systemic hormone is shown to direct local stem cell fate decisions. Given the protective, but mechanistically unclear role of steroid hormones in female colorectal cancer patients, our findings suggest a tumor-suppressive role for steroidal signaling by promoting postmitotic fate when local signaling is deteriorated.

***For correspondence:** reifft@hhu.de

Competing interests: The authors declare that no competing interests exist.

Funding: See page 22

Received: 06 February 2020
Accepted: 07 August 2020
Published: 10 August 2020

Reviewing editor: Elisabeth Knust, Max-Planck Institute of Molecular Cell Biology and Genetics, Germany

Introduction

Reproduction is an energetically costly process triggering multiple physiological adaptations of organs such as liver, pancreas and gastrointestinal tract upon pregnancy in various species (***Hammond, 1997***; ***Roa and Tena-Sempere, 2014***). As a part of the hormonal response to mating and increased metabolic energy consumption, the female *Drosophila melanogaster* midgut is remodeled in size and physiology by stimulating intestinal stem cell (ISC) driven epithelial expansion to achieve an even energy balance (***Cognigni et al., 2011***; ***Klepsatel et al., 2013***; ***Reiff et al., 2015***).

Since the discovery of adult intestinal stem cells (***Micchelli and Perrimon, 2006***; ***Ohlstein and Spradling, 2006***), local signaling pathways such as Notch (N), Jak/Stat, EGFR, Wnt/wingless, Insulin-receptor, Hippo/Warts and Dpp-signaling were shown to contribute to intestinal homeostasis under physiological and challenged conditions like bacterial infections (***Miguel-Aliaga et al., 2018***)(and references therein). The midgut epithelium is maintained by ISC giving rise to only two types of differentiated cells: enteroendocrine cells (EE) and absorptive enterocytes (EC) (***Figure 1A***). Pluripotent ISC are able to self-renew or divide asymmetrically into either committed EC precursor cells called enteroblasts (EB) or enteroendocrine precursor (EEP) cells. EEP, upon timely activation of *scute* in ISC, divide once more prior to terminal differentiation yielding a pair of EE (***Chen et al., 2018***; ***Micchelli and Perrimon, 2006***; ***Ohlstein and Spradling, 2006***; ***Ohlstein and Spradling, 2007***). Nine out of ten ISC mitosis give rise to EB specified by N-activation in EB daughters (***Micchelli and Perrimon, 2006***; ***Ohlstein and Spradling, 2006***; ***Ohlstein and Spradling, 2007***). Post-mitotic EB retain a certain degree of plasticity by: (1) delaying their terminal differentiation through mesenchymal-to-epithelial transition (MET) (***Antonello et al., 2015a***), (2) changing their fate to EE upon loss of the

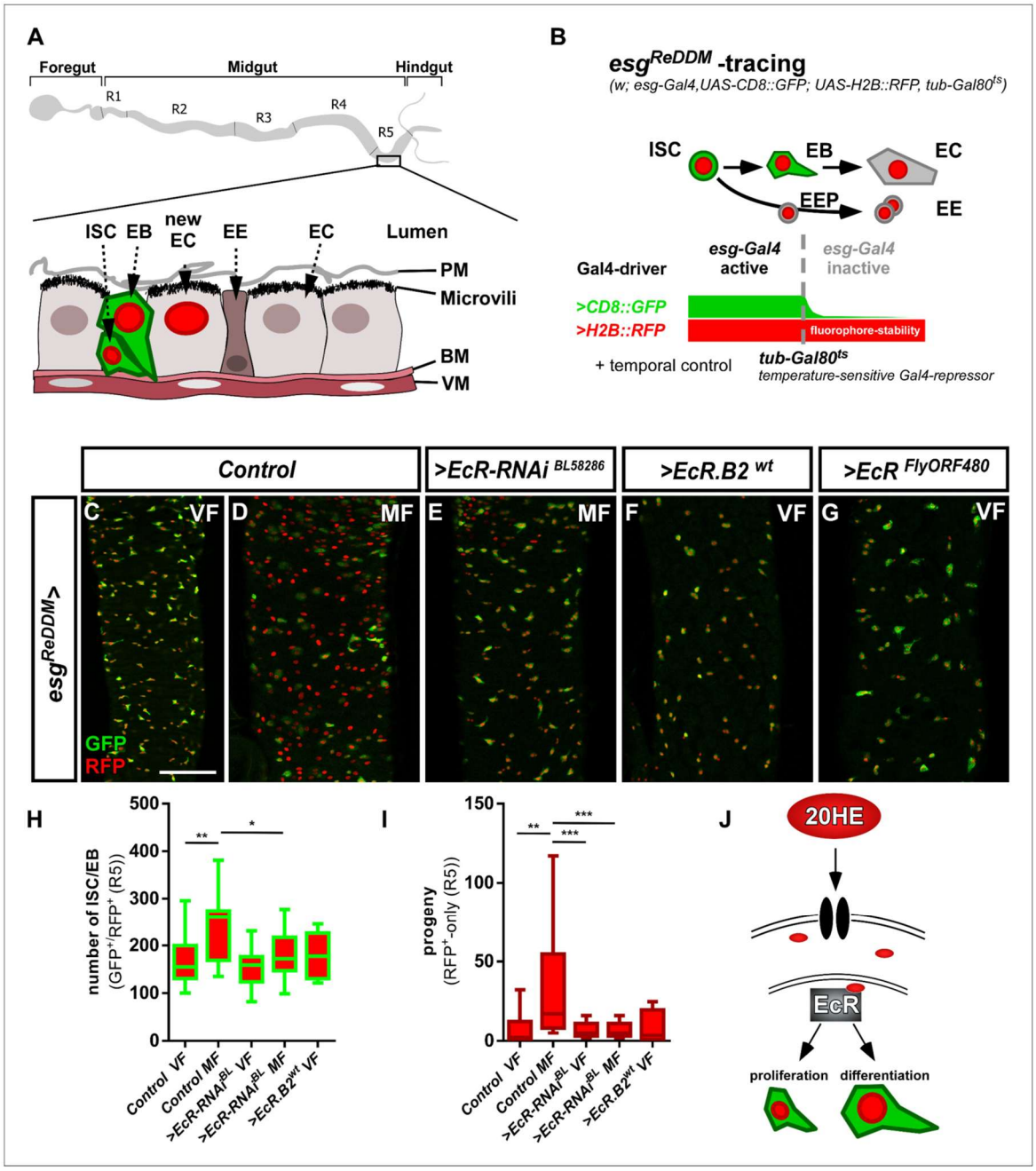

Figure 1. The Ecdysone receptor in intestinal progenitors controls tissue homeostasis. (**A**) Scheme of the adult *Drosophila melanogaster* gastrointestinal tract with cartoon depicting the midgut epithelial monolayer composed of intestinal stem cells (ISC), enteroblasts (EB), enterocytes (EC) and enteroendocrine cells (EE) colored according to the lineage tracing system ReDDM with esg-Gal4 (***Antonello et al., 2015a***). (**B**) Schematic of esg^{ReDDM} tracing including full genotype. *ReDDM* differentially marks cells having active or inactive *Gal4* expression. Combined with *esg-Gal4*, active in

Figure 1 continued on next page

Figure 1 continued

ISC and EB, esg^{ReDDM} double marks ISC and EB driving the expression of *UAS-CD8::GFP* (membrane CD8::GFP, green), *UAS-H2B::RFP* (nuclear H2B::RFP, red) and further UAS-driven transgenes (UAS abbreviated as >hereafter in Figure panels). Newly differentiated EC and EE with inactive *esg-Gal4* are RFP^+-only owing to protein stability of H2B::RFP. Flies are grown at permissive 18˚C in which transgene expression is repressed by ubiquitous tubulin-driven $Gal80^{ts}$. By shifting adult females to the restrictive temperature of 29˚C, $Gal80^{ts}$ is destabilized, in turn enabling ReDDM-tracing marking progeny (EE and EC with H2B::RFP nuclear stain) and in parallel manipulation by allowing transactivation of UAS-sequences through *esg-driven* Gal4-expression (***Antonello et al., 2015a***). Posterior midguts (PMG) after seven days of esg^{ReDDM} tracing of control (crossed with w^{1118}) adult MF (**D**) show mating dependent addition of new EC compared to control VF (**C**) (***Reiff et al., 2015***). (**E**) Knockdown of EcR using UAS-driven RNAi abolishes mating induced new EC generation in MF. (F+G) Overexpression of *>EcR.B2* in VF (**F**) and $>EcRFlyORF^{FlyORF840}$ (**G**) does not induce proliferation or differentiation of progenitors (ISC+EB). (**H–I**) Quantification of progenitor numbers (**H**) and traced progeny encompassing EC and EE (**I**) in R5 PMG (n = 24,17,17,17, 8). Error bars are Standard Error of the Mean (SEM) and asterisks denote significances from one-way ANOVA with Bonferroni's Multiple Comparison Test (*p<0.05, **p<0.01; ***p<0,001; ****p<0.0001). (**J**) Cartoon depicting experimental manipulations on EcR signaling pathway investigated with esg^{ReDDM}. Scale bars = 100 μm.

The online version of this article includes the following source data and figure supplement(s) for figure 1:

Source data 1. Data from ***Figure 1***.
Figure supplement 1. The EcR is expressed in the adult *Drosophila* midgut.
Figure supplement 1—source data 1. Data from ***Figure 1—figure supplement 1***.

transcription factor *klu* (*klumpfuss*) and (3) undergoing apoptosis as an additional homeostatic mechanism (***Korzelius et al., 2019***; ***Reiff et al., 2019***).

Apart from aforementioned local signaling pathways, systemic hormones are released into the hemolymph and act on distant organs (***Figueroa-Clarevega and Bilder, 2015***; ***Kwon et al., 2015***; ***Reiff et al., 2015***). Upon mating, JH released by the neuroendocrine *corpora allata* is able to control ISC proliferation through heterodimers of *Met (methoprene-tolerant)* and *gce (germ cells expressed)* nuclear hormone receptors (***Reiff et al., 2015***). JH coordinates *Drosophila* larval development in concert with the steroid hormone 20-hydroxy-ecdysone (20HE) and both hormones stimulate egg production in adult females (***Bownes et al., 1984***; ***Gilbert et al., 2002***; ***Kozlova and Thummel, 2000***; ***Truman and Riddiford, 2002***). In mated adult female flies, we confirmed an increase of 20HE titers in ovary and detected a similar increase of hemolymph 20HE titers compared to virgin females (***Ameku and Niwa, 2016***; ***Gilbert and Warren, 2005***; ***Harshman et al., 1999***). The anatomical proximity of ovaries and the posterior midgut (PMG) prompted us to investigate a role for the Ecdysone-receptor (EcR) signaling cascade in organ plasticity during reproduction. Downstream of EcR activation, we detected upregulation of *Ecdysone-induced protein 75B (Eip75B)* protein isoforms ensuring absorptive EC production upon mating. Using the established Notch tumor paradigm, we found that 20HE through Eip75B/PPARγ remote controls EB differentiation and suppresses N-loss of function driven hyperplasia. The mechanism identified in this study not only plays a role in the physiology of mating, but also contributes to our understanding of the protective effects of steroid hormone signaling in the pathophysiology of human colorectal cancer.

Results

EcR controls intestinal stem cell proliferation and progenitor differentiation

The female fly intestine undergoes various physiological post-mating adaptations including a size increase of the absorptive epithelium (***Cognigni et al., 2011***; ***Klepsatel et al., 2013***; ***Reiff et al., 2015***). Intrigued by post-mating increases of 20HE titers (***Ameku and Niwa, 2016***; ***Harshman et al., 1999***), we explored a role for EcR-signaling in mating adaptations of the adult *Drosophila melanogaster* intestine.

EcR encodes for three different splice variants: *EcR.A, EcR.B1* and *EcR.B2* (***Cherbas et al., 2003***; ***Talbot et al., 1993***), which we detected by PCR in intestinal tissue with highest expression for *EcR.B2* (***Figure 1—figure supplement 1A***). Using EcR antibodies detecting all splice variants, we found EcR in ISC (positive for the Notch ligand $Delta^+$), EB (Notch responsive element, $NRE\text{-}GFP^+$) and EC (Discs-large-1, $Dlg\text{-}1^+$, ***Figure 1—figure supplement 1B–D'''*** and ***Figure 1A*** for an overview). To investigate a role for the EcR in intestinal tissue homeostasis, we first manipulated EcR function in ISC and EB using the *'ReDDM'* (Repressible Dual Differential Marker, ***Figure 1B***) tracing method to

observe its overall impact on tissue renewal (**Antonello et al., 2015a**). Briefly, *ReDDM* differentially marks cells having active or inactive *Gal4* expression with fluorophores of different stability over a defined period of time. Combined with the enhancer trap *esg-Gal4,* active in progenitors (ISC and EB), esg^{ReDDM} double marks ISC and EB driving the expression of *UAS-CD8::GFP* (*>CD8::GFP*) with short half-life and *>H2B::RFP* with long half-life. Upon epithelial replenishment, CD8::GFP signal is lost and new terminally differentiated EC (Dlg-1^{+}) and EE (Prospero, $Pros^{+}$) stemming from ISC divisions retain a RFP^{+}-nuclear stain due to fluorophore stability (**Figure 1A,B**; **Antonello et al., 2015a**). Crosses are grown at 18˚C in which transgene expression is repressed by ubiquitous tubulin-driven temperature sensitive $Gal80^{ts}$. By shifting adult females to 29˚C, $Gal80^{ts}$ is destabilized, in turn enabling spatiotemporal control of esg^{ReDDM}-tracing and additional UAS-driven transgenes in progenitors (**Figure 1B**).

After seven days of esg^{ReDDM}-tracing, mated females (MF, **Figure 1D**) showed increases of progenitor numbers (**Figure 1H**) and newly generated progeny (EE+EC, **Figure 1I**) in the R5 region of the PMG over virgin females (VF, **Figure 1C**) confirming previous observations (**Reiff et al., 2015**). Reducing *EcR*-levels with two different *>EcR* RNAi stocks in MF resulted in a reduction of ISC/EB numbers (**Figure 1E,H**, **Figure 1—figure supplement 1L**) and newly generated progeny (**Figure 1E, I**, **Figure 1—figure supplement 1L**) to levels comparable to VF controls (**Figure 1C,H,I**). We confirmed knockdown efficiency of *>EcR* RNAi in esg^{ReDDM} by measuring fluorescence intensity of EcR in progenitor cells in situ and found EcR-protein levels significantly decreased in both RNAi lines (**Figure 1—figure supplement 1E–H**).

Independent of EcR-abundance, we found that expressing dominant-negative *EcR.B2* isoforms or *EcR*-heterozygosity using EcR^{M554fs}, a well described loss-of-function (LOF) allele, phenocopy *>EcR* RNAi (**Figure 1—figure supplement 1I–K**). Generally, *EcR* LOF leads to a similar phenotype as JH-receptor knockdown in MF (**Reiff et al., 2015**). To investigate whether EcR-levels affect progenitor behavior, we overexpressed wildtype *EcR.B2* and *pan-EcR* using esg^{ReDDM} in VF. We found neither induction of progenitor numbers nor an increase in new EC (**Figure 1F–I**), suggesting that EcR-dependent proliferation and differentiation of progenitors might be limited by 20HE availability (**Figure 1J**).

Ecdysone titers are increased upon mating and actively transported into progenitors to adapt intestinal physiology

In close anatomical proximity to the PMG, the ovaries are an established ecdysteroidogenic tissue. Determining 20HE titers 48 hr after mating using enzyme immunoassays, we confirmed previous reports of mating dependent increases of ovarian 20HE titers (**Figure 2A**; **Ameku and Niwa, 2016**; **Harshman et al., 1999**) and observed a similar increase in the hemolymph (**Figure 2A**). As a study investigating the *ecdysoneless* mutants suggested that the ovary is the only source for 20HE in adult females (**Garen et al., 1977**), we sought to diminish 20HE titers in adult females. Therefore, we genetically ablated the ovaries using the dominant sterile ovo^{D1} allele in which egg production is blocked prior to vitellogenesis (**Busson et al., 1983**; **Oliver et al., 1987**; **Reiff et al., 2015**; **Figure 2D**). 20HE titers in the hemolymph of ovo^{D1} females are reduced around 40–50% compared to wild-type females (**Figure 2B,A**). Interestingly, 20HE titers in hemolymph and remnants of the ovaries are still significantly increased upon mating of ovo^{D1} females (**Figure 2C**). Consequently, 20HE titers in sterile esg^{ReDDM}/ovo^{D1} MF increase the number of progenitors (**Figure 2E**) and progeny (**Figure 2F**). This suggests that remaining 20HE levels are sufficient to elicit mating related midgut adaptations.

20HE is a polar steroid, which disperses through hemolymph and binds to EcR to activate target gene transcription (**Figure 2D**; **Bownes et al., 1984**; **Gilbert et al., 2002**). Using an established reporter for the activation of 20HE signaling, we found mating induced increases of EcR activity in PMG and ovaries using qPCR (**Figure 2J**). As orally administered 20HE is metabolized and cleared of rapidly, we used the potent non-steroidal EcR agonist RH5849. RH5849 is used as pest control due to its stability, specificity and a 30–60 times higher efficacy compared to 20HE (**Robinson et al., 1987**; **Wing et al., 1988**). Testing concentrations from 1 to 100 µg/ml in timed egg-layings, we observed expected larval molting defects for concentrations from 50 µg/ml upwards (**Figure 2—figure supplement 1A**). Feeding control esg^{ReDDM} VF 50 µg/ml with RH5849, we traced intestinal progenitors with pharmacologically activated EcR-signaling for seven days. RH5849 strongly induces ISC mitosis, reflected by a tenfold increase in newly generated progeny over mating induction

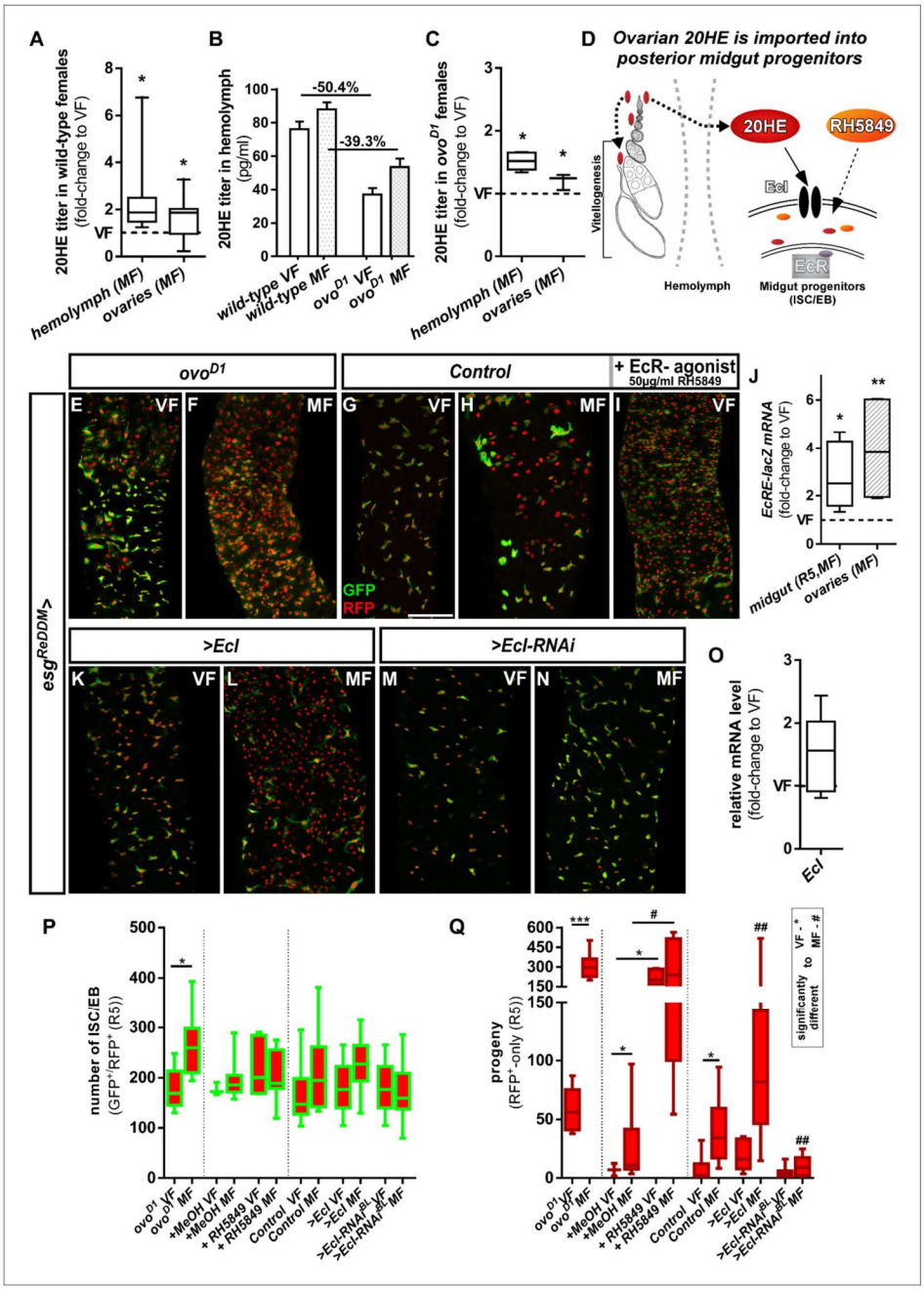

Figure 2. Intracellular 20-Hydroxy-ecdysone levels control ecdysone response through the ecdysone importer. (**A–C**) Determination of 20HE titers in ovaries and hemolymph of wild-type (**A,B**) and *ovo*^{D1} (**B,C**) adult VF and MF 48 hr after mating. (**A,C**) show fold-change increases over VF titer (dotted line at y = 1). (**D**) Cartoon depicting ovarian 20HE release to ISC/EB in the adjacent PMG. Please note that in wild-type females, 20HE is incorporated into developing eggs during vitellogenesis, whereas in *ovo*^{D1} vitellogenesis is absent and might lead to higher (proportional) release into the

Figure 2 continued on next page

Figure 2 continued

hemolymph. 20HE from the hemolymph is absorbed by ISC/EB in the PMG, where the cartoon illustrates specific genetical and pharmacological manipulations on the EcR-signaling pathway. (**E–I**) Representative images of adult PMG after seven days of esg^{ReDDM} tracing of ovo^{D1} VF (**E**), ovo^{D1} MF (**F**) and control VF (**G**) and MF (**H**). (**I**) Control VF PMG after oral administration of RH5849 (50 µg/ml). (**J**) Quantitative RT-PCR on *EcRE* (Ecdysone responsive elements, [***Schwedes et al., 2011***]) driving lacZ expression on intestinal cDNA from VF and MF control flies. Values are normalized to VF levels (dotted line at y = 1) and statistically analysed using student´s t-test (*p<0.05, **p<0.01; ***p<0,001;). (**K–N**) Up- and downregulation of *EcI* in VF (**K,M**) and MF (**L,N**) using UAS driven transgenes after seven days of tracing with esg^{ReDDM}. (**O**) Quantitative RT-PCR of *EcI* on intestinal cDNA from VF and MF control flies. Values are normalized to VF levels (dotted line at y = 1) and statistically analysed using student´s t-test (*p<0.05, **p<0.01; ***p<0,001;). (**P,Q**) Quantification of progenitor numbers (**P**) and traced progeny encompassing EC and EE (**Q**) in R5 PMG (n = 7,9/3,9,5,13/16,13,8,10,10,19). Error bars are Standard Error of the Mean (SEM) and asterisks denote significances from one-way ANOVA with Bonferroni's Multiple Comparison Test (*p<0.05, **p<0.01; ***p<0,001; ****p<0.0001). Scale bars = 100 µm.

The online version of this article includes the following source data and figure supplement(s) for figure 2:

Source data 1. Data from ***Figure 2***.
Figure supplement 1. 20HE regulates physiological adaptations of fatty acid metabolism.
Figure supplement 1—source data 1. Data from ***Figure 2—figure supplement 1***.

(***Figure 2G–I,Q***). Interestingly, RH5849 mediated EcR-activation leads to no accumulation of progenitors (***Figure 2P***) as observed in oncogenic manipulations or disruptions of intestinal homeostasis, suggesting a role for EcR in both, proliferation and differentiation (***Antonello et al., 2015a***; ***Chen et al., 2016***; ***Patel et al., 2015***; ***Reiff et al., 2019***). Given the role of 20HE induced programmed cell death (PCD) in larval metamorphosis and the recently discovered role of EB PCD in adult midgut homeostasis (***Jiang et al., 1997***; ***Jiang et al., 2000***; ***Reiff et al., 2019***), we addressed PCD by activated caspase-3 staining, but found no increase of PCD by RH5849 (data not shown).

Cellular 20HE uptake was recently shown to depend on *Ecdysone Importer (EcI)* belonging to the evolutionary conserved SLCO superfamily of solute carrier transporters. *EcI* LOF causes phenotypes indistinguishable from 20HE and *EcR* deficiencies in vivo (***Okamoto et al., 2018***). To investigate a role of EcI, we confirmed membrane localization of *>EcI* tagged with HA by immunostaining in progenitors using esg^{ReDDM} (***Figure 2—figure supplement 1B***). After seven days, forced expression of *>EcI* using esg^{ReDDM} in VF lead to no increase in progenitor numbers and new EC, underlining that VF 20HE levels are low (***Figure 2K,P,Q***). Further supporting this hypothesis,*>EcI* in MF lead to an increase of newly generated EC exceeding typical mating induction of MF controls by 4.8 fold (***Figure 2L,P,Q***). Blocking 20HE uptake by *EcI-RNAi* in MF abolished ecdysone induced tissue expansion to VF control levels (***Figure 2N,P,Q***). In addition, we tested a function of the *EcI* gene in mating induction, but found no change in *EcI* expression upon mating (***Figure 2O***). Both, pharmacological and genetic experiments, suggest that 20HE titer and import control EcR-activity upon mating (***Figure 2D***).

Upon mating, absorptive EC undergo metabolic adaptations upregulating genes known for lipid uptake (***Reiff et al., 2015***). We found EC immunoreactive for EcR (***Figure 1—figure supplement 1D***) and investigated a function for EcR in mating related upregulation of lipid uptake by measuring the activity of *sterol regulatory element-binding protein* (*Srebp*) (***Reiff et al., 2015***). Therefore, we used a GFP-reporter (*Srebp >CD8::GFP*) that is subjected to the same proteolytic processing as Srebp (***Athippozhy et al., 2011***; ***Reiff et al., 2015***). Confirming previous observations, *Srebp*-activity increases 2.2 fold upon mating (mean fluorescence intensity, ***Figure 2—figure supplement 1C, D***; ***Reiff et al., 2015***). Using the *Srebp*-reporter to drive *>EcR* RNAi in MF, we found reduced *Srebp*-activity comparable VF controls (***Figure 2—figure supplement 1E–F,H***), whereas feeding VF with RH5849 induced *Srebp*-activity 2.4 fold (***Figure 2—figure supplement 1G,H***). Next, we directly addressed lipid uptake with OilRedO-staining on PMG using the EC driver Mex^{ts}. In accordance with *Srebp*-activity (***Figure 2—figure supplement 1C,D,G***), feeding flies with RH5849 (***Figure 2—figure supplement 1K***) and forced expression of EcI (***Figure 2—figure supplement 1L***) significantly induced lipid uptake (***Figure 2—figure supplement 1O***) over controls (***Figure 2—figure supplement 1I,J***). Mex^{ts} > *EcI* RNAi and *>EcR* RNAi did not result in a reduction of lipid uptake below control levels (***Figure 2—figure supplement 1M,N,I***), confirming previous observations of direct fatty acid incorporation into newly produced eggs (***Reiff et al., 2015***).

These data support the idea that mating related synergistic effects of JH- and 20HE-signaling drive adaptation of intestinal homeostasis and physiology. The JH-signal is transduced by the

transcription factor *Krüppel-homolog 1 (Kr-h1)* in adult MF intestines, which prompted us to explore a function for the 'classical' Ecdysone target genes (**Jindra et al., 2013**; **Reiff et al., 2015**).

Ecdysone-induced protein 75b protein isoforms Eip75B-A and Eip75B-C control enteroblast differentiation

During *Drosophila* development, 20HE pulses lead to direct binding of EcR to regulatory regions of early ecdysone response genes *Ecdysone-induced protein 74A (Eip74EF)* and *Ecdysone-induced protein 75B* (*Eip75B*, **Figure 3A**; **Bernardo et al., 2014**; **Karim and Thummel, 1991**; **Segraves and Hogness, 1990**). First, we performed conventional PCR to analyze JH- and Ecdysone target gene expression. Signal for *Kr-h1-A (Kr-h1* in the following), but not *Kr-h1-B*, and for all isoforms of *Eip74EF* and *Eip75B* was found (**Figure 3B**). Using quantitative real time PCR (qPCR) analysis, we confirmed an increase of JH-pathway activity upon mating using *Kr-h1* as control (**Figure 3C**; **Reiff et al., 2015**). To our surprise, we found *Eip74EF* expression unchanged, in contrast to its prominent role in the control of germline stem cell (GSC) proliferation in oogenesis (**Ables and Drummond-Barbosa, 2010**). Instead, we found induction of *Eip75B-A* and *-C* isoforms (**Figure 3C**). *Eip75B* encodes for three protein isoforms (Eip75B-A, -B and –C) that differ in their N-terminal domain structure (**Segraves and Hogness, 1990**) and Eip75B-B lacks one of the two zinc-finger DNA binding domains rendering it incapable of direct DNA binding (**White et al., 1997**).

Intrigued by mating increases of *Eip75B-A /- C* levels, we manipulated Eip75B function using esg^{ReDDM}. Reducing *Eip75B* levels with RNAi, we found a significant increase in ISC and EB numbers (**Figure 3D,E,L**), but not in EC generation compared to VF controls (**Figure 3M**). In MF, *Eip75B* knockdown reduced newly generated EC compared to MF controls, pointing to a role of *Eip75B* in EB differentiation downstream of EcR-activation (**Figure 3E,M**). Interestingly, feeding flies with RH5849 lacking *Eip75B* in their intestinal progenitors (**Figure 3F**) did not result in newly generated progeny (**Figure 3M** compare to **Figure 2Q**), suggesting a central role for Eip75B in the RH5849 response. Additionally, we investigated homozygous *Eip75B-A* mutants using MARCM clonal analysis with a known LOF allele (**Rabinovich et al., 2016**). MARCM clones of *Eip75B-A* ($Eip75B^{A81}$) are significantly larger compared to controls (**Figure 3—figure supplement 1A–D**; **Lee and Luo, 1999**). $Eip75B^{A81}$ deficient clones contain few differentiated EC (GFP^+/Dlg-1^+, **Figure 3—figure supplement 1C**) suggesting disturbed EB to EC differentiation as observed for esg^{ReDDM} *>Eip75* B-RNAi (**Figure 3E**). Together, these LOF experiments hint to a role for mating induced *Eip75B-A /- C* isoforms in EC differentiation of EB downstream of EcR.

Forced expression of Eip75B variants with esg^{ReDDM} resulted in three prominent phenotypes: (1) *Eip75B-A* and *Eip75B-C* strongly drive differentiation into EC (Dlg-1^+, **Figure 3G,J,M**) depleting the entire progenitor pool (**Figure 3G,J,M**). (2) The *Eip75B-B* isoform induces ISC proliferation in VF (**Figure 3I**, **Figure 3—figure supplement 1F**) and raised progenitor numbers suggesting slowed down but not inhibited terminal differentiation (**Figure 3I,L,M**). (3) All Eip75B manipulations strongly reduce the number of newly differentiated EE (**Figure 3—figure supplement 1E**). This suggests that EE differentiation upon *Eip75B-RNAi* and forced expression of the *Eip75B-B* isoform is blocked (**Figure 3I,L**, **Figure 3—figure supplement 1E**). *Eip75B-A* and *Eip75B-C* are sufficient to instantaneously drive progenitors into EC differentiation (**Figure 3G,H,J,K**) even in the absence of 20HE import (**Figure 3H,K**). The immediate strong differentiation stimulus prevents further ISC division and as a consequence also reduces new EE (**Figure 3L,M**, **Figure 3—figure supplement 1E**). Disrupting intestinal homeostasis alters midgut length (**Hudry et al., 2016**) and in line with this, Eip75B manipulations result in a shorter midgut as EC make up around 90% of the whole midgut epithelium (**Figure 3—figure supplement 1G**). Eip75B affects intestinal homeostasis by either slowing down terminal EB to EC differentiation (*Eip75B-B* and *Eip75B-RNAi*) or depleting the ISC and EB pool (*Eip75B-A /– C*, **Figure 3—figure supplement 1G**) preventing sufficient EC production along the gut. When EC production is blocked using *>N* RNAi, the midgut shrinks around one third over a period of seven days (**Chen et al., 2018**; **Guo and Ohlstein, 2015**; **Micchelli and Perrimon, 2006**; **Ohlstein and Spradling, 2006**; **Ohlstein and Spradling, 2007**; **Patel et al., 2015**). Thus, all Eip75B manipulations ultimately lead to an insufficient number of new absorptive EC resulting in a shorter midgut.

Eip75B is a long term predicted *PPARγ*-homologue (*peroxisome proliferator-activated receptor gamma*) in *Drosophila*. A close functional homology got recently confirmed in pharmacogenetic approaches demonstrating that *Eip75B*-mutant flies are irresponsive to PPARγ activating drugs

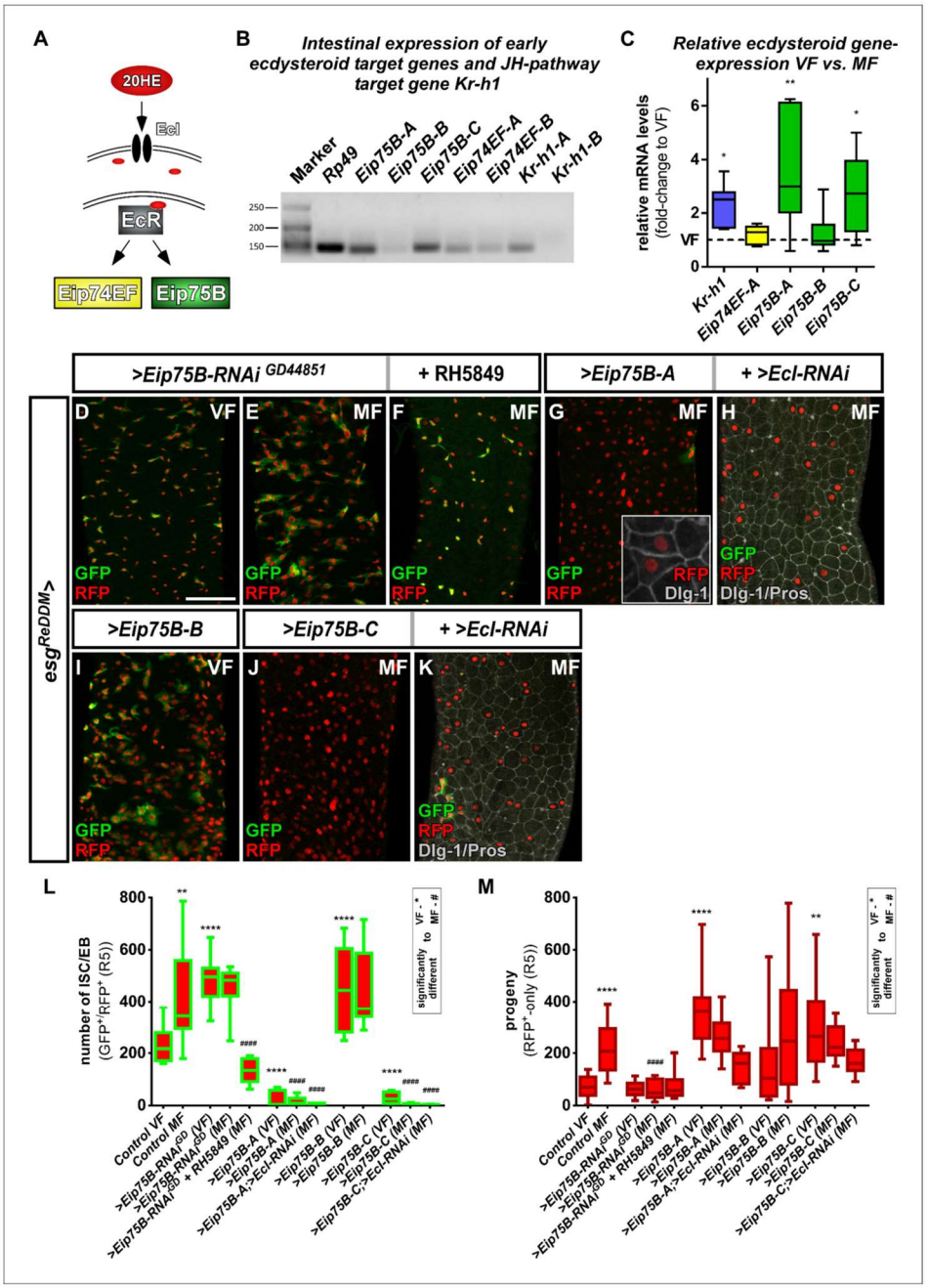

Figure 3. *Ecdysone induced protein 75B* is upregulated upon mating and controls progenitor differentiation. (**A**) Cartoon depicting EcR signaling cascade activating early ecdysteroid target genes. (**B**) Expression analysis of Ecdysone- and JH-signaling target genes including protein isoforms on cDNA transcribed from mRNA isolations from whole midgut dissections of MF. (**C**) Quantitative RT-PCR on early ecdysteroid genes on intestinal cDNA from VF and MF control flies. Values are normalized to VF levels (horizontal line = 1) and statistically analyzed using student´s t-test (n = 6; *p<0.05,

Figure 3 continued on next page

Figure 3 continued

p<0.01;). (D–E**) RNAi-mediated downregulation of *Eip75B* in VF (**D**), MF (**E**) and MF fed with RH5849 (**F**) after seven days of tracing with esg^{ReDDM}. (**G–K**) Representative images of adult PMG with forced expression of *Eip75B* isoforms *Eip75B-A* (**G**), *Eip75B-A and EcI-RNAi* (**H**), *Eip75B-B* (**I**), *Eip75B-C* (**J**), *Eip75B-C* and *EcI-RNAi* (**K**) after seven days of tracing with esg^{ReDDM}. Inset in (**F**) depicts epithelial integration of newly generated Dlg-1^+/RFP^+-EC. (**I–J**) Quantification of progenitor numbers (**I**) and traced progeny encompassing EC and EE (**J**) in R5 PMG (n = 12,13,10,12,11,11,14,8,10,10,10,5,11). Error bars are Standard Error of the Mean (SEM) and asterisks denote significances from one-way ANOVA with Bonferroni's Multiple Comparison Test (*p<0.05, **p<0.01; ***p<0,001; ****p<0.0001, identical p-values are marked by # when compared to MF). Scale bars = 100 µm.
The online version of this article includes the following source data and figure supplement(s) for figure 3:

Source data 1. Data from ***Figure 3***.
Figure supplement 1. Analysis of *Eip75B-A* MARCM clones.
Figure supplement 1—source data 1. Data from ***Figure 3—figure supplement 1***.
Figure supplement 2. EB specific genetic manipulation of Eip75B using klu^{ReDDM}.
Figure supplement 2—source data 1. Data from ***Figure 3—figure supplement 2***.

(***Joardar et al., 2015***; ***King-Jones and Thummel, 2005***). This homology is of particular interest, as human PPARγ plays a role in i) pregnancy related adaptations of lipid metabolism (***Waite et al., 2000***) and ii) as target in colorectal cancer (CRC) (***Sarraf et al., 1999***). Thus, we tested pharmacological activation of Eip75B/PPARγ with the established agonist Pioglitazone, a drug used in Diabetes mellitus treatment (***Gillies and Dunn, 2000***; ***Jafari et al., 2007***). Flies fed with food containing Pioglitazone show a strong increase in the number of progenitor cells (***Figure 4B,E***) and newly generated EC (***Figure 4F***) compared to controls (***Figure 4A***). Strikingly, knockdown of Eip75B led to irresponsiveness to Pioglitazone (***Figure 4C,D,F***) suggesting that Pioglitazone activates Eip75B in intestinal progenitors.

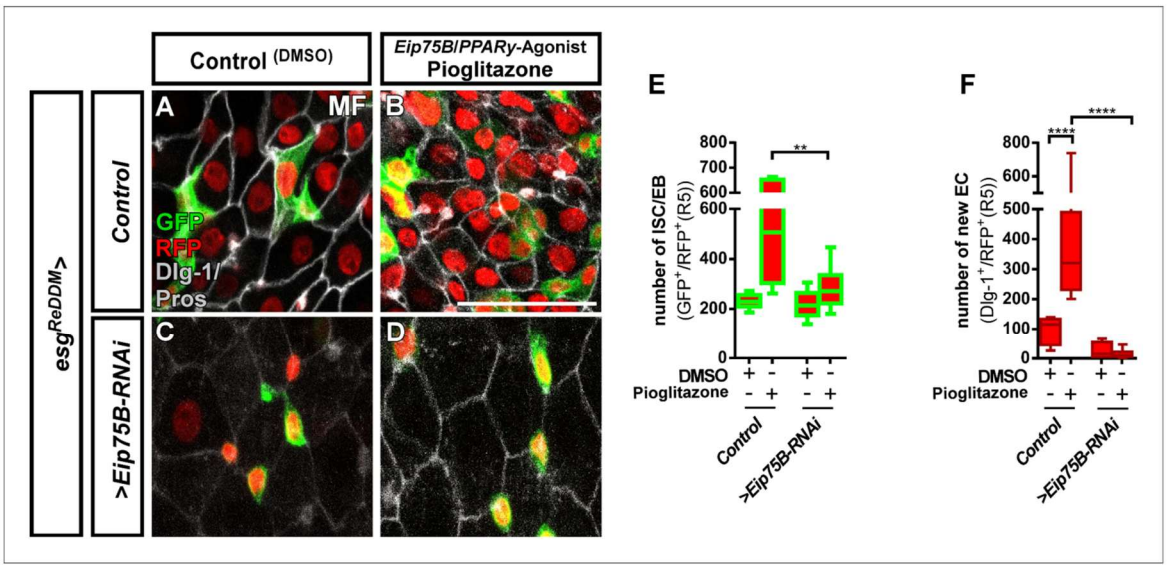

Figure 4. The Eip75B/PPARγ agonist Pioglitazone acts through Eip75B to stimulate progenitor differentiation. (**A–D**) Representative images of adult PMG after seven days of esg^{ReDDM} tracing of control MF (**A,B**) and *>Eip75* B-RNAi MF (**C,D**) fed with DMSO as control (A,C, 2.5 µl/ml food) and Pioglitazone (B,D; 0,002 mg in DMSO/ml food). (E+F) Quantification of progenitor numbers (**E**) and newly generated EC (**F**) in R5 PMG (n = 7,6,10,11). Error bars are Standard Error of the Mean (SEM) and asterisks denote significances from one-way ANOVA with Bonferroni's Multiple Comparison Test (*p<0.05, **p<0.01; ***p<0,001; ****p<0.0001,. Scale bars = 100 µm.
The online version of this article includes the following source data for figure 4:

Source data 1. Data from ***Figure 4***.

Taken together, these findings strongly suggested a role for *Eip75B* in EB differentiation. EB are specified by N-signaling and their lineage is maintained by the transcription factor *klumpfuss* (*klu*). *klu*$^{+}$-EB retain some plasticity to change fate to EE upon reduction of *klu*-levels (**Korzelius et al., 2019**; **Reiff et al., 2019**). We used *klu*^{ReDDM} to explore the function of *EcR* and *Eip75B* in EB lineage identity (**Figure 3—figure supplement 2A**). No changes in EB fate decisions towards EE differentiation were observed upon knockdown of *EcR* and *Eip75B* (**Figure 3—figure supplement 2A,B–D**). *Eip75B-A* and *Eip75B-C* expression with *klu*^{ReDDM} phenocopied EB to EC differentiation effects observed in *esg*^{ReDDM} (**Figure 3—figure supplement 2G,I,J,K**) without non-autonomously inducing proliferation in wild-type ISC of VF and MF (**Figure 3—figure supplement 2J,K**). Expressing *Eip75B-B* in *klu*^{ReDDM} lead to delayed EB differentiation similar to *esg*^{ReDDM} and non-autonomous induction of ISC mitosis (**Figure 3I**, **Figure 3—figure supplement 2J,L**; **Patel et al., 2015**; **Reiff et al., 2019**). Having identified *Eip75B-A /- C* as mating induced differentiation effector of 20HE signaling, we hypothesized and investigated a synergism of 20HE and JH hormonal signaling pathways controlling epithelial expansion upon mating.

The interplay between JH and 20HE in intestinal progenitors

Our data suggest that mating induced JH and 20HE signaling affect ISC proliferation and EB differentiation through their effectors *Kr-h1* and *Eip75B-A /- C* (**Figure 5K**; **Reiff et al., 2015**). In VF lacking mating induction of both hormones (**Figure 2A–C**; **Ameku and Niwa, 2016**; **Harshman et al., 1999**; **Reiff et al., 2015**), forced >*Kr* h1 expression doubles progenitor numbers reproducing previous results (**Figure 5B,I**; **Reiff et al., 2015**). Initially, we aimed to perform a full genetic epistasis analysis for *Eip75B* and *Kr-h1*, but this analysis was hampered as we failed to recombine *Kr-h1-RNAi* with *Eip75B* isoform expressing stocks.

However, we were able to analyze midguts of MF with forced *Kr-h1*-expression and simultaneous *Eip75B-RNAi* (**Figure 5C,D**), which increases progenitor numbers (**Figure 5I**) with only few newly generated EC (**Figure 5J**). This finding supports the requirement of *Eip75B* in EB differentiation (**Figure 3E**) and *Kr-h1* in ISC proliferation (**Figure 5A**). Simultaneous double knockdown of >*Kr-h1-RNAi*/*Eip75B-RNAi* (**Figure 5H**) in MF did not show mating induction. Progenitor numbers and differentiated progeny are reduced (**Figure 5I,J**) phenocopying single >*Kr* h1-RNAi (**Reiff et al., 2015**). Surprisingly, we observed a strong increase of progenitor numbers forcing *Kr-h1* and *Eip75B-B* expression (**Figure 5F,I,J**). These results indicate an additive role of forced *Eip75B-B* and *Kr-h1*-expression on ISC proliferation, whereas the latter transduces the mating related proliferation response (**Figure 3C**). The stimulus inducing *Eip75B-B* expression yet needs to be identified (**Figure 5K**).

Most interestingly, *Eip75B-A* and *–C*, despite of raised *Kr-h1*-levels, drive progenitors into EC differentiation largely phenocopying sole *Eip75B-A* and *-C* expression (compare **Figures 3G,J** and **5E, G,I,J**). Our data on *Eip75B-A* and *-C* corroborate a potent role for Ecdysone-induced EB differentiation. ISC fate decisions in the adult midgut rely on N-signaling (**Micchelli and Perrimon, 2006**; **Ohlstein and Spradling, 2006**; **Ohlstein and Spradling, 2007**). During *Drosophila* follicle cell development N opposes EcR-function (**Sun et al., 2008**), which prompted us to investigate *Eip75B-A /- C* as effectors of EcR-signaling in the context of N-dependent EB differentiation.

Ecdysone signaling through *Eip75B-A* and *Eip75B-C* controls enteroblast differentiation in a notch deficiency tumor model

In the *Drosophila* and mammalian intestinal stem cell niche, N-signaling specifies EE and EC fate (**Jensen et al., 2000**; **Micchelli and Perrimon, 2006**; **Ohlstein and Spradling, 2006**; **Ohlstein and Spradling, 2007**; **VanDussen et al., 2012**). In *Drosophila*, mitosis of *N* mutant ISC generates only ISC-like progenitor cells and EE, which results in an intestinal epithelium accumulating a lack of newly produced EC and compensatory proliferation (**Figure 6A,B**; **Chen et al., 2018**; **Guo and Ohlstein, 2015**; **Micchelli and Perrimon, 2006**; **Ohlstein and Spradling, 2006**; **Ohlstein and Spradling, 2007**; **Patel et al., 2015**).

Using N-LOF tumors as an experimental paradigm lacking EC production, we sought to investigate the differentiation inducing properties of Eip75B-A /- C. Reduction of N by RNAi or a dominant-negative N-receptor using *esg*^{ReDDM} lead to tumors of different sizes, which we quantified and classified according to their number (**Figure 6B**). We predominantly found tumors of 5–10 cells

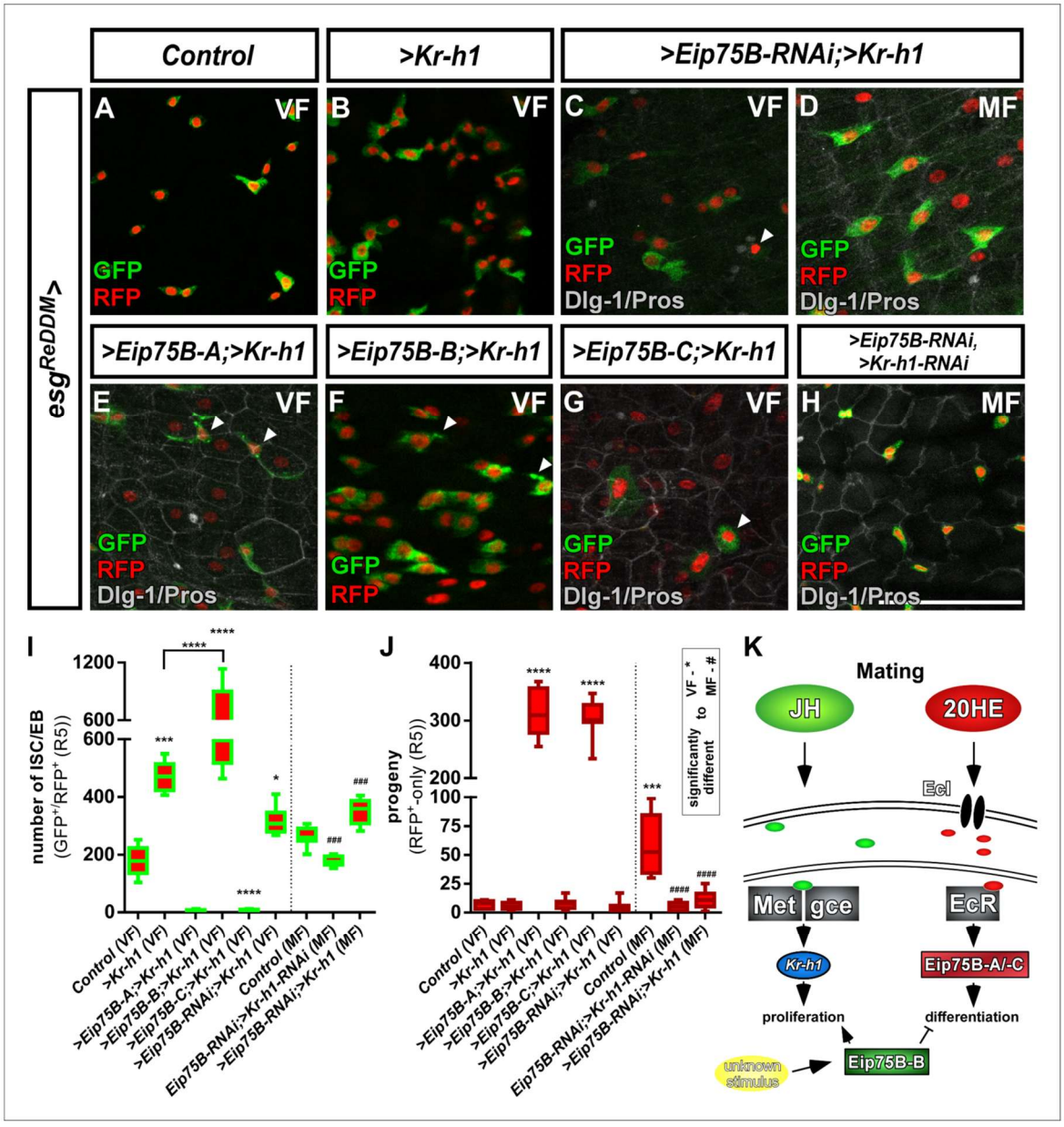

Figure 5. Crosstalk between JH- and Ecdysone-signaling pathways controlling intestinal progenitor proliferation and differentiation. (**A–B**) Images of adult PMG of control VF (**A**) and forced expression of > *Kr* h1 (**B**) traced for seven days with esg^{ReDDM}. (**C–H**) Images of adult PMG with forced expression of > *Kr* h1 with > *Eip75* B-RNAi in VF and MF (**C,D**) and expression of *Eip75B* isoforms > *Eip75* B-A (**E**),>*Eip75* B-B (**F**),>*Eip75* B-C (**G**) and double > *Eip75B-RNAi/>Kr-h1-RNAi* (**H**) after seven days of tracing with esg^{ReDDM}. Please note that genotypes of (**C–G**) were accompanied with semi-lethality even at permissive 18˚C, suggesting for example background transgene expression or position effects most probably caused by the total number of six transgenes including esg^{ReDDM}. PMG of > *Kr* h1 combinations also showed some progenitor lethality indicated by membrane-blebbing and irregularities (arrowheads, (**E–G**) as described in ***Reiff et al., 2019***. (**J**) Quantification of progenitor numbers (**I**) and traced progeny encompassing

Figure 5 continued on next page

Figure 5 continued

EC and EE (**J**) in R5 PMG (n = 12,5,9,8,7,13,8,8,13). Error bars are Standard Error of the Mean (SEM) and asterisks denote significances from one-way ANOVA with Bonferroni's Multiple Comparison Test (*p<0.05, **p<0.01; ***p<0,001; ****p<0.0001, identical p-values are marked by # when compared to MF). Scale bars = 50 μm (**K**) Cartoon depicting transcriptional effectors of JH- and Ecdysone signaling pathways. The JH receptor is formed by a heterodimer of *Methoprene tolerant (Met)* and *germ cells expressed (gce)*. Ligand bound receptor activates the transcription of *krüppel homolog 1 (Kr-h1)* mediating mating effects in the adult intestine (***Reiff et al., 2015***) Forced expression of Eip75B-B affects proliferation and differentiation through an yet unknown stimulus.

The online version of this article includes the following source data for figure 5:

Source data 1. Data from ***Figure 5***.

(***Figure 6B***, ***Figure 6—figure supplement 1A***), but also few tumors containing more than 100 ISC/EE-like cells with indistinguishable single or multiple ISC origin (*class IV*, ***Figure 6B***, ***Figure 6—figure supplement 1A***).

Co-expression of *Eip75B-A /- C* with N-LOF strongly reduced total tumor number (***Figure 6C,D, F***) and smaller *class I*, *II* and *III* tumors (***Figure 6—figure supplement 1A***), whereas *Eip75B-RNAi* results in confluent *class IV* tumors all along the PMG (***Figure 6E***). Although tumor number is strongly reduced (***Figure 6F***), occasional *class IV* tumors (<1/PMG) are able to escape suppressive Eip75B-A /- C showing no reduction in tumor size (***Figure 6—figure supplement 1A***). Additional tumorigenic mechanisms such as Upd- or EGF-ligand upregulation may counteract the tumor suppressive function of 20HE signaling in *class IV* tumors (***Patel et al., 2015***).

Since Eip75B-A and Eip75B-C re-enable EC differentiation despite the lack of N (***Figure 6C,D***; Dlg-1^{+}/RFP^{+}), we investigated whether the EcR-pathway and pharmacological Eip75B-activation are able to trigger EC fate in a N-LOF context. Activation of Eip75B using Pioglitazone led to more newly generated EC (***Figure 6H,I***) compared to controls (***Figure 6G***). In addition, we observed a slight, but significant reduction in the number of N-tumors upon feeding Pioglitazone (***Figure 6J***).

Given the protective role of steroid hormone signaling in colorectal cancer (CRC), we sought to investigate N tumor numbers upon EcR-signaling activation (***Chen et al., 1998***; ***Hendifar et al., 2009***; ***Lin et al., 2012***). We activated EcR-signaling with RH5849 (***Figure 7B***) or by raising intracellular levels of 20HE expressing > *EcI* in *esg^{ReDDM}*(***Figure 7D***). Either manipulation resulted in numerous confluent tumors reflecting the previously observed role of 20HE in proliferation (***Figure 7F***). In line with this,>*EcI* RNAi- and >*EcR* RNAi significantly reduced tumor burden (***Figure 7C,E,F***).

More importantly, ecdysone-pathway activation led to significantly higher numbers of newly generated EC (arrowheads in ***Figure 7B,D,G***), suggesting an upregulation of *Eip75B-A* and *Eip75B-C* in Notch tumors upon EcR-activation through RH5849 and > *EcI*. To exclude remaining N activity, we generated MARCM clones mutant for *N* (*N^{55e11}*) (***Guo and Ohlstein, 2015***). In agreement with our previous observations, activating 20HE signaling in N clones led to a tenfold increase in EC numbers over controls (***Figure 7—figure supplement 1A–C***) and forced expression of > *E75* A/-C to instant EC formation (***Figure 7—figure supplement 1D–E***). Interestingly, in the presence of N, its activity is increased upon RH5849 feeding (***Figure 7—figure supplement 1F***), which suggests an interplay between Notch and EcR-signaling that might converge on *Eip75B* (this study) and *klu* (***Korzelius et al., 2019***; ***Reiff et al., 2019***).

Taken together, our data establish 20HE as a systemic signal controlling reproductive adaptations in synergism with JH (***Figure 7H***). Focusing on EcR-signaling in ISC and EB, we found the mating induced *Eip75B-A /- C* isoforms acting as differentiation factors in EB. Eip75B-A /- C induces EC fate even in Notch-deficient midgut progenitors, an experimental paradigm used to recapitulate early steps of tumorigenesis. Notch dependent fate decisions in midgut precursor cells are conserved between flies and humans. Thus, our findings suggest a new mechanism how steroid hormone signaling might suppress tumor growth by promoting post-mitotic cell fate in intestinal neoplasms marked by a lack of fate specification.

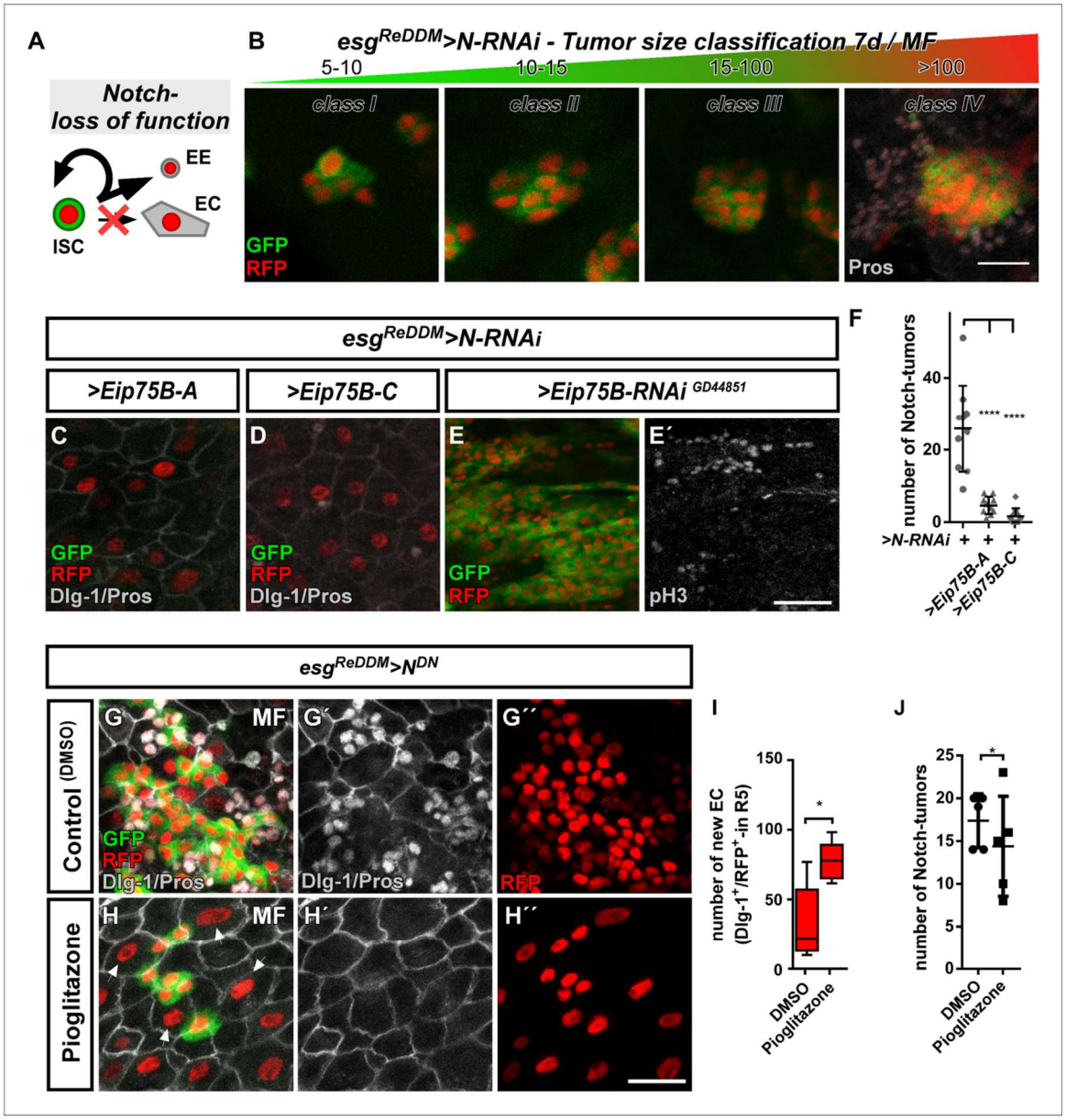

Figure 6. *Ecdysone induced protein 75B* promotes EB differentiation in a Notch tumor paradigm. (**A**) Cartoon depicting cell fate changes upon N-LOF combined with esg^{ReDDM} coloring (***Ohlstein and Spradling, 2006***; ***Ohlstein and Spradling, 2007***). (**B**) > *N* RNAi driven by esg^{ReDDM} leads to different tumor sizes after seven days of tracing that were classified in four classes according to size. Note, ISC-like/EE clusters up to four cells are not quantified as they occasionally occur in controls too. Progenitors are double labelled (GFP^+/RFP^+), where newly generated EE are identified by immunostaining for Prospero (Pros) and H2B::RFP trace from esg^{ReDDM}. (**C–D**) Co- expression of *Eip75B* isoforms > *Eip75* B-A (**C**) and > *Eip75* B-C (**D**) after seven days of tracing with esg^{ReDDM} > *N* RNAi in MF. Note additional Dlg-1^+-immunoreactivity in (grey,C+D) demonstrating epithelial integration of newly generated cells as EC (Dlg-$1^+/RFP^+$). (E+E') RNAi-mediated downregulation of *Eip75B* in MF shows confluent N-tumors (**E**) accompanied by increased mitosis (**E'**). (**F**) Quantification of ISC progeny encompassing ISC-like and EE total N-tumor number in R5 PMG (n = 10,10,10). (**G–J**) Feeding of the

Figure 6 continued on next page

Figure 6 continued

Eip75B/PPARγ agonist Pioglitazone to $esg^{ReDDM} > N^{DN}$ flies leads to the generation of newly generated EC ((**H,I**), Dlg-1^{+}/RFP^{+}) after seven days of tracing compared to DMSO controls (**G,I**). (**I–J**) Quantification of ISC progeny encompassing ISC-like and EE total N-tumor number in R5 PMG (n = 5,5). Error bars are Standard Error of the Mean (SEM) and asterisks denote significances from one-way ANOVA with Bonferroni's Multiple Comparison Test (*p<0.05, **p<0.01; *** p$$BOX_TXT_END$$. <0,001; ****p<0.0001). Scale bars = 25 μm.

The online version of this article includes the following source data and figure supplement(s) for figure 6:

Source data 1. Data from ***Figure 6***.

Figure supplement 1. Size distribution of different Notch-tumor classes.

Figure supplement 1—source data 1. Data from ***Figure 6—figure supplement 1***.

Discussion

Systemic hormones and intestinal remodeling upon mating

Growing offspring involves significant metabolic adaptations to raised energy demands in mothers. *Drosophila melanogaster* uses a classical r-selected reproductive strategy with high number of offspring and minimal parental care (***Pianka, 1970***). Upon mating, egg production is increased tenfold supported by metabolic and behavioral adaptations such as food intake and transit, nutrient preference and a net increase of absorptive tissue in the PMG depending on JH release (***Carvalho et al., 2006***; ***Cognigni et al., 2011***; ***Reiff et al., 2015***; ***Ribeiro and Dickson, 2010***).

Here, we describe a role for the steroid-hormone ecdysone controlling intestinal tissue remodeling upon mating through EcR-signaling. The unliganded heterodimer of EcR and ultraspiracle (USP) binds its DNA consensus sequences serving as a repressor. Upon ligand binding, the EcR/USP heterodimer turns into an activator inducing the expression of early response genes *Eip74EF, Eip75B* and *broad (br)* (***Schwedes et al., 2011***; ***Uyehara and McKay, 2019***). Initially, we investigated knockdown of *USP, br* and *Eip74EF* in intestinal progenitors and observed effects on progenitor survival independent of mating status (***Figure 3C***, Zipper and Reiff, *unpublished data*).

Our data support the idea that 20HE and JH synergistically concert intestinal adaptations balancing nutrient uptake to the increased energy demands after mating (***Figures 1–5***). We confirmed that mating induces ovarian ecdysteroid biosynthesis stimulating egg production by ovarian GSC (***Figure 2A***; ***Ables and Drummond-Barbosa, 2010***; ***Ameku and Niwa, 2016***; ***Ameku et al., 2017***; ***Harshman et al., 1999***; ***König et al., 2011***; ***Morris and Spradling, 2012***; ***Uyehara and McKay, 2019***). In accordance with an inter-organ signaling role for 20HE, we also detected increased 20HE titers in the hemolymph (***Figure 2A***). Surprisingly, we found this mating dependent increase of 20HE titers still present upon partial genetic ablation of the ovaries using ovo^{D1} (***Figure 2B***; ***Reiff et al., 2015***). This can be explained by either (i) other source(s) for 20HE in adult females like the brain (***Chen et al., 2014***; ***Itoh et al., 2011***) or (ii) 20HE release from remaining germarial cells in stage 1–4 eggs of ovo^{D1} VF and MF. Indeed, germarial cells have been shown to express the ecdysteroidogenic *Halloween* genes (***Ameku and Niwa, 2016***; ***Ameku et al., 2017***). In addition, ovo^{D1} MF lack ovarian 20HE uptake during vitellogenesis (***Figure 2D***) of later egg stages, which potentially contributes to 20HE titer in the hemolymph of ovo^{D1} females and intestinal epithelium expansion (***Figure 2D,E,J,K***; ***Enya et al., 2014***).

The epithelial expansion upon mating of ovo^{D1} females has been observed before (***Reiff et al., 2015***) and might be comparably high due to the different genetic background of ovo^{D1} flies compared to w^{1118} (***Figure 2Q***). While this work was in review, genetic ablation of ovarian ecdysteroidogenic enzymes was performed in female flies and resulted in a reduction of mitotic ISC. However, a direct assessment of 20HE titers was not performed and a mating dependent context was not analyzed (***Ahmed et al., 2020***). Taken together, current data cannot clearly dissect whether the ovary is the exclusive source of 20HE (***Garen et al., 1977***). In future experiments, 20HE titers have to be directly addressed to investigate whether other sources like the brain might be involved in 20HE release upon mating and other physiological stimuli (***Chen et al., 2014***; ***Itoh et al., 2011***).

In the adjacent posterior midgut, we describe the impact of 20HE on *Eip75B-A /- C* expression (***Figure 7H***) and show that 20HE import triggers EcR-activation: i) in VF with low ovarian 20HE levels, overexpression of wild-type *EcR* and *EcI* are unable to elicit neither ISC proliferation nor differentiation effects (***Figures 1–2***). ii) pharmacological activation through RH5849 and Pioglitazone (***Figures 2***

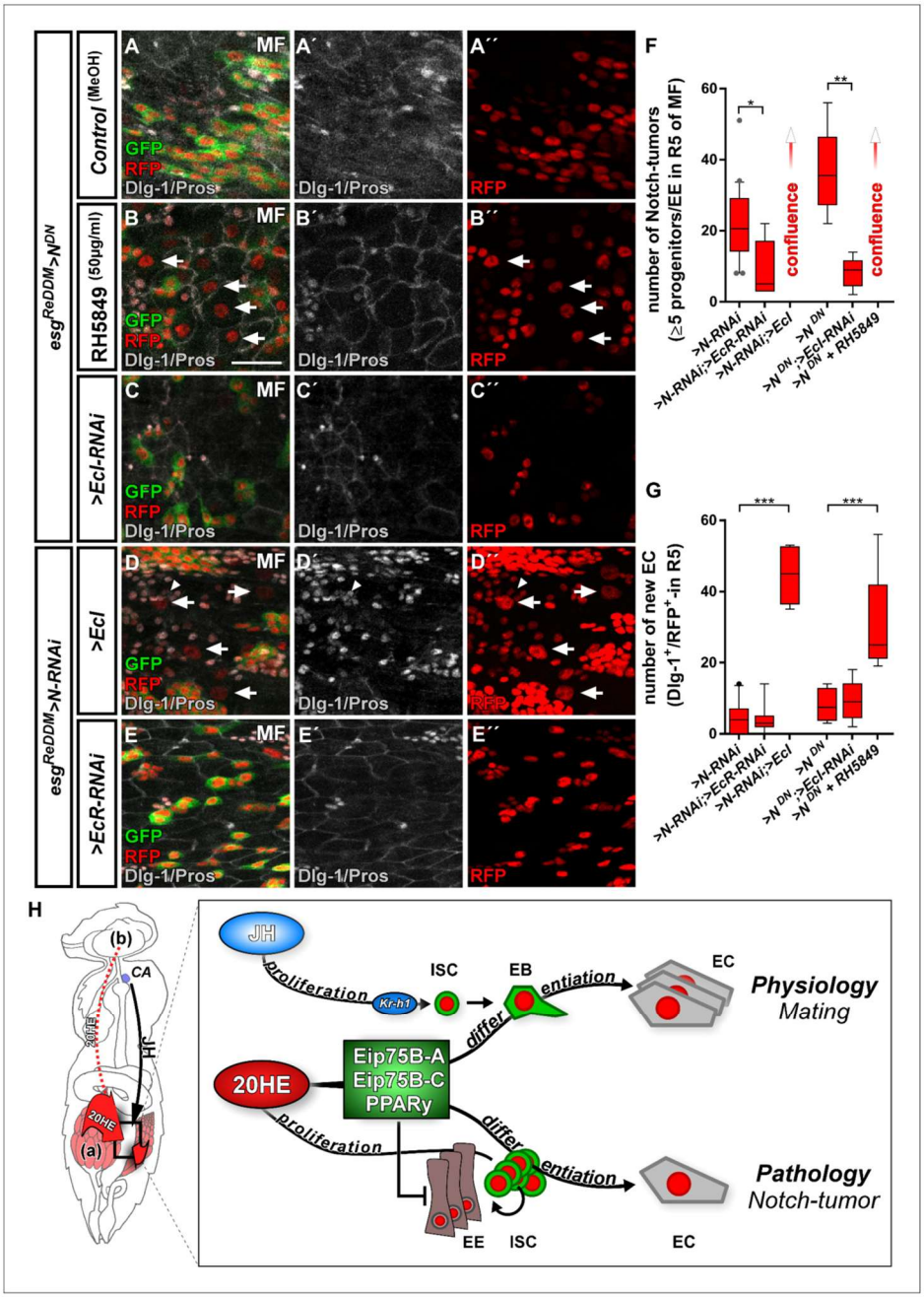

Figure 7. Ecdysone signaling promotes EC-fate in a Notch tumor paradigm. (**A–E''**) Pharmacological and genetic manipulation of Ecdysone signaling. Adult PMG of MF with N-LOF (>*N* RNAi or > N^{DN}) treated with MeOH as control (**A–A''**) or RH5849 (**B–B''**) to activate Ecdysone signaling. Arrowheads highlight newly generated Dlg-1^{+}/RFP^{+}-EC (B+B'') after seven days of esg^{ReDDM} > N^{DN}. (**C–C''**) RNAi-mediated downregulation of *Ecl* in esg^{ReDDM} > N^{DN}, forced expression of >*Ecl* (**D–D''**) and >*EcR* RNAi (**E–E''**) in esg^{ReDDM} > *N* RNAi MF after seven days of tracing. Arrowheads highlight

Figure 7 continued on next page

Figure 7 continued

newly generated Dlg-1^{+}-EC (D+D''), scale bars = 25 µm. (**F**) Quantification of ISC progeny encompassing ISC-like, EC and EE classified after tumor size in R5 PMG (n = 13,5,7,4,6,9). Error bars are Standard Error of the Mean (SEM) and asterisks denote significances from one-way ANOVA with Bonferroni's Multiple Comparison Test (*p<0.05, **p<0.01; ***p<0,001; ****p<0.0001). (**G**) Quantification of newly generated EC (Dlg-1^{+}/RFP^{+}) in R5 PMG (n = 13,5,7,4,6,9). Error bars are Standard Error of the Mean (SEM) and asterisks denote significances from one-way ANOVA with Bonferroni's Multiple Comparison Test (*p<0.05, **p<0.01; ***p<0,001; ****p<0.0001). (**H**) Model of 20HE and JH hormonal pathways influencing physiological and pathological turnover in the intestine. Upon mating, JH from the neuroendocrine CA (*corpora allata*, [***Reiff et al., 2015***]) as well as ovarian 20HE (**a**) synergize on progenitor cells in the posterior midgut of adult female flies. The source of 20HE could not be definitely determined in this current study and 20HE might as well stem from the brain (**b**). JH induces ISC proliferation through Kr-h1, whereas 20HE signaling transduced by Eip75B-A /- C/PPARγ, ensures that newly produced EB differentiate into EC. New EC lead to a net increase in absorptive epithelium and thus ensures physiological adaptation of intestinal size to the new metabolic energy requirements of pregnancy. In the adult intestine, early steps of tumor-pathology are recapitulated when EC fate is inhibited by the lack of Notch signaling in progenitors (***Patel et al., 2015***). Notch mutant ISC divisions only produces ISC-like progenitors and EE. We show in this study that 20HE signaling, through Eip75B-A /- C/PPARγ, is capable to alleviate Notch tumor growth by driving intestinal progenitors into post-mitotic absorptive EC fate.

The online version of this article includes the following source data and figure supplement(s) for figure 7:

Source data 1. Data from ***Figure 7***.
Figure supplement 1. Analysis of *Notch* mutant MARCM clones and consequences of clonal EcR-activation.
Figure supplement 1—source data 1. Data from ***Figure 7—figure supplement 1***.

and ***4***) as well as (iii) forced *EcI* expression induce proliferation and EB differentiation in MF mediated by *Eip75B-A /- C* (***Figures 2***, ***3***, ***6*** and ***7***). Together with the previous findings on JH upon mating (***Reiff et al., 2015***), our current data suggest a concerted role for JH on proliferation and 20HE on differentiation of midgut progenitors.

The interplay between *Eip75B* and *Kr-h1* controls intestinal size adaptation

Downstream of the EcR, we found differential regulation of *Eip75B* isoforms upon mating. *Eip75B* activates egg production in ovarian GSC (***Ables and Drummond-Barbosa, 2010***; ***König et al., 2011***; ***Morris and Spradling, 2012***; ***Uyehara and McKay, 2019***) and its knockdown reduces germarial size and number. In accordance with differentiation defects found in EB in our work, the number of cystoblasts, the immediate daughters of GSC, is reduced as well (***Ables and Drummond-Barbosa, 2010***; ***Morris and Spradling, 2012***).

In our study, we dissected specific roles for *Eip75B* isoforms. *Eip75B-B* expression is at the lower detection limit (***Figure 3B***) and unchanged upon mating (***Figure 3C***). Thus, our finding that forced *Eip75B-B* expression raised ISC mitosis in VF (***Figure 3—figure supplement 1F***) might be due to ectopic expression. *Eip75B-B* mutants are viable and fertile and *Eip75B-B* is interacting with DNA only upon forming heterodimers with *Hormone receptor 3 (Hr3)* temporarily repressing gene expression (***Bialecki et al., 2002***; ***Sullivan and Thummel, 2003***; ***White et al., 1997***). Further studies of *Eip75B-B,* especially its expression pattern and transcriptional regulation, are necessary to elucidate in which physiological context, else than mating, *Eip75B-B* controls ISC proliferation.

Mating induction of *Eip75B-A /- C*, but not *Eip75B-B*, underlines their differential transcriptional regulation (***Segraves and Hogness, 1990***). This idea is supported by the finding that larval epidermis from *Manduca sexta* exposed to heightened JH-levels is sensitized to 20HE, which results in a 10-fold increase of *Eip75B-A*, but not of *Eip75B-B* expression (***Dubrovskaya et al., 2004***; ***Zhou et al., 1998***). An in silico analysis of 4 kb regulatory regions upstream of *Kr-h1* using JASPAR revealed several EcR/USP and Met consensus sequences (***Khan et al., 2018***), suggesting that both hormonal inputs may also converge on *Kr-h1* driving ISC proliferation (***Figure 5B***; ***Reiff et al., 2015***). We propose a synergistic interplay between JH- and 20HE-signaling upon mating, in which the JH pathway effector *Kr-h1* increases proliferation in ISC and the EcR effectors *Eip75B-A /- C* drive EB into differentiation. The combined action of *Kr-h1* and *Eip75B-A /- C* ensures mating induced organ size growth (***Figures 5K*** and ***7H***). The experimental investigation of *Eip75B* and *Kr-h1* regulatory regions incorporating endocrine signals from at least two different organs and leading to differential activity and function in ISC and EB will be a fascinating topic for future studies.

Eip75B/PPARγ and progenitor fate commitment in physiology and pathology

A key discovery of our study is that systemic 20HE directs local intestinal progenitor differentiation. Upon EcR activation, we found *Eip75B-A /- C* promoting EB to EC differentiation. When tissue demand arises, EB are thought to physically separate from ISC and become independent of N. Detached EB acquire motility and are able to postpone their terminal epithelial integration after initial specification (**Antonello et al., 2015a**; **Antonello et al., 2015b**; **Martin et al., 2018**; **Siudeja et al., 2015**). Epithelial integration of progenitors can be initiated experimentally by *nubbin (nub)* mediated downregulation of *esg* and the nub-RB isoform is sufficient to initiate EC formation downstream of Notch signaling (**Korzelius et al., 2014**; **Tang et al., 2018**).

Our data suggest, that the ecdysone pathway acting through *Eip75B-A /- C* provides a similar, remotely inducible signal for terminal EB differentiation. This idea is supported by several lines of evidence: i) EB-specific knockdown of *Eip75B* stalls their differentiation using klu^{ReDDM} (**Figure 3—figure supplement 2E**), suggesting *Eip75B* functions after initial N-input. ii) klu^{+}-EB do not change fate upon *Eip75B* knockdown, suggesting a more mature EB differentiation status that already lost plasticity (**Figure 3—figure supplement 2A–D**; **Korzelius et al., 2019**; **Reiff et al., 2019**). iii) Forced *Eip75B-A /- C* expression in EB leads to their immediate differentiation independent of N-input (**Figure 6C,D**, **Figure 7—figure supplement 1D,E**). In addition, *Eip75B* was found to be highly expressed in EB in a recent study from the Perrimon lab (**Hung et al., 2018**), raising the question about its transcriptional regulation.

A plethora of studies established *Eip75B* as an early response gene downstream of the Ecdysone pathway (**Ables and Drummond-Barbosa, 2010**; **König et al., 2011**; **Morris and Spradling, 2012**; **Thummel, 1996**; **Uyehara and McKay, 2019**). Another pathway stimulating *Eip75B* expression in EB might be the N pathway. N activation leads to immediate EC differentiation of progenitors and thus phenocopies *Eip75B-A /- C* expression (**Hudry et al., 2016**; **Reiff et al., 2019**). Indeed, 20HE- and Notch-signaling have been shown to converge on target genes in various tissues and functions (**Mitchell et al., 2013**; **Sun et al., 2008**; **Xu et al., 2018**) and both pathways acetylate H3K56 modifying multiple regulatory genomic regions including *Eip75B* (**Skalska et al., 2015**). We observed that 20HE-signaling leads to the differentiation of progenitors to EC in a N LOF context (**Figures 5** and **6**, **Figure 7—figure supplement 1**). This is probably the result from strong genetic and pharmacological stimuli (**Figures 6** and **7**, **Figure 7—figure supplement 1**) acting through Eip75B. 20HE signaling might facilitate the expression of differentiation factors like *Eip75B* as well as *klu* in the presence of N signaling under normal physiological conditions (**Figure 7—figure supplement 1F**). Future in-depth analysis of *Eip75B* regulatory regions and the generation of *Eip75B* reporter flies will help to understand the interplay of 20HE and N signaling acting on *Eip75B*.

Confirming a close relationship between fly *Eip75B* and human *PPARγ*, we found midgut progenitors responding to the known PPARγ agonist Pioglitazone. In patients, PPARγ plays a role in i) pregnancy related adaptations of lipid metabolism (**Waite et al., 2000**) and ii) as target in colorectal cancer (CRC) (**Sarraf et al., 1999**). Decreased PPARγ levels are associated with development of insulin resistance and failure of lipolysis in obese pregnant women (**Rodriguez-Cuenca et al., 2012**; **Vivas et al., 2016**). Mating upregulates PPARγ/Eip75B (**Figure 3**) and we also describe increased lipid uptake upon EcR-activation (**Figure 2—figure supplement 1**) in absorptive EC. Srebp, a gene with known function in fatty acid metabolism, is also activated (**Horton et al., 2003**; **Reiff et al., 2015**; **Seegmiller et al., 2002**). Studying this interplay between SREBP, PPARγ and steroid hormone signaling will shed light on to which extent adaptation of intestinal size and lipid metabolism contribute to pathophysiological conditions like diabetes.

In CRC, *PPARγ* loss-of-function mutations are observed in around 8% of patients (**Sarraf et al., 1999**). *PPARγ* expression correlates with good prognosis and *PPARγ* is epigenetically silenced during CRC progression (**Ogino et al., 2009**; **Pancione et al., 2010**). In agreement with our in vivo experiments on Eip75B-A /- C in EB differentiation (**Figures 3–7**), in vitro studies identified *PPARγ* promoting differentiation in various colon cancer cell lines (**Cesario et al., 2006**; **Shimizu and Moriwaki, 2008**; **Yamazaki et al., 2007**; **Yoshizumi et al., 2004**).

In a CRC mouse model, biallelic loss of *PPARγ* leads to a 4-fold increase tumor incidence and reduced survival in female mice over males ($Apc^{Min/+}$/$PPARγ^{-/-}$) (**McAlpine et al., 2006**), whereas males develop around three times more colon tumors with wild type *PPARγ* (**Cooper et al., 2005**).

In line with this, ovariectomized $Apc^{Min/+}$ mice develop significantly more tumors and have decreased *PPARγ* expression, highlighting a possible link between *PPARγ* and estrogen signaling. Meta-analyses of hormone replacement studies have shown that estrogen confers a lower risk to develop CRC and better survival rates for female CRC patients (**Chen et al., 1998**; **Hendifar et al., 2009**; **Lin et al., 2012**).

It is tempting to speculate that this mechanism of steroid hormones signaling through EcR/ER (estrogen receptor) to activate *Eip75B/PPARγ* is conserved from flies to humans. Indeed, human estradiol and 20HE activate the EcR with similar affinity and elicit *Eip75B* transcription by binding to *EcRE* (Ecdysone-Responsive Elements). *EcRE* can be converted to functional *ERE* (estrogen responsive elements) by a simple change of nucleotide spacing suggesting high conservation (**Martinez et al., 1991**; **Schwedes et al., 2011**).

Taken together, our findings reveal that mating induced steroid hormone release, which signals to adjacent intestinal stem cells, controls their proliferation and, more importantly, differentiation of committed precursor cells through *Eip75B/PPARγ*. Ecdysone control of cell fate ensures the production of absorptive enterocytes during mating related intestinal adaptations and induces enterocyte fate in a *Drosophila* intestinal tumor model marked by loss of enterocyte differentiation. Mechanistically, we propose that *Eip75B/PPARγ* exerts an anti-neoplastic role by promoting progenitor differentiation into postmitotic enterocyte fate, thereby reducing the pool of mitotically active cells. Our findings might be a first step towards understanding the protective, but so far mechanistically unclear tumor suppressive role of steroid hormones in female colorectal cancer patients. Downstream of steroidal signaling, Eip75B/PPARγ promotes postmitotic cell fate when local signaling is deteriorated and thus might reflect a promising target for future studies in colorectal cancer models.

Materials and methods

Key resources table

Reagent type (species) or resource	Designation	Source or reference	Identifiers	Additional information
Genetic reagent (*Drosophila melanogaster*)	esg^{ReDDM}	**Antonello et al., 2015a** DOI: 10.15252/embj.201591517		**Figures 1–7**; **Figure 1—figure supplement 1**; **Figure 3—figure supplement 1**
Genetic reagent (*D. melanogaster*)	esg^{ReDDM} > *Eip75B-A*	**Rabinovich et al., 2016** DOI: 10.1016/j.cell.2015.11.047		**Figure 3**; **Figure 3—figure supplement 1**
Genetic reagent (*D. melanogaster*)	esg^{ReDDM} > *Eip75B-B*	**Rabinovich et al., 2016** DOI: 10.1016/j.cell.2015.11.047		**Figure 3**; **Figure 3—figure supplement 1**
Genetic reagent (*D. melanogaster*)	esg^{ReDDM} > *Eip75B-C*	**Rabinovich et al., 2016** DOI: 10.1016/j.cell.2015.11.047		**Figure 3** ; **Figure 3—figure supplement 1**
Genetic reagent (*D. melanogaster*)	*Srebp > CD8::GFP*	**Reiff et al., 2015** DOI: 10.7554/eLife.06930		**Figure 2—figure supplement 1**
Genetic reagent (*D. melanogaster*)	*Mex* > ^{ts}	**Phillips and Thomas, 2006** DOI: 10.1242/jcs.02839		**Figure 2—figure supplement 1**
Genetic reagent (*D. melanogaster*)	*MARCM (FRT2A)*	**Lee and Luo, 1999** DOI: 10.1016/S0896-6273 (00)80701–1		**Figure 3—figure supplement 1**
Genetic reagent (*D. melanogaster*)	$Eip75^{A81}$*-MARCM (FRT2A)*	**Rabinovich et al., 2016** DOI: 10.1016/j.cell.2015.11.047		**Figure 3—figure supplement 1**
Genetic reagent (*D. melanogaster*)	klu^{ReDDM}	**Reiff et al., 2019** DOI: 10.15252/embj.2018101346		**Figure 3—figure supplement 2**
Genetic reagent (*D. melanogaster*)	N^{55e11}*-MARCM (FRT19A)*	**Guo and Ohlstein, 2015** DOI: 10.1126/science.aab0988		**Figure 7—figure supplement 1**
Chemical compund, drug	RH5849	DrEhrenstorfer	DRE-C16813000	340 µM final concentration
Chemical compund, drug	Pioglitazone	Sigma-Aldrich	Sigma-Aldrich 112529-15-4	14 µM final concentration

Genetics and fly husbandry/fly strains

OregonR and w^{1118} flies served as wild-type controls. The following transgenes and mutations were employed: esg^{ReDDM} (**Antonello et al., 2015a**), klu^{ReDDM} (**Reiff et al., 2019**), *UAS-EcI-Flag-HA* (**Okamoto et al., 2018**), *UAS-EcI* (**Okamoto et al., 2018**), *UAS-EcI-RNAi* (**Okamoto et al., 2018**), *UAS-Eip75B-A-Flag* (**Rabinovich et al., 2016**), *UAS-Eip75B-B-Flag* (**Rabinovich et al., 2016**), *UAS-Eip75B-C-Flag* (**Rabinovich et al., 2016**), $UAS\text{-}N^{DN}$ (J. Treisman), *Dl::GFP* (F. Schweisguth), N^{55e11} *FRT19A* (**Guo and Ohlstein, 2015**), *Srebp-GAL4* (**Kunte et al., 2006**), *Mex-Gal4* (**Phillips and Thomas, 2006**), *Gbe+Su(H)dsRed* (T. Klein). From Bloomington *Drosophila* Stock Center (BDSC): *UAS-EcR-RNAi* (*BL58286*), *UAS-EcR.B2* (*BL4934*), $UAS\text{-}EcR.B2^{W650A}$ (BL9449), $UAS\text{-}EcR.B2^{F645A}$ (BL9450), EcR^{M554fs} (BL4894), *EcRE-lacZ (BL4516)*, $Eip75B^{A81}$(BL23654), *UAS-CD8::GFP* (*BL5137*), ovo^{D1} (BL1309), *NRE::GFP* (*BL30727*), *NRE::GFP* (*BL30728*), *Dlg-1::GFP* (BL59417), From Kyoto *Drosophila* Stock Center: *UAS-Kr-h1* (DGRC120052). From FlyORF, Switzerland: *UAS-EcR-HA (F000480)*, *UAS-Kr-h1 (F000495)*. From Vienna *Drosophila* Resource Center (VDRC) *UAS-EcR-RNAi (GD37059)*, *UAS-Eip75B-RNAi (GD44851)*, *UAS-Eip75B-RNAi (KK108399)*, *UAS-N-RNAi (GD14477)*.

MARCM clones

Mosaic analysis with repressible cell marker (MARCM; **Lee and Luo, 1999**) clones were induced in midguts by Flippase under control of a *heat-shock* promoter. Expression of the Flippase was activated for 45 min in a 37˚C-water bath to induce positively marked clones. Guts were dissected 5 days after induction. Clones in experimental and control flies were induced in parallel.

Food composition and fly keeping

Fly food contained 1424 g corn meal, 900 g malt extract, 800 g sugar beet syrup, 336 g dried yeast, 190 g soy fluor, 100 g agarose, 90 ml propionic acid and 30 g NIPAGIN powder (antimycotic agent) in 20 l H_2O. Food was cooked for about an hour to reduce bioburden, then filled into small plastic vials and cooled down to RT. Flies were kept at 25˚C except for crosses with temperature-sensitive $GAL80^{ts}$ (GAL4 repressor) which were kept at 18˚C (permissive temperature) until shifted to 29˚C (restrictive temperature) to activate GAL4-mediated transgene expression. Crosses with esg^{ReDDM} and klu^{ReDDM} were carried out as described previously (**Antonello et al., 2015a**; **Reiff et al., 2015**; **Reiff et al., 2019**). Due to persisting problems with mucous formation on food surface in vials with VF, all experiments distinguishing between mated and virgin female flies were run on food with twice the amount of NIPAGIN. Mucous formation was avoided because of massive induction of tissue renewal by pathogenic stress.

Hormone analogue treatments

A vial of fly food was reheated in the microwave until it became liquid, the hormone analogues were added, thoroughly mixed and filled into a new vial. For each ml of food 5 µl of RH5849 (340 µM final concentration; 20 µg/µl stock solution, diluted in MeOH; DRE-C16813000, DrEhrenstorfer) was added. As a control, an equivalent volume of carrier solution (MeOH) was added to the food. Hormone analogue treatments were performed for the period of the 7 days *ReDDM* (**Antonello et al., 2015a**) shift.

PPARγ agonist treatments

A vial of fly food was reheated in the microwave until it became liquid, the PPARγ agonist was added, thoroughly mixed and filled into a new vial. For each ml of food 2.5 µl Pioglitazone (14 µM final concentration, 2 µg/µl stock solution, diluted in DMSO; Sigma-Aldrich, St. Louis, USA) were added. The equivalent amount of DMSO served as control. Flies were starved in an empty vial for at least six hours to ensure synchronized feeding when set to Pioglitazone. Food was renewed after three days and fly midguts were dissected after five days.

Immunohistochemistry

Guts were dissected in PBS and transferred into 4% PFA immediately after dissection and staining was performed on an orbital shaker. After 45 min of fixation guts were washed once with PBS for 10 min. Antibodies were diluted in 0.5% PBT + 5% normal goat serum. The incubation with primary antibodies (1:250 anti-Dlg-1 [mouse; Developmental studies Hybridoma Bank (DSHB)]; 1:50 anti-Pros

[mouse; DSHB]; 1:2000 anti-pH3 [rabbit; Merck Millipore, 06–570]; 1:50 anti-EcR common Ag10.2 [mouse; DSHB]; 1:500 anti-HA High Affinity 3F10 [rat; Merck, Sigma-Aldrich]; 1:1500 anti-ß-Galactosidase preabsorbed [rabbit; Cappel Research Products]) was performed at 4˚C over night. After washing with PBS guts were incubated with secondary antibodies (1:500 Goat anti-MouseAlexa647 [Invitrogen]; 1:500 Goat anti-RatAlexa647 [Invitrogen]; 1:500 Goat anti-RabbitAlexa647 [Invitrogen]) and DAPI (1:1000; 100 µg/ml stock solution in 0.18 M Tris pH 7.4; DAPI No. 18860, Serva, Heidelberg) for at least 3 hr at RT. Guts were washed a last time with PBS prior to mounting in Fluoromount-G Mounting Medium (Electron Microscopy Sciences).

X-Gal staining of *Drosophila* midguts

Guts were dissected in PBS and transferred into 4% PFA immediately after dissection. After 20 min of fixation, guts were washed three times with 0.3% PBT. Stainingbuffer (0.15M NaCl; 1 mM $MgCl_2$; 10 mM Na-phosphate buffer pH 7.2; 3.3 mM F3Fe(CN)6, 3.3 mM K4Fe(CN)6; 0.3% Triton X-100) was heated to 65˚C and 3% X-Gal added. The guts were stained for at least 1 hr at 37˚C until a dark blue staining became visible. Guts were washed two times in 0.3% PBT prior to mounting in Fluoromount-G Mounting Medium (Electron Microscopy Sciences). Stained midguts were imaged using an Axiophot2 microscope (Carl Zeiss) equipped with an AxioCam MRc (Carl Zeiss).

OilRedO staining of *Drosophila* midguts

Guts were dissected in PBS and transferred into 4% PFA immediately after dissection. After 45 min of fixation, guts were washed in consecutive applications of 1xPBS, double-distilled H_2O, and 60% isopropanol. Guts were stained in a 6:4 dilution of OilRedO (Sigma-Aldrich, 0.1% stock solution diluted in isopropanol) in dH_2O for 20 min, then washed in 60% isopropanol and dH_2O. After mounting in Fluoromount-G Mounting Medium (Electron Microscopy Sciences, emsdiasum) PMG were imaged using an Axiophot2 microscope (Carl Zeiss) equipped with an AxioCam MRc (Carl Zeiss). OilRedO staining intensity was analyzed using Fiji. RGB channels were split and the green channel was subtracted from the red channel to eliminate background signal. A fixed threshold was set, and guts were manually outlined as a ROI. The mean intensity of the resulting signal within the ROI was measured.

Image acquisition

Posterior midguts were imaged using an LSM 880 Airyscan confocal microscope (Carl Zeiss) using 'Plan-Apochromat 10x/0.45 M27', 'Plan-Apochromat 20x/0.8 M27' and 'C-Apochromat 40x/1.20 W Corr M27' objectives. Image resolution was set to at least 2048 × 2048 pixels. At least three focal planes (1 µm distance) were combined into a Z-stack to image one cell layer and to compensate for gut curvature.

For determining whole midgut length, an Axio Zoom.V16 (Carl Zeiss) was employed with DAPI filter and 1x/0.25-objective.

Quantification of proliferation and intensity measurements

Maximum intensity projections were calculated from Z-stack images of PMG by Fiji (ImageJ 1.51 n, Wayne Rasband, National Institutes of Health, USA). Total cell number and RFP-positive cell count of *ReDDM* (**Antonello et al., 2015a**) guts were analyzed semi-automatically by a self-written macro for Fiji whereas GFP-positive cells were counted manually (macro available from the authors).

For fluorescence or OilRedO intensity measurements, intestines were scanned with fixed laser/exposure time settings and measured in Fiji. The region of interest was selected manually, and mean intensity of the area was determined. This way, relative EcR and ß-Galactosidase protein levels were measured in antibody-stainings, relative SREBP activity was analyzed in PMG cells expressing *mCD8::GFP* under the control of *Srebp-GAL4*, and amount of triglycerides was analyzed by OilRedO stainings.

Jaspar

The open-access webtool JASPAR (**Khan et al., 2018**) was utilized to predict transcription factor binding sites within the 5'-UTR of *EcI*. It was specifically scanned for binding motifs related to Ecdysone and Juvenile Hormone signaling.

RNA isolation and cDNA synthesis

The R5 regions or ovaries of at least three female flies were dissected and transferred into a droplet of RNA*later* Solution (Invitrogen by Thermo Fisher Scientific) on ice. The tissue was homogenized in 100 µl peqGOLD TriFast (VWR Life Science) and total RNA was isolated as specified by the manufacturer. The following cDNA synthesis was performed with 250 ng of total RNA and the SuperScript IV Reverse Transcriptase (Invitrogen by Thermo Fisher Scientific) using a 1:1 mixture of oligo-dT primers and random hexamers directly upon RNA isolation. Prior to Real-time qPCR, cDNA samples were diluted 1:2 in dH_2O.

Verification of gene expression in the adult midgut by PCR

To verify gene expression in the adult *Drosophila* midgut, PCRs were performed with primer pairs specific for *ovo* and the *Svb* isoform, or isoform-specific primer pairs for *EcR* spanning at least one exon-exon boundary. PCRs were performed with Q5 High-Fidelity DNA Polymerase (NEB) for at least 30 cycles. Reaction products were loaded on an agarose gel (1.5%) and separated by electrophoresis to verify lengths of PCR products.

Primer	Forward (5′–3′)	Reverse (5′–3′)
EcR.A	GGGGTCTAAGAAACATTTTGAGG	CCATTTGCAGCTGCAGCCGACGT
EcR.B1	GCACGTACGAAGCCCGATCGCGT	CCGGACTCGTTGCCGCAGAGCC
EcR.B2	GCACGTACGAAGCCCGATCGCGT	CTCTTCCCTCTGTTCACGCCC
ovo	CGCAGAGCCAAGATGTACGTG	GATAGTGGACCTCCGGCT
Svb^{Rep}	ACAGTAAGTTGCGAGCCGG	TGTTTTGGGGTGTCCTTTCGTG

Real-time qPCR

Expression levels of Ecdysone signaling pathway-associated genes were determined in VF and MF. Eclosed *OregonR* or *EcRE-LacZ* flies were aged for 4d before mating. After 72 hr of mating, RNA was isolated and cDNA synthetized before running qPCRs. After an enzyme activation step (20 s 95˚C), 40 cycles of denaturation (2 s 95˚C), primer annealing (20 s 58˚C) and elongation (20 s 72˚C) were run. Primers were designed to anneal at 59˚C. Reaction was set up with KAPA SYBR FAST Universal (Roche) in a total volume of 10 µl. All qPCR results were normalized to the house-keeping gene *rp49*.

Primer	Forward (5′–3′)	Reverse (5′–3′)
Eip74EF-A	AGAAACTTCGAGGCAATAGGGT	TGTGCGGCCTCATCTCAAG
Eip74EF-B	TGGCCATCCCACAACGC	GGGCGGAAATGAACCTGTTG
Eip75B-A	CCTGTGCCAGAAGTTCGATGA	AAGAATCCATCGGCATCTTCGT
Eip75B-B	CGTCTAGCTCGATTCCTGATCTA	CGGAAGAATCCCTTGCAACC
Eip75B-C	CTGTGGTTCCGGCGGATT	TCGAATTCTATGTTGAGTTCTGGTT
EcI	TGCAGTGCCGCTCTCAACTGTACC	TCACAGTAACCGTTGACCGCCTCC
EcR.A	GTGTTCGGTGAAAAACGCAA	TCCTAGCAACTGAGCTTTTGTAGAC
EcR.B1	TTAACGGTTGTTCGCTCGCA	AGTGCGGGAAACAATCAGAGCAT
EcR.B2	GTTAACGGTTGTTCGCTCGC	TGCGGGAAACAATCAGAGCATA
Kr-h1(A)	ACAATTTTATGATTCAGCCACAACC	GTTAGTGGAGGCGGAACCTG
Kr-h1(B)	AAATCTTGGGCACCCAAACAA	GTTGTGGCTGAATCTTTCGC
Lac-Z	ATCAGGATATGTGGCGGATGAGCG	AGTACAGCGCGGCTGAAATCATC
rp49	TGGTTTCCGGCAAGCTTCAA	TGTTGTCGATACCCTTGGGC

20-HE isolation and titer determination

20-HE titers were determined in VF and MF of the same age. Eclosed *OregonR* or heterozygous ovo^{D1} mutant flies were aged for 3d before mating. After 24 hr or 48 hr at least 20 adult female flies were pierced in the thorax with a needle and put into a 150 µl-PCR tube that was punctured in its very bottom. Hemolymph was harvested by centrifugation (5.000x g 5 min RT) and collected in a 1.5 ml-reaction tube. Total weight of flies was determined before and after centrifugation. Typical yields of hemolymph were around 0.6–1 mg. The isolated hemolymph was mixed with 500 µl MeOH, centrifuged (12.000x g 20 min 4˚C) and the supernatant was transferred into a new 1.5 ml-reaction tube. MeOH was evaporated at 30˚C in a vacuum centrifuge (Eppendorf concentrator plus) and 20HE was resuspended in 100 µl EIA buffer and stored at −20˚C until usage.

Ecdysone levels were determined using the 20-Hydroxyecdysone Enzyme Immunoassay kit according to manufacturer's instructions (#A05120.96 wells; Bertin Bioreagent). 20HE titer was normalized to hemolymph yield.

Statistical analysis

Figures of quantifications were assembled, and statistics were run in GraphPad Prism 6.01. For single comparisons, data sets were analyzed by two-sided unpaired t-test. For multiple comparisons, data sets were analyzed by one-way ANOVA and Tukey's post-hoc test. Significant differences are displayed as * for $p \leq 0.05$, ** for $p \leq 0.01$, *** for $p \leq 0.001$ and **** for $p \leq 0.0001$.

Acknowledgements

We thank Maria Dominguez, Thomas Klein, Oren Schuldiner, Francois Schweisguth, Naoki Yamanaka, the Bloomington *Drosophila* Stock Center (NIHP400D018537), the Transgenic RNAi Project (TRiP) at Harvard Medical School (NIK/NIGMS R01-GM084947) and the Vienna *Drosophila* Resource Center (VDRC, http://www.vdrc.at) for providing transgenic fly stocks. We thank the Center for Advanced Imaging (CAi) at HHU for providing microscopy services. TR thanks Maria Dominguez in whose lab he initiated this project and Thomas Klein for being a very supportive host. We also thank Zeus Antonello, Nahuel Villegas, Hendrik Pannen and Thomas Klein for comments on the manuscript. The project is funded by a Deutsche Forschungsgesellschaft (DFG-Sachbeihilfe RE 34532–1) grant. LZ is supported by the Wilhelm Sander-Stiftung (2018.145.1).

Additional information

Funding

Funder	Grant reference number	Author
Deutsche Forschungsgemeinschaft	RE 34532-1	Tobias Reiff
Wilhelm Sander-Stiftung	2018.145.1	Lisa Zipper

The funders had no role in study design, data collection and interpretation, or the decision to submit the work for publication.

Author contributions

Lisa Zipper, Denise Jassmann, Sofie Burgmer, Bastian Görlich, Investigation; Tobias Reiff, Conceptualization, Funding acquisition, Investigation, Writing - original draft, Writing - review and editing

Author ORCIDs

Tobias Reiff https://orcid.org/0000-0001-6610-6148

Decision letter and Author response

Decision letter https://doi.org/10.7554/eLife.55795.sa1
Author response https://doi.org/10.7554/eLife.55795.sa2

Additional files

Supplementary files

- Transparent reporting form

Data availability

All data generated or analysed during this study are included in the manuscript and supporting files. Source data files have been provided in a separate Excel File.

References

Ables ET, Drummond-Barbosa D. 2010. The steroid hormone ecdysone functions with intrinsic chromatin remodeling factors to control female germline stem cells in *Drosophila*. *Cell Stem Cell* **7**:581–592. DOI: https://doi.org/10.1016/j.stem.2010.10.001

Ahmed SMH, Maldera JA, Krunic D, Paiva-Silva GO, Pénalva C, Teleman AA, Edgar BA. 2020. Fitness trade-offs incurred by ovary-to-gut steroid signalling in *Drosophila*. *Nature* **584**:415–419. DOI: https://doi.org/10.1038/s41586-020-2462-y

Ameku T, Yoshinari Y, Fukuda R, Niwa R. 2017. Ovarian ecdysteroid biosynthesis and female germline stem cells. *Fly* **11**:185–193. DOI: https://doi.org/10.1080/19336934.2017.1291472, PMID: 28631993

Ameku T, Niwa R. 2016. Mating-Induced increase in germline stem cells via the neuroendocrine system in *female Drosophila*. *PLOS Genetics* **12**:e1006123. DOI: https://doi.org/10.1371/journal.pgen.1006123, PMID: 27310920

Antonello ZA, Reiff T, Ballesta-Illan E, Dominguez M. 2015a. Robust intestinal homeostasis relies on cellular plasticity in enteroblasts mediated by miR-8-Escargot switch. *The EMBO Journal* **34**:2025–2041. DOI: https://doi.org/10.15252/embj.201591517, PMID: 26077448

Antonello ZA, Reiff T, Dominguez M. 2015b. Mesenchymal to epithelial transition during tissue homeostasis and regeneration: patching up the *Drosophila* midgut epithelium. *Fly* **9**:132–137. DOI: https://doi.org/10.1080/19336934.2016.1140709, PMID: 26760955

Athippozhy A, Huang L, Wooton-Kee CR, Zhao T, Jungsuwadee P, Stromberg AJ, Vore M. 2011. Differential gene expression in liver and small intestine from lactating rats compared to age-matched virgin controls detects increased mRNA of cholesterol biosynthetic genes. *BMC Genomics* **12**:95. DOI: https://doi.org/10.1186/1471-2164-12-95, PMID: 21291544

Bernardo TJ, Dubrovskaya VA, Xie X, Dubrovsky EB. 2014. A view through a chromatin loop: insights into the ecdysone activation of early genes in *Drosophila*. *Nucleic Acids Research* **42**:10409–10424. DOI: https://doi.org/10.1093/nar/gku754, PMID: 25143532

Bialecki M, Shilton A, Fichtenberg C, Segraves WA, Thummel CS. 2002. Loss of the ecdysteroid-inducible E75A orphan nuclear receptor uncouples molting from metamorphosis in *Drosophila*. *Developmental Cell* **3**:209–220. DOI: https://doi.org/10.1016/S1534-5807(02)00204-6, PMID: 12194852

Bownes M, Dübendorfer A, Smith T. 1984. Ecdysteroids in adult males and females *of Drosophila melanogaster*. *Journal of Insect Physiology* **30**:823–830. DOI: https://doi.org/10.1016/0022-1910(84)90019-2

Busson D, Gans M, Komitopoulou K, Masson M. 1983. Genetic analysis of three dominant Female-Sterile mutations located on the X chromosome of *Drosophila melanogaster*. *Genetics* **105**:309–325. PMID: 17246162

Carvalho GB, Kapahi P, Anderson DJ, Benzer S. 2006. Allocrine modulation of feeding behavior by the sex peptide of *Drosophila*. *Current Biology* **16**:692–696. DOI: https://doi.org/10.1016/j.cub.2006.02.064, PMID: 16581515

Cesario RM, Stone J, Yen WC, Bissonnette RP, Lamph WW. 2006. Differentiation and growth inhibition mediated via the RXR:ppargamma heterodimer in Colon cancer. *Cancer Letters* **240**:225–233. DOI: https://doi.org/10.1016/j.canlet.2005.09.010, PMID: 16271436

Chen MJ, Longnecker MP, Morgenstern H, Lee ER, Frankl HD, Haile RW. 1998. Recent use of hormone replacement therapy and the prevalence of colorectal adenomas. *Cancer Epidemiology Biomarkers Prevention* **7**:227–230.

Chen W, Liu Z, Li T, Zhang R, Xue Y, Zhong Y, Bai W, Zhou D, Zhao Z. 2014. Regulation of *Drosophila* circadian rhythms by miRNA let-7 is mediated by a regulatory cycle. *Nature Communications* **5**:5549. DOI: https://doi.org/10.1038/ncomms6549, PMID: 25417916

Chen J, Xu N, Huang H, Cai T, Xi R. 2016. A feedback amplification loop between stem cells and their progeny promotes tissue regeneration and tumorigenesis. *eLife* **5**:e14330. DOI: https://doi.org/10.7554/eLife.14330, PMID: 27187149

Chen J, Xu N, Wang C, Huang P, Huang H, Jin Z, Yu Z, Cai T, Jiao R, Xi R. 2018. Transient scute activation via a self-stimulatory loop directs enteroendocrine cell pair specification from self-renewing intestinal stem cells. *Nature Cell Biology* **20**:152–161. DOI: https://doi.org/10.1038/s41556-017-0020-0

Cherbas L, Hu X, Zhimulev I, Belyaeva E, Cherbas P. 2003. EcR isoforms in *Drosophila*: testing tissue-specific requirements by targeted blockade and rescue. *Development* **130**:271–284. DOI: https://doi.org/10.1242/dev.00205, PMID: 12466195

Cognigni P, Bailey AP, Miguel-Aliaga I. 2011. Enteric neurons and systemic signals couple nutritional and reproductive status with intestinal homeostasis. *Cell Metabolism* **13**:92–104. DOI: https://doi.org/10.1016/j.cmet.2010.12.010, PMID: 21195352

Cooper HS, Chang WC, Coudry R, Gary MA, Everley L, Spittle CS, Wang H, Litwin S, Clapper ML. 2005. Generation of a unique strain of multiple intestinal neoplasia (Apc(+/Min-FCCC)) mice with significantly increased numbers of colorectal adenomas. *Molecular Carcinogenesis* **44**:31–41. DOI: https://doi.org/10.1002/mc.20114, PMID: 15937958

Dubrovskaya VA, Berger EM, Dubrovsky EB. 2004. Juvenile hormone regulation of the E75 nuclear receptor is conserved in diptera and lepidoptera. *Gene* **340**:171–177. DOI: https://doi.org/10.1016/j.gene.2004.07.022, PMID: 15475158

Enya S, Ameku T, Igarashi F, Iga M, Kataoka H, Shinoda T, Niwa R. 2014. A halloween gene noppera-bo encodes a glutathione S-transferase essential for ecdysteroid biosynthesis via regulating the behaviour of cholesterol in *Drosophila*. *Scientific Reports* **4**:6586. DOI: https://doi.org/10.1038/srep06586, PMID: 25300303

Figueroa-Clarevega A, Bilder D. 2015. Malignant *Drosophila* tumors interrupt insulin signaling to induce cachexia-like wasting. *Developmental Cell* **33**:47–55. DOI: https://doi.org/10.1016/j.devcel.2015.03.001, PMID: 25850672

Garen A, Kauvar L, Lepesant JA. 1977. Roles of ecdysone in *Drosophila* development. *PNAS* **74**:5099–5103. DOI: https://doi.org/10.1073/pnas.74.11.5099, PMID: 16592466

Gilbert LI, Rybczynski R, Warren JT. 2002. Control and biochemical nature of the ecdysteroidogenic pathway. *Annual Review of Entomology* **47**:883–916. DOI: https://doi.org/10.1146/annurev.ento.47.091201.145302, PMID: 11729094

Gilbert LI, Warren JT. 2005. A molecular genetic approach to the biosynthesis of the insect steroid molting hormone. *Vitamins and Hormones* **73**:31–57. DOI: https://doi.org/10.1016/S0083-6729(05)73002-8, PMID: 16399407

Gillies PS, Dunn CJ. 2000. Pioglitazone. *Drugs* **60**:333–343. DOI: https://doi.org/10.2165/00003495-200060020-00009, PMID: 10983737

Guo Z, Ohlstein B. 2015. Stem cell regulation bidirectional notch signaling regulates *Drosophila* intestinal stem cell multipotency. *Science* **350**:aab0988. DOI: https://doi.org/10.1126/science.aab0988, PMID: 26586765

Hammond KA. 1997. Adaptation of the maternal intestine during lactation. *Journal of Mammary Gland Biology and Neoplasia* **2**:243–252. DOI: https://doi.org/10.1023/a:1026332304435, PMID: 10882308

Harshman LG, Loeb AM, Johnson BA. 1999. Ecdysteroid titers in mated and *unmated Drosophila melanogaster* females. *Journal of Insect Physiology* **45**:571–577. DOI: https://doi.org/10.1016/S0022-1910(99)00038-4, PMID: 12770342

Hendifar A, Yang D, Lenz F, Lurje G, Pohl A, Lenz C, Ning Y, Zhang W, Lenz HJ. 2009. Gender disparities in metastatic colorectal Cancer survival. *Clinical Cancer Research* **15**:6391–6397. DOI: https://doi.org/10.1158/1078-0432.CCR-09-0877, PMID: 19789331

Horton JD, Shah NA, Warrington JA, Anderson NN, Park SW, Brown MS, Goldstein JL. 2003. Combined analysis of oligonucleotide microarray data from transgenic and knockout mice identifies direct SREBP target genes. *PNAS* **100**:12027–12032. DOI: https://doi.org/10.1073/pnas.1534923100, PMID: 14512514

Hudry B, Khadayate S, Miguel-Aliaga I. 2016. The sexual identity of adult intestinal stem cells controls organ size and plasticity. *Nature* **530**:344–348. DOI: https://doi.org/10.1038/nature16953, PMID: 26887495

Hung R-J, Hu C, Kirchner R, Li F, Xu C. 2018. A cell atlas of the adult *Drosophila* midgut. *PNAS* **117**:1514–1523. DOI: https://doi.org/10.1073/pnas.1916820117

Itoh TQ, Tanimura T, Matsumoto A. 2011. Membrane-bound transporter controls the circadian transcription of clock genes in *Drosophila*. *Genes to Cells* **16**:1159–1167. DOI: https://doi.org/10.1111/j.1365-2443.2011.01559.x, PMID: 22077638

Jafari M, Khodayari B, Felgner J, Bussel II, Rose MR, Mueller LD. 2007. Pioglitazone: an anti-diabetic compound with anti-aging properties. *Biogerontology* **8**:639–651. DOI: https://doi.org/10.1007/s10522-007-9105-7, PMID: 17628757

Jensen J, Pedersen EE, Galante P, Hald J, Heller RS, Ishibashi M, Kageyama R, Guillemot F, Serup P, Madsen OD. 2000. Control of endodermal endocrine development by Hes-1. *Nature Genetics* **24**:36–44. DOI: https://doi.org/10.1038/71657, PMID: 10615124

Jiang C, Baehrecke EH, Thummel CS. 1997. Steroid regulated programmed cell death during *Drosophila metamorphosis*. *Development* **124**:4673–4683. PMID: 9409683

Jiang C, Lamblin AF, Steller H, Thummel CS. 2000. A steroid-triggered transcriptional hierarchy controls salivary gland cell death during *Drosophila metamorphosis*. *Molecular Cell* **5**:445–455. DOI: https://doi.org/10.1016/S1097-2765(00)80439-6, PMID: 10882130

Jindra M, Palli SR, Riddiford LM. 2013. The juvenile hormone signaling pathway in insect development. *Annual Review of Entomology* **58**:181–204. DOI: https://doi.org/10.1146/annurev-ento-120811-153700, PMID: 22994547

Joardar A, Menzl J, Podolsky TC, Manzo E, Estes PS, Ashford S, Zarnescu DC. 2015. PPAR gamma activation is neuroprotective in a *Drosophila* model of ALS based on TDP-43. *Human Molecular Genetics* **24**:1741–1754. DOI: https://doi.org/10.1093/hmg/ddu587, PMID: 25432537

Karim FD, Thummel CS. 1991. Ecdysone coordinates the timing and amounts of E74A and E74B transcription in *Drosophila*. *Genes & Development* **5**:1067–1079. DOI: https://doi.org/10.1101/gad.5.6.1067, PMID: 2044954

Khan A, Fornes O, Stigliani A, Gheorghe M, Castro-Mondragon JA, van der Lee R, Bessy A, Chèneby J, Kulkarni SR, Tan G, Baranasic D, Arenillas DJ, Sandelin A, Vandepoele K, Lenhard B, Ballester B, Wasserman WW, Parcy

F, Mathelier A. 2018. JASPAR 2018: update of the open-access database of transcription factor binding profiles and its web framework. *Nucleic Acids Research* **46**:D260–D266. DOI: https://doi.org/10.1093/nar/gkx1126, PMID: 29140473

King-Jones K, Thummel CS. 2005. Nuclear receptors — a perspective from *Drosophila*. *Nature Reviews Genetics* **6**:311–323. DOI: https://doi.org/10.1038/nrg1581

Klepsatel P, Gáliková M, De Maio N, Ricci S, Schlötterer C, Flatt T. 2013. Reproductive and post-reproductive life history of wild-*caught Drosophila melanogaster* under laboratory conditions. *Journal of Evolutionary Biology* **26**:1508–1520. DOI: https://doi.org/10.1111/jeb.12155, PMID: 23675912

König A, Yatsenko AS, Weiss M, Shcherbata HR. 2011. Ecdysteroids affect *Drosophila* ovarian stem cell niche formation and early germline differentiation. *The EMBO Journal* **30**:1549–1562. DOI: https://doi.org/10.1038/emboj.2011.73, PMID: 21423150

Korzelius J, Naumann S, Loza-Coll M A, Sk Chan J, Dutta D. 2014. Escargot maintains stemness and suppresses differentiation in *Drosophila* intestinal *stem cells. Embo J.* **33**:2967–2982. DOI: https://doi.org/10.15252/embj.201489072

Korzelius J, Azami S, Ronnen-Oron T, Koch P, Baldauf M, Meier E, Rodriguez-Fernandez IA, Groth M, Sousa-Victor P, Jasper H. 2019. The WT1-like transcription factor klumpfuss maintains lineage commitment of enterocyte progenitors in the *Drosophila* intestine. *Nature Communications* **10**:4123. DOI: https://doi.org/10.1038/s41467-019-12003-0, PMID: 31511511

Kozlova T, Thummel CS. 2000. Steroid regulation of postembryonic development and reproduction in *Drosophila*. *Trends in Endocrinology & Metabolism* **11**:276–280. DOI: https://doi.org/10.1016/S1043-2760(00)00282-4, PMID: 10920384

Kunte AS, Matthews KA, Rawson RB. 2006. Fatty acid auxotrophy in *Drosophila* larvae lacking SREBP. *Cell Metabolism* **3**:439–448. DOI: https://doi.org/10.1016/j.cmet.2006.04.011, PMID: 16753579

Kwon Y, Song W, Droujinine IA, Hu Y, Asara JM, Perrimon N. 2015. Systemic organ wasting induced by localized expression of the secreted insulin/IGF antagonist ImpL2. *Developmental Cell* **33**:36–46. DOI: https://doi.org/10.1016/j.devcel.2015.02.012, PMID: 25850671

Lee T, Luo L. 1999. Mosaic analysis with a repressible cell marker for studies of gene function in neuronal morphogenesis. *Neuron* **22**:451–461. DOI: https://doi.org/10.1016/S0896-6273(00)80701-1, PMID: 10197526

Lin BR, Huang MT, Chen ST, Jeng YM, Li YJ, Liang JT, Lee PH, Chang KJ, Chang CC. 2012. Prognostic significance of TWEAK expression in colorectal Cancer and effect of its inhibition on invasion. *Annals of Surgical Oncology* **19 Suppl 3**:385–394. DOI: https://doi.org/10.1245/s10434-011-1825-x, PMID: 21681381

Martin JL, Sanders EN, Moreno-Roman P, Jaramillo Koyama LA, Balachandra S, Du X, O'Brien LE. 2018. Long-term live imaging of the *Drosophila* adult midgut reveals real-time dynamics of division, differentiation and loss. *eLife* **7**:e36248. DOI: https://doi.org/10.7554/eLife.36248, PMID: 30427308

Martinez E, Givel F, Wahli W. 1991. A common ancestor DNA motif for invertebrate and vertebrate hormone response elements. *The EMBO Journal* **10**:263–268. DOI: https://doi.org/10.1002/j.1460-2075.1991.tb07946.x, PMID: 1846802

McAlpine CA, Barak Y, Matise I, Cormier RT. 2006. Intestinal-specific PPARgamma deficiency enhances tumorigenesis in ApcMin/+ mice. *International Journal of Cancer* **119**:2339–2346. DOI: https://doi.org/10.1002/ijc.22115, PMID: 16858678

Micchelli CA, Perrimon N. 2006. Evidence that stem cells reside in the adult *Drosophila* midgut epithelium. *Nature* **439**:475–479. DOI: https://doi.org/10.1038/nature04371, PMID: 16340959

Miguel-Aliaga I, Jasper H, Lemaitre B. 2018. Anatomy and physiology of the digestive tract of *Drosophila melanogaster*. *Genetics* **210**:357–396. DOI: https://doi.org/10.1534/genetics.118.300224, PMID: 30287514

Mitchell NC, Lin JI, Zaytseva O, Cranna N, Lee A, Quinn LM. 2013. The ecdysone receptor constrains wingless expression to pattern cell cycle across the *Drosophila* wing margin in a cyclin B-dependent manner. *BMC Developmental Biology* **13**:28. DOI: https://doi.org/10.1186/1471-213X-13-28, PMID: 23848468

Morris LX, Spradling AC. 2012. Steroid signaling within *Drosophila* ovarian epithelial cells sex-specifically modulates early germ cell development and meiotic entry. *PLOS ONE* **7**:e46109. DOI: https://doi.org/10.1371/journal.pone.0046109, PMID: 23056242

Ogino S, Shima K, Baba Y, Nosho K, Irahara N, Kure S, Chen L, Toyoda S, Kirkner GJ, Wang YL, Giovannucci EL, Fuchs CS. 2009. Colorectal Cancer expression of peroxisome proliferator-activated receptor gamma (PPARG, PPARgamma) is associated with good prognosis. *Gastroenterology* **136**:1242–1250. DOI: https://doi.org/10.1053/j.gastro.2008.12.048, PMID: 19186181

Ohlstein B, Spradling A. 2006. The adult *Drosophila* posterior midgut is maintained by pluripotent stem cells. *Nature* **439**:470–474. DOI: https://doi.org/10.1038/nature04333, PMID: 16340960

Ohlstein B, Spradling A. 2007. Multipotent *Drosophila* intestinal stem cells specify daughter cell fates by differential notch signaling. *Science* **315**:988–992. DOI: https://doi.org/10.1126/science.1136606

Okamoto N, Viswanatha R, Bittar R, Li Z, Haga-Yamanaka S, Perrimon N, Yamanaka N. 2018. A membrane transporter is required for steroid hormone uptake in *Drosophila*. *Developmental Cell* **47**:294–305. DOI: https://doi.org/10.1016/j.devcel.2018.09.012, PMID: 30293839

Oliver B, Perrimon N, Mahowald AP. 1987. The ovo locus is required for sex-specific germ line maintenance in *Drosophila*. *Genes & Development* **1**:913–923. DOI: https://doi.org/10.1101/gad.1.9.913, PMID: 3428601

Pancione M, Sabatino L, Fucci A, Carafa V, Nebbioso A, Forte N, Febbraro A, Parente D, Ambrosino C, Normanno N, Altucci L, Colantuoni V. 2010. Epigenetic silencing of peroxisome proliferator-activated receptor γ is a biomarker for colorectal Cancer progression and adverse patients' outcome. *PLOS ONE* **5**:e14229. DOI: https://doi.org/10.1371/journal.pone.0014229, PMID: 21151932

Patel PH, Dutta D, Edgar BA. 2015. Niche appropriation by *Drosophila* intestinal stem cell tumours. *Nature Cell Biology* **17**:1182–1192. DOI: https://doi.org/10.1038/ncb3214, PMID: 26237646

Phillips MD, Thomas GH. 2006. Brush border spectrin is required for early endosome recycling in *Drosophila*. *Journal of Cell Science* **119**:1361–1370. DOI: https://doi.org/10.1242/jcs.02839, PMID: 16537648

Pianka ER. 1970. On r- and K-Selection. *The American Naturalist* **104**:592–597. DOI: https://doi.org/10.1086/282697

Rabinovich D, Yaniv SP, Alyagor I, Schuldiner O. 2016. Nitric oxide as a switching mechanism between axon degeneration and regrowth during developmental remodeling. *Cell* **164**:170–182. DOI: https://doi.org/10.1016/j.cell.2015.11.047, PMID: 26771490

Reiff T, Jacobson J, Cognigni P, Antonello Z, Ballesta E, Tan KJ, Yew JY, Dominguez M, Miguel-Aliaga I. 2015. Endocrine remodelling of the adult intestine sustains reproduction in *Drosophila*. *eLife* **4**:e06930. DOI: https://doi.org/10.7554/eLife.06930, PMID: 26216039

Reiff T, Antonello ZA, Ballesta-Illán E, Mira L, Sala S, Navarro M, Martinez LM, Dominguez M. 2019. Notch and EGFR regulate apoptosis in progenitor cells to ensure gut homeostasis in *Drosophila*. *The EMBO Journal* **38**:e101346. DOI: https://doi.org/10.15252/embj.2018101346, PMID: 31566767

Ribeiro C, Dickson BJ. 2010. Sex peptide receptor and neuronal TOR/S6K signaling modulate nutrient balancing in *Drosophila*. *Current Biology* **20**:1000–1005. DOI: https://doi.org/10.1016/j.cub.2010.03.061, PMID: 20471268

Roa J, Tena-Sempere M. 2014. Connecting metabolism and reproduction: roles of central energy sensors and key molecular mediators. *Molecular and Cellular Endocrinology* **397**:4–14. DOI: https://doi.org/10.1016/j.mce.2014.09.027, PMID: 25289807

Robinson PD, Morgan ED, Wilson ID, Lafont R. 1987. The metabolism of ingested and injected [3H]ecdysone by final instar larvae of Heliothis armigera. *Physiological Entomology* **12**:321–330. DOI: https://doi.org/10.1111/j.1365-3032.1987.tb00757.x

Rodriguez-Cuenca S, Carobbio S, Velagapudi VR, Barbarroja N, Moreno-Navarrete JM, Tinahones FJ, Fernandez-Real JM, Orešic M, Vidal-Puig A. 2012. Peroxisome proliferator-activated receptor γ-dependent regulation of lipolytic nodes and metabolic flexibility. *Molecular and Cellular Biology* **32**:1555–1565. DOI: https://doi.org/10.1128/MCB.06154-11, PMID: 22310664

Sarraf P, Mueller E, Smith WM, Wright HM, Kum JB, Aaltonen LA, de la Chapelle A, Spiegelman BM, Eng C. 1999. Loss-of-Function mutations in ppary associated with human Colon cancer. *Molecular Cell* **3**:799–804. DOI: https://doi.org/10.1016/S1097-2765(01)80012-5

Schwedes C, Tulsiani S, Carney GE. 2011. Ecdysone receptor expression and activity in adult *Drosophila melanogaster*. *Journal of Insect Physiology* **57**:899–907. DOI: https://doi.org/10.1016/j.jinsphys.2011.03.027, PMID: 21507325

Seegmiller AC, Dobrosotskaya I, Goldstein JL, Ho YK, Brown MS, Rawson RB. 2002. The SREBP pathway in *Drosophila*: regulation by Palmitate, not sterols. *Developmental Cell* **2**:229–238. DOI: https://doi.org/10.1016/s1534-5807(01)00119-8, PMID: 11832248

Segraves WA, Hogness DS. 1990. The E75 ecdysone-inducible gene responsible for the 75B early puff in *Drosophila* encodes two new members of the steroid receptor superfamily. *Genes & Development* **4**:204–219. DOI: https://doi.org/10.1101/gad.4.2.204, PMID: 2110921

Shimizu M, Moriwaki H. 2008. Synergistic effects of PPARgamma ligands and retinoids in Cancer treatment. *PPAR Research* **2008**:181047. DOI: https://doi.org/10.1155/2008/181047, PMID: 18528526

Siudeja K, Nassari S, Gervais L, Skorski P, Lameiras S, Stolfa D, Zande M, Bernard V, Frio TR, Bardin AJ. 2015. Frequent somatic mutation in adult intestinal stem cells drives neoplasia and genetic mosaicism during aging. *Cell Stem Cell* **17**:663–674. DOI: https://doi.org/10.1016/j.stem.2015.09.016, PMID: 26607382

Skalska L, Stojnic R, Li J, Fischer B, Cerda-Moya G, Sakai H, Tajbakhsh S, Russell S, Adryan B, Bray SJ. 2015. Chromatin signatures at Notch-regulated enhancers reveal large-scale changes in H3K56ac upon activation. *The EMBO Journal* **34**:1889–1904. DOI: https://doi.org/10.15252/embj.201489923, PMID: 26069324

Sullivan AA, Thummel CS. 2003. Temporal profiles of nuclear receptor gene expression reveal coordinate transcriptional responses during *Drosophila* development. *Molecular Endocrinology* **17**:2125–2137. DOI: https://doi.org/10.1210/me.2002-0430, PMID: 12881508

Sun J, Smith L, Armento A, Deng WM. 2008. Regulation of the endocycle/gene amplification switch by notch and ecdysone signaling. *Journal of Cell Biology* **182**:885–896. DOI: https://doi.org/10.1083/jcb.200802084, PMID: 18779369

Talbot WS, Swyryd EA, Hogness DS. 1993. *Drosophila* tissues with different metamorphic responses to ecdysone express different ecdysone receptor isoforms. *Cell* **73**:1323–1337. DOI: https://doi.org/10.1016/0092-8674(93)90359-X, PMID: 8324824

Tang X, Zhao Y, Buchon N, Engström Y. 2018. The POU/Oct transcription factor nubbin controls the balance of intestinal stem cell maintenance and differentiation by Isoform-Specific regulation. *Stem Cell Reports* **10**:1565–1578. DOI: https://doi.org/10.1016/j.stemcr.2018.03.014, PMID: 29681543

Thummel CS. 1996. Flies on *steroids–Drosophila* metamorphosis and the mechanisms of steroid hormone action. *Trends in Genetics* **12**:306–310. DOI: https://doi.org/10.1016/0168-9525(96)10032-9, PMID: 8783940

Truman JW, Riddiford LM. 2002. Endocrine insights into the evolution of metamorphosis in insects. *Annual Review of Entomology* **47**:467–500. DOI: https://doi.org/10.1146/annurev.ento.47.091201.145230, PMID: 11729082

Uyehara CM, McKay DJ. 2019. Direct and widespread role for the nuclear receptor EcR in mediating the response to ecdysone in *Drosophila*. *PNAS* **116**:9893–9902. DOI: https://doi.org/10.1073/pnas.1900343116, PMID: 31019084

VanDussen KL, Carulli AJ, Keeley TM, Patel SR, Puthoff BJ, Magness ST, Tran IT, Maillard I, Siebel C, Kolterud Å, Grosse AS, Gumucio DL, Ernst SA, Tsai YH, Dempsey PJ, Samuelson LC. 2012. Notch signaling modulates proliferation and differentiation of intestinal crypt base columnar stem cells. *Development* **139**:488–497. DOI: https://doi.org/10.1242/dev.070763, PMID: 22190634

Vivas Y, Díez-Hochleitner M, Izquierdo-Lahuerta A, Corrales P, Horrillo D. 2016. Peroxisome proliferator activated receptor gamma 2 modulates late pregnancy homeostatic metabolic adaptations. *Molecular Medicine* **22**:724–736. DOI: https://doi.org/10.2119/molmed.2015.00262

Waite LL, Person EC, Zhou Y, Lim KH, Scanlan TS, Taylor RN. 2000. Placental peroxisome proliferator-activated receptor-gamma is up-regulated by pregnancy serum. *The Journal of Clinical Endocrinology and Metabolism* **85**:3808–3814. DOI: https://doi.org/10.1210/jcem.85.10.6847, PMID: 11061543

White KP, Hurban P, Watanabe T, Hogness DS. 1997. Coordination of *Drosophila* metamorphosis by two ecdysone-induced nuclear receptors. *Science* **276**:114–117. DOI: https://doi.org/10.1126/science.276.5309.114, PMID: 9082981

Wing KD, Slawecki RA, Carlson GR. 1988. RH 5849, a nonsteroidal ecdysone agonist: effects on larval lepidoptera. *Science* **241**:470–472. DOI: https://doi.org/10.1126/science.241.4864.470, PMID: 17792610

Xu K, Liu X, Wang Y, Wong C, Song Y. 2018. Temporospatial induction of homeodomain gene *cut* dictates natural lineage reprogramming. *eLife* **7**:e33934. DOI: https://doi.org/10.7554/eLife.33934, PMID: 29714689

Yamazaki K, Shimizu M, Okuno M, Matsushima-Nishiwaki R, Kanemura N, Araki H, Tsurumi H, Kojima S, Weinstein IB, Moriwaki H. 2007. Synergistic effects of RXR alpha and PPAR gamma ligands to inhibit growth in human Colon cancer cells–phosphorylated RXR alpha is a critical target for Colon cancer management. *Gut* **56**:1557–1563. DOI: https://doi.org/10.1136/gut.2007.129858, PMID: 17604322

Yoshizumi T, Ohta T, Ninomiya I, Terada I, Fushida S, Fujimura T, Nishimura G, Shimizu K, Yi S, Miwa K. 2004. Thiazolidinedione, a peroxisome proliferator-activated receptor-gamma ligand, inhibits growth and metastasis of HT-29 human Colon cancer cells through differentiation-promoting effects. *International Journal of Oncology* **25**:631–639. PMID: 15289864

Zhou B, Hiruma K, Jindra M, Shinoda T, Segraves WA, Malone F, Riddiford LM. 1998. Regulation of the transcription factor E75 by 20-hydroxyecdysone and juvenile hormone in the epidermis of the tobacco hornworm, Manduca sexta, during larval molting and metamorphosis. *Developmental Biology* **193**:127–138. DOI: https://doi.org/10.1006/dbio.1997.8798, PMID: 9473318

Supplemental figures

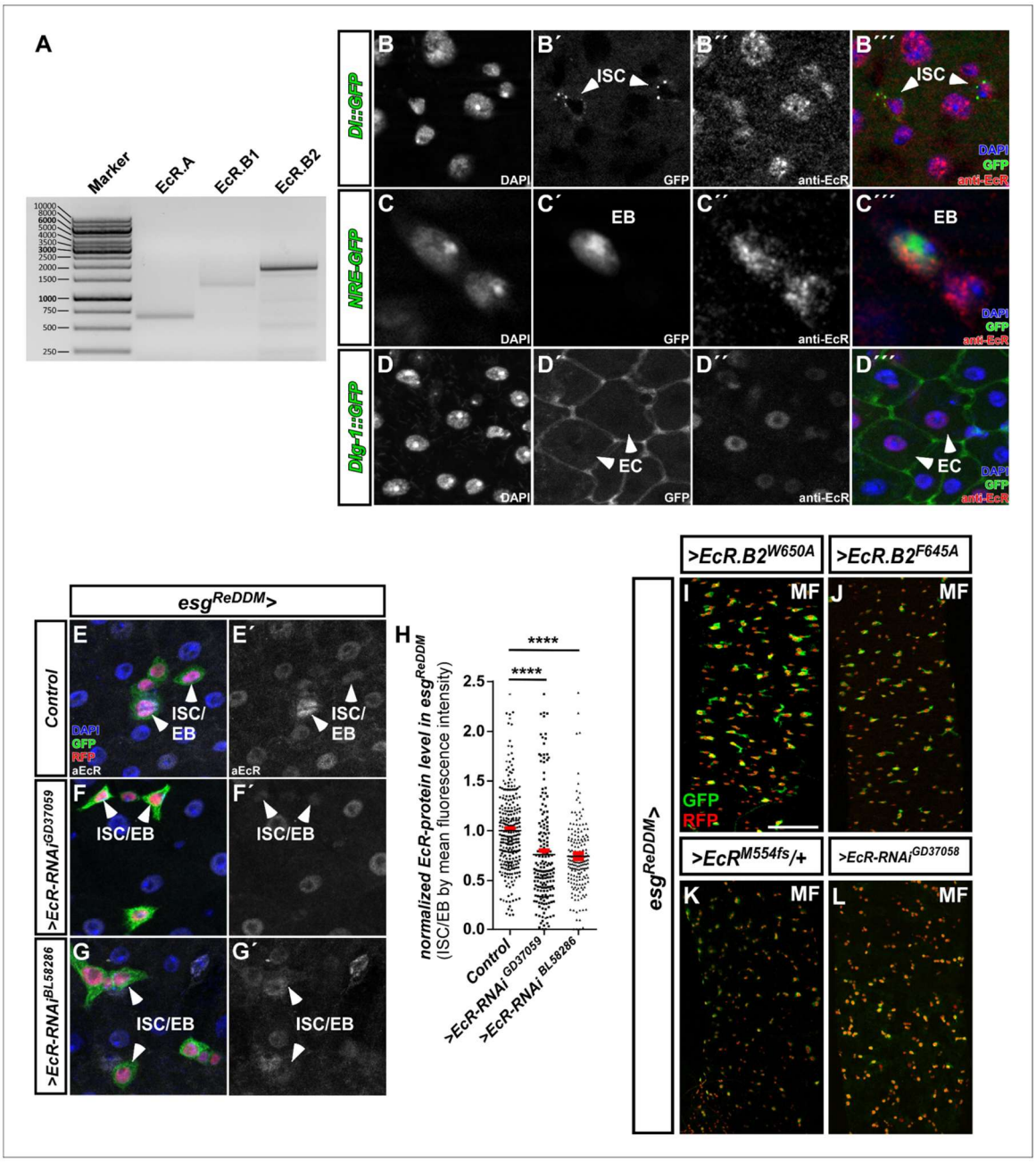

Figure 1—figure supplement 1. The EcR is expressed in the adult *Drosophila* midgut. (**A**) Expression analysis of Ecdysone-receptor splice variants with specific primer sets performed on cDNA transcribed from mRNA isolations of whole midgut dissections of adult MF. (**B–D**) Antibody staining against all EcR variants in PMG of adult MF using transgenic lines for the ISC-specific Notch-ligand Delta tagged with GFP (Dl::GFP, B-B''' inset magnification) and Notch responsive element marking EB (NRE-GFP, C-C''' inset magnification). Absorptive differentiated EC were identified using the GFP-tagged

Figure 1—figure supplement 1 continued on next page

Figure 1—figure supplement 1 continued

septate junction marker Dlg-1 (**D–D'''**). Shown are single fluorescence channels including DAPI and merge (**B'''–D'''**). (**E–H**) Representative images of esg^{ReDDM} driving EcR-RNAis showing reduction of EcR immunoreactivity (**F–G'**). (**H**) in situ quantification of EcR levels by fluorescence intensity measurements in esg^{ReDDM} after seven days of tracing. Confocal images were taken at identical excitation and emission settings. Single GFP^+/RFP^+ progenitor cell nuclei were measured using Fiji and statistically analyzed (n = 272,179,179) using one-way ANOVA with Bonferroni's Multiple Comparison Test (*p<0.05, **p<0.01; ***p<0,001; ****p<0.0001). (**I–L**) Forced expression of dominant-negative *EcR.B2*-variants (I+J), heterozygosity with the EcR^{M554fs}-allele (**K**) and a second *EcR-RNAi* (**L**) after seven days of esg^{ReDDM}-tracing in adult PMG of MF. Scale bars = 100 µm.

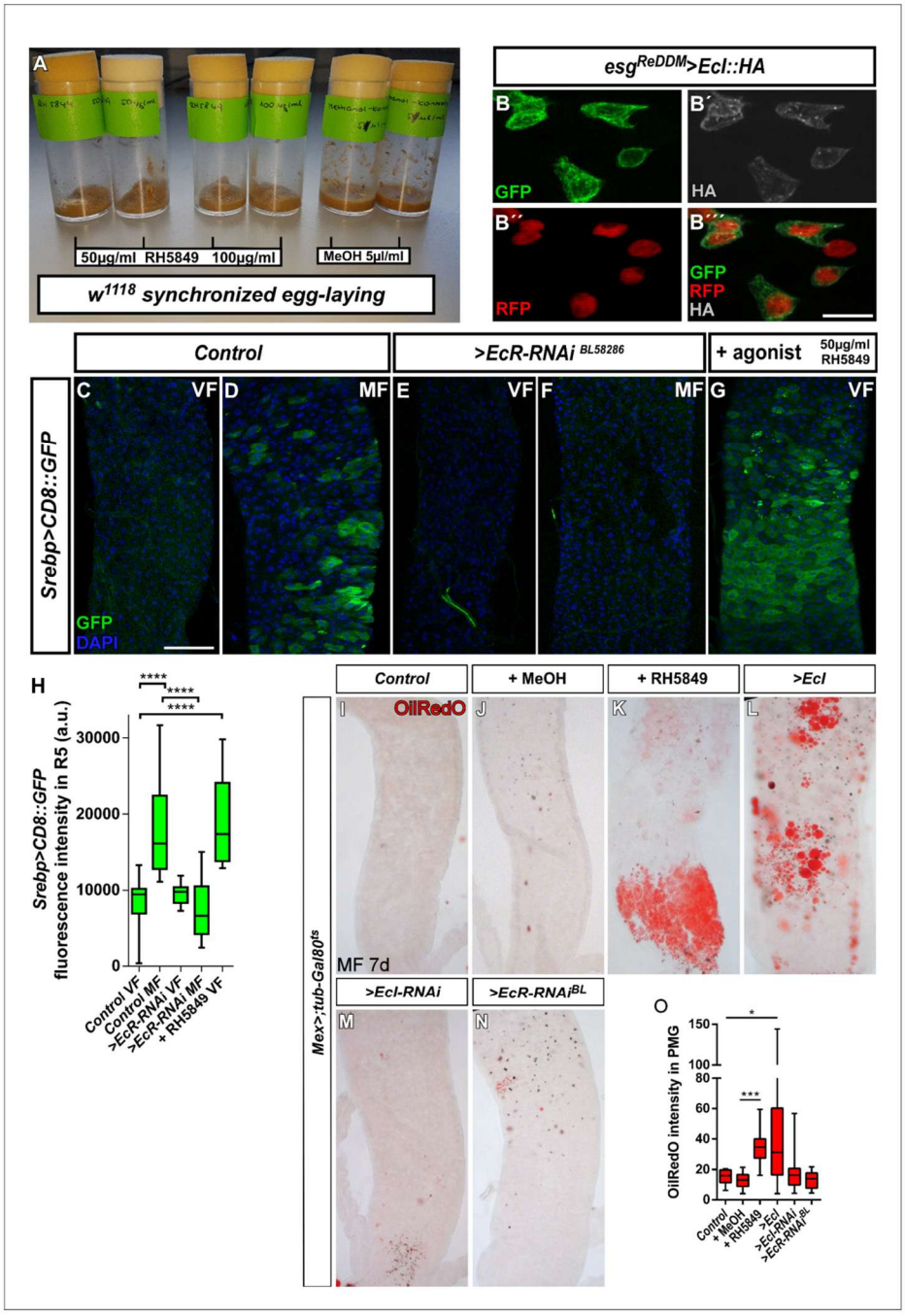

Figure 2—figure supplement 1. 20HE regulates physiological adaptations of fatty acid metabolism. (**A**) *Drosophila* food tubes of w^{1118} control egg layings to determine concentrations of RH5849. Please note that there is no crawling L3-larvae and puparium formation in both RH5849 concentrations.

Figure 2—figure supplement 1 continued on next page

Figure 2—figure supplement 1 continued

MeOH is the carrier solution and serves as control in all performed pharmacological experiments using RH5849. (**B–B'''**) Forced expression of *>Ecl::HA* using esg^{ReDDM} with subsequent immunohistochemistry using HA-antibodies reveals correct membrane localization of tagged Ecl::HA (**B'**) in ISC/EB (**B**) (***Okamoto et al., 2018***). (**C–G**) *Srebp-Gal4 > CD8::GFP* carrying VF and MF were crossed with w^{1118} (C+D),*>EcR* RNAi (E+F) or treated with RH5849 (**G**) for three days. The *Srebp-Gal4* line used is subjected to the same proteolytic processing as wild-type *Srebp*, thus reflecting upregulation of lipid uptake gene expression (***Athippozhy et al., 2011***; ***Reiff et al., 2015***). (**H**) Mean GFP-fluorescence intensities in R5 PMG of according genotypes in (**C–G**) were measured using Fiji imaging software and statistically analyzed (n = 12, 15, 13, 18, 9) using one-way ANOVA with Bonferroni's Multiple Comparison Test (*p<0.05, **p<0.01; ***p<0,001; ****p<0.0001). Scale bars = 100 µm. (**I–N**) Representative images of direct assessment of lipid content in PMG with OilRedO-staining of the indicated genotypes. Mex-Gal4, tub-$Gal80^{ts}$ was used to temporally control EC manipulation of indicated genes. (**I–N**) Control flies (I+J), fed with RH5849 (**K**), *>Ecl* (**L**), *>Ecl* RNAi (**M**) and *>EcR* RNAi (**N**) were kept for seven days at 29°C to allow transgene activation. (**O**) Quantification of OilRedO intensity and statistical analysed (n = 11,17,12,16,8,9) using student's t-test. Unluckily, we were unable to combine these fly stocks with ovo^{D1} to reveal whether egg production obscures a reduction of Ecl-RNAi and EcR-RNAi in EC lipid uptake as shown in ***Reiff et al., 2015***.

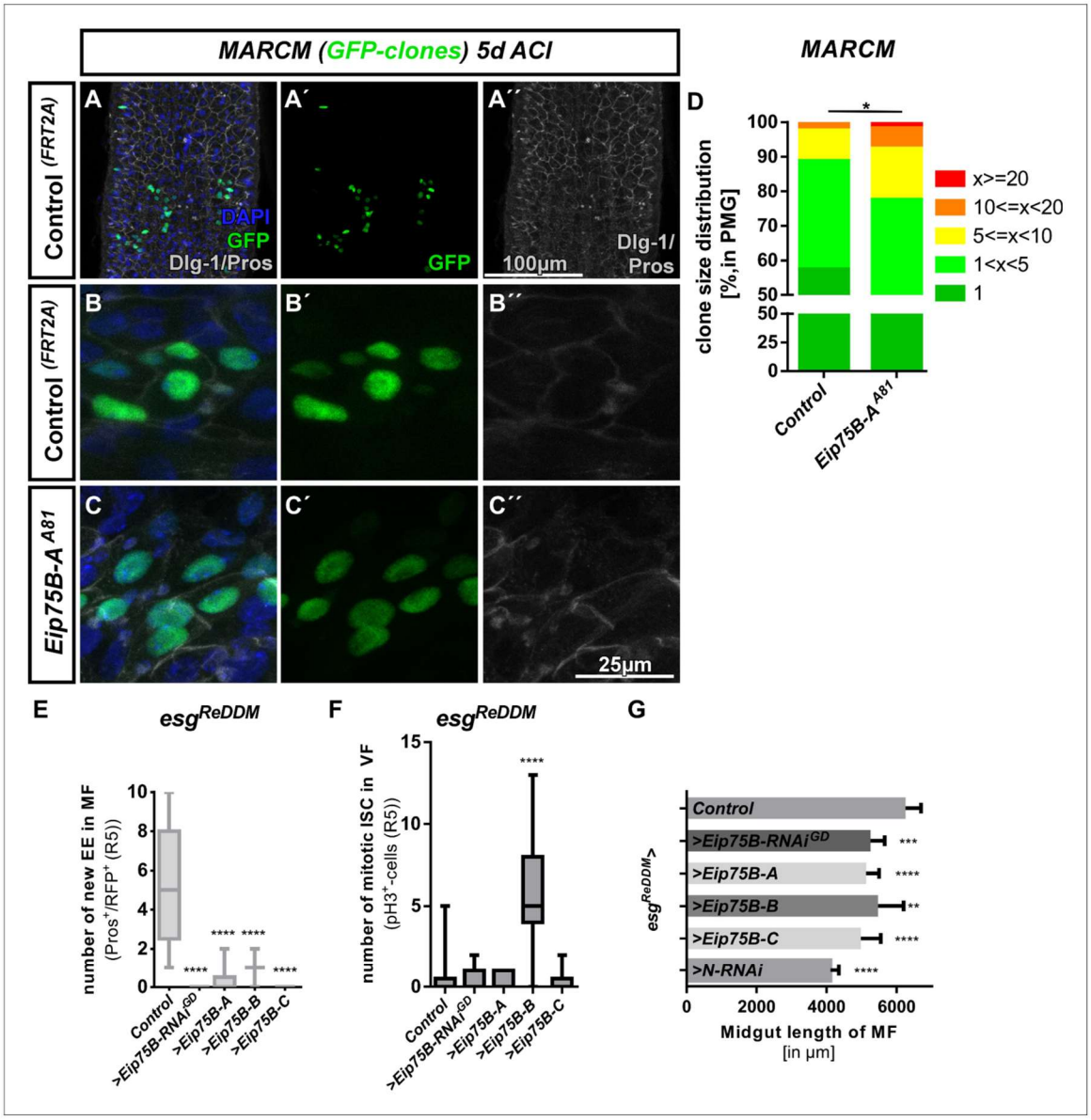

Figure 3—figure supplement 1. Analysis of *Eip75B-A* MARCM clones. (**A–E´´**) Representative images of MARCM clones of the indicated allele five days after clone induction (ACI) counterstained with Dlg-1 and Pros immunohistochemistry. Control clones lead to proper EC formation (big GFP^+-nuclei/$Dlg\text{-}1^+$) and EE (small GFP^+ diploid nuclei/$Pros^+$, arrowheads in B). *Eip75B-A* null mutant clones (**C–C´´**) do not contain properly differentiated EC (big GFP^+ nuclei without Dlg-1). Scale bars indicated in the images (**A,B–C**). (**D**) Quantification of GFP-MARCM clone size in R5 PMG (n = 294,252 clones analyzed). Error bars are Standard Error of the Mean (SEM) and asterisks denote significances from unpaired Student´s t-test (*p<0.05). (**E**) Quantification of EE (n = 12,13,10,12,11) and (**F**) pH3 (n = 9,11,7,10,10) in R5 PMG. Error bars are Standard Error of the Mean (SEM) and asterisks denote significances from one-way ANOVA with Bonferroni's Multiple Comparison Test (*p<0.05, **p<0.01; ***p<0,001; ****p<0.0001). (**G**) Overall length in µm of midguts from proventriculus to mid-/hindgut boundary of indicated genotypes. > *N* RNAi is a genetic condition in which no new EC are generated (***Figure 5***), thus reflecting the maximum midgut length reduction when no new EC are added.

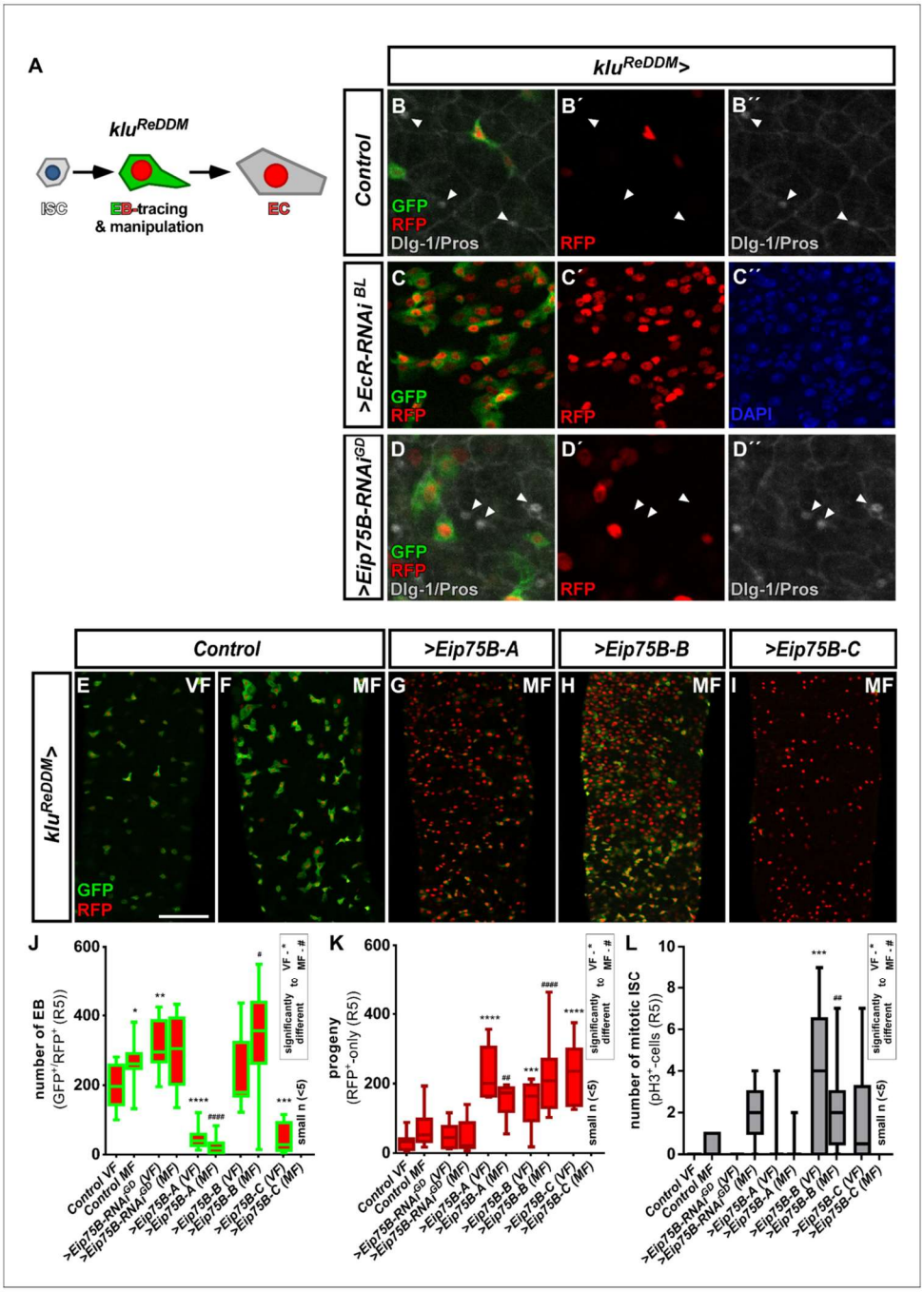

Figure 3—figure supplement 2. EB specific genetic manipulation of Eip75B using *klu*^{ReDDM}. (**A**) Cartoon depicting *klu*^{ReDDM}-tracing. *klu-Gal4* is active in EC-committed EB only and EC progeny is labelled with nuclear H2B::RFP (***Reiff et al., 2019***). (**B–D''**) Representative images of MF controls (**B–B''**)

Figure 3—figure supplement 2 continued on next page

Figure 3—figure supplement 2 continued

and EB-specific knockdown of *EcR* (C-C'') and *Eip75B* (**D–D''**) using klu^{ReDDM} after seven days of tracing. Differentiated progeny was identified in (B+D) with Dlg-1 and Pros immunohistochemistry. (**E–I**) Representative images of adult PMG of control VF (**E**) and MF (**F**) and forced expression of *Eip75B* gene products *Eip75B-A* (**G**), *Eip75B-B* (**H**) and *Eip75B-C* (**I**) after seven days of tracing with klu^{ReDDM}. (**J–L**) Quantification of EB number (**J**), traced progeny encompassing EC and EE (**K**) and ISC mitosis (**L**) in R5 PMG (n = 11,13,10,10,10,10,6,10,10,10). Error bars are Standard Error of the Mean (SEM) and asterisks denote significances from one-way ANOVA with Bonferroni's Multiple Comparison Test (*p<0.05, **p<0.01; ***p<0,001; ****p<0.0001, identical p-values are marked by # when compared to MF). Scale bars = 100 µm.

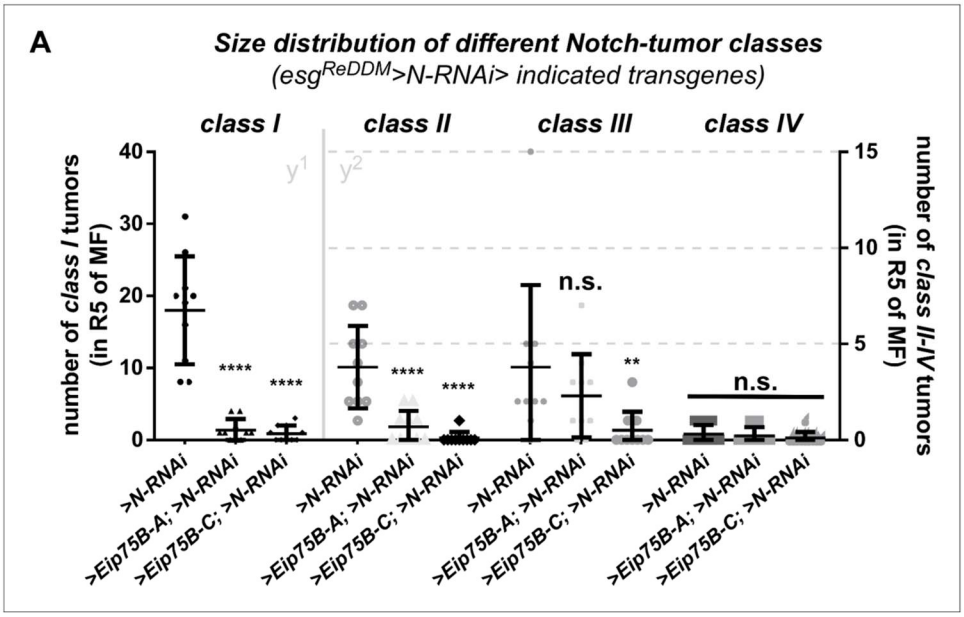

Figure 6—figure supplement 1. Size distribution of different Notch-tumor classes. (**A**) Quantification of ISC progeny encompassing ISC-like, EC and EE classified after tumor size (*classes I to IV*) in R5 PMG of *esg*^{ReDDM} > *N* RNAi (n = 10,10,10). Error bars are Standard Error of the Mean (SEM) and asterisks denote significances from one-way ANOVA with Bonferroni's Multiple Comparison Test (*p<0.05, **p<0.01; ***p<0,001; ****p<0.0001).

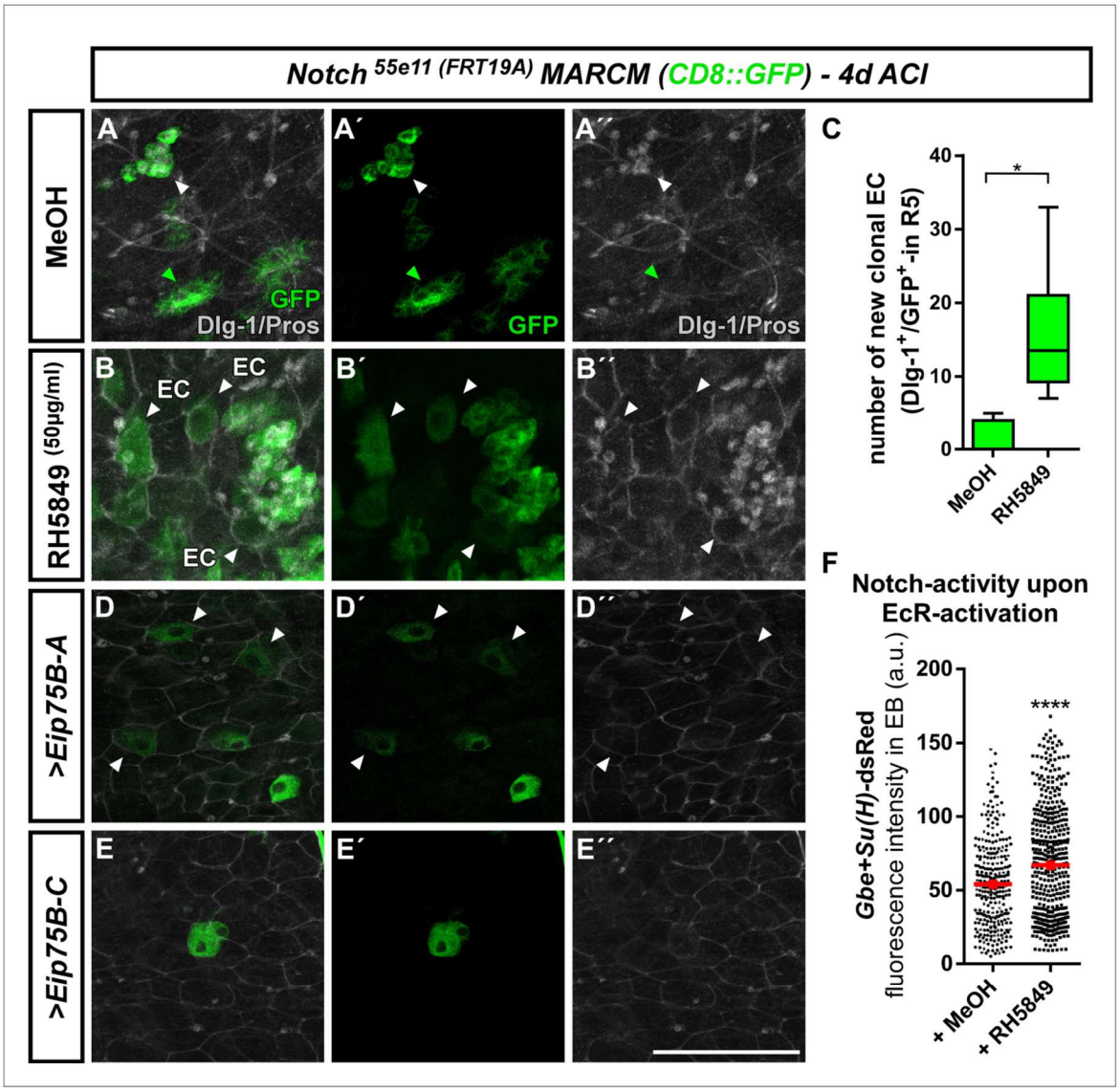

Figure 7—figure supplement 1. Analysis of *Notch* mutant MARCM clones and consequences of clonal EcR-activation. (**A–E''**) Representative images of MARCM clones for the Notch receptor (N^{55e11}) in MF PMG four days after clone induction (ACI) counterstained with Dlg-1 and Pros antibodies. Control *Notch* clones (MeOH) contain GFP-labelled clones containing ISC-like cells (GFP-only, green arrowheads) or EE (small GFP^+ diploid nuclei/$Pros^+$, white arrowheads). *Notch* null mutant clones (**B–B''**) treated with RH5849 contain differentiated EC in adjacent to Notch tumors ($Dlg1^+$/GFP^+) arrowheads). (**C**) Quantification of GFP-labelled EC in *Notch* MARCM clones in R5 PMG (n = 7,6). Error bars are Standard Error of the Mean (SEM) and asterisks denote significances from unpaired Student´s t-test (*p<0.05, p=0,0129). (D+E) Forced expression of > *Eip75* B-A (**D**) and > *Eip75* B-C (**E**) leads to the immediate formation of single cell clones that immediately differentiated into EC (arrowheads). (**F**) Notch activity addressed by Gbe-SuH activity fluorescence activity in RH5849 fed flies vs. control flies (>250 EB in n > 3 midguts, Error bars are Standard Error of the Mean (SEM) and asterisks denote significances from unpaired Student´s t-test (****p<0.001). Scale bars = 100 µm.

So far, the impact of 20HE/oestrogen and its downstream factor Eip75B/hPPARγ on intestinal tumour progression have only been investigated in a benign tumour-model of N-deficient ISC (Paper I Figure 6, Figure 6-figure supplement 1, Figure 7 and Figure 7-figure supplement 1). The aim was to establish a novel *Drosophila* model which resembles malignant tumours of human CRC patients. For this purpose, CRISPR/Cas9 was used to target tumour suppressor genes of the most frequently altered signalling pathways in CRC, combined with expression of oncogenic Ras^{G12V}. CRISPR/Cas9 mediated mutagenesis is induced by using esg^{ReDDM} complemented with expression of Cas9. At the same time ReDDM-tracing enables labelling of tumour stem cells and tracing of their progeny. The generation and first characterizations of the novel *Drosophila* CRC model have been published as part of paper II.

2.2 Paper II: The MicroRNA miR-277 Controls Physiology and Pathology of the Adult *Drosophila* Midgut by Regulating the Expression of Fatty Acid β-Oxidation-Related Genes in Intestinal Stem Cells

metabolites

MDPI

Article

The MicroRNA *miR-277* Controls Physiology and Pathology of the Adult *Drosophila* Midgut by Regulating the Expression of Fatty Acid β-Oxidation-Related Genes in Intestinal Stem Cells

Lisa Zipper [1,†], Sai Batchu [2,†], Nida Hatice Kaya [3], Zeus Andrea Antonello [2,4,†] and Tobias Reiff [1,*,†]

1 Institute of Genetics, Department of Biology, The Faculty of Mathematics and Natural Sciences, Heinrich-Heine-Universität Düsseldorf, 40225 Düsseldorf, Germany; lisa.zipper@hhu.de
2 Cooper Medical School, Rowan University, Camden, NJ 08102, USA; batchu94@rowan.edu (S.B.); antonello@rowan.edu (Z.A.A.)
3 Institute for Zoology and Organismic Interactions, Department of Biology, The Faculty of Mathematics and Natural Sciences, Heinrich-Heine-Universität Düsseldorf, 40225 Düsseldorf, Germany; nida.kaya@hhu.de
4 Cooper University Hospital, Cooper University Health Care, Cooper Medical School, Rowan University, Camden, NJ 08102, USA
* Correspondence: reifft@hhu.de
† These authors contributed equally to this work.

Abstract: Cell division, growth, and differentiation are energetically costly and dependent processes. In adult stem cell-based epithelia, cellular identity seems to be coupled with a cell's metabolic profile and vice versa. It is thus tempting to speculate that resident stem cells have a distinct metabolism, different from more committed progenitors and differentiated cells. Although investigated for many stem cell types in vitro, in vivo data of niche-residing stem cell metabolism is scarce. In adult epithelial tissues, stem cells, progenitor cells, and their progeny have very distinct functions and characteristics. In our study, we hypothesized and tested whether stem and progenitor cell types might have a distinctive metabolic profile in the intestinal lineage. Here, taking advantage of the genetically accessible adult *Drosophila melanogaster* intestine and the availability of ex vivo single cell sequencing data, we tested that hypothesis and investigated the metabolism of the intestinal lineage from stem cell (ISC) to differentiated epithelial cell in their native context under homeostatic conditions. Our initial in silico analysis of single cell RNAseq data and functional experiments identify the *microRNA miR-277* as a posttranscriptional regulator of fatty acid β-oxidation (FAO) in the intestinal lineage. Low levels of *miR-277* are detected in ISC and progressively rising *miR-277* levels are found in progenitors during their growth and differentiation. Supporting this, *miR-277*-regulated fatty acid β-oxidation enzymes progressively declined from ISC towards more differentiated cells in our pseudotime single-cell RNAseq analysis and in functional assays on RNA and protein level. In addition, in silico clustering of single-cell RNAseq data based on metabolic genes validates that stem cells and progenitors belong to two independent clusters with well-defined metabolic characteristics. Furthermore, studying FAO genes in silico indicates that two populations of ISC exist that can be categorized in mitotically active and quiescent ISC, of which the latter relies on FAO genes. In line with an FAO dependency of ISC, forced expression of *miR-277* phenocopies RNAi knockdown of FAO genes by reducing ISC size and subsequently resulting in stem cell death. We also investigated *miR-277* effects on ISC in a benign and our newly developed CRISPR-Cas9-based colorectal cancer model and found effects on ISC survival, which as a consequence affects tumor growth, further underlining the importance of FAO in a pathological context. Taken together, our study provides new insights into the basal metabolic requirements of intestinal stem cell on β-oxidation of fatty acids evolutionarily implemented by a sole microRNA. Gaining knowledge about the metabolic differences and dependencies affecting the survival of two central and cancer-relevant cell populations in the fly and human intestine might reveal starting points for targeted combinatorial therapy in the hope for better treatment of colorectal cancer in the future.

check for updates

Citation: Zipper, L.; Batchu, S.; Kaya, N.H.; Antonello, Z.A.; Reiff, T. The MicroRNA *miR-277* Controls Physiology and Pathology of the Adult *Drosophila* Midgut by Regulating the Expression of Fatty Acid β-Oxidation-Related Genes in Intestinal Stem Cells. *Metabolites* **2022**, *12*, 315. https://doi.org/10.3390/metabo12040315

Academic Editor: Claire Pecqueur

Received: 15 March 2022
Accepted: 28 March 2022
Published: 31 March 2022

Publisher's Note: MDPI stays neutral with regard to jurisdictional claims in published maps and institutional affiliations.

Keywords: intestinal stem cell; metabolism; fatty acid oxidation; *Drosophila*; midgut

1. Introduction

The ability of organisms to maintain their internal conditions in balance requires energy uptake. An organism's body is considered to be homeostatic while it constantly compensates for fluctuating wear and tear, injuries, changes in environment, and energetical in- and effluxes. To cope with these unpredictable conditions, evolution generated plastic and context-dependent ways to adapt to changes in e.g., nutrients availability. Nutrient-related adaptations go down until the cellular level, affecting the way each cell utilizes resources of energy. Growth, division, and differentiation are genetically encoded processes and are thought to adapt their gene expression in a plastic and context-dependent manner [1–4].

Prime candidates for such a complex regulation of gene expression of entire pathways and networks are microRNAs, which regulate approximately half of the transcriptome [1,2]. Indeed, apart from established roles in key processes such as cytoskeletal dynamics, cell migration, stemness, and metabolic phenotype [3–6], microRNAs have been implicated in the control of glucose and lipid metabolism [7].

In adult *Drosophila melanogaster* females, lipid metabolism is upregulated in a regionalized subpopulation of differentiated intestinal cells upon mating to sustain egg production [5–7]. Such regional differences of intestinal cell types have not only been reported regarding metabolism, but localization also seems to be connected with stem cell (SC) identity and proliferation behavior [8–10]. Together, this leads to the intriguing question on which metabolic phenotype intestinal stem cells (ISC) rely and whether their metabolism is involved in SC behavior.

In general, in vivo data on SC metabolism is scarce owing to the lack of proper genetic sensors and tools. Here, we employed the fruit fly *Drosophila melanogaster,* taking advantage of its exhaustive genetic toolbox to study SC metabolism in an adult organism during physiological homeostasis and in the pathological context of tumoral growth. Briefly, the fly intestine harbors around one thousand multipotent ISC, showing regional differences in proliferation behavior and cellular anatomy [8,9,11–13]. ISC are able to self-renew, but mainly divide asymmetrically to generate two types of precursor cells: postmitotic enteroblasts (EB) capable of differentiation to absorptive enterocytes (EC) and enteroendocrine precursor cells (EEP) that perform a singular symmetric division giving rise to two enteroendocrine cells (EE) [11,12,14].

For a long time, it was generally assumed that SC harbor immature mitochondria allowing no or limited ATP production through oxidative phosphorylation (OXPHOS). Recent and widespread literature on SC metabolism has provided new insights, revealing that the metabolic phenotype of SC varies depending on species, age, and developmental stage, as well as tissue localization [15]. Studies of embryonic, mesenchymal, neural, and induced pluripotent SC also show that their metabolic phenotype varies from glycolysis, over β-oxidation of fatty acids (FAO) to OXPHOS as an energy source [15,16], suggesting that there is no SC metabolism per se. An important commonality of these studies is that the vast majority was performed in vitro where the sheer availability of oxygen and metabolites in culture media might affect metabolic (re-)programming of cultured SC.

In the adult *Drosophila* intestine, a few studies hint to metabolic pathways for energy allocation in ISC and how this influences homeostatic processes. In aging ISC, energy supply from nutrient stores is reduced, negatively affecting tissue homeostasis in old flies [17]. A few in vivo studies shed first light on ISC metabolism. Schell and colleagues demonstrated a requirement of mitochondrial metabolism in ISC for intestinal homeostasis in *Drosophila* and intestinal organoids, which suggests OXPHOS as a possible energy source for *Drosophila* ISC.

A second study suggests a direct link between ISC metabolic state and nutrient availability. By manipulating a key enzyme of the hexosamine biosynthesis pathway, Mattila and colleagues were able to shift the balance between OXPHOS and glycolysis, linking nutrient content directly to ISC proliferation [18,19]. Recent work from the Edgar lab confirms metabolic changes in EB while differentiating and describes that EGFR signaling increases glycolysis, FAO, and mitochondrial biogenesis [19,20]. In addition, input from EGFR signaling was shown to specifically affect EB survival, supporting the idea of different metabolism and thus nutrient requirements of ISC and EB [21]. Downregulation of key metabolic enzymes for glycolysis and OXPHOS does not affect ISC numbers, suggesting that both metabolic pathways are dispensable for basal metabolism controlling ISC survival [18,20,22]. However, genetic manipulations in both studies were performed using the *esg-Gal4* driver line which is active in ISC and EB, thus not allowing discrimination between metabolic requirements in stem or maturing precursor cells [22].

Here, building on in silico data from clustering of metabolic genes and pathways in *Drosophila* ISC, we set out to functionally identify and characterize the role of FAO genes in ISC metabolism in vivo. Investigating physiology and pathology of genetic manipulations of FAO enzymes, we add to the growing knowledge of metabolic essentials of intestinal stem cells.

2. Results

2.1. Identification of miR-277 as a Regulator of Cellular Metabolism

Changing cell metabolism requires fundamental adaptations of genetic networks and gene expression, which is why we aimed at microRNAs regulating such complex genetic networks. Approximately half of the transcriptome is regulated by microRNAs, which makes them a perfect candidate for the control of such metabolic networks [23,24]. Taking advantage of in silico resources [8,13], putative target gene lists from four different miRNA prediction algorithms were compared (Figure 1a). Predicted target genes of individual miRNAs showing up in at least three out of four miRNA prediction algorithms were then subjected to Gene Ontology Mapping using FatiGO Babelomics 4.0 (http://www.babelomics.org/, accessed on 5 November 2021).

To our surprise, from eight investigated microRNAs, only *microRNA miR-277* showed a significant enrichment of a set of predicted target genes all mapping to metabolic pathways (Figure S1). Analyzing and assigning this gene set using KEGG pathways revealed that eight of the *miR-277* regulated genes possess enzymatic functions in fatty acid metabolism (Figure 1b) and a known role in branched chain amino acid catabolism [25]. Furthermore, *miR-277* was linked to lipid metabolism in *Aedes aegypti* before [26].

The direct regulation of predicted target genes by *miR-277* was investigated using quantitative real- time PCR. Relative mRNA levels of predicted target genes were decreased in whole guts of adult *Drosophila* upon forced expression of *miR-277* in EC (Figure 1d), indicating that all eight target genes involved in fatty acid metabolism are in fact regulated by *miR-277*. β-oxidation of fatty acids (FAO) provides an important energy source by degrading fatty acids fueling the citrate cycle with acetyl-CoA (Figure 1b). Together with our previous data showing activation of lipid uptake in the posterior midgut upon mating [6], we aimed to investigate the role of *miR-277* and FAO in intestinal progenitors.

2.2. miR-277 Is Expressed in Differentiating EB and EC in the Adult Drosophila Intestine

Intrigued by these results, we tested for *miR-277* expression in the posterior region of the female adult *Drosophila* intestine and found pre-miRNA-277 expressed in the adult midgut by PCR (Figure 1c). Therefore, we used *miR-277* sensor flies containing a transgene consisting of *miR-277* consensus sequences fused to a sequence coding for GFP (Figure 2a). Presence of *miR-277* results in mRNA degradation and therefore reduced GFP-levels compared to control flies lacking these consensus sequences [27,28]. Crossing these flies with a reporter for Notch-signaling activity (*NRE-mcherry or Gbe+Su(H)dsRed,* marking EB) enabled us to decipher ISC from EB and epithelial EC and EE (Figure 2b,b‴) [11,29].

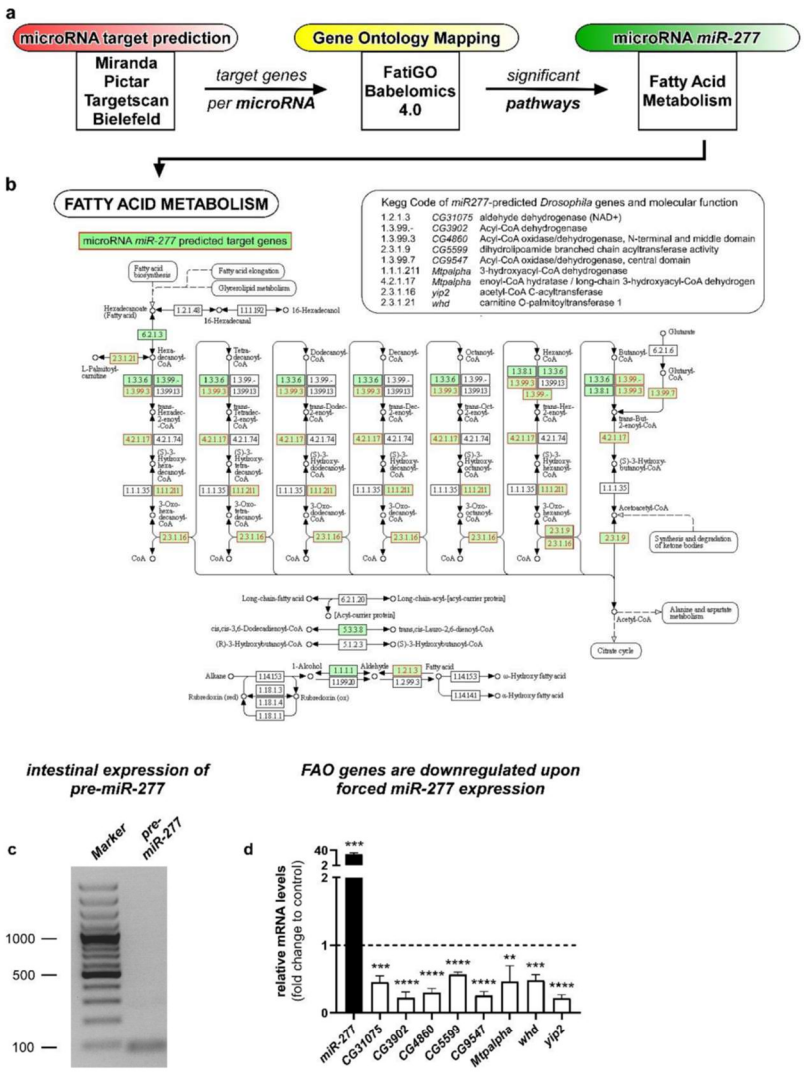

Figure 1. Workflow of the identification process for Gene Ontology Networks from microRNA target gene prediction and subsequent Gene Ontology mapping and proof of actual target gene regulation by *miR-277*. (**a**) Putative target gene lists for different miRNAs were obtained and analyzed from four microRNA prediction algorithms. Target genes that showed up in at least three out of four prediction algorithms were subjected to FatiGO prediction for Gene Ontology networks on Babelomics 4.0 servers (Barcelona, Spain) and resulting GO-terms (Gene Ontology) with a *p*-value $p < 0.05$ were considered. (**b**) Summary of predicted *miR-277* target genes involved in fatty acid metabolism: shown is the involvement of *miR-277* regulated genes in KEGG nomenclature with red lettering and green background. The table (top-right) lists all targeted genes from the KEGG pathway prediction for fatty acid metabolism, the according *Drosophila melanogaster* genes, and functions. KEGG involvement image modified, copyright by Kanehisa Laboratories. (**c**) PCR reaction using specific primer sets for the *pre-miR-277* reveal *miR-277* on adult *Drosophila* midgut cDNA; (**d**) relative mRNA levels of predicted *miR-277* target genes involved in fatty acid metabolism were decreased in whole guts upon forced expression of *UAS-miR-277* in EC using a Mex^{ts}*-Gal4* driver ($n = 3$; unpaired *t*-test: ** $p < 0.01$, *** $p < 0.001$, **** $p < 0.0001$).

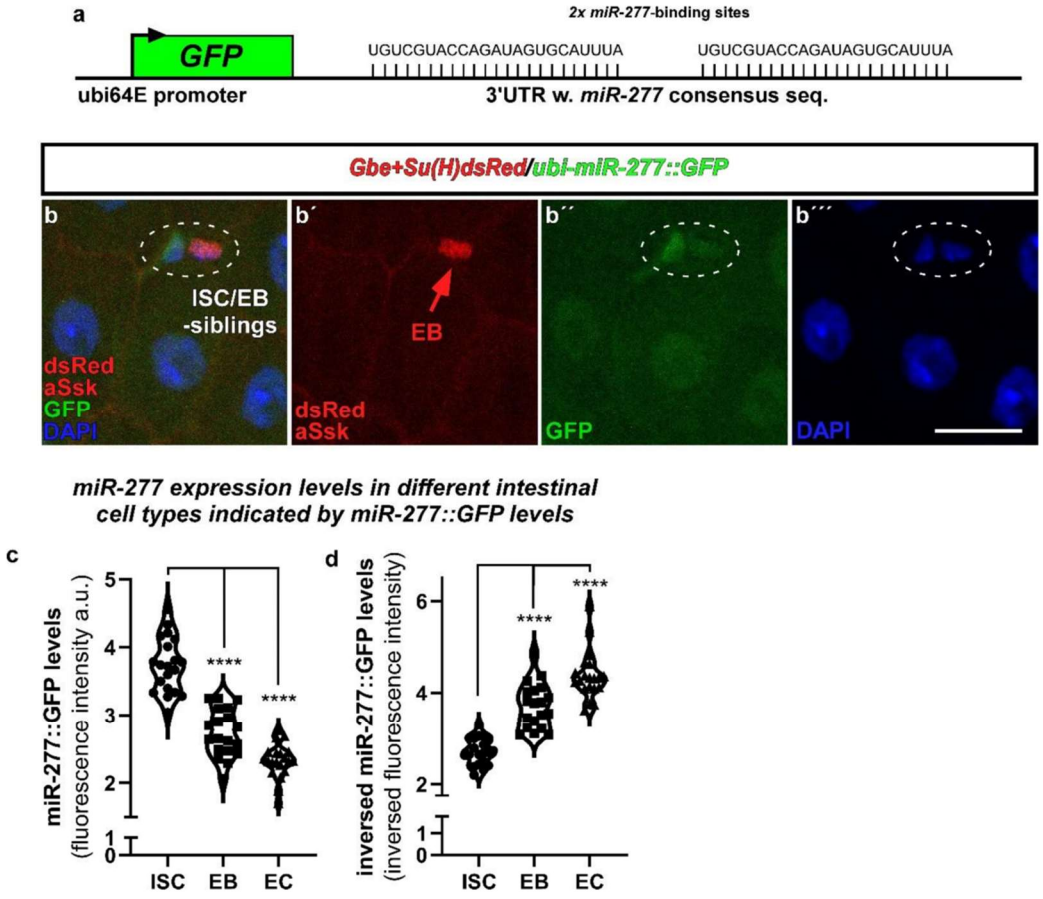

Figure 2. *miR-277*-expression in ISC, EB and EC revealed by *miR-277::GFP* sensor flies in the R5 region of the posterior midgut. (**a**) miR-277-expression in R5 regions of adult posterior midguts was analyzed using a transgenic sensor for *miR-277*. The sensor is expressed ubiquitously by ubi-promoter sequences and consists of *miR-277* consensus sequences fused to the coding sequence of GFP. Thus, raised *miR-277* levels directly reduce GFP signals. (**b–b‴**) Flies carrying the *miR-277* sensor were crossed with flies carrying the Notch-activity reporter *Gbe+Su(H)dsRed* labelling EB. After seven days at 25 °C, images were taken with fixed 488 nm laser settings to enable comparison of GFP-intensity (**b″**). *Ubi-miR-277::GFP* flies reveal a significant decrease in GFP-signal in EB and epithelial EC (identified by big nuclear size and aSsk staining of septate junctions) compared to GFP signal detected in ISC. (**c**,**d**) Quantification of GFP-fluorescence intensity of ISC, EB and EC corrected to control *ubi-GFP* flies ((**c**); see materials and methods; $n = 20, 19, 20$; ANOVA, **** $p < 0.001$) and numerical inversion for comprehensibility (**d**). (Scale bar is 10 µm).

ISC and EB usually occur as duplets (Figure 2b) and maturing EB separate from their mother ISC to differentiate into EC [3,21,30]. We addressed *miR-277* expression levels by measuring GFP fluorescence in ISC, EB, and EC. Presence of endogenous *miR-277* leads to degradation of GFP encoding mRNA and thus fluorescence intensity. Highest GFP fluorescence was measured in ISC (Figure 2b,c), reflecting low endogenous *miR-277* levels (Figure 2d). Differentiating EB and terminally differentiated EC have significantly lower GFP-levels, suggesting higher *miR-277* levels (Figure 2c,d), which in turn might reflect less FAO activity. We validated the reactivity of the *miR-277* sensor flies to changes in

miR-277 expression by crossing *miR-277::GFP* flies with overexpression (*UAS-miR-277*) or knockdown of *miR-277* using an miR-277 sponge genetic construct (*UAS-miR-277-sp*, Figure 6e). MicroRNA sponges contain multiple complementary binding sites to the seed sequence of a microRNA of interest (Figure 6e) and reduce endogenous microRNA levels in both flies and human cell culture [31,32]. Upon overexpression of *miR-277* in ISC/EB, *miR-277::GFP* intensities were decreased, while knockdown of *miR-277* resulted in increased GFP intensities (Figure S4f–i). These results prove that the sensor is reflecting *miR-277* expression levels and underlines endogenous *miR-277* expression in ISC/EB. Next, we set out to determine FAO gene transcription in existing scRNAseq datasets of intestinal cell types [13].

2.3. miR-277 Target Gene Expression in Reconstructed Intestinal Lineage Trajectories from scRNAseq

To investigate the expression of *miR-277* target genes and possible metabolic differences between ISC/EB and differentiated progeny, we used the updated 2019 single-cell sequencing dataset [13] to perform a cell clustering and lineage reconstruction based only on metabolic genes [33,34]. To infer cell lineage, we used only ISC/EB, differentiating EC, EC (anterior (aEC), mid (mEC) and posterior EC (pEC)), and EEs, and excluded all other cell types following a previous analysis [13].

Four main lineages were reconstructed: (i) ISC/EB→differentiating EC (dEC)→anterior EC (aEC), (ii) ISC/EB→dEC→mid EC (mEC), (iii) ISC/EB→dEC→posterior EC (pEC) and (iv) ISC/EB→EE (Figure 3a). ISC/EB and each EC subtype (aEC, mEC and pEC) showed clustering with a small dispersion indicating a homogenous metabolic profile from anterior to posterior EC (Figure S2a–c). EE instead showed the highest dispersion/metabolic heterogeneity in accordance with a high variety of EE subtypes [35] (Figure 3a). Pseudotime analysis of predicted *miR-277* target genes indicates that most genes of the FAO pathways predicted to be regulated by *miR-277* are progressively inhibited in dEC towards terminally differentiated EC lineages and in the lineage specification of EE as well (Figure 3b).

In detail, the reconstructed lineage towards pEC shows that FAO metabolic genes *CG31075, CG4860, CG5599, CG9547,* and *whd* diminish, while *yip2* and *CG3902* progressively increase (Figure 3b). *Mtpalpha* diminishes during the differentiation to then increase again in the terminally differentiated pEC (Figure 3b). In the reconstructed lineage towards anterior EC, the expression profile is similar to the posterior midgut with the difference of *yip2*, which progressively increases, and *whd*, which decreases during differentiation to then increase in terminally differentiated anterior EC, similarly to *Mtpalpha* for pEC (Figure 3b). In the mid midgut, reconstructed lineages also show similar patterns to the pEC, with the exception of *CG5599* which increases progressively, *CG3902* which initially increases in the process of differentiation to then diminish in terminally differentiated mEC, and *yip2* which increases initially and then diminishes. Although few FAO genes seem to be more expressed in differentiated cells or seem to be fluctuate in the process of differentiation, altogether these data show that FAO genes expression levels diminish towards differentiated cells.

This is in accordance with our in vivo data showing that *miR-277* levels increase towards EC fate (Figure 2c,d) and further indicates that *miR-277* post-transcriptionally represses FAO genes (Figure 1d). To confirm our in silico pseudotime analysis, we investigated flies carrying a GFP-tagged CG9547 fusion protein under control of endogenous regulatory sequences (Figure S5a). We found highest CG9547 protein levels in Notch ligand Delta (Dl) positive ISC (FigureS 5d and S5b–b‴). Using specific markers for intestinal cells [5,11,12,21,29,36], we were able to validate our pseudotime analysis of an expression decline for CG9547 towards epithelial EC cell fates on protein level (Figure 5d). In addition, we could prove that CG9547 protein levels are reduced upon overexpression of *miR-277* (Figure S5e,e′,h) or knockdown of *CG9547* by RNAi (Figure S5g,g′,h) compared to controls (Figure S5d,d′,h). Upon knockdown of *miR-277* using *miR-277-sp* CG9547 protein levels increase (Figure S5f,f′,h). This observation supports our results showing endoge-

nous expression and regulation of the predicted target genes involved in FAO by *miR-27* 7 in ISC/EB.

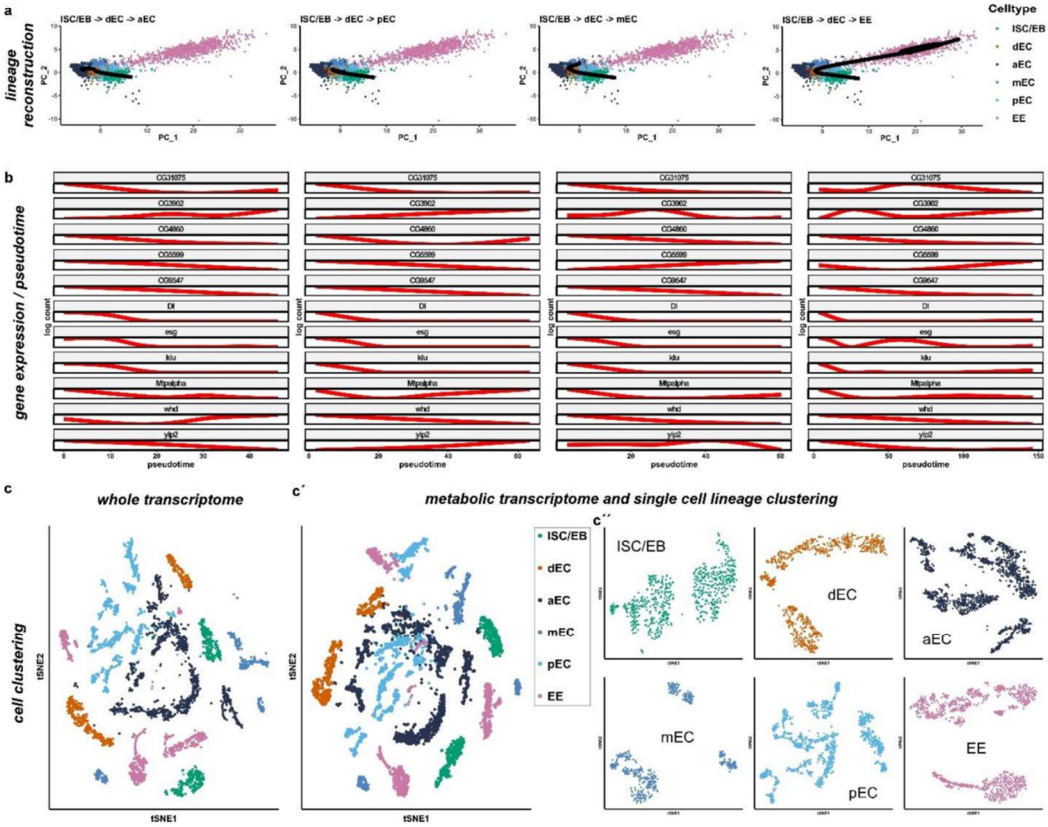

Figure 3. Metabolic transcriptome analysis of single-cell sequencing data from the cell atlas of the *Drosophila* midgut. (**a**) Cell lineages based on metabolic genes expression were inferred using Slingshot. Four lineages were constructed starting from ISC/EB and ending in each differentiated cell type (anterior EC (aEC), middle EC (mEC), posterior EC (pEC), and EE). (**b**) Plot of gene expression as a function of pseudotime for each lineage. Target genes of *miR-277* are shown together with the known markers of ISC and EB (*esg*, *Dl*, *klu* and *pros*). (**c**–**c″**) Comparison of whole transcriptomic (**c**) and only metabolic genes (**c′**–**c″**) cell clustering with correspondent activity score. (**c′**,**c″**) Metabolic cell clusters separated by cell type (**c′**) and single cell lineage clustering (**c″**) as previously described.

The finding of CG9547 FAO enzyme expression in ISC and its regulation by *miR-277* strongly underlines our metabolic analysis from scRNAseq. Our observations suggest that fatty acids in ISC are used for energy production through FAO and might rather be used for membrane build-up in dEC and EC in an anabolic way. Together with the finding that FAO regulating *miR-277* levels are low in ISC, we wanted to investigate the hypothesis whether fatty acids might be used differently between ISC and EB.

2.4. FAO defines Differences among Intestinal Stem Cells and Enteroblasts

Stem cells and progenitor cells, although both undifferentiated progenitor cell types, are fundamentally different. In the adult *Drosophila* intestine, ISC are the only cell type capable of self-renewal, while EB are postmitotic and committed towards EC differentiation. EB are a transient but discrete cell type capable of delaying terminal differentiation

for sustained periods of time. During differentiation, EB obtain functional mitochondria and endoreplicate [3,5,19–21,30]. To investigate whether expression of genes involved in metabolic pathways in ISC and EB have differences reflecting their functional differences, we subdivided the ISC/EB cluster obtained in the principal component analysis of metabolic genes (Figure 3c–c″) using previously described cell type specific markers such as *Dl* (ISC), *esg* (ISC+EB), *klu* (EB) and *pros* (EE) [5,11,12,21,29,36] (Figure 4a).

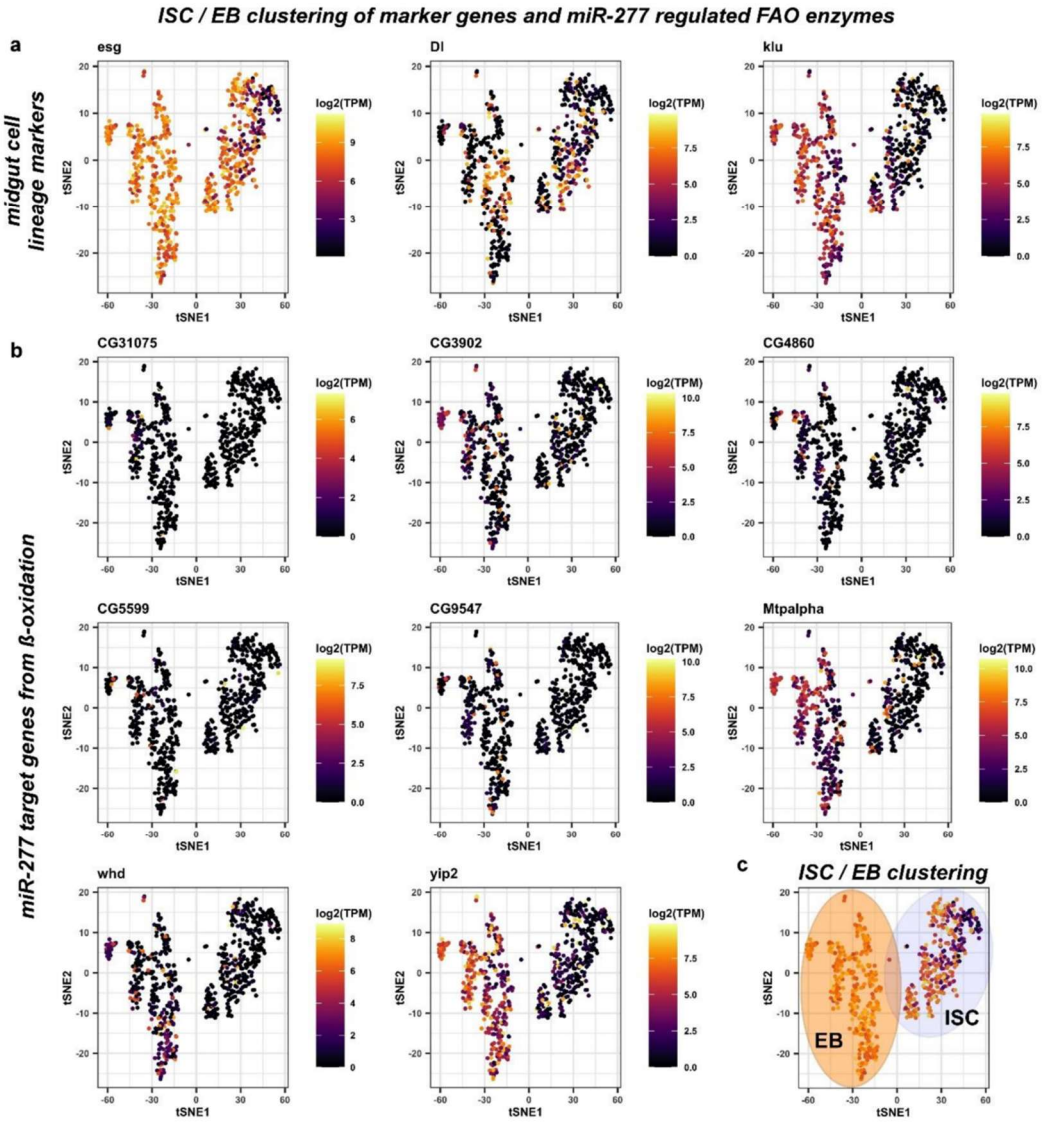

Figure 4. Analysis of midgut progenitor cell markers and *miR-277* target genes from ß-oxidation in metabolic cell clusters of ISC/EB. (**a**) Two distinct ISC/EB clusters in the metabolic cell clusters were identified being positive for *esg* expression. The ISC marker *Dl* is expressed in cells of both clusters that are negative for expression of the EB marker *klu*. (**b**) Analysis of *miR-277* target genes from FAO in metabolic cell clusters of ISC/EB (**c**) ISC/EB clusters can be subdivided into two distinct metabolic clusters, ISC (grey circle) and EB (orange circle) analyzing expression of *Dl* and *klu* marker genes.

Escargot (esg) marks both ISC and EB, as previously demonstrated [3,37,38]. However, *esg* has been shown to overlap with EE [3,37–39]. First, we observed and excluded a very small number of $pros^+$ cells within the esg^+ ISC/EB population from the analysis (Figure S3a). The Notch ligand *Delta (Dl)* has been shown to be a sufficient but not necessary marker of ISC *per se*, as it is only necessary during stem cell division for EB cell fate determination by Delta/Notch signaling [1,12,21,31,32]. In EB, the Notch target gene *klumpfuss (klu)* has been shown to be a sufficient and necessary marker for EB, preventing the EE fate and committing towards the EC fate [21,36]. We hence initially defined ISC as 'esg^+, Dl^+, klu^-, and $pros^-$', and EB as 'esg^+, Dl^-, klu^+, and $pros^-$' (Figure 4a). Using these criteria for mapping, *miR-277* targeted FAO enzymes are found to be expressed in ISC/EB (Figure 4b) and two distinct populations of ISC and EB can be distinguished (Figure 4c). Despite that, we found a high variety of genes contradicting only one ISC population in terms of metabolic gene expression.

After an exhaustive search, we isolated and termed a third group, reflecting a second population of ISC that is Dl^- ('esg^+, Dl^-, klu^- and $pros^-$', Figure 5a,f) built on our metabolic mapping, marker gene expression, and a previous unpublished observation that under very low turnover conditions, the majority of ISC of virgin females are negative for the mitosis marker pH3 and importantly esg^+/Dl^- [6] (Antonello and Reiff, unpublished results). We also observed that reprogramming towards lipid uptake upon mating [6] may already cause an upregulation of CG9547 protein levels in MF compared to VF (Figure S5c). Using these criteria, Dl^+ proliferating ISC (pISC) have high expression of cell cycle genes *CycD*, *CycE*, and *stg* (*string*, *CDC25A*) (Figure 5b), whereas quiescent ISC (qISC) have high levels of *nub* (*POU/OCT1*) involved in quiescence [40,41] (Figure 5b). E2F1 is also high in qISC, where it might exert its known role as repressor of OXPHOS and mitochondrial function [42,43] and promote FAO to support self-renewal and drug resistance via NANOG in tumor-initiating stem-like cells [43] (Figure 5a). EB show higher levels of endoreplication genes (*Orc1*, *dup*), cellular growth (*mTor*, *Myc*) and *Eip75B* [5] (Figure 5b).

Strikingly, qISC and pISC are characterized by high expression of the FAO genes *CG5599*, *Mtpalpha*, and *yip2* and, respectively, *CG3902*, *CG4860*, *CG9547*, and *whd* in comparison to EB (Figure 5c). As an exception from *miR-277* target genes showing clear expression differences among populations, *CG31075* sticks out being high in a small number of EB (Figure 5c). *CG31075* is predicted to code for an orthologue of human ALDH1A, an alcohol dehydrogenase, and is thus not involved in FAO but is part of KEGG pathway 'Fatty Acid Metabolism' (Figure 1b). As *CG31075* knockdown also results in reduced ISC sizes (Figure S4d,e), it is a tempting candidate for future studies involving metabolism of ISC.

These data suggest that *miR-277* target genes are differently regulated between Dl^- and Dl^+ ISC and enriched in both populations (Figure 5c,d) compared to the cell types of the intestinal lineage. In accordance with our in silico data on ISC metabolic gene expression, this suggests that ISC are characterized by FAO and that ISC, from a metabolic point of view, are dissimilar to EB that can be clearly distinguished by published marker genes (Figure 5b–d) [5,20,44]. Together, our analysis and experiments show high expression of FAO genes in qISC gradually declining towards terminal EC differentiation (Figure 5e), a tempting lead towards understanding of ISC metabolism, which we sought to experimentally address in the following.

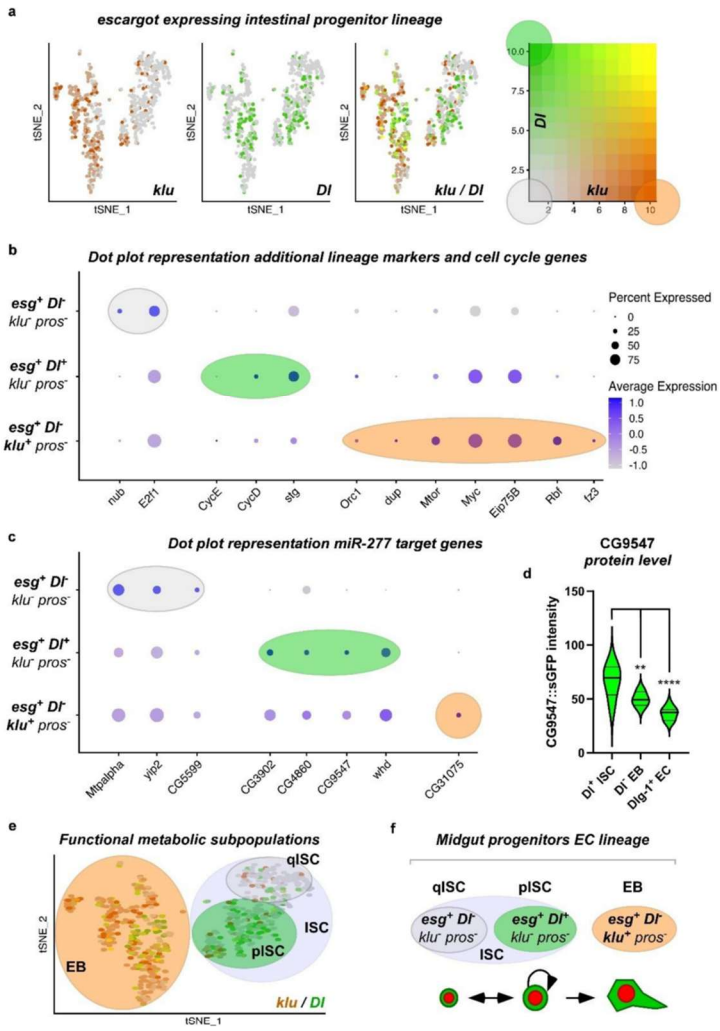

Figure 5. Subclustering of ISC/EB using combined expression of *esg*, *Dl*, *klu*, and *pros* identify quiescent and proliferating ISC within the ISC cluster. (**a**) The analysis of *Dl* and *klu* expression levels in the escargot positive intestinal progenitor lineage identifies 3 populations within the esg^+ ISC/EB cell cluster: klu^+, Dl^- (red), Dl^+, klu^- (green), and Dl^-, klu^- (grey). Double positive cells are not identified confirming the mutual exclusivity of these markers. (**b**) Dot plot representation of additional lineage markers and cell cycle genes shows high expression of quiescence marker *nub* in esg^+, Dl^-, klu^-, and $pros^-$ quiescent ISC (qISC), whereas expression of cell cycle genes *CycE*, *CycD*, and *stg* is high in esg^+, Dl^+, klu^-, and $pros^-$ proliferating ISC (pISC) and expression of EB markers like *Eip75B* is highest in esg^+, Dl^-, klu^+, and $pros^-$ EB cell cluster. (**c**) Dot plot representation of *miR-277* target genes identify the differentially expressed FAO genes *Mtpalpha*, *yip2*, and *CG5599* as quiescent ISC (Dl^-) markers. *CG3902*, *CG4860*, *CG9547*, and *whd* are higher expressed in proliferating ISC (esg^+, Dl^+, klu^-, and $pros^-$). *CG31075* is the only *miR-277* target gene showing higher expression in EB (esg^+, Dl^-, klu^+, and $pros^-$). (**d**) CG9547 protein expression levels significantly decline in the ISC lineage (n = 6, 8, 9; ANOVA: ** $p < 0.01$, **** $p < 0.0001$). (**e**,**f**) cartoons depicting esg^+ intestinal progenitor lineage clusters can be further subdivided in qISC (grey circle), pISC (green circle) and EB (orange circle) upon expression of *Dl*, *klu*, and *pros*.

2.5. miR-277 Levels affect Midgut Homeostasis and Progenitor Survival

Taking advantage of the accessible and versatile genetic toolbox of *Drosophila*, we set out to investigate whether there are consequences of altered expression levels of genes involved in FAO metabolism in ISC. Like its human counterpart, the adult *Drosophila* midgut is replenished by tightly controlled ISC division and differentiation of progenitors into absorptive enterocytes (EC) and secretory enteroendocrine cells (EE) [11,12,14] (Figure 6a). To better understand the function of *miR-277* in intestinal homeostasis , we employed the ' *ReDDM*' tracing system (Repressible Dual Differential Marker) [3,21,30]. *ReDDM* allows determination of tissue turnover with temporal control of tracing and simultaneous expression of further UAS-driven transgenes. The spectrum of possible effects that we can detect and decipher using *ReDDM* ranges from proliferation, differentiation, and over apoptosis to aberrant cellular morphology [3,5,6,21,30].

The principle of *ReDDM* relies on differential marking of cells having active or inactive *Gal4* expression with fluorophores of different stability. Combined with the enhancer trap *esg-Gal4*, esg^{ReDDM}, double marks qISC, pISC, and EB driving the expression of *UAS-CD8::GFP* (>*CD8::GFP*) with short half-life and >*H2B::RFP* with long half-life (Figure 6a). Crosses are grown at 18°C in which transgene expression is repressed by ubiquitous tubulin-driven temperature sensitive $Gal80^{ts}$. By shifting adult females to 29 °C, $Gal80^{ts}$ is destabilized, in turn enabling spatiotemporal control of esg^{ReDDM} tracing and additional UAS-driven transgenes including *UAS-Cas9,* important in experiments making use of CRISPR-Cas9 (Figure S7a–f, $esg^{ReDDMCas9}$). Upon epithelial replenishment, newly differentiated epithelial EC and EE stemming from ISC divisions retain RFP^+-nuclei due to fluorophore stability and show gradual renewal of the intestinal epithelium (Figure 6b–d) [3].

By crossing esg^{ReDDM} with flies carrying either UAS-constructs encoding for *miR-277* or a *miR-277-sponge (miR-277-sp)*, we investigated overexpression and knockdown of *miR-277*. MicroRNA sponges contain multiple complementary binding sites to the seed sequence of a microRNA of interest (Figure 6e) and reduce endogenous microRNA levels in both flies and human cell culture [31,32]. Intriguingly, raised levels of *miR-277* led to significantly reduced ISC and EB numbers compared to controls after seven days of tracing and transgene expression (Figure 6f,h,i). Consequently, numerical loss of ISC and EB (Figure 6h) impairs intestinal homeostasis reflected by the lack of newly generated EC (Figure 6i). Strikingly, forced *miR-277* levels affect ISC and EB survival displayed by membrane-blebbing and nuclear fragmentation (Figure 6f inset, Figure S4a), both hallmarks of apoptotic progenitors in the intestine [21].

Conversely, knockdown of *miR-277* using miR-277 sponges leads to accumulation of mature EB accompanied by low numbers of small diploid ISC (Figure 6g, morphological identification of esg^{+3}). Progenitor numbers and tissue renewal is significantly increased compared to controls (Figure 6h,i), which suggests a requirement for optimal *miR-277* levels in ISC survival and differentiation of EB to epithelial EC. EE differentiation was addressed by immunostaining with the EE marker prospero [11,12,29], but is not affected by *miR-277* manipulations (data not shown).

In addition, the survival of ISC and EB upon forced *miR-277* expression is rescued by baculoviral P35 (Figure S4b,b') underlining that the observed form of cell death is apoptosis [45]. However, rescued progenitors remain small in size and rarely divide suggestive for an additional proliferation and growth-related impact of *miR-277* (Figure S4b'). Apoptosis of ISC upon *miR-277* expression reveals their dependence on proper *miR-277* levels, which led us to hypothesize that ISC depend on proper regulation of genes involved in FAO metabolism. As microRNAs are known to post transcriptionally regulate many genes, we sought to directly address FAO with RNAi against individual FAO genes in the next experiments.

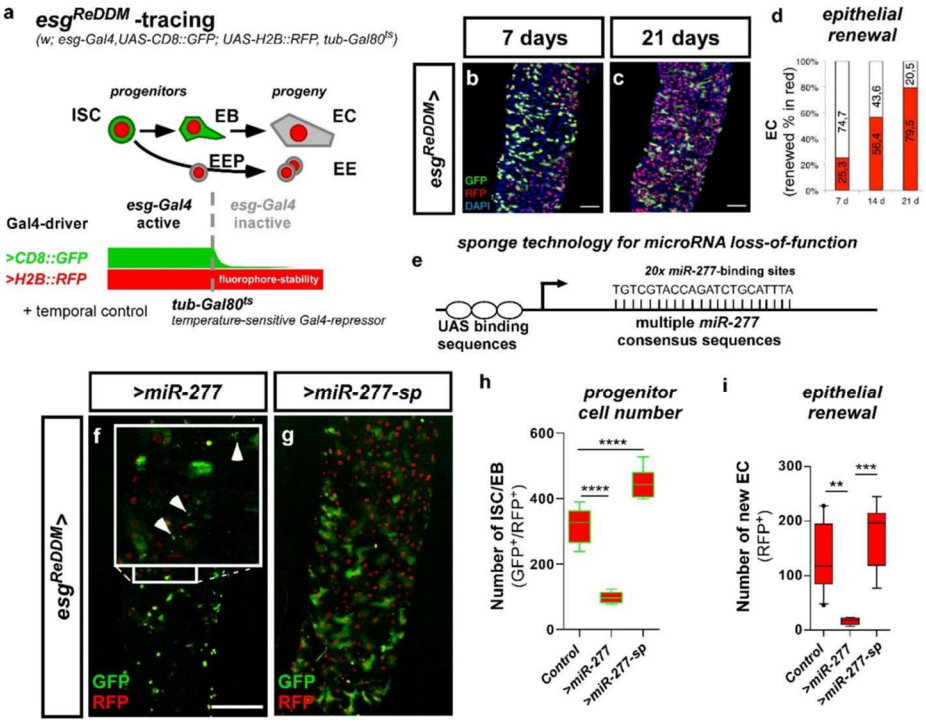

Figure 6. *esg*^{ReDDM} tracing of stem cell production and manipulation of *miR-277* in ISC and EB. (**a**) The expression of two different fluorophores (*CD8::GFP* and *H2B::RFP*) is driven by the ISC and EB specific driver *esg-Gal4*. EB differentiating to epithelial EC loose *esg-Gal4* driven CD8::GFP, while stable H2B::RFP persists. Also, the enteroendocrine precursors (EEP) and their progeny (EE) loose the *esg-Gal4* driven CD8::GFP, but retain the H2B::RFP. The expression of UAS-driven transgenes is temporally controlled by a ubiquitously expressed temperature-sensitive Gal80^{ts} repressor, which is inactivated by a temperature shift to 29 °C. (**b**,**c**) show tracing in control (*esg*^{ReDDM}>/*w*^{1118}) adult *Drosophila* mated females. EB integrate in the epithelium as EC or EE (GFP$^-$/RFP$^+$) revealing midgut turnover rate under physiological conditions after 7 days (**b**) and 21 days at 29 °C (**c**). (**d**) Quantification of epithelial renewal in adult PMG traced for 7–21 days (**a**–**d**, modified from Antonello et al., 2015). (**e**) Schematic of loss-of-function by microRNA sponges achieved by the expression of multiple consensus sequences for the according microRNA. (**f**) *esg*^{ReDDM} driven overexpression of *miR-277* resulting in cell death of presumably small GFP$^+$/RFP$^+$-ISC (inset arrowheads). (**g**) Depletion of *miR-277* with a UAS-driven sponge titrating intracellular *miR-277* levels. (**h**,**i**) Quantification of ISC/EB-numbers (**h**) and EC renewal (**i**) in *miR-277* overexpression and knockdown after 7 days in R5a/b (n = 13, 5, 8; ANOVA: ** $p < 0.01$, *** $p < 0.001$, **** $p < 0.0001$). (scale bar is 50 µm in (**b**,**c**,**f**,**g**)).

2.6. miR-277 and FAO Deficiency affect ISC Morphology and Subsequently Survival in Physiology and Pathology

Our findings of *miR-277*-induced apoptosis are of great interest as apoptotic mechanisms controlling ISC survival are unknown and harbor therapeutic potential as ISC are the cells of origin for colorectal cancer (CRC). Cellular growth, mitochondrial maturation and endoreplication are hallmarks during the differentiation process from ISC to EC [3,5,19–21,30]. In previous experiments (Figures 6f and S4a) we observed that when *miR-277* induced apoptosis is blocked with p35, ISC survive although much smaller in size (Figure S4b' arrowheads). Thus, we sought to address consequences of *miR-277*-mediated

FAO gene knockdown and individual FAO gene RNAi knockdown on ISC size and survival using esg^{ReDDM} [3,30].

After seven days of knockdown using esg^{ReDDM}, we found no indication of apoptosis, but significantly decreased ISC size upon forced *miR-277* expression (Figure 7b) and after knockdown of individual FAO genes (*CG4860*, *CG9547*, *Mtpalpha* and *yip2*, Figure 7d–h), possibly reflecting a disruption of metabolic energy supply for metabolic growth. Conversely, knockdown of *miR-277* using *miR-277-sponges* increased ISC size (Figure 7c,h). Strikingly, *yip2*, the enzyme catalyzing the last step of FAO, also revealed the strongest impact on ISC size (Figure 7h) and followed the pseudotime differentiation (Figures 3b and 5b). Together, these experiments show a strong impact of FAO genes for ISC growth and that our observation of *miR-277*-induced apoptosis is not caused by the regulation of other *miR-277* targets.

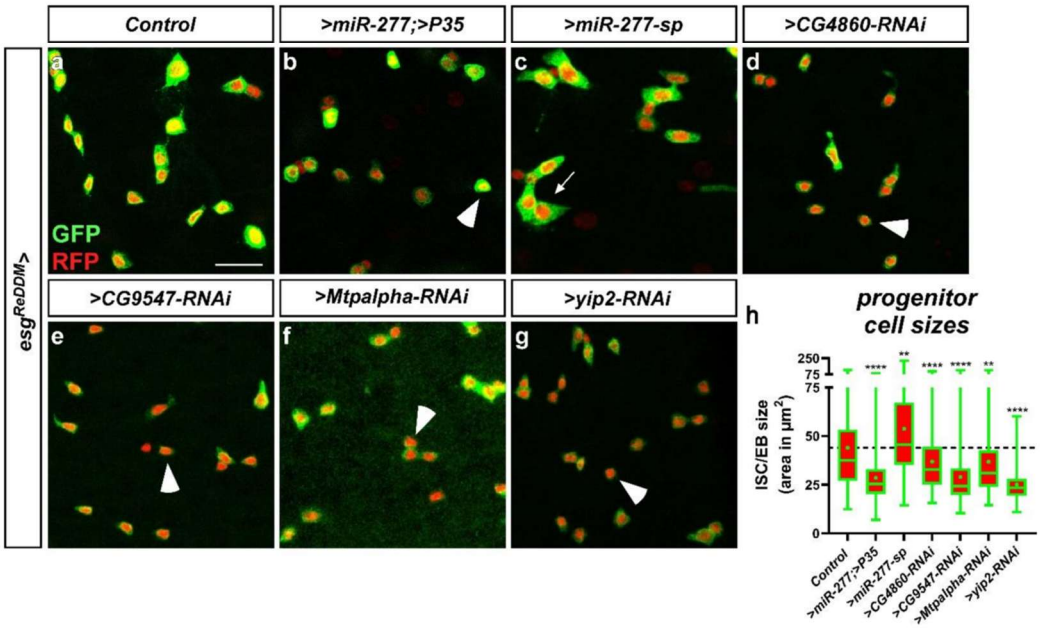

Figure 7. esg^{ReDDM} tracing with manipulation of *miR-277* and *miR-277* target genes from FAO in ISC/EB. (**a**) Confocal image of control PMG (R5a/b) after 7 days showing normal ISC and EB-numbers and sizes. (**b**) Forced expression of *miR-277* with block of apoptosis by P35. Arrowheads point to small ISC, whereas arrows indicate particularly and unusually big ISC. (**c**) Knockdown of *miR-277* using *miR-277-sponges* increases the number of ISC/EB with enlarged size (**c**,**h**). (**d**–**g**) knockdown of *miR-277* target genes from FAO results in a higher number of small ISC ((**d**–**h**), arrowheads). (**h**) Quantification of ISC/EB-sizes in manipulations of *miR-277* and knockdown of *miR-277* target genes after 7 days in R5a/b (n = 200, 199, 150, 150, 199, 150, 150; ANOVA: ** $p < 0.01$, **** $p < 0.0001$). (scale bar is 20 µm).

In contrast to *miR-277*, FAO gene RNAi did not result in ISC apoptosis after seven days. However, after 21 days of RNAi-mediated *CG5599* and *Mtpalpha* knockdown, we observed membrane-blebbing and nuclear fragmentation indicating apoptosis in progenitors (Figure S5j,k, arrowheads). Generally, RNAi-mediated knockdown should resemble downregulation comparable to forced expression of a microRNA. Our data in Figure S5 suggests that RNAi is probably less effective than an endogenous microRNA evolved to regulate these genes, which might account for this phenotypic delay. Together these data suggest a crucial role of FAO as energy source for ISC that is subsequently essential for

their survival. Intrigued by the effects of FAO gene depletion reduction on ISC survival, we wanted to study ISC survival with greater detail in a benign pathological context.

2.7. miR-277 in a Benign ISC Tumor Model

The discovery of *miR-277*-mediated ISC survival is intriguing, as ISC are known to resist radiation and chemically induced apoptosis. ISC have been established as cell of origin for colorectal cancer (CRC) in the mammalian and fly intestine [46–49]. While several mitogenic factors have been described, no factors regulating ISC survival have been identified [50] and might bear high therapeutic value. We previously described that revealing cell death in vivo is challenging as dying cells are cleared off rapidly from the intestinal epithelium by macrophages [21], which hampers quantification and might result in underestimation of apoptotic cell loss.

Here, we sought to circumvent this issue by raising the number of ISC using the established Notch (N) loss-of-function (LOF) tumor model (Figure 8a) [5,51]. N LOF results in the accumulation of ISC-like cells that are unable to differentiate (Figure 8a,b) [21]. Using esg^{ReDDM} tracing in combination with N LOF and forced *miR-277* expression (Figure 8c), we found no effect on tumor number (Figure 8e), composition (Figure S6b), and size (Figure S6a). Strikingly, we found N-tumors with forced *miR-277* expression to undergo high rates of apoptotic cell death (Figures 8f and S6c,c') and ISC-like cells are significantly reduced in size (Figure 8h). In addition, new epithelial EC differentiate from the tumors, which might reflect an escape from apoptosis through differentiation (Figure 8g).

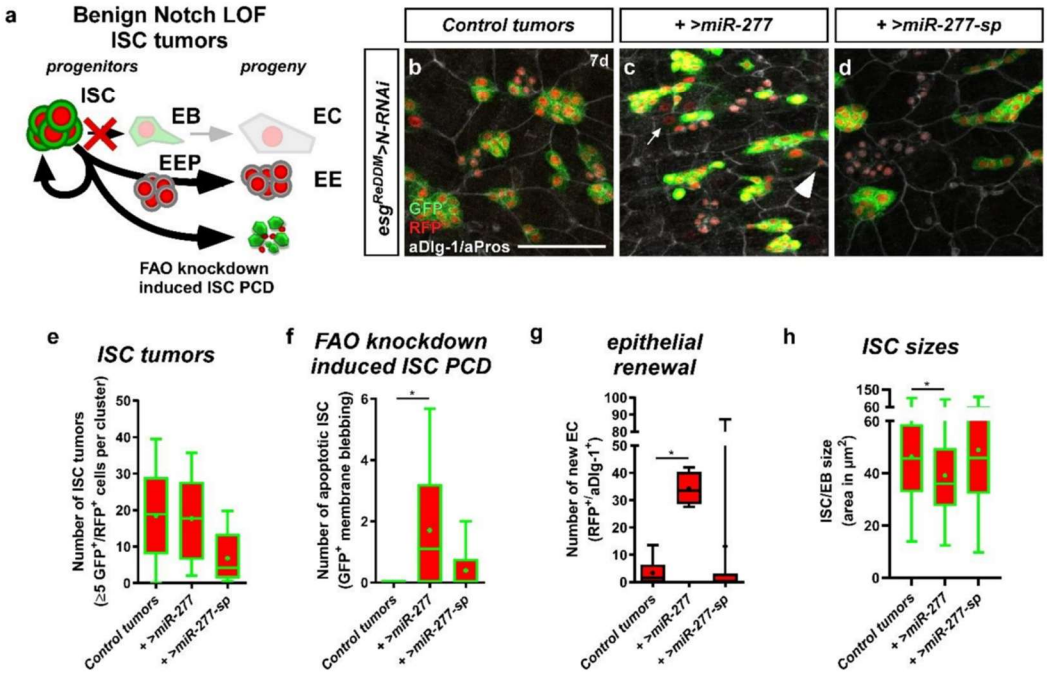

Figure 8. esg^{ReDDM} tracing and manipulation of *miR-277* in the benign Notch tumor model. (**a**) N LOF in ISC/EB prevents EB specification through N signaling and EC production, thus resulting in a stochastic rate of symmetric ISC divisions (ISC tumor formation) and the production of EE (EE tumor formation). We added ISC apoptosis caused by overexpression of *miR-277* as a possible outcome for ISC division (apoptotic ISC, aCasp3 positive, Figure S6c–c'). (**b**) esg^{ReDDM} tracing combined with *N-*

RNAi driven in ISC and EB results in the formation of ISC tumors (GFP^+/RFP^+) and EE tumors ($GFP^-/RFP^+/aPros^+$) and a reduced number of renewed EC ($GFP^-/RFP^+/aDlg\text{-}1^+$) in midguts of mated female flies after 7 d at 29 °C. (**c**) Simultaneous overexpression of *miR-277* in the Notch tumor model is not affecting ISC nor EE tumor formation, but shows a significant increase in apoptotic ISC indicated by membrane blebbing (**c**,**f**, arrowhead), an increased production of newly differentiated EC (**c**,**g**, $GFP^-/RFP^+/aDlg\text{-}1^+$, arrow), and significantly reduced ISC size (**h**). (**d**–**g**) Knockdown of *miR-277* in the Notch tumor model has no effect on tumor formation (**e**), number of apoptotic ISC (**f**), nor the number of renewed EC (**g**). (**e**–**g**) Quantification of number of ISC tumors (**e**), number of apoptotic ISC (**f**), and number of new EC (**g**) of *miR-277* manipulations in the Notch tumor model after 7 days in R5a/b normalized to an area of 100,000 μm^2. (**h**) Quantification of ISC sizes (n = 8, 6, 7/8, 8, 7/8, 8, 7/75, 150, 121; ANOVA: * $p < 0.05$). (scale bar is 50 µm).

Loss of programmed cell death is observed during tumorigenesis and is a hallmark of malignant growth. The basis of the used benign model, LOF of N receptors, is not a frequent alteration observed in CRC tumorigenesis, which is why we designed and established the first *Drosophila* model of CRC that is based on CRISPR-Cas9-induced gene excision (Figures 9a and S7a). Individual conditional CRISPR-Cas9 gene editing of single tumor suppressors was recently shown to induce similar benign intestinal tumors [52]. We chose to mimic sporadic CRC development by targeting frequently mutated genes simultaneously that were previously shown to induce all hallmarks of CRC [49]. For that purpose, we advanced a cloning protocol for multiplex single-guideRNA arrays involving 'scarless' ligation with high efficiency (Figure S9) [53].

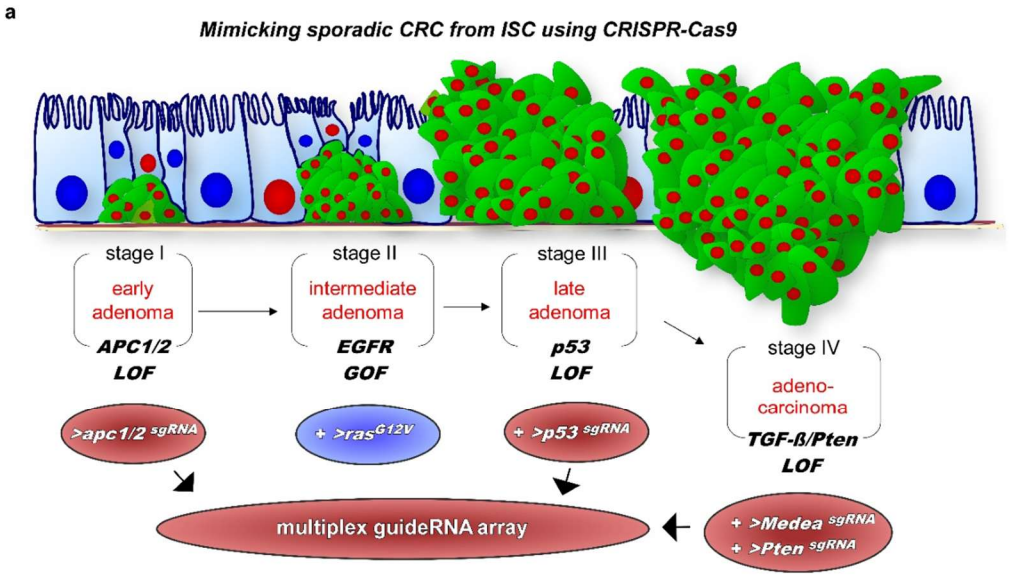

Figure 9. *Cont.*

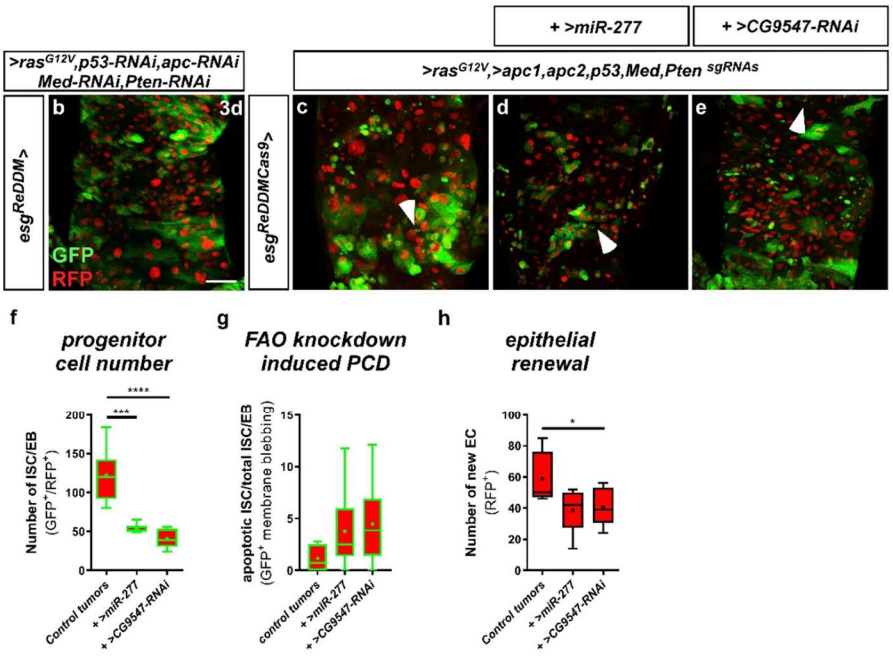

Figure 9. esg^{ReDDM} tracing and overexpression of *miR-277* in a newly established colorectal cancer (CRC) model based on CRISPR-Cas9 excision. (**a**) A newly established *Drosophila* model for CRC combines the esg^{ReDDM} tracing system with expression of *Cas9* and single guideRNAs (sgRNAs) targeting the *Drosophila* orthologs of the most frequently mutated tumor suppressors in CRC patients. Early adenoma-like lesions and hyperactive Wnt/wg signaling are induced by knockout of the Apc orthologs *apc1* and *apc2*. Additional expression of an oncogenic ras^{G12V} leads to an activation of EGFR signaling, knockout of *p53*, and knockouts of the TGF-ß ortholog *Medea* and *Pten* mimic sporadic CRC patient-like carcinoma. In this model, the hallmarks of colorectal cancer, namely, (i) an increased SC proliferation, (ii) decreased differentiation to epithelial cells, (iii) a decreased apoptosis rate, and (iv) cell migration through the basal membrane, can be modeled and analyzed. Here, we used this model to investigate *miR-277* overexpression in CRC-like modified ISC. (**b**) esg^{ReDDM} tracing combined with the RNAi-based *Drosophila* CRC model established by Bangi et al. 2016 results in the formation of ISC/EB cell clusters (GFP^+/RFP^+) and an increased EB growth in midguts of mated female flies after 7 d at 29 °C. (**c**) $esg^{ReDDMCas9}$ tracing combined with our new CRISPR-Cas9-induced CRC model reflects all CRC characteristics previously observed by Bangi and colleagues [49]. In detail, Cas9 excision of sporadic CRC associated genes leads to the formation of ISC/EB cell clusters, increased EB growth and PCD of ISC/EB indicated by membrane blebbing (arrowheads) in midguts of mated female flies after 3 d at 29 °C. As a consequence, overall survival of CRC flies is strongly reduced to about one week. (**d**,**e**) Simultaneous overexpression of *miR-277* (**d**) or RNAi mediated knockdown of *CG9547* (**e**) in the CRISPR-Cas9-induced CRC model reduces the number of ISC/EB compared to control tumors and reduces EB differentiation. (**f**–**h**) Quantification of ISC/EB numbers (**f**), number of apoptotic ISC/EB (**g**), and number of newly differentiated EC (**h**) of the newly established CRISPR-Cas9 induced CRC model and simultaneous overexpression of *miR-277* after 3 days in an area of 40,000 μm^2 in R5a/b (n = 7,6,6/7,6,6/7,6,6; ANOVA: * $p < 0.05$, *** $p < 0.001$, **** $p < 0.0001$). (scale bar is 50 µm).

GuideRNAs in our model are under control of a UAS promoter and target *apc1, apc2 (adenomatous polyposis coli 1&2), p53, Medea (dSmad4)* and *Pten (Phosphatase and tensin homolog)* (Figure S7g,h). Transgenic flies were injected and subsequently recombined with flies harboring oncogenic $>ras^{G12V}$, reflecting EGFR signaling gain of function (Figure 9a).

To allow simultaneous Cas9 excisions, tracing, and UAS-driven genetic manipulations in ISC, we recombined an *UAS-Cas9.P2* transgene into the esg^{ReDDM} tracing flies ($esg^{ReDDMCas9}$) (Figure S7a–c). In control experiments, ISC and EB appear more rounded upon Cas9.P2 expression (Figure S7c) in accordance with a previous study [52], but their numbers remain constant comparable to esg^{ReDDM} controls (Figure S7b) and also tissue homeostasis is not disrupted after seven days (Figure S7d,e). Additionally, we approached the efficiency of CRISPR-Cas9 events and found a 99% reduction crossing single guideRNA flies targeting CD8::GFP in esg^{ReDDM} (Figure S7f), proving highly efficient excision. One of several advantages of our CRISPR/Cas9-based model over previous CRC models [49] is the irreversibility of Cas9 excision, which also excludes possible compensation of RNAi-mediated knockdown.

2.8. miR-277 and Colorectal Tumorigenesis

Firstly, we compared the CRC model from Bangi et al., 2016 [49] (Figure 9b) with our new model with CRISPR-Cas9 excision of *apc1/2, p53, Medea,* and *Pten* in conjunction with oncogenic ras^{G12V} (Figure 9a). Using $esg^{ReDDMCas9}$ as an ISC-specific driver for intestinal tumorigenesis [46–49], virtually all ISC should be converted into aberrant CRC tumor stem cells (Figure S7f). Intestines of both CRC models showed strong proliferation, defective differentiation, overgrowth of progenitor cells, and multilayering (Figure 9c,d) revealed by additional esg^{ReDDM} tracing. Traced ISC and their progeny can be differentiated using specific markers for EC and EE (not shown). Progenitor cell production as well as turnover of the midgut is dramatically accelerated and after only 48–72h, the remaining hypotrophic epithelium consists of new EC only. Of note, complete renewal of the midgut epithelium in non-tumoral controls usually takes about 4 weeks [3,30].

Reprogramming of fatty acid metabolism was previously observed in various tumor entities [54]. We thus wanted to address whether *miR-277*, and thus expression levels of FAO genes, is affected in our CRC model. Therefore, we crossed the *miR-277* sensor flies to our CRC model and investigated whether *miR-277* levels change upon tumor induction (Figure S8a). esg^{ReDDM} tracing allows distinguishing between manipulated tumoral and unmodified intestinal cells (inset Figure S8b–c'). By determining GFP fluorescence intensity, we found that GFP levels inside of tumoral tissue are significantly higher than in the surrounding cells (Figure S8d). Thus, *miR-277* levels are reduced in cells of the tumoral tissue, suggesting higher expression of FAO genes (Figure S8e).

Finally, we aimed at testing a putative favorable role of *miR-277* and FAO genes and investigated whether forced *miR-277* expression in our CRC model affects ISC-like cell survival, like in benign Notch tumors (Figure 8c,f,h). In our CRC model tumors, sporadic CRC gene deletions induce pleiotropic phenotypes including proliferation, differentiation, cellular growth, and multilayering (Figure 9a,c–e). On top of that, intestines with forced *miR-277* expression (Figure 9d) or RNAi-mediated knockdown of *CG9547* (Figure 9e), and thus, reduced levels of FAO gene expression, present further clearly distinct phenotypes (Figure 9c–e): (i) progenitor cells undergo apoptosis but with a similar frequency as controls (Figure 9g), which is probably owed to p53 deletion (Figure 9a); (ii) progenitor cell number (Figure 9f) and progeny are strongly reduced (Figure 9h).

In summary, our findings suggest an important role of *miR-277*-regulated FAO genes in intestinal stem cell metabolism. Using physiological and pathological paradigms, we show that suppressed FAO gene expression clearly affect intestinal stem cell size and once *miR-277*, in its role as a pan-FAO gene regulator, is forcedly expressed, ISC even become apoptotic, hampering tumoral growth. These findings are especially important in a pathological context as so far, no specific triggers for intestinal stem cell survival have been described. Our in vivo findings on intestinal stem cell metabolic gene expression might thus pave the way for future investigation of fatty acid oxidation as a promising new therapeutic target in colorectal cancer, but also other tumor entities relying on similar metabolic cues.

3. Discussion

Physiological in vivo data on stem cell metabolism is scarce owing to the complexity of experimental setup and availability of proper genetic sensors and tools. Here, we employed the fruit fly *Drosophila melanogaster,* taking advantage of its exhaustive genetic toolbox to study SC metabolism in an adult organism and investigated the metabolic gene expression profile of intestinal stem cells following leads from combined in silico resources. Building on the identification of *miR-277* as a negative regulator of fatty acid β-oxidation (FAO), our data hint to a new and quiescent ISC population that depends on lipids as an energy source. In contrast to dispensable OXPHOS [20], a previous study discovered lipolysis involved in ISC survival [55]. In functional experiments, we discovered that FAO gene expression is essential for ISC survival, providing detailed insight on the metabolic cues by identifying *miR-277* as controller of the majority of FAO enzymes, and show that they are capable of eliciting ISC starvation and subsequent apoptosis. Our data however cannot exclude effects of a *miR-277*-dependent regulation of further pathways, like BCAA catabolism [25], and further *miR-277*-regulated genes involved in similar phenotypes. ISC apoptosis can be triggered under physiological conditions, in turn disrupting tissue homeostasis, but importantly, is also observed in pathological contexts in a benign tumor model. In addition, FAO-deprived ISC show strongly reduced tumor size in a new CRISPR-Cas9 fly model of colorectal cancer.

3.1. A Putative Role of Fatty Acid β-Oxidation in Controlling Quiescence in Stem Cells and their Lineage

The most important cue of our study, that requires and definitely warrants future investigation, is the discovery that ISC can be metabolically subdivided into a quiescent and an active ISC population using established markers [11,12,21,29,36] and existing scRNAseq data [13]. Although our data only provide a first step towards understanding the metabolic differences between quiescent and active ISC, several of our functional investigations support this hypothesis: (i) direct FAO downregulation by *miR-277* and (ii) specific individual knockdown of FAO enzymes affects ISC size and (iii) subsequently their survival.

Stalling FAO as an energy source is thought to cause rapid depletion of acetyl-CoA [56]. Studies in yeast show that acetyl-CoA levels serve as checkpoint between quiescent and proliferative state. Furthermore, high acetyl-CoA drives the acetylation of histones with loci encoding for growth regulatory genes [57,58]. EB growth has previously been shown to depend on input from EGFR-Ras signaling and occurs in parallel with endoreplication and glycolysis during EB differentiation to polyploid absorptive EC [3,20,30,44,59]. Cellular growth is a crucial process that might require the anabolic generation of cell membrane from fatty acids. It is tempting to speculate that *miR-277* expression reflects a switching mechanism for fatty acid usage between metabolic energy generation in quiescent ISC and cell membrane generation necessary in mitotically active ISC and growing EB. In line with this, SC in the *Drosophila* testis requires mitochondria and accumulates fatty acids when mitochondrial fusion is genetically ablated [60]. Interestingly, it was previously observed that knockdown of FAO enzymes phenocopy mitochondrial fusion defects [60,61]. A single study observed mitochondria in long cellular protrusions of intestinal progenitors, but did not perform any functional studies [62]. Studying the interplay between FAO and mitochondrial function in ISC and EB will be a fascinating topic for future studies.

The prime candidate pathway switching from quiescence to active ISC state and progenitor maturation is EGFR-Ras signaling. Apart from growth, EGFR stimulates proliferation in ISC under homeostatic conditions [20,44,59,63] and deprivation of EGFR signaling leads to programmed cell death of EB [21]. Interestingly, ISC are spared from blockade of EGFR-induced apoptosis and survive as mitotically inactive singletons supported by lineage tracing in two publications [21,59]. This further supports the idea that quiescent ISC are capable of surviving without EGFR input probably by relying on FAO as an energy source. Future efforts will aim to further dissect this metabolic switch. Central to resolve

this issue is to reveal specific signals and conditions driving stem cells into FAO metabolism, such as is already known for fasting [64].

3.2. miR-277, Fatty Acid Oxidation and ISC Apoptosis

A commonality of all investigated FAO genes is their role in mitochondrial FAO and high levels of FAO genes in ISC further support the hypothesis that ISC harbor immature mitochondria [20]. Direct molecular interactions linking apoptosis and FAO have been described in various in vitro approaches, including human CRC cell lines [65–67]. In accordance with our data and a role for FAO in metabolism and subsequent ISC loss, our data shows that the CPT1A orthologue, *whd* (*withered)*, diminishes progressively in the reconstructed lineages (Figure 3b). The *whd* orthologue catalyzes the transport of long-chain fatty acids from the cytoplasm to the mitochondria and *whd* mutants are highly sensitive to starvation and oxidative stress [68]. Further FAO genes follow that expression pattern from ISC declining to EC lineage: *CG3902 (acyl-CoA dehydrogenase), CG5599 (dihydrolipoamide branched chain transacylase E2), CG9547 (glutaryl-CoA dehydrogenase), Mtpalpha (mitochondrial trifunctional protein),* and *yip2 (acetyl-CoA C-acetyltransferase)* (Figures 3b and 5c), which catalyzes the last step of FAO [69].

Studies in yeast support the idea of a connection between FAO and apoptosis induced at mitochondria as the *yip2* orthologue ACAA2 interacts with proapoptotic BNIP3, a known interactor of Bcl-2, controlling cell survival [69]. Furthermore, murine ISC induce FAO upon fasting which in turn improves regeneration. The same authors found that ISC diminish over time when Cpt1a, the rate-limiting carnitine palmitoyltransferase in FAO, is genetically disrupted [56,64]. In our functional experiments, we could show that FAO knockdown in ISC phenocopies *miR-277*-induced starvation and subsequent apoptosis (Figure 7a–h).

In a previous study we found that progenitors undergoing apoptosis are cleared off rapidly e, which we circumvented by genetically increasing the number of ISC with the benign Notch tumor model. FAO depletion upon forced *miR-277* expression drives a significant number of ISC into apoptosis, despite the pro-survival signal from N LOF [21]. The same experiments also showed that significantly more progenitors from N tumors escape cell death by differentiating to EC fate. This N-independent differentiation behavior was observed before for factors inducing EC fate [5,21,40]. In our case it might reflect a locally controlled metabolic switch of ISC to an early EB fate allowing OXPHOS by activating mitochondrial energy production and thus FAO independent survival and differentiation to EC.

It was also observed that mitotically active ISC in N tumors are located at the outer rim of the ISC clusters, where they are capable of receiving mitogens like the EGF-ligand *spitz* [51]. Thus, central ISC in an N tumor mass might become quiescent and, in case of additional >*miR-277,* undergo apoptosis because FAO cannot be activated (Figure 8f). Unfortunately, we and others failed to obtain reliable cleaved caspase 3 stainings in N tumors (Parthive Patel, personal communication) [51]. *miR-277*-induced apoptosis would in turn select for FAO-independent pISC, which might provide an explanation for the tendency of higher cell numbers (Figure S6a) found in our experiments. It will be an interesting topic for future studies to elucidate which factors sense and stimulate the necessity to enter quiescence.

3.3. The Role of miR-277 and FAO Genes in a CRC Model

Our observed dependence of ISC on FAO is of high importance as ISC are the established cells of origin for CRC in the mammalian intestine [46–49,55]. Furthermore, *Drosophila* ISC are known to resist radiation and chemically induced apoptosis [21,50], and in rodents, quiescent +4 ISC, but not LGR5^{+} ISC, are indispensable for intestinal homeostasis following radiation [70–74]. It is thus tempting to speculate that *Drosophila* and mouse ISC and patient CRC-SC have similar apoptotic dependencies. Until now, no other factors than FAO regulating ISC survival have been described [50,55,64]. Survival in

various tumor entities depends on EGFR signaling, which is strongly altered in about two thirds of sporadic CRC patients [49]. The drugs Cetuximab and Panitumumab containing antibodies targeting EGFR signaling have become standard therapy [49,75]. Both drugs are highly effective in neoadjuvant therapy as tumor mass is strongly reduced, which facilitates timely resection before therapy resistance develops. However, resection remains the indispensable step for successful treatment as the vast reduction of tumor mass after treatments results from the reduction of transient-amplifying (TA)-like cells through (i) reduced EGFR-dependent ISC proliferation resulting in less TA cells, but more strikingly from (ii) a reduction of the more numerous, rapidly dividing TA cells. Additionally, data in *Drosophila* suggests that the analogous cell type to mammalian TA cells, the EB, respond to EGFR inhibition with apoptosis [21].

Unfortunately, fly ISC and human CRC stem cells do not share the apoptotic sensitivity of TA cells to EGFR antibody treatments, but are driven into quiescence [76]. It is tempting to speculate that quiescence and change to FAO metabolism enable CSC to survive treatment and in turn might explain rapid CRC recurrence after treatment. Drug therapy is known to exert selective pressure additionally promoting for e.g., oncogenic RAS or BRAF variants and thus contribute to the active selection for therapy-resistant tumor stem cells. Interestingly, using our newly developed CRC model, we found that introducing a mutational pattern resembling spontaneous CRC into ISC renders ISC resistant to *miR-277*/FAO-induced apoptosis. During the stepwise and stage-specific tumorigenesis, p53 mutation results in aberrant survival of tumor cells. As a consequence of loss of pro-apoptotic p53 in our CRC model, we found that ISC gain capability to withstand forced *miR-277* expression (Figure 9f) in contrary to benign Notch tumors in which apoptosis can still take place normally (Figure 8f).

Loss of p53 is a key event in human colorectal tumorigenesis and our findings may add to the understanding of metabolic changes conferring survival and possibly also further tumor properties. Indeed, data from other tumor entities shows that cancer SC utilize FAO for self-renewal and resistance to chemotherapy [43,77]. The dependence of adult stem cells on mitochondrial FAO and lipid metabolism for their maintenance is not only highlighted in our study, but has also been evidenced in mammalian hematopoietic and neural SCs [78,79]. Our data provides additional understanding underlining the dependency of ISC on FAO and its control by a microRNA. In follow up studies, the possibilities of combinatorial treatments of FAO together with targeting EGFR might be investigated and their therapeutic combined value will be evaluated to help improve future cancer treatment.

4. Materials and Methods

4.1. In Silico microRNA Target Prediction

Targets of miRNAs are usually predicted by scanning for consensus sequences of their seed sequence in mRNA. Several online tools are available that generate lists of genes predicted to be regulated by a given miRNA. Depending on the stringency of the algorithm used in a particular prediction tool, dozens, up to the magnitude of thousands, of genes are predicted to be targets of a particular microRNA. To combine lists from four different prediction tools (Miranda, Pictar, Targetscan and a miRNA target collection from Bielefeld), we extracted multiple hits from all four tools and restricted the final list of eight genes that showed up in at least three of four predicted target lists (see Figure 1). The list of investigated microRNAs encompasses *miRs-7, 8, 14, 34, 124, 277, 278, 315.*

An earlier in silico study on *miR-277* also identified the BCAA degradation pathway. However, it did not identify multiple hits in endocytosis nor fatty acid metabolism like our study, probably due to the early developmental state of prediction tools for miRNA targets [25,80]. As the vast majority of genes stemmed from FAO, our study focused on FAO metabolism and the role of *miR-277* in ISC.

4.2. Genetics and fly Husbandry/Fly Strains

The following transgenic flies were employed: *esg^{ReDDM}* [3], *NRE::mCherry* [81], *Gbe+Su(H)dsRed* (T. Klein), *UAS-miR-277* [25], *Mex-Gal4*, *UAS-P35* (Bruce A. Hay), *UAS-ras^{G12V},UAS-p53-RNAi,UAS-apc-RNAi;UAS-Med-RNAi,UAS-Pten-RNAi* [49]. *Ubi-GFP* and *Ubi-miR-277::GFP* sensor flies are kindly provided by Klaus Förstemann. From Bloomington Drosophila Stock Center (BDSC): *UAS-miR-277-sponge* (BL61408), *UAS-CG4860-RNAi* (BL67769), *UAS-CG9547-RNAi* (BL53327), UAS-Mtpα-RNAi (BL32873), *UAS-yip2-RNAi* (BL36874), *UAS-CG4389-RNAi* (BL32873), *UAS-CG5599-RNAi* (BL32876), *UAS-Cas9.P2* (BL58985), *vas-phiC31;attP51C* (BL24482), *vas-phiC31;;attP86Fb* (BL24749), *UAS-ras^{G12V}* (II) (BL64195), *UAS-ras^{G12V} (III)* (BL64196), *U6-EGFP-sgRNA* (BL79393), *UAS-CG31075-RNAi* (BL50654), *UAS-mCherrymitoOMM* (BL66532). From Vienna Drosophila Resource Center (VDRC): *UAS-N-RNAi* (GD14477), *CG9547::sGFP* (v318106).

4.3. Food Composition and Fly Keeping

Fly food contained 1424 g corn meal, 900 g malt extract, 800 g sugar beet syrup, 336 g dried yeast, 190 g soy fluor, 100 g agarose, 90 mL propionic acid, and 30 g NIPAGIN powder (antimycotic agent) in 20 L H_2O. Food was cooked for about an hour to reduce bioburden, then filled into small plastic vials and cooled down to RT. Flies were kept at 25 °C except for crosses with temperature-sensitive GAL80ts (GAL4 repressor) which were kept at 18 °C (permissive temperature) until shifted to 29 °C (restrictive temperature) to activate GAL4-mediated transgene expression. Crosses with *esg^{ReDDM}* were carried out as described previously [3,6,30]. Due to persisting problems with mucous formation on food surface in vials with VF, all experiments distinguishing between mated and virgin female flies were run on food with twice the amount of NIPAGIN. Mucous formation was avoided because of massive induction of tissue renewal by pathogenic stress.

4.4. RNA Isolation and cDNA Synthesis

The midguts from at least 5 mated female flies were dissected and transferred into a droplet of RNA *later* Solution (Invitrogen by Thermo Fisher Scientific, Bremen, Germany) on ice. The dissected tissue was homogenized in 100 µL peqGOLD TriFast (VWR Life Science) and total RNA was isolated as specified by the manufacturer. The following cDNA synthesis was performed with 250 ng of total RNA and the SuperScript IV Reverse Transcriptase (Invitrogen by Thermo Fisher Scientific) using a 1:1 mixture of oligo-dT primers and random hexamers directly upon RNA isolation. Prior to Real-time qPCR, cDNA samples were diluted 1:4 in dH_2O.

4.5. Real-Time qPCR and Conventional PCR

Expression levels of predicted *miR-277* target genes were determined upon forced expression of *miR-277* in enterocytes of midguts from adult *Drosophila*. *Mex^{ts}>* flies were crossed to *w^{1118}* (control) or *>miR-277* flies at 18 °C and their progeny shifted to 29 °C for 24 h prior to RNA isolation and cDNA synthesis before running the qPCRs. After an enzyme activation step (2 min 95 °C), 40 cycles of denaturation (15 s 95 °C), primer annealing (20 s 58 °C) and elongation (30 s 72 °C) were run. SYBR Green intensities were measured at the end of every elongation step and a melting curve was calculated at the end of the PCR reaction. Primers were designed to anneal at 59 °C. Reaction was set up with KAPA SYBR FAST Universal (Roche) in a total volume of 10 µL. All qPCR results were normalized to the house-keeping gene *rp49*. For gel visualization (Figure 1c), the qPCR protocol was used and visualized on 2% agarose gel (Table 1).

Table 1. List of primers used in real-time qPCR to investigate expression levels of predicted target genes of *miR-277*.

Primer	Forward (5′-3′)	Reverse (5′-3′)
Rp49	TGGTTTCCGGCAAGCTTCAA	TGTTGTCGATACCCTTGGGC
miR-277	GCGTGTCAGGAGTGCATTTG	GATTGTACGTTCTGGAATGTCGT
CG31075	TCCGAGGGAGATAAGGCTGA	GAATGCCTTGTCCCGATCCA
CG3902	CTTCTCCCTGAAGACCGTCG	GGATGGCTACCGTGGCATTA
CG4860	CGACCGGGAGGAGCTTTATC	TCCAATCCGGAACCACCATAC
CG5599	TCGATGACGGAATCCCTGAAAA	TCTCCTTGGCCACTAACTGC
CG9547	CAAGCTGATTGGTGCCTTTGG	GCGCACTAGTAATCCACGTCT
MtpAlpha	CCAGTCCTTCGTCATGGACA	CACGGATCACATCGAGAATCTTCA
whd	AACTTCTACGGCACGGATGC	TGCCCTGAACCATGATAGGC
Yip2	CATGAGTTGCAGCGCAAGAAG	GCTGTAGGATTAGACAGCCTCG

4.6. Plasmid Cloning

For cloning of multiple sgRNAs into the pCFD6 plasmid [82], a SapI restriction site in pCFD6 was removed by site-directed mutagenesis (SDM) using a pfu polymerase (Promega) following the QuikChange II-E-Site-Directed Mutagenesis Kit Manual (Agilent). The following primers were used for SDM: pCFD6_SDM_noSapI_for TTGCGTATTGGGCGCACTTC-CGCTTCC and pCFD6_SDM_noSapI_rev GGAAGCGGAAGTGCGCCCAATACGCAA to generate the pCFD6_noSapI plasmid. Successful removal of the SapI restriction site was verified by Sanger Sequencing.

4.7. gRNA Design

The CRISPR Optimal Target Finder [83] was used to design gRNAs and to search for possible off-targets. Gene regions of the tumor suppressors *apc1, apc2, p53, Med, and Pten*, which are orthologous to the most frequently mutated genes in CRC patients [49], were copied into the target finder. Additionally, a gRNA targeting the EGFR signaling repressor *capicua (cic)* was designed to induce an activation of EGFR signaling, which is the second most common step in colon carcinogenesis. CRISPR targets with a length of 20 bp and a 5′ NGG were identified using *Drosophila melanogaster* (reference genome, r_6) as reference. The specificities of identified CRISPR targets were evaluated using the CRISPR Optimal Target Finder [83] with maximum stringency searching for NGG and NAG PAMs in the *Drosophila melanogaster* (reference genome, r_6) reference genome. For each gene the CRISPR target with the lowest number of off-targets was selected (Table 2).

Table 2. List of genes and the specific sequence targeted in the CRC model with number of off-targets predicted by the CRISPR Optimal Target Finder [83].

Targeted Gene	Target Sequence	Number of Off-Targets
apc1	GGGCATCGCCGAGCTCAGTC	3
apc2	GGAGAGACGATCCGCTCAGA	5
cic	GGCTTGCCCGGGGAGCTTAG	4
p53	GGCTATTACGTGCCCCAATA	5
Med	GGTGAAGGACGAATACTCAG	1
Pten	GACGGTTTCTGAATAGGCCC	4

Forward primers for gRNA amplification were designed containing a BbsI or SapI restriction site, the selected guide sequence, and a sequencecomplementary to the gRNA-

core on the pCFD6_noSapI plasmid (5′-3′). Reverse primers for gRNA amplification were designed containing a BbsI or SapI restriction site matching the forward primer, two SapI or BbsI restriction sites contrariwise to the flanking restriction sites, and a sequence complementary to the tRNA sequence of the pCFD6_noSapI plasmid (5′-3′). A linker between the flanking BbsI or SapI restriction sites and the remaining primer sequence was added to enable seamless cloning of multiple gRNAs. The last guide sequence targeting Pten was added to a final reverse primer, which lacks additional restriction sites. PCR reactions were performed using the Q5® High-Fidelity DNA Polymerase (NEB, New England Biolabs) and the pCFD6_noSapI as template DNA. Resulting in fragments of gRNA, gRNAcore, tRNA and two SapI or BbsI restriction sites flanked by BbsI or SapI restriction sites (Figure S9).

The pCFD6_noSapI plasmid contains a gRNAcore followed by a tRNA sequence which are flanked by BbsI restriction sites. The DNA fragment containing the first gRNA1 followed by the gRNAcore sequence, the tRNA sequence, and two SapI restriction sites is also flanked by BbsI restriction sites. This fragment is combined with the plasmid by cutting with the BbsI restriction enzyme prior to ligation. The next DNA fragment contains the second target sequence, gRNA2, and two BbsI restriction sites. This fragment is flanked by SapI restriction sites and added to the plasmid by cutting with the SapI restriction enzyme and ligation. The third DNA fragment is designed as the first one with except for the gRNA sequence, along with others. To create these fragments, primer pairs were designed with forward primers binding the gRNAcore sequence on the plasmid and the specific gRNA sequence and flanking restriction site in a primer extension. The reverse primers consist of a sequence complementary to the tRNA sequence in the plasmid and the specific restriction sites in an extension (Table 3).

Table 3. List of Primers used to amplify gRNA constructs for the CRC model (Colors recapitulate Figure S9).

Primer	Sequence (5′-3′)
BbsI_apc1_for	ATAAGAAGACCTTGCAGGGCATCGCCGAGCTCAGTCGTTTCAGAGCTATGCTGGAAAC
SapI_apc2_for	ATAAGCTCTTCCTGCAGGAGAGACGATCCGCTCAGAGTTTCAGAGCTATGCTGGAAAC
BbsI_cic_for	ATAAGAAGACCTTGCAGGCTTGCCCGGGGAGCTTAGGTTTCAGAGCTATGCTGGAAAC
SapI_p53_for	ATAAGCTCTTCCTGCAGGCTATTACGTGCCCCAATAGTTTCAGAGCTATGCTGGAAAC
BbsI_Med_for	ATAAGAAGACCTTGCAGGTGAAGGACGAATACTCAGGTTTCAGAGCTATGCTGGAAAC
final_rev_Pten_BbsI	ATAAGAAGACCCAAACGACGGTTTCTGAATAGGCCCTGCACCAGCCGGGAATCGAACC
universal_rev_2xSapI_BbsI	ATAAGAAGACCCAAACTGAAGAGCTGAACGGCTCTTCTGCACCAGCCGGGAATCGAACC
universal_rev_2xBbsI_SapI	ATAAGCTCTTCAAACTGGTCTTCTGAAGGGAAGACTATGCACCAGCCGGGAATCGAACC

The pCFD6_noSapI plasmid and the DNA fragment containing the first gRNA flanked by BbsI restriction sites were cut by the BbsI restriction enzyme (NEB, New England Biolabs) prior to ligation of the fragment into the plasmid using a T4 ligase (NEB, New England Biolabs). In the next step, the created plasmid now containing the two SapI restriction sites 3′ of the first gRNA and the second DNA fragment containing the next gRNA flanked by SapI restriction sites were cut by the SapI restriction enzyme (NEB, New England Biolabs) prior to ligation. These steps were repeated until the gRNAs of all six genes were ligated into the pCFD6_noSapI plasmid. The resulting construct was injected into flies containing a phiC31 integrase and an attP docking site.

Transformant flies carrying the construct were identified by eye color produced by a mini-white gene which is inserted into the construct. These flies were used to establish stocks in single crosses. Later successful excisions mediated by the gRNA construct and the Cas9 protein were verified by PCR using primers flanking the targeted gene regions and genomic DNA from fly guts of $esg^{ReDDMCas9}$ controls and $esg^{ReDDMCas9}$>*apc1,apc2,cic,Med,p53,Pten* ^{sgRNAs}

as templates. A knockout of *cic* could not be verified; instead, the *UAS-ras*^{G12V} transgene was added to activate EGFR signaling and the *cic-sgRNA* was left out in the genotypic description.

4.8. Immunohistochemistry

Dissected guts from mated female flies were fixed in 4% PFA in 1XPBS for 45 min. After fixation the guts were washed with 1XPBS for 10 min and stained with primary antibodies 1:500 anti-Ssk (rabbit; [84]); 1:250 anti-Dlg-1 [mouse; Developmental studies Hybridoma Bank (DSHB)]; 1:250 anti-Pros [mouse; Developmental studies Hybridoma Bank (DSHB)], 1:200 anti-Casp3 [rabbit, Cell signalling technology cleaved caspase-3 (Asp175)], 1:200 anti-GFP [chicken, Abcam (ab13970)], 1:200 anti-Dl [mouse, Developmental studies Hybridoma Bank (DSHB, C594.9B)]) diluted in 0.5% PBT (0.5% Triton (Sigma-Aldrich) in 1XPBS) + 5% normal goat serum (Thermo Fisher Scientific, Berman, Germany). Primary antibody staining was performed at 4 °C over night on an orbital shaker. Next, guts were washed with 1XPBS for 10 min and incubated with secondary antibodies (1:500 Goat anti-RabbitAlexa568 [Invitrogen], 1:500 Goat anti-MouseAlexa647 [Invitrogen], 1:500 Goat anti-RabbitAlexa647 [Invitrogen], 1:500 Goat anti-chickenAlexa488 [Invitrogen]) and DAPI (1:1000; 100 µg/mL stock solution in 0.18 M Tris pH 7.4; DAPI No. 18860, Serva, Heidelberg) for at least 1.5 h at RT. After washing with 1XPBS for 10 min the stained guts were mounted in Fluoromount-G Mounting Medium (Electron Microscopy Sciences).

4.9. Image Acquisition

The posterior parts of stained midguts were imaged using a LSM 710 confocal microscope (Carl Zeiss) using 'Plan-Apochromat 20 × /0.8 M27' and 'C-Apochromat 40 × /1.20 W Corr M27' objectives. Image resolution was set to at least 2048 × 2048 pixels. Focal planes with 1 µm distance were scanned and combined into Z-stacks to image one cell layer of the tubular gut and to compensate for gut curvature.

4.10. Quantification of Proliferation, Cell Size and Fluorophore Intensity Measurements

Quantification of progenitor cell number and epithelial renewal and fluorescence intensity measurements were performed as described previously [5]. Fiji (ImageJ 1.51 n, Wayne Rasband, National Institutes of Health, USA) was used to calculate maximum intensity images from z-stack images. GFP positive progenitor cells of *esg*^{ReDDM} [3] guts were counted manually whereas RFP positive renewed epithelial cells were counted semi-automatically by a self-written macro for Fiji. Cell size measurements were performed in Fiji by outlining the single cells by hand and measuring the area.

Midguts of *Ubi-miR-277::GFP* sensor flies and the *Ubi-GFP* controls or *CG9547::sGFP* flies were scanned with fixed laser settings and exposure times. Mean intensities of manually selected areas were determined using Fiji.

4.11. Statistical Analysis

GraphPad Prism 9.0.0 was used to run statistical analysis and create graphs of quantifications. For single comparisons, data sets were analyzed by two-sided unpaired *t*-test. Multiple comparisons were analyzed by one-way ANOVA and Turkey's post-hoc test. Significant differences are displayed as * for $p \leq 0.05$, ** for $p \leq 0.01$, *** for $p \leq 0.001$ and **** for $p \leq 0.0001$.

4.12. Metabolic Landscape of Adult Drosophila Midgut at Single Cell Level

4.12.1. Preprocessing

Previously published single-cell RNA sequencing data derived from 10,605 midgut epithelial cells from 7-d-old females were retrieved from Gene Expression Omnibus accession GSE120537 [13]. Gene expression values were gene length normalized in TPM (transcripts per million) space and $\log_2$ transformed. For genes associated with multiple transcripts, the longest transcript length was used. Transcript lengths were obtained from Ensembl Biomart (https://m.ensembl.org/index.html, accessed on 5 November 2021). Missing gene

expression values were input using scImpute algorithm with default settings and only applied to genes with dropout rates larger than 50% to prevent over-input [85]. Metabolic gene lists were downloaded from KEGG database (http://www.kegg.jp/, accessed on 5 November 2021). Input expression values were used for t-SNE clustering [86] using Rtsne package with default settings after Krijthe, J. H. Rtsne: T-Distributed Stochastic Neighbor Embedding using Barnes-Hut Implementation. https://github.com/jkrijthe/Rtsne, 2015, accessed on 5 November 2021].

4.12.2. Normalization

Four normalization methods were evaluated. Upper-quartile [87] and trimmed mean of M-values [88] were implemented using calcNormFactors function from the edgeR package [88]. Relative log expression [89] was implemented from DESeq2 [90], Deconvolution normalization using the scran package computed tumor subgroup-specific size factors [91]. Read counts were divided by size factors corresponding to tumor subgroup and then transformed back to TPM. Only genes with dropout rate <0.75 were used as reference genes for normalization to avoid noise from low-expressed genes. Performance of the methods was evaluated using the distributions of relative gene expression values amongst different cell types. The deconvolution normalization derived expression values were used, as it was most effective in minimizing the differences in the distributions of relative gene expression levels between the cell types (Figure S2c).

4.12.3. Pathway Activity Analysis

The pathway score analysis from Xiao et al. was used with the input and deconvolution-normalized values [92]. The pathway activity score is defined as the relative gene expression values averaged over all genes in a specific pathway and all subgroup cells of this type [92]. Statistical significance of pathway activities in specific subgroups was calculated by random permutation test, where subgroup labels were randomly shuffled 5000 times to simulate null distribution, followed by comparison of pathway activity scores to original scores.

All code is available from the authors upon request.

Supplementary Materials: The following supporting information can be downloaded at: https://www.mdpi.com/article/10.3390/metabo12040315/s1. Figure S1: Overview of metabolic pathways in biological systems, Figure S2: Analysis of metabolic pathways and their activity in different cell types, Figure S3: Subclustered quiescent ISC (esg^+, Dl^- and klu^-) within the metabolic ISC cluster are negative for expression of the EE marker pros, Figure S4: esgReDDM tracing of ISC/EB with forced miR-277 expression and block of apoptosis, Figure S5: esgReDDM tracing and manipulation of miR-277 target genes CG4389 and CG5599 for 21 days and endogenous CG9547 expression in different cell types, Figure S6: esgReDDM tracing and manipulation of miR-277 in the Notch tumor model, Figure S7: Comparison of the esgReDDM and esgReDDMCas9 system and schematic composition of the newly developed CRISPR-Cas9 CRC model, Figure S8: miR-277-expression in CRC tumors revealed by miR-277::GFP sensor flies, Figure S9: schematic illustration of the strategy for seamless cloning of multiple gRNAs into the pCFD_noSapI plasmid.

Author Contributions: Conceptualization, Z.A.A. and T.R.; Formal analysis, L.Z. and S.B.; Funding acquisition, T.R.; Investigation, L.Z. and N.H.K.; Software, S.B.; Supervision, Z.A.A. and T.R.; Visualization, T.R.; Writing—original draft, L.Z., Z.A.A. and T.R.; Writing—review & editing, L.Z., Z.A.A. and T.R. All authors have read and agreed to the published version of the manuscript.

Funding: The research was funded by Wilhelm Sander Stiftung: 2018.145.1; Deutsche Forschungsgemeinschaft: RE-3453/3-1 and The Camden Health Research Initiative (CHRI) Award: 2020–2023.

Institutional Review Board Statement: Not applicable.

Informed Consent Statement: Not applicable.

Data Availability Statement: The data presented in this study are available in the article and supplementary materials.

Acknowledgments: We thank Klaus Förstemann, Thomas Klein, Michael Krahn, the Bloomington Drosophila Stock Center (NIHP400D018537), the Transgenic RNAi Project (TRiP) at Harvard Medical School (NIK/NIGMS R01-GM084947) and the Vienna Drosophila Resource Center (VDRC, http://www.vdrc.at, accessed on 5 November 2021) for providing transgenic fly stocks. We would like to acknowledge the Center for Advanced Imaging (CAi) at Heinrich Heine University for providing support with imaging and access to the Zeiss LSM 880 microscope system (DFG INST 208/746-1 FUGG) and Zeiss LSM 710 microscope system (DFG INST 208/539-1 FUGG). TR and ZA thank Maria Dominguez in whose lab we initiated this project and Thomas Klein for being a very supportive host. The project is funded by a Deutsche Forschungsgesellschaft (DFG-Sachbeihilfe RE 3453/2–1) grant. LZ is supported by the Wilhelm Sander-Stiftung (2018.145.1).

Conflicts of Interest: The authors declare no conflict of interest.

References

1. Lai, X.; Wolkenhauer, O.; Vera, J. Understanding microRNA-mediated gene regulatory networks through mathematical modelling. *Nucleic Acids Res.* **2016**, *44*, 6019–6035. [CrossRef] [PubMed]
2. Lamouille, S.; Subramanyam, D.; Blelloch, R.; Derynck, R. Regulation of epithelial–mesenchymal and mesenchymal–epithelial transitions by microRNAs. *Curr. Opin. Cell Biol.* **2013**, *25*, 200–207. [CrossRef] [PubMed]
3. A Antonello, Z.; Reiff, T.; Ballesta-Illan, E.; Dominguez, M. Robust intestinal homeostasis relies on cellular plasticity in enteroblasts mediated by miR-8–Escargot switch. *EMBO J.* **2015**, *34*, 2025–2041. [CrossRef] [PubMed]
4. Hu, S.; Jiang, Q.; Luo, D.; Zhao, L.; Fu, X.; Chen, Y.; Song, X.; Li, L.; Zhao, H.; He, Y.; et al. miR-200b is a key regulator of tumor progression and metabolism targeting lactate dehydrogenase A in human malignant glioma. *Oncotarget* **2016**, *7*, 48423–48431. [CrossRef]
5. Zipper, L.; Jassmann, D.; Burgmer, S.; Görlich, B.; Reiff, T. Ecdysone steroid hormone remote controls intestinal stem cell fate decisions via the PPARγ-homolog Eip75B in Drosophila. *eLife* **2020**, *9*, e55795. [CrossRef]
6. Reiff, T.; Jacobson, J.; Cognigni, P.; Antonello, Z.; Ballesta, E.; Tan, K.J.; Yew, J.Y.; Dominguez, M.; Miguel-Aliaga, I. Endocrine remodelling of the adult intestine sustains reproduction in Drosophila. *eLife* **2015**, *4*, e06930. [CrossRef]
7. Ahmed, S.M.H.; Maldera, J.A.; Krunic, D.; Paiva-Silva, G.O.; Pénalva, C.; Teleman, A.A.; Edgar, B.A. Fitness trade-offs incurred by ovary-to-gut steroid signalling in Drosophila. *Nature* **2020**, *584*, 415–419. [CrossRef]
8. Dutta, D.; Dobson, A.; Houtz, P.L.; Gläßer, C.; Revah, J.; Korzelius, J.; Patel, P.; Edgar, B.A.; Buchon, N. Regional Cell-Specific Transcriptome Mapping Reveals Regulatory Complexity in the Adult Drosophila Midgut. *Cell Rep.* **2015**, *12*, 346–358. [CrossRef]
9. Buchon, N.; Osman, D.; David, F.P.; Fang, H.Y.; Boquete, J.P.; Deplancke, B.; Lemaitre, B. Morphological and molecular characterization of adult midgut compartmentalization in Drosophila. *Cell Rep.* **2013**, *3*, 1725–1738. [CrossRef]
10. Stine, R.R.; Sakers, A.P.; TeSlaa, T.; Kissig, M.; Stine, Z.E.; Kwon, C.W.; Cheng, L.; Lim, H.-W.; Kaestner, K.H.; Rabinowitz, J.D.; et al. PRDM16 Maintains Homeostasis of the Intestinal Epithelium by Controlling Region-Specific Metabolism. *Cell Stem. Cell* **2019**, *25*, 830–845.e8. [CrossRef]
11. Ohlstein, B.; Spradling, A. The adult Drosophila posterior midgut is maintained by pluripotent stem cells. *Nature* **2006**, *439*, 470–474. [CrossRef] [PubMed]
12. Micchelli, C.A.; Perrimon, N. Evidence that stem cells reside in the adult Drosophila midgut epithelium. *Nature* **2006**, *439*, 475–479. [CrossRef] [PubMed]
13. Hung, R.J.; Hu, Y.; Kirchner, R.; Liu, Y.; Xu, C.; Comjean, A.; Tattikota, S.G.; Li, F.; Song, W.; Sui, S.H.; et al. A cell atlas of the adult Drosophila midgut. *Proc. Natl. Acad. Sci. USA* **2020**, *117*, 1514–1523. [CrossRef] [PubMed]
14. Chen, J.; Xu, N.; Wang, C.; Huang, P.; Huang, H.; Jin, Z.; Yu, Z.; Cai, T.; Jiao, R.; Xi, R. Transient Scute activation via a self-stimulatory loop directs enteroendocrine cell pair specification from self-renewing intestinal stem cells. *Nat. Cell Biol.* **2018**, *20*, 152–161. [CrossRef]
15. Hu, C.; Fan, L.; Cen, P.; Chen, E.; Jiang, Z.; Li, L. Energy Metabolism Plays a Critical Role in Stem Cell Maintenance and Differentiation. *Int. J. Mol. Sci.* **2016**, *17*, 253. [CrossRef]
16. Shyh-Chang, N.; Daley, G.Q.; Cantley, L.C. Stem cell metabolism in tissue development and aging. *Development* **2013**, *140*, 2535–2547. [CrossRef]
17. Biteau, B.; Karpac, J.; Supoyo, S.; DeGennaro, M.; Lehmann, R.; Jasper, H. Lifespan Extension by Preserving Proliferative Homeostasis in Drosophila. *PLoS Genet.* **2010**, *6*, e1001159. [CrossRef]
18. Mattila, J.; Kokki, K.; Hietakangas, V.; Boutros, M. Stem Cell Intrinsic Hexosamine Metabolism Regulates Intestinal Adaptation to Nutrient Content. *Dev. Cell* **2018**, *47*, 112–121.e3. [CrossRef]
19. Deng, H.; Takashima, S.; Paul, M.; Guo, M.; Hartenstein, V. Mitochondrial dynamics regulates Drosophila intestinal stem cell differentiation. *Cell Death Discov.* **2018**, *4*, 81. [CrossRef]
20. Jin, Y.; Zhang, C.; Marchetti, M.; Hammouda, O.; Edgar, B. EGFR Signaling Activates Intestinal Stem Cells by Promoting Mitochondrial Biogenesis. *SSRN Electron. J.* **2021**. [CrossRef]
21. Reiff, T.; Antonello, Z.A.; Ballesta-Illán, E.; Mira, L.; Sala, S.; Navarro, M.; Martinez, L.M.; Dominguez, M. Notch and EGFR regulate apoptosis in progenitor cells to ensure gut homeostasis in Drosophila. *EMBO J.* **2019**, *38*, e101346. [CrossRef] [PubMed]

22. Schell, J.C.; Wisidagama, D.R.; Bensard, C.; Zhao, H.; Wei, P.; Tanner, J.; Flores, A.; Mohlman, J.; Sorensen, L.K.; Earl, C.S.; et al. Control of intestinal stem cell function and proliferation by mitochondrial pyruvate metabolism. *Nat. Cell Biol.* **2017**, *19*, 1027–1036. [CrossRef] [PubMed]
23. Urbich, C.; Kuehbacher, A.; Dimmeler, S. Role of microRNAs in vascular diseases, inflammation, and angiogenesis. *Cardiovasc. Res.* **2008**, *79*, 581–588. [CrossRef] [PubMed]
24. Friedman, R.C.; Farh, K.K.-H.; Burge, C.B.; Bartel, D.P. Most mammalian mRNAs are conserved targets of microRNAs. *Genome Res.* **2009**, *19*, 92–105. [CrossRef] [PubMed]
25. Esslinger, S.M.; Schwalb, B.; Helfer, S.; Michalik, K.M.; Witte, H.; Maier, K.C.; Martin, D.; Michalke, B.; Tresch, A.; Cramer, P.; et al. Drosophila miR-277 controls branched-chain amino acid catabolism and affects lifespan. *RNA Biol.* **2013**, *10*, 1042–1056. [CrossRef]
26. Ling, L.; Kokoza, V.A.; Zhang, C.; Aksoy, E.; Raikhel, A.S. MicroRNA-277 targets insulin-like peptides 7 and 8 to control lipid metabolism and reproduction in Aedes aegypti mosquitoes. *Proc. Natl. Acad. Sci. USA* **2017**, *114*, E8017–E8024. [CrossRef]
27. Schertel, C.; Rutishauser, T.; Förstemann, K.; Basler, K. Functional Characterization of Drosophila microRNAs by a Novel in Vivo Library. *Genetics* **2012**, *192*, 1543–1552. [CrossRef]
28. Brennecke, J.; Hipfner, D.R.; Stark, A.; Russell, R.B.; Cohen, S.M. Bantam Encodes a Developmentally Regulated microRNA that Controls Cell Proliferation and Regulates the Proapoptotic Gene hid in Drosophila. *Cell* **2003**, *113*, 25–36. [CrossRef]
29. Ohlstein, B.; Spradling, A. Multipotent Drosophila Intestinal Stem Cells Specify Daughter Cell Fates by Differential Notch Signaling. *Science* **2007**, *315*, 988–992. [CrossRef]
30. Antonello, Z.A.; Reiff, T.; Dominguez, M. Mesenchymal to epithelial transition during tissue homeostasis and regeneration: Patching up the Drosophila midgut epithelium. *Fly* **2015**, *9*, 132–137. [CrossRef]
31. Ebert, M.S.; Neilson, J.R.; Sharp, P.A. MicroRNA sponges: Competitive inhibitors of small RNAs in mammalian cells. *Nat. Methods* **2007**, *4*, 721–726. [CrossRef] [PubMed]
32. Horwich, M.D.; Zamore, P.D. Design and delivery of antisense oligonucleotides to block microRNA function in cultured Drosophila and human cells. *Nat. Protoc.* **2008**, *3*, 1537–1549. [CrossRef] [PubMed]
33. Leader, D.P.; A Krause, S.; Pandit, A.; A Davies, S.; Dow, J.A.T. FlyAtlas 2: A new version of the Drosophila melanogaster expression atlas with RNA-Seq, miRNA-Seq and sex-specific data. *Nucleic Acids Res.* **2017**, *46*, D809–D815. [CrossRef] [PubMed]
34. Street, K.; Risso, D.; Fletcher, R.B.; Das, D.; Ngai, J.; Yosef, N.; Purdom, E.; Dudoit, S. Slingshot: Cell lineage and pseudotime inference for single-cell transcriptomics. *BMC Genom.* **2018**, *19*, 477. [CrossRef] [PubMed]
35. Guo, X.; Yin, C.; Yang, F.; Zhang, Y.; Huang, H.; Wang, J.; Deng, B.; Cai, T.; Rao, Y.; Xi, R. The Cellular Diversity and Transcription Factor Code of Drosophila Enteroendocrine Cells. *Cell Rep.* **2019**, *29*, 4172–4185.e5. [CrossRef]
36. Korzelius, J.; Azami, S.; Ronnen-Oron, T.; Koch, P.; Baldauf, M.; Meier, E.; A Rodriguez-Fernandez, I.; Groth, M.; Sousa-Victor, P.; Jasper, H. The WT1-like transcription factor Klumpfuss maintains lineage commitment of enterocyte progenitors in the Drosophila intestine. *Nat. Commun.* **2019**, *10*, 4123. [CrossRef]
37. Korzelius, J.; Naumann, S.K.; A Loza-Coll, M.; Chan, J.S.; Dutta, D.; Oberheim, J.; Gläßer, C.; Southall, T.D.; Brand, A.; Jones, D.L.; et al. Escargot maintains stemness and suppresses differentiation in Drosophila intestinal stem cells. *EMBO J.* **2014**, *33*, 2967–2982. [CrossRef]
38. A Loza-Coll, M.; Southall, T.D.; Sandall, S.L.; Brand, A.; Jones, D.L. Regulation of Drosophila intestinal stem cell maintenance and differentiation by the transcription factor Escargot. *EMBO J.* **2014**, *33*, 2983–2996. [CrossRef]
39. Li, Y.; Pang, Z.; Huang, H.; Wang, C.; Cai, T.; Xi, R. Transcription Factor Antagonism Controls Enteroendocrine Cell Specification from Intestinal Stem Cells. *Sci. Rep.* **2017**, *7*, 988. [CrossRef]
40. Tang, X.; Zhao, Y.; Buchon, N.; Engström, Y. The POU/Oct Transcription Factor Nubbin Controls the Balance of Intestinal Stem Cell Maintenance and Differentiation by Isoform-Specific Regulation. *Stem Cell Rep.* **2018**, *10*, 1565–1578. [CrossRef]
41. Tsuji, T.; Hasegawa, E.; Isshiki, T. Neuroblast entry into quiescence is regulated intrinsically by the combined action of spatial Hox proteins and temporal identity factors. *Development* **2008**, *135*, 3859–3869. [CrossRef] [PubMed]
42. Blanchet, E.; Annicotte, J.-S.; Lagarrigue, S.; Aguilar, V.; Clapé, C.; Chavey, C.; Fritz, V.; Casas, F.; Apparailly, F.; Auwerx, J.; et al. E2F transcription factor-1 regulates oxidative metabolism. *Nat. Cell Biol.* **2011**, *13*, 1146–1152. [CrossRef] [PubMed]
43. Chen, C.-L.; Kumar, D.B.U.; Punj, V.; Xu, J.; Sher, L.; Tahara, S.M.; Hess, S.; Machida, K. NANOG Metabolically Reprograms Tumor-Initiating Stem-like Cells through Tumorigenic Changes in Oxidative Phosphorylation and Fatty Acid Metabolism. *Cell Metab.* **2015**, *23*, 206–219. [CrossRef] [PubMed]
44. Xiang, J.; Bandura, J.; Zhang, P.; Jin, Y.; Reuter, H.; Edgar, B.A. EGFR-dependent TOR-independent endocycles support Drosophila gut epithelial regeneration. *Nat. Commun.* **2017**, *8*, 15125. [CrossRef] [PubMed]
45. A Hay, B.; Wolff, T.; Rubin, G.M. Expression of baculovirus P35 prevents cell death in Drosophila. *Development* **1994**, *120*, 2121–2129. [CrossRef]
46. Barker, N.; Ridgway, R.A.; Van Es, J.H.; Van De Wetering, M.; Begthel, H.; van den Born, M.; Danenberg, E.; Clarke, A.R.; Sansom, O.J.; Clevers, H. Crypt stem cells as the cells-of-origin of intestinal cancer. *Nature* **2009**, *457*, 608–611. [CrossRef]
47. Sato, T.; Vries, R.G.; Snippert, H.J.; Van De Wetering, M.; Barker, N.; Stange, D.E.; Van Es, J.H.; Abo, A.; Kujala, P.; Peters, P.J.; et al. Single Lgr5 stem cells build crypt-villus structures in vitro without a mesenchymal niche. *Nature* **2009**, *459*, 262–265. [CrossRef]
48. Barker, N.; Van Es, J.H.; Kuipers, J.; Kujala, P.; Van Den Born, M.; Cozijnsen, M.; Haegebarth, A.; Korving, J.; Begthel, H.; Peters, P.J.; et al. Identification of stem cells in small intestine and colon by marker gene Lgr5. *Nature* **2007**, *449*, 1003–1007. [CrossRef]

49. Bangi, E.; Murgia, C.; Teague, A.G.; Sansom, O.J.; Cagan, R.L. Functional exploration of colorectal cancer genomes using Drosophila. *Nat. Commun.* **2016**, *7*, 13615. [CrossRef]
50. Xing, Y.; Su, T.T.; Ruohola-Baker, H. Tie-mediated signal from apoptotic cells protects stem cells in Drosophila melanogaster. *Nat. Commun.* **2015**, *6*, 7058. [CrossRef]
51. Patel, P.H.; Dutta, D.; Edgar, B.A. Niche Appropriation by Drosophila Intestinal Stem Cell Tumors. *Nat. Cell Biol.* **2015**, *17*, 1182–1192. [CrossRef] [PubMed]
52. Bahuguna, S.; Redhai, S.; Zhou, J.; Wang, T.; Port, F.; Boutros, M. Conditional CRISPR-Cas Genome Editing in *Drosophila* to Generate Intestinal Tumors. *Cells* **2021**, *10*, 3156. [CrossRef] [PubMed]
53. Port, F.; Strein, C.; Stricker, M.; Rauscher, B.; Heigwer, F.; Zhou, J.; Beyersdörffer, C.; Frei, J.; Hess, A.; Kern, K.; et al. A large-scale resource for tissue-specific CRISPR mutagenesis in Drosophila. *eLife* **2020**, *9*, e53865. [CrossRef] [PubMed]
54. Koundouros, N.; Poulogiannis, G. Reprogramming of fatty acid metabolism in cancer. *Br. J. Cancer* **2019**, *122*, 4–22. [CrossRef] [PubMed]
55. Singh, S.R.; Zeng, X.; Zhao, J.; Liu, Y.; Hou, G.; Liu, H.; Hou, S.X. The lipolysis pathway sustains normal and transformed stem cells in adult Drosophila. *Nature* **2016**, *538*, 109–113. [CrossRef] [PubMed]
56. Tiwari, S.K.; Toshniwal, A.G.; Mandal, S.; Mandal, L. Fatty acid β-oxidation is required for the differentiation of larval hematopoietic progenitors in Drosophila. *eLife* **2020**, *9*, e53247. [CrossRef] [PubMed]
57. Cai, L.; Sutter, B.M.; Li, B.; Tu, B.P. Acetyl-CoA Induces Cell Growth and Proliferation by Promoting the Acetylation of Histones at Growth Genes. *Mol. Cell* **2011**, *42*, 426–437. [CrossRef] [PubMed]
58. Shi, L.; Tu, B.P. Acetyl-CoA and the Regulation of Metabolism: Mechanisms and Consequences. *Curr. Opin. Cell Biol.* **2015**, *33*, 125–131. [CrossRef]
59. Jiang, H.; Grenley, M.O.; Bravo, M.-J.; Blumhagen, R.Z.; Edgar, B.A. EGFR/Ras/MAPK Signaling Mediates Adult Midgut Epithelial Homeostasis and Regeneration in Drosophila. *Cell Stem. Cell* **2011**, *8*, 84–95. [CrossRef]
60. Demarco, R.S.; Uyemura, B.S.; D'Alterio, C.; Jones, D.L. Mitochondrial fusion regulates lipid homeostasis and stem cell maintenance in the Drosophila testis. *Nat. Cell Biol.* **2019**, *21*, 710–720. [CrossRef]
61. Torroja, L.; Ortuño-Sahagún, D.; Ferrús, A.; Hämmerle, B.; Barbas, J.A. scully, an Essential Gene of Drosophila, is Homologous to Mammalian Mitochondrial Type II l-3-hydroxyacyl-CoA Dehydrogenase/Amyloid-β Peptide-binding Protein. *J. Cell Biol.* **1998**, *141*, 1009–1017. [CrossRef] [PubMed]
62. A Endow, S.; E Miller, S.; Ly, P.T. Mitochondria-enriched protrusions are associated with brain and intestinal stem cells in Drosophila. *Commun. Biol.* **2019**, *2*, 427. [CrossRef] [PubMed]
63. Liang, J.; Balachandra, S.; Ngo, S.; O'Brien, L.E. Feedback regulation of steady-state epithelial turnover and organ size. *Nature* **2017**, *548*, 588–591. [CrossRef] [PubMed]
64. Mihaylova, M.M.; Cheng, C.-W.; Cao, A.; Tripathi, S.; Mana, M.D.; Bauer-Rowe, K.E.; Abu-Remaileh, M.; Clavain, L.; Erdemir, A.; Lewis, C.A.; et al. Fasting Activates Fatty Acid Oxidation to Enhance Intestinal Stem Cell Function during Homeostasis and Aging. *Cell Stem. Cell* **2018**, *22*, 769–778.e4. [CrossRef] [PubMed]
65. Boren, J.; Brindle, K.M. Apoptosis-induced mitochondrial dysfunction causes cytoplasmic lipid droplet formation. *Cell Death Differ.* **2012**, *19*, 1561–1570. [CrossRef] [PubMed]
66. Escudero, S. Direct Regulation of Mitochondrial Fatty Acid Oxidation by Anti-Apoptotic MCL-1. Ph.D. Thesis, Harvard University, Cambridge, MA, USA, 2017.
67. Iuchi, K.; Ema, M.; Suzuki, M.; Yokoyama, C.; Hisatomi, H. Oxidized unsaturated fatty acids induce apoptotic cell death in cultured cells. *Mol. Med. Rep.* **2019**, *19*, 2767–2773. [CrossRef] [PubMed]
68. Strub, B.R.; Parkes, T.L.; Mukai, S.T.; Bahadorani, S.; Coulthard, A.B.; Hall, N.; Phillips, J.P.; Hilliker, A.J. Mutations of the withered (whd) gene in Drosophila melanogaster confer hypersensitivity to oxidative stress and are lesions of the carnitine palmitoyltransferase I (CPT I) gene. *Genome* **2008**, *51*, 409–420. [CrossRef]
69. Cao, W.; Liu, N.; Tang, S.; Bao, L.; Shen, L.; Yuan, H.; Zhao, X.; Lu, H. Acetyl-Coenzyme A acyltransferase 2 attenuates the apoptotic effects of BNIP3 in two human cell lines. *Biochim. Biophys. Acta Gen. Subj.* **2008**, *1780*, 873–880. [CrossRef]
70. Montgomery, R.K.; Carlone, D.L.; Richmond, C.A.; Farilla, L.; Kranendonk, M.E.G.; Henderson, D.E.; Baffour-Awuah, N.Y.; Ambruzs, D.M.; Fogli, L.K.; Algra, S.; et al. Mouse telomerase reverse transcriptase (mTert) expression marks slowly cycling intestinal stem cells. *Proc. Natl. Acad. Sci. USA* **2010**, *108*, 179–184. [CrossRef]
71. Sangiorgi, E.; Capecchi, M.R. Bmi1 is expressed in vivo in intestinal stem cells. *Nat. Genet.* **2008**, *40*, 915–920. [CrossRef]
72. Yan, K.S.; Chia, L.A.; Li, X.; Ootani, A.; Su, J.; Lee, J.Y.; Su, N.; Luo, Y.; Heilshorn, S.C.; Amieva, M.R.; et al. The intestinal stem cell markers Bmi1 and Lgr5 identify two functionally distinct populations. *Proc. Natl. Acad. Sci. USA* **2011**, *109*, 466–471. [CrossRef] [PubMed]
73. Powell, A.E.; Wang, Y.; Li, Y.; Poulin, E.J.; Means, A.L.; Washington, M.K.; Higginbotham, J.N.; Juchheim, A.; Prasad, N.; Levy, S.E.; et al. The Pan-ErbB Negative Regulator Lrig1 Is an Intestinal Stem Cell Marker that Functions as a Tumor Suppressor. *Cell* **2012**, *149*, 146–158. [CrossRef] [PubMed]
74. Barker, N.; van Oudenaarden, A.; Clevers, H. Identifying the Stem Cell of the Intestinal Crypt: Strategies and Pitfalls. *Cell Stem. Cell* **2012**, *11*, 452–460. [CrossRef] [PubMed]
75. You, B.; Chen, E.X. Anti-EGFR Monoclonal Antibodies for Treatment of Colorectal Cancers: Development of Cetuximab and Panitumumab. *J. Clin. Pharmacol.* **2012**, *52*, 128–155. [CrossRef] [PubMed]

76. Basak, O.; Beumer, J.; Wiebrands, K.; Seno, H.; van Oudenaarden, A.; Clevers, H. Induced Quiescence of Lgr5+ Stem Cells in Intestinal Organoids Enables Differentiation of Hormone-Producing Enteroendocrine Cells. *Cell Stem. Cell* **2017**, *20*, 177–190.e4. [CrossRef] [PubMed]
77. Samudio, I.; Harmancey, R.; Fiegl, M.; Kantarjian, H.; Konopleva, M.; Korchin, B.; Kaluarachchi, K.; Bornmann, W.; Duvvuri, S.; Taegtmeyer, H.; et al. Pharmacologic inhibition of fatty acid oxidation sensitizes human leukemia cells to apoptosis induction. *J. Clin. Investig.* **2010**, *120*, 142–156. [CrossRef]
78. Knobloch, M.; Braun, S.; Zurkirchen, L.; Von Schoultz, C.; Zamboni, N.; Araúzo-Bravo, M.J.; Kovacs, W.; Karalay, Ö.; Suter, U.; Machado, R.A.M.; et al. Metabolic control of adult neural stem cell activity by Fasn-dependent lipogenesis. *Nature* **2012**, *493*, 226–230. [CrossRef]
79. Ito, K.; Carracedo, A.; Weiss, D.; Arai, F.; Ala, U.; Avigan, D.E.; Schafer, Z.T.; Evans, R.M.; Suda, T.; Lee, C.-H.; et al. A PML–PPAR-δ pathway for fatty acid oxidation regulates hematopoietic stem cell maintenance. *Nat. Med.* **2012**, *18*, 1350–1358. [CrossRef]
80. Stark, A.; Brennecke, J.; Russell, R.B.; Cohen, S.M. Identification of Drosophila MicroRNA Targets. *PLOS Biol.* **2003**, *1*, e60. [CrossRef]
81. Housden, B.; Millen, K.; Bray, S.J. Drosophila Reporter Vectors Compatible with ΦC31 Integrase Transgenesis Techniques and Their Use to Generate New Notch Reporter Fly Lines. *G3 Genes | Genomes | Genetics* **2012**, *2*, 79–82. [CrossRef]
82. Port, F.; Bullock, S.L. Augmenting CRISPR applications in Drosophila with tRNA-flanked sgRNAs. *Nat. Methods* **2016**, *13*, 852–854. [CrossRef] [PubMed]
83. Gratz, S.J.; Ukken, F.P.; Rubinstein, C.D.; Thiede, G.; Donohue, L.K.; Cummings, A.M.; O'Connor-Giles, K.M. Highly Specific and Efficient CRISPR/Cas9-Catalyzed Homology-Directed Repair in Drosophila. *Genetics* **2014**, *196*, 961–971. [CrossRef] [PubMed]
84. Izumi, Y.; Motoishi, M.; Furuse, K.; Furuse, M. A tetraspanin regulates septate junction formation in Drosophila midgut. *J. Cell Sci.* **2016**, *129*, 1155–1164. [CrossRef] [PubMed]
85. Li, W.V.; Li, J.J. An accurate and robust imputation method scImpute for single-cell RNA-seq data. *Nat. Commun.* **2018**, *9*, 997. [CrossRef]
86. Van Der Maaten, L.; Hinton, G. Visualizing data using t-SNE. *J. Mach. Learn. Res.* **2008**, *9*, 2579–2625.
87. Bullard, J.H.; Purdom, E.; Hansen, K.D.; Dudoit, S. Evaluation of statistical methods for normalization and differential expression in mRNA-Seq experiments. *BMC Bioinform.* **2010**, *11*, 94. [CrossRef]
88. Robinson, M.D.; McCarthy, D.J.; Smyth, G.K. EdgeR: A Bioconductor package for differential expression analysis of digital gene expression data. *Bioinformatics* **2010**, *26*, 139–140. [CrossRef]
89. Anders, S.; Huber, W. Differential expression analysis for sequence count data. *Genome Biol.* **2010**, *11*, R106. [CrossRef]
90. Love, M.I.; Huber, W.; Anders, S. Moderated estimation of fold change and dispersion for RNA-seq data with DESeq2. *Genome Biol.* **2014**, *15*, 550. [CrossRef]
91. LLun, A.T.; Bach, K.; Marioni, J.C. Pooling across cells to normalize single-cell RNA sequencing data with many zero counts. *Genome Biol.* **2016**, *17*, 75. [CrossRef]
92. Xiao, Z.; Dai, Z.; Locasale, J.W. Metabolic landscape of the tumor microenvironment at single cell resolution. *Nat. Commun.* **2019**, *10*, 3763. [CrossRef] [PubMed]

Supplementary Figure S1

iPath metabolome indicating miR-277 target genes in red

a

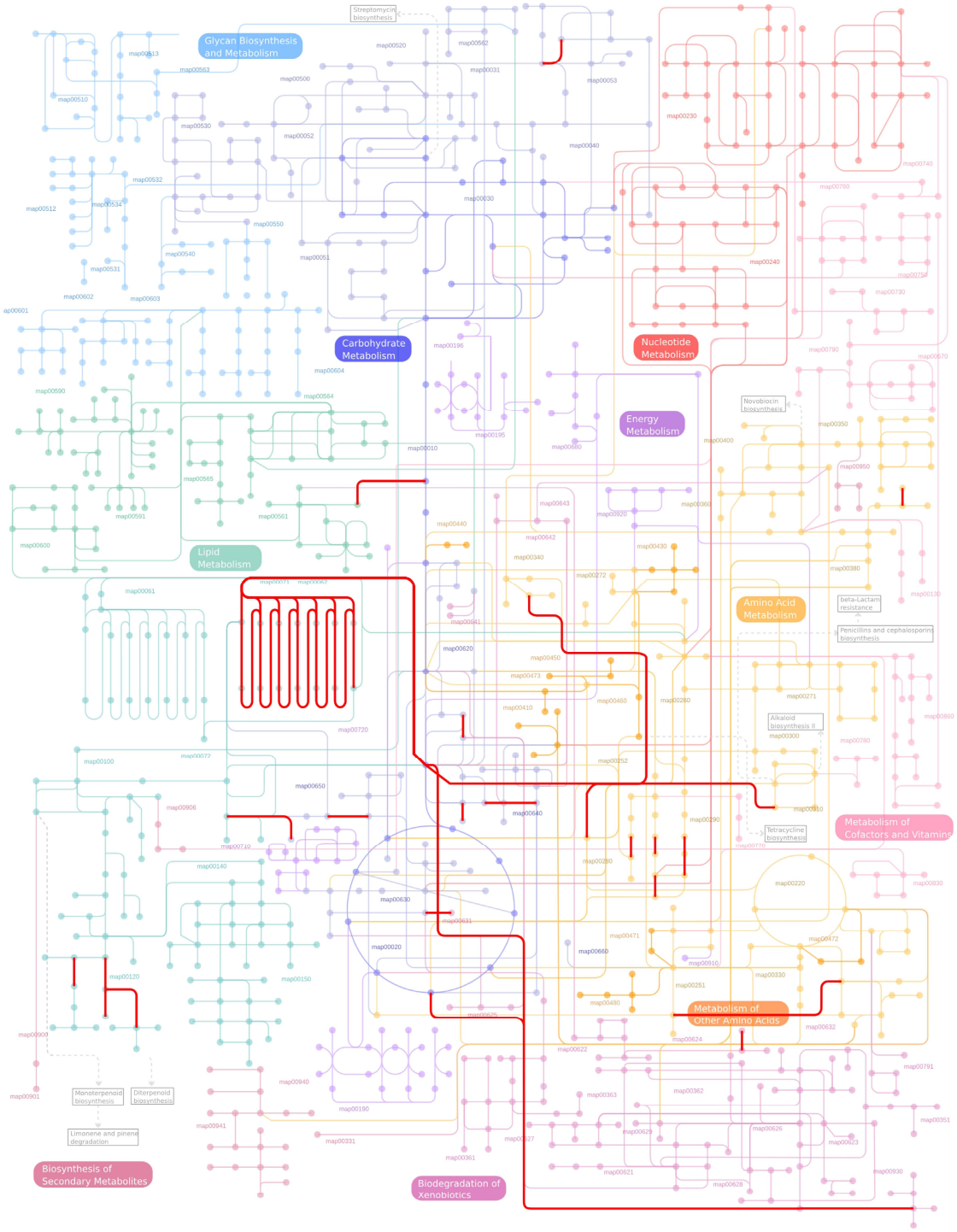

Supplementary Figure S2

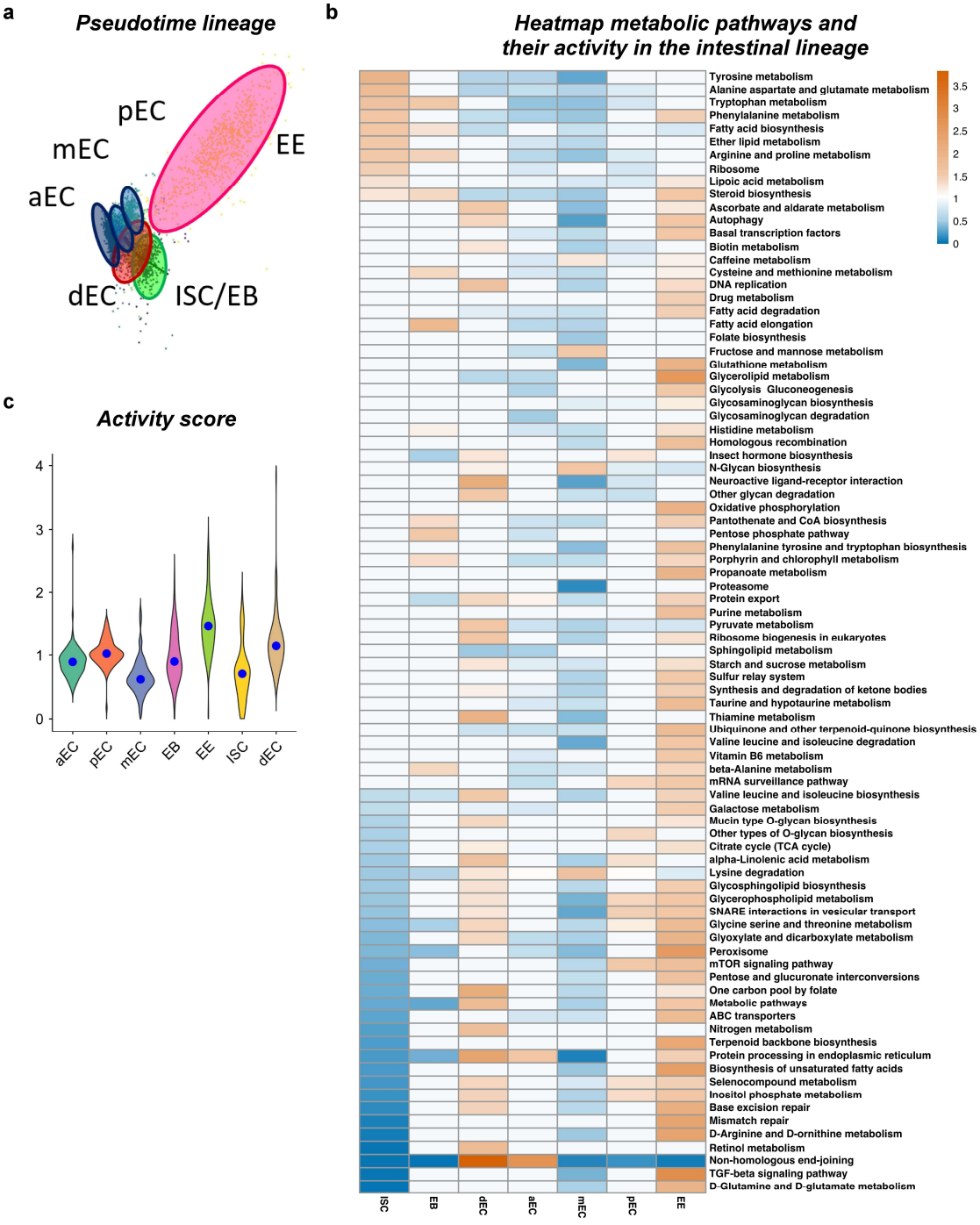

Supplementary Figure S3

a

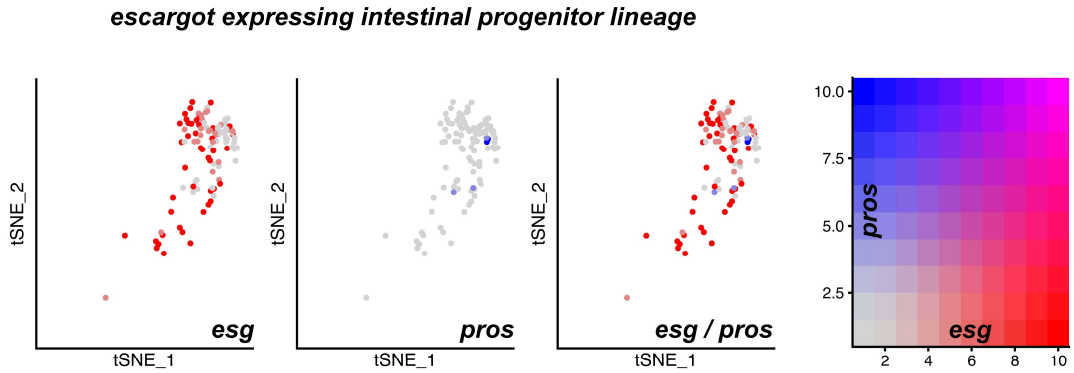

Supplementary Figure S4

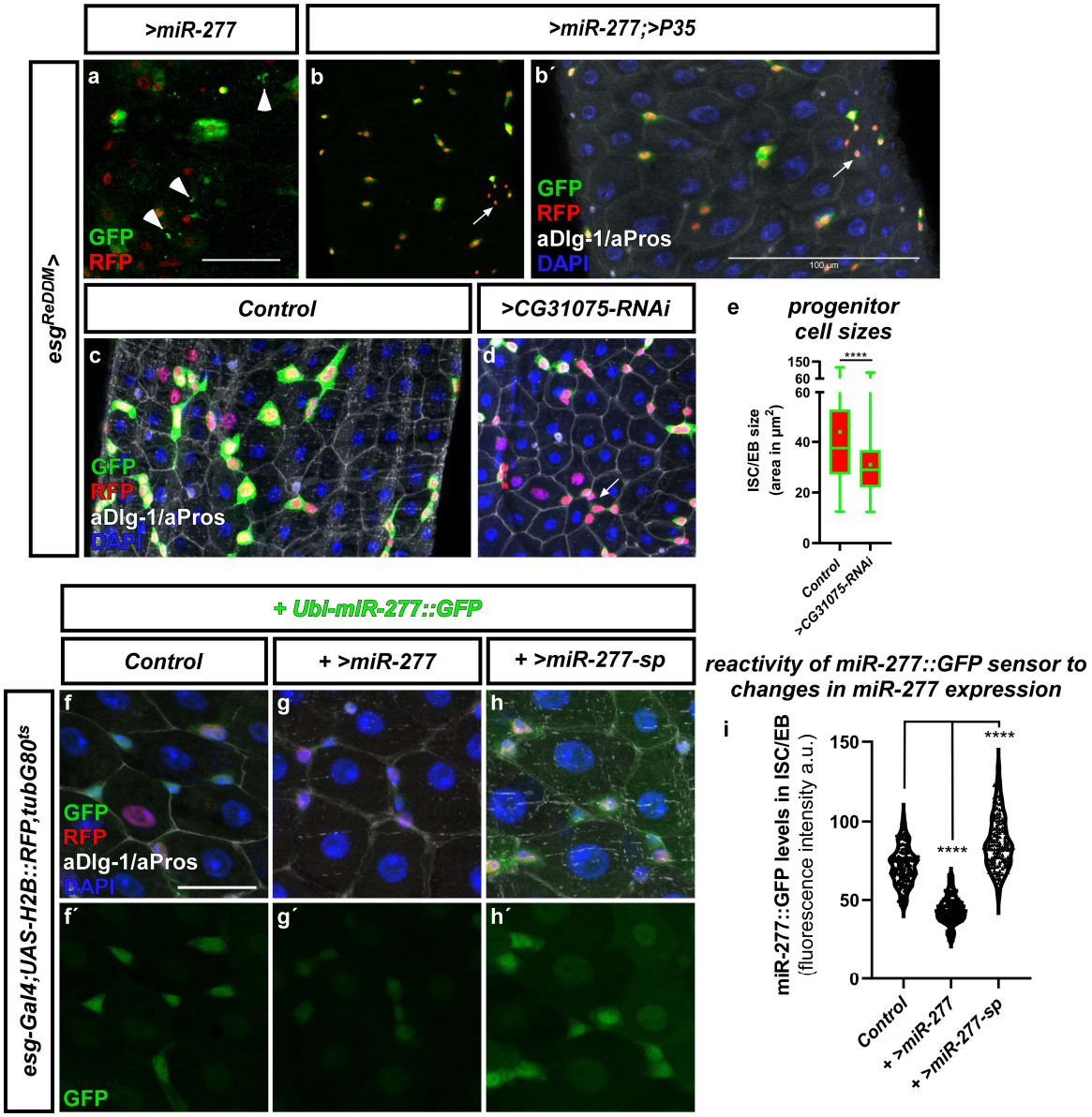

Supplementary Figure S5

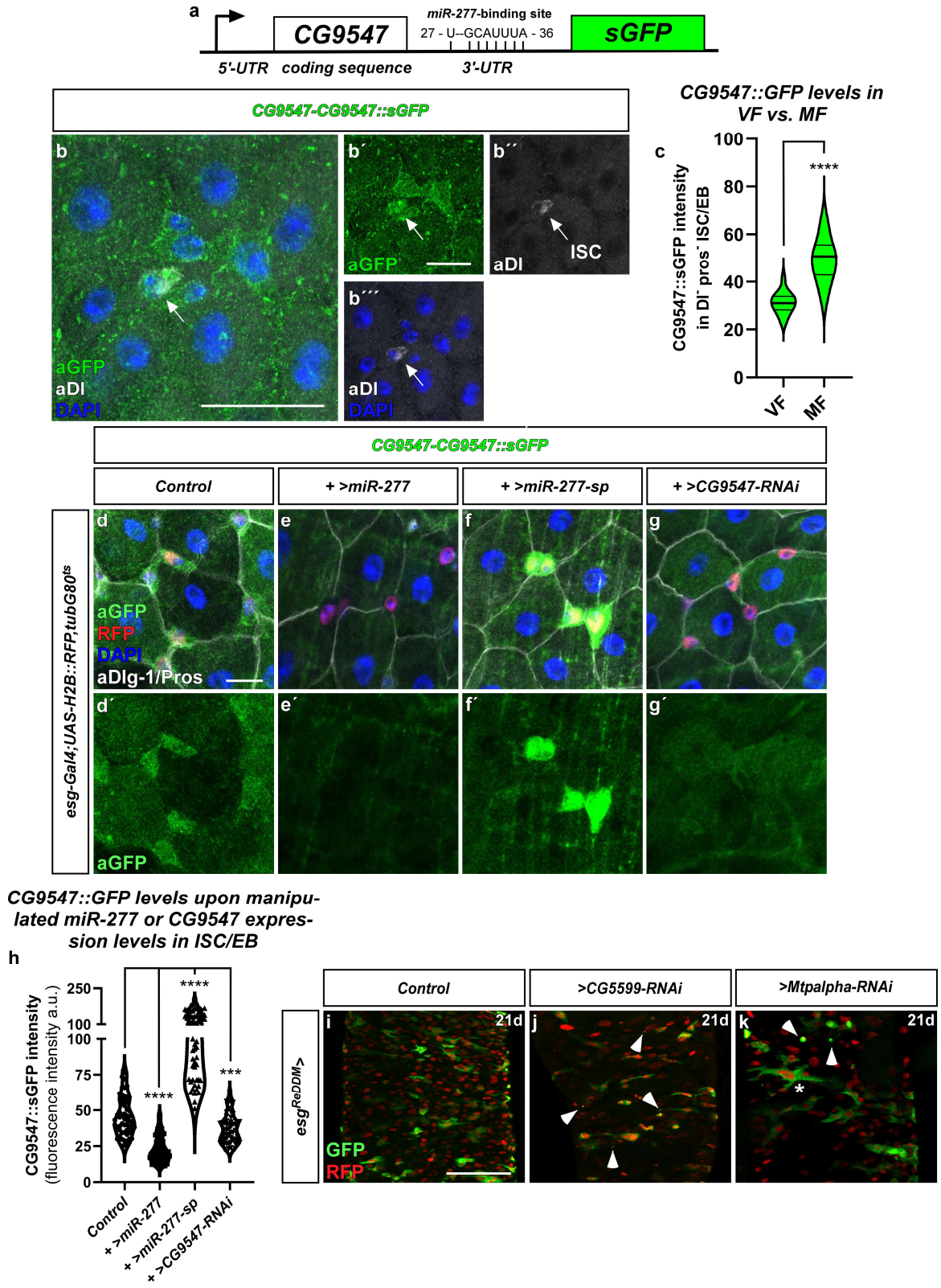

Supplementary Figure S6

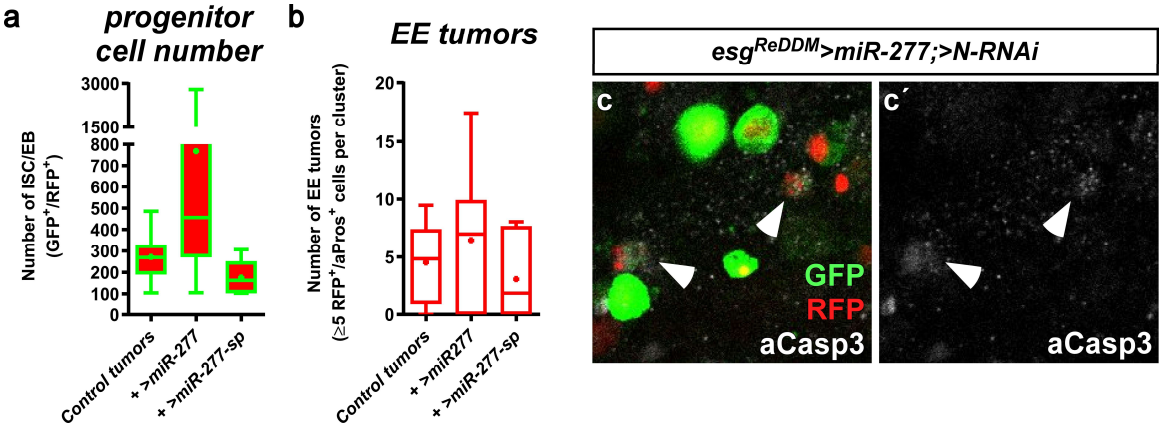

Supplementary Figure S7

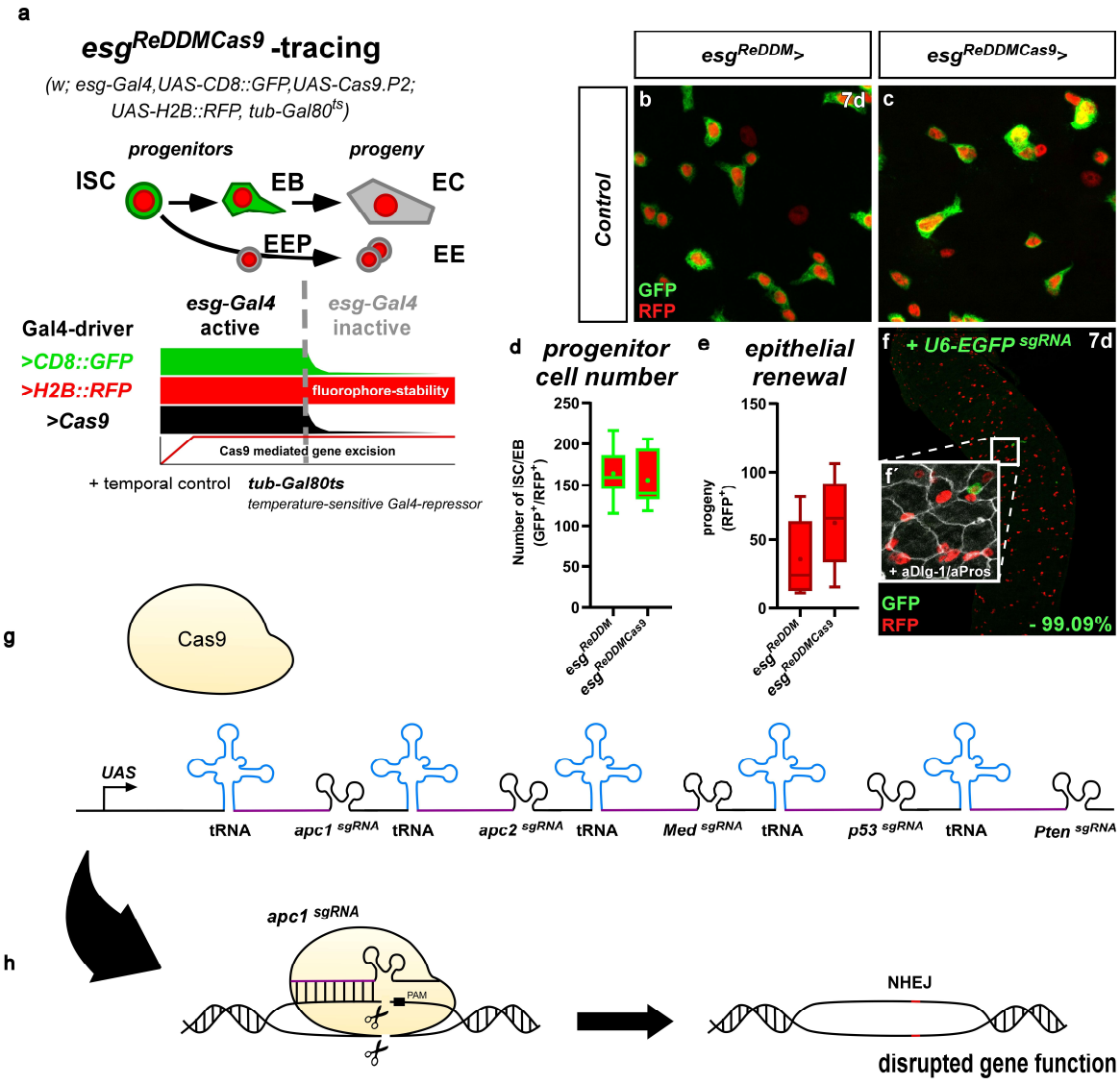

Supplementary Figure S8

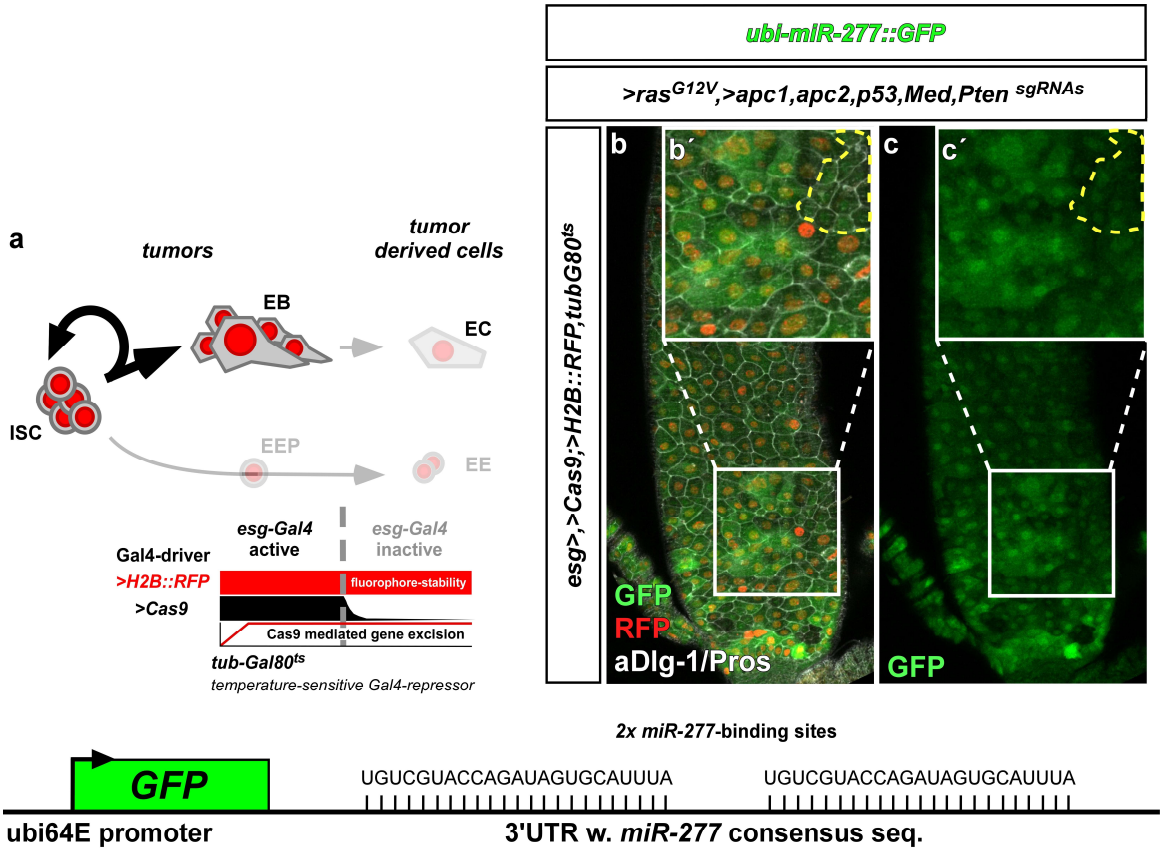

miR-277 expression levels outside and inside tumors indicated by miR-277::GFP intensities

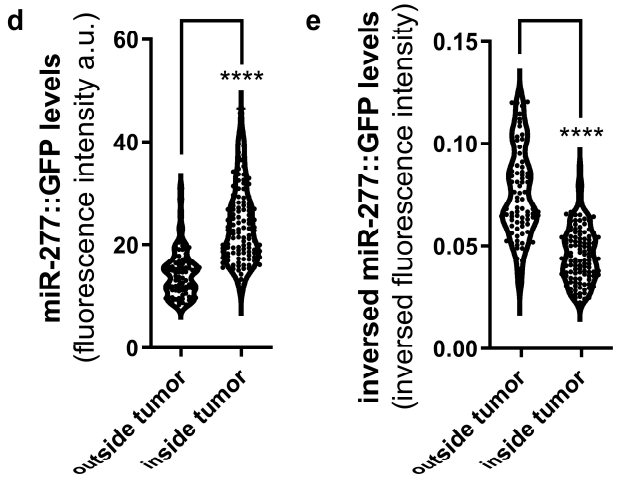

Supplementary Figure S9

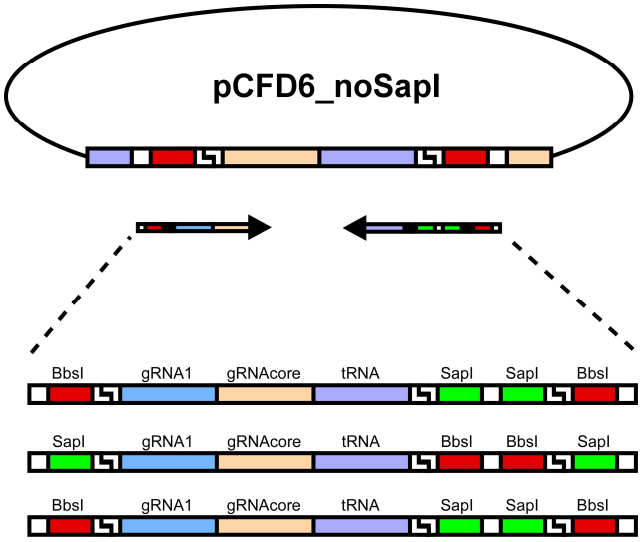

2.3 Paper III: Steroid hormone-induced wingless ligands tune female intestinal size in *Drosophila*

nature communications

Article

Steroid hormone-induced wingless ligands tune female intestinal size in *Drosophila*

Received: 10 November 2023

Accepted: 19 December 2024

Published online: 06 January 2025

Check for updates

Lisa Zipper[1], Bernat Corominas-Murtra[2] & Tobias Reiff[1]

Female reproduction comes at great expense to energy metabolism compensated by extensive organ adaptations including intestinal size. Upon mating, endocrine signals orchestrate a 30% net increase of absorptive epithelium. Mating increases production of the steroid hormone Ecdysone released by the *Drosophila* ovaries that stimulates intestinal stem cell (ISC) divisions. Here, we uncover the transcription factor *crooked legs (crol)* as an intraepithelial coordinator of Ecdysone-induced ISC mitosis. For the precise investigation of non-autonomous factors on ISC behaviour, we establish Rapport, a spatiotemporally-controlled dual expression and tracing system for the analysis of paracrine genetic manipulation while tracing ISC behaviour. Rapport tracing reveals that Ecdysone-induced Crol controls mitogenic Wnt/Wg-ligand expression from epithelial enterocytes activating ISC mitosis. Paracrine Wg stimulation is counterbalanced by Crol-repression of *string/CDC25* and *CyclinB* autonomously in ISC. Rapport-based ISC tumours confirm paracrine stimulation through the Ecdysone-Crol-Wg axis on mitotic behaviour, whereas the autonomous anti-proliferative role of Crol in ISC is conserved in models of colorectal cancer. Finally, mathematical modelling corroborates increasing enterocyte numbers and Wnt/Wg-degradation to set a stable post-mating intestinal size. Together, our findings provide insights into the complex endocrine growth control mechanisms during mating-induced adaptations and might help untangling pleiotropic hormonal effects observed in gastrointestinal tumorigenesis.

Generation of offspring is an energetically costly process that triggers multiple physiological adaptations of organs such as liver, pancreas and gastrointestinal tract in various species[1,2]. Survival and fitness of progeny relies on tight control of alimentary tract adaptations to metabolic demands in small rodents, in which daily food uptake during lactation can equal the mother´s body weight[1,3]. It is key to understand regulatory mechanisms for hyperplasia and -trophy of the intestine, as it underlies both, physiological tissue functionality and potential malfunctioning in common diseases such as diabetes, obesity and cancer. Physiological adaptations to mating and pregnancy offer a unique opportunity to explore the nature of the underlying interorgan communication.

In *Drosophila melanogaster* females, gut size is increased to match energy consumption when egg production is initiated[4–8]. Endocrine interorgan communication orchestrates this organ size re-set yielding an enlarged intestine with about a third more absorptive enterocytes (EC)[7,8]. This expansion is orchestrated by systemic release of juvenile hormone (JH) from the neuroendocrine corpora allata and the steroid hormone 20-Hydroxy-Ecdysone (20HE) from the ovaries. Both hormones converge on intestinal progenitors increasing intestinal stem cell (ISC) proliferation and enteroblast (EB) differentiation towards EC fate[4,7–10]. 20HE-dependent increases in ISC proliferation depend on presence of

[1]Department of Biology, Institute of Genetics, The Faculty of Mathematics and Natural Sciences, Heinrich Heine University Düsseldorf, Düsseldorf, Germany. [2]Department of Biology, University of Graz, Graz, Austria. e-mail: reifft@hhu.de

the Ecdysone-receptor (EcR) and early response genes *Broad, Eip75B* and *Hr3*[4,8], but mating-dependent molecular control mechanisms of how active 20HE-signalling affects the cell cycle in ISC, remained unknown.

Here, we report and characterize how *crooked legs* (*crol*) relays endocrine 20HE into local intraepithelial ISC division control. We detected 20HE-dependent *crol* activation in ISC and epithelial EC. Interestingly, functional experiments revealed antagonizing mitogenic effects of *crol* manipulation in the ISC population on one hand and the EC population on the other hand, a function of Crol that is also exerted by its human orthologue ZNF267. This observation prompted us to invent and establish 'Rapport', a bipartite spatiotemporally controlled tracing and expression system, which enabled us to manipulate EC while tracing non-autonomous effects on labelled stem cell progeny. We designed Rapport to offer highest flexibility and compatibility with existing genetic tools and combined it with a driver for epithelial enterocytes in this study. Using Rapport, we discover that Crol relays systemic 20HE signalling in EC into locally acting paracrine Wnt/Wg ligands. This finding is of high interest as EC are the largest cell population in the midgut and Wnt/Wg signalling pathway is central in homeostasis and malignancies of the fly and mammalian gut[11,12]. Manipulation of the 20HE-Crol-Wg axis in microenvironmental EC non-autonomously controls ISC proliferation during mating-dependent intestinal growth and in neoplastic tumours. Quite the contrary, *crol* expression in ISC acts antiproliferative through the CDC25-orthologue *string* and the mitotic cyclin *Cyclin B*, suggestive for a Crol-dependent mitotic balance.

Mathematical modelling supports our hypothesis of opposing autonomous and non-autonomous mitogenic effects of Crol on ISC and that EC numbers are indeed stabilizing mating-adapted organ size depending on 20HE levels. Interestingly, our discovered dynamic pattern is highly robust and can be derived from the fundamental properties of diffusion and degradation of Wnt/Wg ligands. These opposing cell type-dependent consequences of a single hormonal stimulus on stem cell proliferation inside the same epithelium underpin complex hormonal action on epithelial growth during pregnancy-induced hyperplasia and pleiotropic effects observed in cancer of the intestine.

Results

Crooked legs responds to mating-dependent 20HE steroid hormone release

The female fly intestine undergoes a variety of post-mating adaptations including a net increase of the absorptive epithelium[5–7]. Mating-dependent enteroplasticity is orchestrated by two hormones, JH and 20HE, which act directly on ISC mitosis increasing the number of absorptive EC[4,7,8]. Aiming to elaborate Ecdysone-responsive genes exerting ISC division control, we followed leads from developmental studies[13–15] and sequencing approaches that suggested expression of *crooked legs* in the adult *Drosophila* midgut[16,17].

Transgenic flies in which Crol is GFP-tagged (Crol::GFP) confirmed *crol*-expression in the adult midgut of female and male flies. We detected GFP-signal in all four major cell types of the intestine: ISC positive for the Notch-ligand Delta (N and Dl, Fig. S1A-A"), EB identified by N-activity (N-reporter GBE+Su(H)-dsRed, Fig. S1B-B"), EE positive for Pros (Prospero, Fig. S1C-C") and EC, positive for the septate junction marker Dlg1 (Discs large 1, Fig. S1C-C"). It was previously shown that mating induces a physiological adaptation of the posterior midgut (PMG) by size and cell number, which is most pronounced in the R5 region of the PMG[7,8]. Mating induces an ovary-to-gut release of 20HE (Fig. 1E)[8], which we also found to significantly increase Crol::GFP levels when comparing adult mated females (MF) with virgin females (VF) (Fig. 1A-B', E, F). As mating induces both, JH and 20HE, we next confirmed *crol* responsiveness to pharmacological EcR activation by feeding the EcR agonist RH5849 to female (Fig. 1E) and male flies[8]. RH5849 significantly increased Crol::GFP fluorescence intensity in control females (Fig. 1C-D', F) whereas no difference was detected in male flies fed with RH5849 (Fig. S1G–I) underlining previously described differences in hormone responsiveness and sexual identity of cells in the female and male midgut[4,8,18,19]. Previous studies showed that manipulation of 20HE levels can be achieved by genetic ovariectomy using the dominant ovo^{D1} stock, which diminishes later egg stages of vitellogenesis in ovarioles as a sink for 20HE while keeping the main population of ovary cells producing 20HE active[8,20]. In line with a regulation of *crol* by 20HE, we detected a significant increase of Crol::GFP fluorescence in ovariectomized MF (Fig. S1D–D',F). Interestingly, *crol* responded to mating (Fig. 1A-B'), RH5849 (Fig. 1C-D') and 20HE-induction by ovariectomy (Fig. S1D-F) in ISC/EB (Fig. 1A', B', C', D', Fig. S1D', E' encircled $Arm^{+}/Pros^{-}$-cells) as well as epithelial EC (Fig. 1A', B', C', D', Fig. S1D', E' arrows) by significant increases in Crol::GFP intensity (Fig. 1F, Fig. S1F).

Recent studies showed that 20HE is taken up through the Ecdysone importer (EcI) in larval development[21] and the adult midgut[8]. Using heat-shock induced Flp-out clones, we investigated whether Crol::GFP levels respond to EcI-overexpression and knockdown (Fig. 1G-H'). Clones positively marked by *UAS-RFP* (> RFP, '>' abbreviates Gal4/UAS regulation) also overexpress >*EcI*. In line with previous results[8], >*EcI* facilitates 20HE uptake which led to increased Crol::GFP levels in ISC/EB ($Arm^{+}/Pros^{-}$) as well as EC (Fig. 1G, G', I) when compared to wild type ISC/EB and EC (Fig. 1G, G', outlined cells). Reciprocally, a clonal reduction of 20HE uptake by *EcI-RNAi* reduces Crol::GFP levels in ISC/EB and EC (Fig. 1H, H', J) compared to non-clonal ISC/EB and EC (Fig. 1H, H'). Having identified *crol* as 20HE target in the adult midgut cells, we investigated its role in intestinal tissue homeostasis by separately addressing Crol in ISC/EB progenitors and epithelial EC (Fig. 1E).

Crol and its functional human orthologue ZNF267 control proliferation of intestinal stem cells

First, we manipulated *crol* autonomously in ISC and EB using the *'ReDDM'* (Repressible Dual Differential Marker, Fig. S2A) tracing method to observe overall impact on tissue renewal with spatiotemporal control of tracing onset and gene manipulation[22]. Briefly, *ReDDM* differentially marks cells having active or inactive *Gal4* expression with fluorophores of different stability. Combined with the enhancer trap *esg-Gal4*, active in progenitors (ISC and EB), esg^{ReDDM} double marks ISC and EB driving the expression of *UAS-CD8::GFP* (> *CD8::GFP*, '>' abbreviates Gal4/UAS regulation and '>>' lexA/AoP regulation in the following) with short half-life and >*H2B::RFP* with long half-life. Upon epithelial replenishment, newly differentiated EC and EE stemming from ISC divisions retain an RFP^{+}-nuclear stain due to fluorophore stability[22]. Crosses are grown at 18 °C in which transgene expression is repressed by ubiquitous tubulin-driven temperature sensitive $Gal80^{ts}$. By shifting adult females to 29 °C, $Gal80^{ts}$ is destabilized, in turn enabling temporal control of esg^{ReDDM}-tracing and additional UAS-driven transgenes in progenitors (Fig. S2A).

After seven days of tracing adult female intestines using esg^{ReDDM}, we found that overexpression of *crol* has an antiproliferative effect decreasing the number of progenitor cells (Fig. 2B, B') about 12-fold (Fig. 2E) compared to controls (Fig. 2A). Reciprocally, RNAi-knockdown (Fig. 2C) and guideRNA (gRNA) mediated excision of *crol* (Fig. S2G) using $esg^{ReDDMCas9}$ tracing significantly increased the number of progenitors (Fig. 2E, Fig. S2H), new epithelial cells (Fig. S2B) and stimulated ISC division (Fig. S2C) compared to controls (Fig. S2D). Similar results were obtained using independent overexpression and loss-of-function transgenics of *crol* (Fig. S2B, E–H). Underlining functionality of both, the reporter and RNAi stock, *crol-RNAi* driven by *esg*> in ISC and EB reduces Crol::GFP fluorescence (Fig. S2I–L).

We next sought to identify human orthologues of *crooked legs* and by mining databases for zinc finger transcription factors with a high

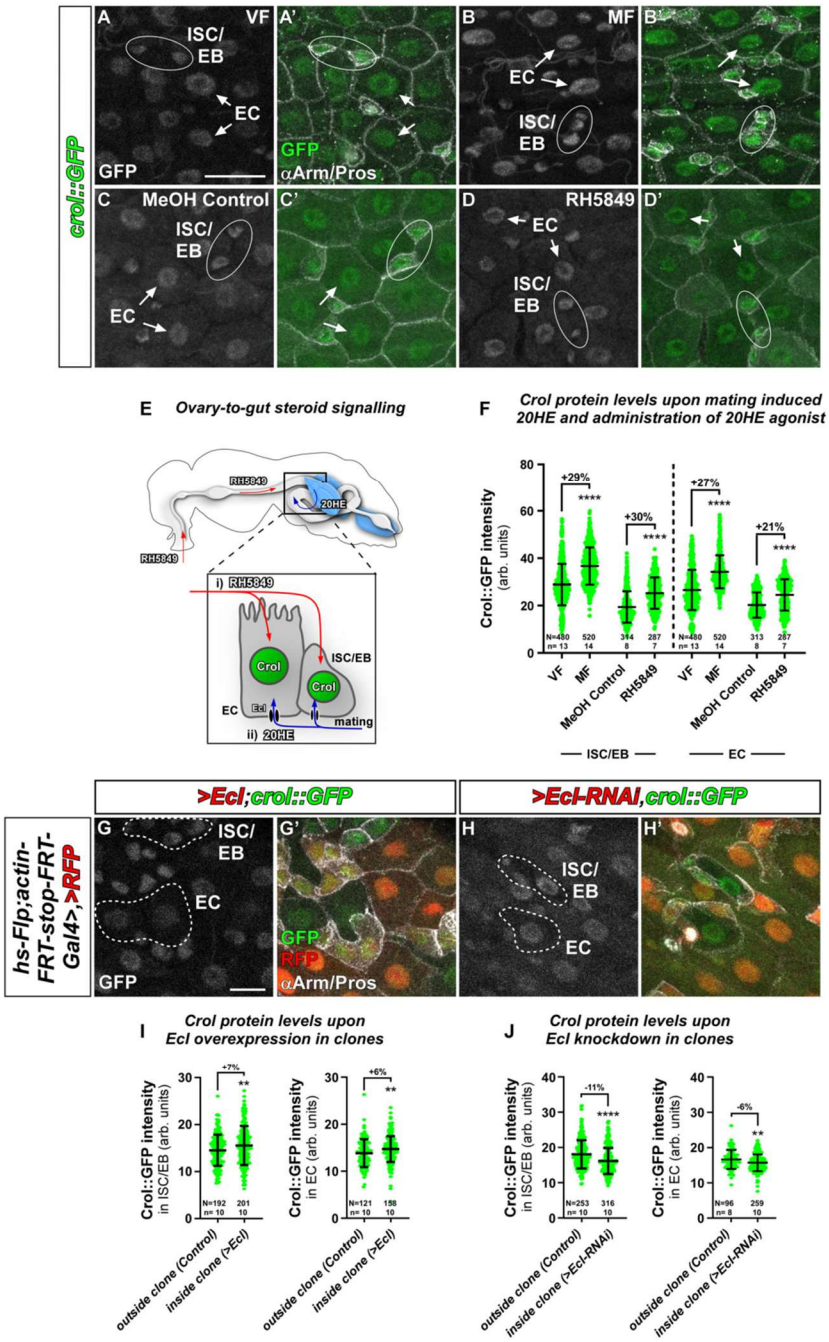

degree of sequence homology to Crol. We isolated the human Krüppel-like zinc finger transcription factor ZNF267 with a high degree of sequence homology (Fig. S2M) using in silico prediction resources (Flybase). To explore the ability of human ZNF267 (hZNF267) to substitute Crol function in intestinal progenitors, we depleted endogenous *crol* by RNAi and expressed hZNF267 at the same time (Fig. 2D) and observed rescue of *crol-RNAi*-induced progenitor accumulations by hZNF267 (Fig. 2D, E). In line with a role for Crol and hZNF267 in mitosis, hZNF267 regulates cell proliferation and differentiation in liver tissue[23,24]. Crol (Fig. S1) and hZNF267 show wide-ranged expression across human intestinal cell types (GTEx, Proteinatlas) and, like *crol* (Fig. 1I, J), is induced by steroid hormone signalling[25]. This prompted us to investigate how steroid hormones may affect ISC proliferation downstream of Crol and hZNF267.

Fig. 1 | Crol responds to 20HE steroid hormone release. A–D' Crol::GFP in R5 of adult midguts of (**A–A'**) virgin female (VF) flies compared to (**B–B'**) mated females (MF), (**C–C'**) MF fed with MeOH (MeOH Control) compared to (**D–D'**) MF fed with RH5849. **A–D** Sole Crol::GFP signal in greyscale and (**A'–D'**) in green colour combined with Arm and Pros antibody staining to identify duplets of ISC/EB (white ellipses) and EC (white arrows). Scale bar is 20 μm. **E** Female fly with midgut and ovaries. Oral RH5849 is (i) absorbed from the midgut lumen into ISC/EB and EC., 20HE from the ovaries travels through the hemolymph (ii) from where it is imported by the Ecdysone importer (EcI). **F** Crol::GFP intensities in ISC/EB and EC upon mating and oral administration of 20HE agonist RH5849. **G–H'** Confocal images showing heat-shock induced Flp-out clones in R5 regions positively marked by *UAS-RFP* and combined with *crol::GFP* and (**G–G'**) *UAS-EcI* or (**H–H'**) *UAS-EcI-RNAi*. (**G–H'**, UAS abbreviated as '>' hereafter in figure panels). Sole Crol::GFP signal is shown in greyscale and (**G'–H'**) in green colour combined with RFP for identification of clones and αArm/Pros for cell type identification. **G–H** Non-clonal areas including ISC/EB and EC are outlined in white dashed lines. Scale bar is 10 μm. **I-J** Quantification of Crol::GFP levels in ISC/EB and EC outside of clones and inside of clones with (**I**) > *EcI* or (**J**) > *EcI-RNAi*. **F, I–J** Scatter dot plots show individual values with indication of means ± SD. *N* and *n* values represent number of cells and number of biological replicas, respectively. Asterisks denote significances from (**F, I–J**) two-sided Mann Whitney *U* tests, and (**I**) unpaired two-sided *t*-tests used for comparison of Crol::GFP intensities in ISC/EB ($p = 0.0082$), (**$p < 0.01$;****$p < 0.0001$). Fold changes are shown in percentages. Source data are provided as a Source Data file.

Crol controls ISC proliferation through String and Cyclin B

During *Drosophila* development, it was shown that the tyrosine protein phosphatase *string* (*stg*, CDC25-orthologue) and the mitotic B-type Cyclin *CycB* are targets of EcR activity[26,27]. Supporting the idea that EcR-signalling controls ISC proliferation through Stg and CycB, EcR agonists not only increase ISC mitosis[4,8], but also *stg* and *CycB* transcript levels (Fig. 2J). In line with previous observations[28,29], up- and downregulation of *stg* levels in *esg*^{ReDDM} traced guts (Fig. 2F, H) reciprocally controlled ISC lineage production encompassing progenitor cells and newly differentiated cells produced by ISC (Fig. 2K). Confirming a function of Stg in mitotic control by Crol downstream of EcR-signalling, ISC proliferation and subsequent increase in lineage production upon >*crol-RNAi* is abolished when >*stg-RNAi* is co-expressed (Fig. 2C, I, K, L). Vice versa, co-expression of >*crol* and >*stg* (Fig. 2G) rescues ISC lineage production (Fig. 2K) and sporadic ISC mitosis as visualized by anti-pH3 staining (Fig. S3F). Comparable results were obtained when we investigated simultaneous depletion of Crol and CycB (Fig. S3A–G). Together, these data suggest an endocrine control of ISC cell cycle exit by Crol (Fig. 2M) acting on *stg* and *CycB* in line with observations during larval development[14,27].

This data suggested an anti-proliferative role for Crol in ISC, whereas we previously observed 20HE signalling in differentiation processes of the intestinal lineage[8]. A function of Crol in ISC proliferation rather than a role in differentiation of EB, is further supported by several lines of evidence: (i) EB express the EB lineage-specifying transcription factor *klumpfuss (klu)* and become postmitotic during lineage progression into EC[30–33]. When we manipulated *crol* using *klu*^{ReDDM} (Fig. S3H)[34], we revealed no increase in the number of EB nor new EC numbers upon *crol* up- and downregulation (Fig. S3I–M) suggesting no major role in differentiation when compared to strong Ecdysone-induced effectors of differentiation such as Eip75B-A/C[8]. (ii) Klu is described as transcriptional repressor[35], which directly binds *CycB* regulatory regions and is thought to mediate EB cell cycle exit[33]. Interestingly, we detected highest Crol::GFP levels in *klu*-positive EB (Fig. S3Q) pointing to a similar anti-proliferative role for Crol, further supported by our Crol and CycB manipulations (Fig. S3A–G)[27]. (iii) Additionally pointing to a role for Crol and CycB in proliferation control of ISC and EB, *crol-RNAi* (Fig. S3N) and forced *CycB* expression (Fig. S3O) using EB-specific *klu*^{ReDDM} result in cell cycle re-entry reflected by occasional mitotic pH3-positive EB (Fig. S3P). Together, our data highlights *crooked legs* as effector of Ecdysone-signalling that autonomously promotes ISC cell cycle exit involving *stg* and *CycB* (Fig. 2M).

The 20HE-Crol-Wg axis in enterocytes controls non-autonomous Wnt/Wg activity in intestinal stem cells

Intriguingly, *hZNF267*[23,24] as well as *crol*[13,14,27] connect steroid hormone and Wnt/Wg-signalling, which prompted us to investigate whether Crol controls Wnt/Wg-expression downstream of systemic 20HE-signalling during physiological mating-induced intestinal adaptations. Using transgenic flies in which Wg, the primary Wnt-ligand in *Drosophila*, is GFP-tagged (Wg::GFP), we confirmed strong Wg signal at the mid-/hindgut boundary (MHB)[36], the most posterior midgut region known to be patterned by Wnt/Wg signalling[37]. Anterior to the MHB, we detected robust Wg::GFP signal in EC of the mating-responsive R5 region (Fig. 3A–D')[38,39]. This suggests that Wg acts on ISC in a paracrine manner, which we analysed using the established *frizzled3* (*fz3)* sensor flies for Wnt/Wg signalling pathway activity (Fig. 3K)[40,41]. Examining *fz3-RFP* intensity in posterior midguts, we confirmed Wnt/Wg pathway activity at the MHB[41] and supporting the idea of EC-derived Wg (Fig. 3A–D') acting on ISC in a paracrine manner, we detected fz3-RFP signal in intestinal progenitors (Arm^{+}/Pros^{-}, Fig. 3E–H')[42] in R5 under homeostatic conditions.

Quantification of fluorescence intensities revealed that the EcR agonist RH5849 and *ovo*^{D1} increase Wg::GFP fluorescence in EC (Fig. 3A–D', I, J) and fz3-RFP in ISC/EB (Fig. 3E–J), suggestive for active Wnt/Wg signalling from EC to ISC (Fig. 3K). Mating also increased Wg::GFP (Fig. S4A–C) and fz3-RFP levels (Fig. S4D–F), which is suggestive for a role for paracrine Wnt/Wg signalling during physiological midgut adaptations. Previous work in challenged guts showed autocrine Wnt/Wg signalling between ISC and EB[43]. In contrast, we found that under homeostatic conditions[34] depletion of Wg using >*wg-RNAi* driven in *esg*^{ReDDM} flies did not significantly alter intestinal turnover (Fig. S5A–E) nor Wnt/Wg signalling activity using *fz3-RFP* sensor flies (Fig. S5F–I). Together, these findings pointed to EC being the source for Wnt/Wg ligands under homeostatic conditions.

Given Crol::GFP-responsiveness to 20HE (Fig. 1A-B', F, G–J, Fig. S1D–F) and Wg::GFP (Fig. 3C-D', Fig. S4A–C) signal in EC, we examined whether *wg* expression is controlled by 20HE and Crol in EC. Therefore, we combined the established EC-driver (*mex >)*[44] with *fz3-RFP*, which enables Wnt/Wg activity assessment in ISC/EB and manipulation of Wnt/Wg ligands from EC employing *tub-Gal80*^{ts} for temporal control (Fig. 4A). In line with the idea of a 20HE-Crol-Wg axis, we found that increasing 20HE signalling pathway activity by EC-specific expression of *EcI*[8,21], *crol* as well as *wg* significantly increased *fz3* activity in adjacent ISC/EB (Fig. 4B, E–G', I, I'). Reciprocally, depletion of *EcI*, *crol* and *wg* in EC, non-autonomously reduced *fz3* activity measured in ISC/EB (Fig. 4B, J-K', M, M'). Consequently, Wg-depletion downstream of forced *crol* expression reduced paracrine *fz3* activity measured in ISC/EB (Fig. 4C, H, H'), whereas *hZNF267* expression in endogenous *crol*-depleted EC stimulated *wg* expression (Fig. 4D, L, L'). Further supporting Crol acting on *wg* expression control in EC[14,27], we detected a 5.2-fold increase in Wg::GFP intensity upon >*crol* expression (Fig. 4N-O', Q) and a significant decrease upon >*crol-RNAi* (Fig. 4P–Q).

Combined with previous findings[14,27], our data involves *wg* as a central transcriptional target of Crol in intestinal EC, which in turn non-autonomously stimulates Wnt/Wg signalling pathway activity in ISC/EB. Intrigued by these observations, we investigated whether Wnt/Wg activation in epithelial EC through the 20HE-Crol-Wg axis translates into stem cell driven intestinal homeostasis and size adaptation[4,7,8].

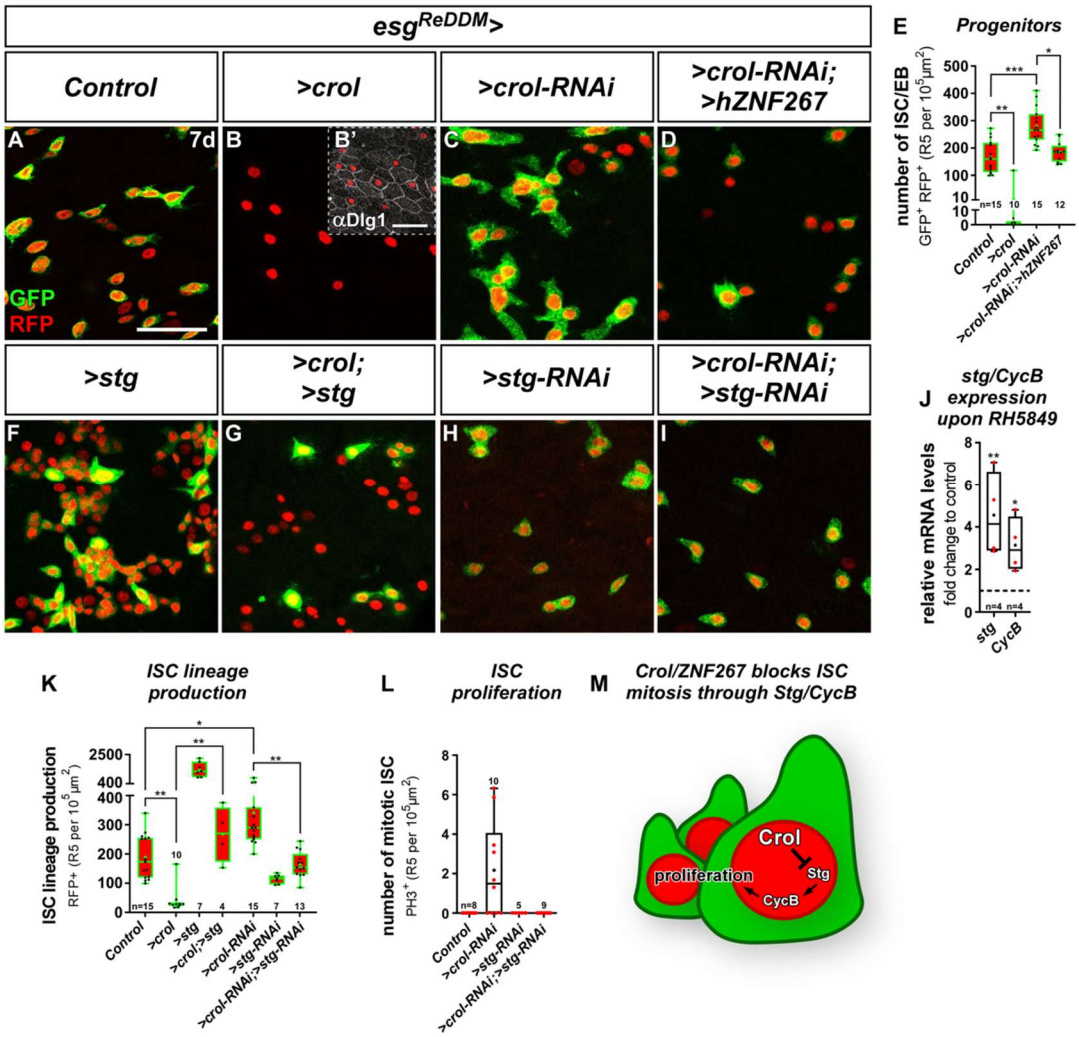

Fig. 2 | Crol and hZNF267 control ISC proliferation through String/Cyclin B. **A**–**D** Confocal images showing R5 regions of MF midguts after seven days (7 d) of esg^{ReDDM} tracing showing (**A**) controls with active *esg*> in ISC/EB driving expression of >*CD8::GFP* (membrane GFP) and >*H2B::RFP* (nuclear RFP), (**B**) ISC/EB specific overexpression (OE) of *crol* (F003414) with (**B'**) showing anti-Discs large 1 (Dlg1) staining in septate junctions of EC, (**C**) >*crol-RNAi* (BL41669), and (**D**) simultaneous expression of >*crol-RNAi* (BL41669) and the human Crol orthologue ZNF267 (>*hZNF267*). Scale bar is 50 µm. **E** Quantification of progenitor numbers upon esg^{ReDDM} manipulations of *crol* ($p = 0.0041$; $p = 0.0007$; $p = 0.011$). **F**–**I** Confocal images of MF midguts after 7 d showing (**F**) ISC/EB specific OE of *string* (*stg*) (F000926), (**G**) combined with >*crol* (BL58359), and (**H**) specific KD of *stg* by RNAi (**I**) combined with >*crol-RNAi* (BL41669). **J** Quantitative RT-qPCR on midgut cDNA of MF fed with RH5849 showing relative mRNA levels of *stg* and *Cyclin B* (*CycB*) normalized to MeOH control ($p = 0.0052$; $p = 0.0459$). **K**, **L** Quantification of (**K**) ISC lineage production (ISC/EB and newly differentiated cells, $p = 0.002$; $p = 0.0111$; $p = 0.0012$; $p = 0.0039$), and (**L**) number of αPH3+ ISC in R5 upon combined manipulations of *crol* and *stg*. **E**, **J**, **K**, **L** For Box-and-whisker plots: the center is the median, minima and maxima are 25th and 75th quartile and whiskers indicate full range of values. All individual values with '*n*' representing numbers of biological replicas are shown by dots and means are indicated by '+'. Asterisks denote significances from multiple comparisons by Kruskal-Wallis test (*$p < 0.05$; **$p < 0.01$; ***$p < 0.001$). Source data are provided as a Source Data file. **M** Schematic showing inhibition of Stg and CycB by Crol within ISC thereby controlling proliferation.

'Rapport' tracing reveals non-autonomous control of intestinal homeostasis through 20HE-Crol-Wg

For the investigation of paracrine effects on stem cell behaviour, we developed 'Rapport' ('Repressible activity paracrine reporter'), a dual binary expression system that combines spatiotemporally controlled transgene expression with ReDDM tracing of stem cell progeny. To preserve advantage of the existing established Gal4/UAS drivers and toolbox, we created an entirely new and Gal4-independent lexA/Aop-based '$esg^{lexReDDM}$' (*esg* > > *CD8::GFP*, >>*H2B::mCherry::HA*, *tub-Gal80^{ts}*) tracing system. Importantly, when combined with *mex-Gal4* (*mex* >) for EC specific expression[44], the lexA-operator driven in $esg^{lexReDDM}$ as well as Gal4 driven by *mex* are repressed by temperature-sensitive Gal80^{ts}, which allows simultaneous temporally controlled onset of UAS-transgenes as well as $esg^{lexReDDM}$ tracing and Aop-transgenes (Fig. 5A)[45]. Thanks to the compactness of the $esg^{lexReDDM}$-cassette on one chromosome, we readily created eight 'flavours' of Rapport

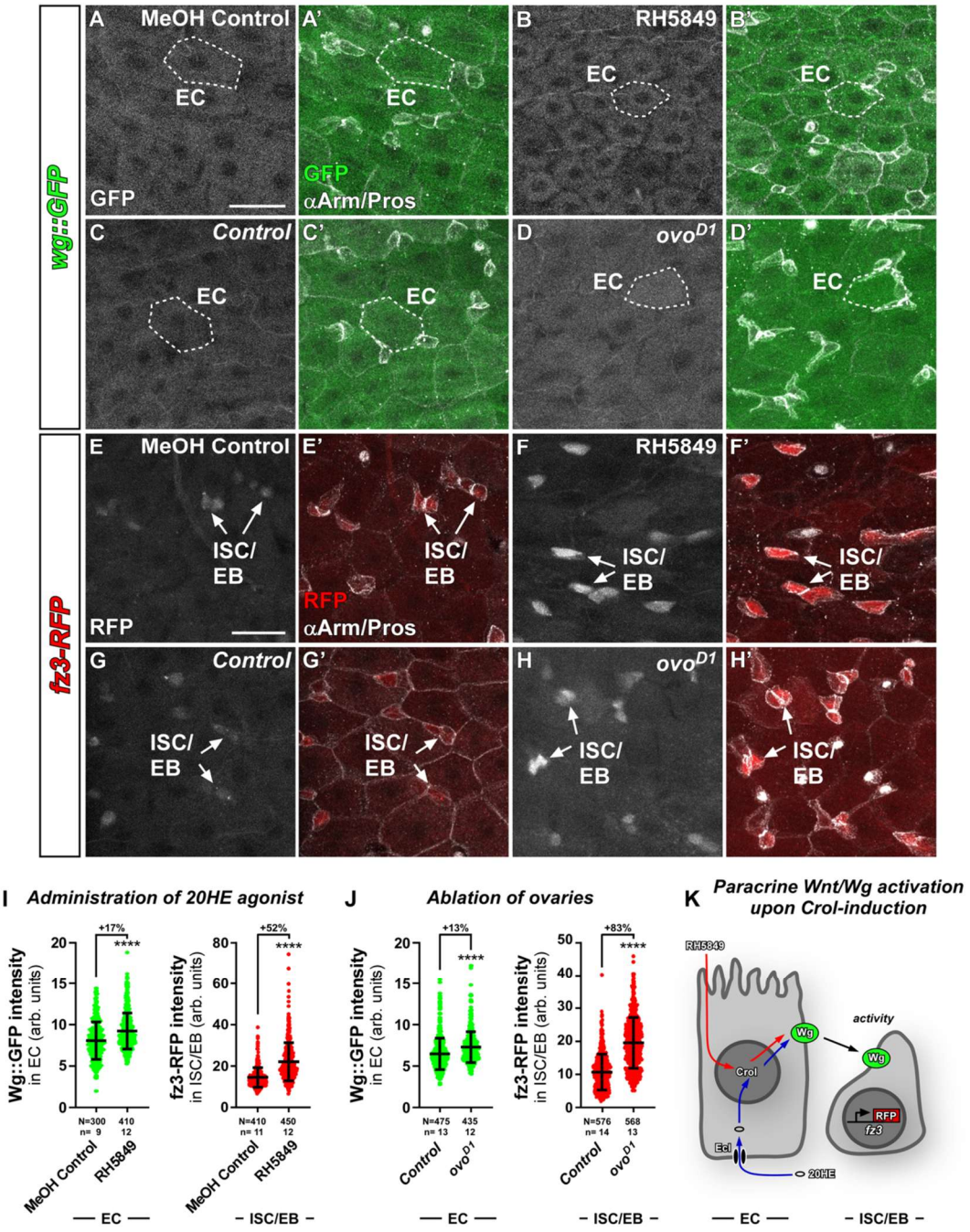

encompassing all major intestinal cell types and adjacent tissues (Table 1).

We confirmed Rapport tracing functionality by tracing outcrossed controls over three weeks (Fig. S6A–C) and observed an expected linear increase in intestinal renewal (Fig. S6E), while ISC/EB numbers remained constant (Fig. S6D) and comparable to the established Gal4/UAS-based *ReDDM*-tracing[22]. Previous reports described autocrine EGFR-stimulation resulting in ISC proliferation and lineage production[28], which we confirmed by crossing Rapport with *mex>* to flies expressing the EGF ligand *Spitz* (>*spi*, TGF alpha homologue)[46] resulting in strongly induced progenitor production (Fig. S6F).

Next, we assessed whether 20HE and Crol controlled Wnt/Wg activity (Fig. 4) stimulates ISC division resulting in EC production and organ size adaptation using Rapport (Fig. 5A). Forced expression of

Fig. 3 | 20HE induces Wnt/Wg ligand expression in EC and consequently Wnt/Wg signalling activity in ISC/EB. A–D' Confocal images of GFP-tagged Wingless ligand (*wg::GFP*) in R5 regions of midguts from (**A–A'**) MF fed with MeOH Control compared to (**B–B'**) MF fed with RH5849, and (**C–C'**) w^{1118} control flies compared to (**D–D'**) dominant ovo^{D1} MF. **A–D** Sole Wg::GFP signal is shown in greyscale and (**A'–D'**) in green colour combined with αArm and αPros to identify ISC/EB,EE and EC. Exemplary measured EC are outlined by white dashed lines. Scale bar is 20 μm. **E–H'** R5 regions of MF midguts with RFP expressed under control of the fz3 promotor (*fz3-RFP*) showing Wnt/Wg activity in (**E–E'**) MF fed with MeOH Control compared to (**F–F'**) MF fed with RH5849, and (**G–G'**) w^{1118} control flies compared to (**H–H'**) dominant ovo^{D1} MF. Exemplary ISC/EB are marked by white arrows. Scale bar is 20 μm. **I–J** Wg::GFP intensities in EC and fz3-RFP intensities in ISC/EB upon (**I**) RH5849 and (**J**) ovo^{D1}. **I–J** Scatter dot plots show individual values with indication of means ± SD. *N* and *n* values represent number of cells and number of biological replicas, respectively. Asterisks denote significances from two-sided Mann-Whitney *U* tests (****$p < 0.0001$). Fold changes are shown in percentages. Source data are provided as a Source Data file. **K** Schematic of paracrine Wnt/Wg activation in ISC/EB upon 20HE increment. RH5849 is incorporated into EC from the midgut lumen, whereas 20HE from surrounding haemolymph is imported into EC by EcI. Within EC 20HE hormone and RH5849 activate expression of Crol and Wg. Wg ligand then non-autonomously activates Wnt/Wg signalling in ISC/EB visualized by fz3-RFP activity.

>EcI, *>crol*/ *>hZNF267* and *>wg* (Fig. 5C–F) non-autonomously increased progenitor cell number (Fig. 5J) and *>EcI* and *>crol* increase ISC progeny numbers (Fig. 5K) compared to controls (Fig. 5B). Reciprocally, depletion of *EcI, crol* and *wg* reduced progenitor numbers (Fig. 5G–J). Importantly, although *>wg-RNAi* significantly reduces *>crol*-induced progenitor numbers (Fig. 5L–N), this rescue is not fully penetrant (Fig. 5J), which might be related to methodological hurdles such as RNAi-efficiency and additional, unknown mitogens acting non-autonomously on ISC proliferation under the control of Crol.

Our results on the autonomous response to Crol in progenitors suggests that Crol is involved in cell cycle exit in klu^{+}-positive EB by repressing *CycB* (Fig. S3A–Q)[33]. When expressing *>wg* with Rapport, we detected an upregulation of *CycB* (Fig. 5O) that might point to a derepression of the CycB promoter by Wg leading to the increase in progenitor production (Fig. 5F, J) and is quite similar in strength to RH5849 induction observed upon EcR-activation (Fig. 2J). Indeed, Wg was previously connected with CycB regulation[27,47] although it is far better known for the regulation of Cyclin D1[48]. Together, our data reveals a direct relay of 20HE activity by Crol into mitogenic paracrine Wnt/Wg signal in enterocytes that is balanced by anti-proliferative Crol autonomously in stem cells. Following this fascinating involvement of endocrine 20HE, Crol and Wg in proliferation control, we sought to investigate their role in intestinal tumour models.

The 20HE-Crol-Wg mitotic balance is conserved in intestinal tumours

Wnt/Wg signalling is a well-known driver of tumorigenesis with a key role in cancers of the intestine. hZNF267 is upregulated in colorectal cancer (CRC) and regulates cell proliferation and differentiation in epithelial cancer entities[23,24]. We found that hZNF267 expression levels positively and negatively correlate with members of the Wnt/Wg signalling pathway (Fig. S7A). CRC originates from ISC[49], which prompted us to investigate *crol* and hZNF267 in two established intestinal tumour models.

Investigating the autonomous role of Crol/hZNF267 in N loss-of-function (LOF, Fig. S7B) tumours[28,30–32] showed that forced expression of *crol* and *hZNF267* within ISC reduced tumour number (Fig. 6A–C, E) further underlining their anti-proliferative function. Furthermore, *>crol* did not induce new EC, which additionally argues for Crol acting on ISC proliferation rather than factors such as *Eip75B* acting on 20HE-induced differenitation[8]. Reciprocally, we did not observe the expected increase in tumour number upon *>crol-RNAi* (Fig. 6D, E), which is probably attributed to already strong mitotic stimuli such as EGF signalling acting on Stg and Cyclins during tumorigenesis outweighing reduced antiproliferative Crol effects[28,50]. Growing evidence proves that microenvironmental Wnt/Wg ligands are an important contributor to the multifaceted process of colorectal tumorigenesis[51–55]. We thus thought to extend Rapport for the investigation of N-LOF tumours. Therefore, we recombined Aop-driven *>>N-RNAi* with *mex-Gal4* yielding a fly stock with ISC-specific *>>N-LOF* that renders ISC incapable of EC lineage production and instead accumulates ISC- and EEP-like tumoral cells[28,30–32] and allows simultaneous EC-specific manipulations (Fig. S7C, Fig. 6F). Using this model, we investigated non-autonomous effects of Crol/hZNF267 manipulations in EC and found that *>crol* boosts ISC tumour cell mass by 4-fold leading to confluent tumours along the midgut (Fig. 6G, J) comparable to tumour-induction by microenvironmentally-derived mitogenic EGF ligands[46,56]. Albeit at a lower rate, *>hZNF267* significantly increases tumour number (Fig. 6H, J), whereas lowering of non-autonomous Wg by *>crol-RNAi* (Fig. 6I–J) and direct depletion by *>wg-RNAi* in EC, does not affect N-tumour growth pointing to stronger mitotic stimulus outweighing paracrine Wg in N-tumours[28,50].

Even though Notch-tumours recapitulate important steps of CRC tumorigenesis[28], N is not frequently mutated in CRC patients. Therefore, we also investigated an autonomous function for Crol/hZNF267 in a CRISPR-Cas9 based model of sporadic CRC[57] targeting the most frequently mutated genes (*Apc1,Apc2,p53,Med* and *Pten*) with a multiplex guideRNA array combined with expression of oncogenic $>Ras^{G12V}$ (Fig. 6O)[57–59]. Initiating these mutations using spatiotemporal induction by $esg^{ReDDMCas9}$, CRC from ISC results in severe and pleiotropic cellular phenotypes (Fig. 6K) and early fly demise (Fig. S7D)[57]. Underlining the protective autonomous role of *crol* and hZNF267 (Fig. 6E), their forced expression in CRC avatars significantly improved fly survival (Fig. 6P).

An apparent phenotype of CRC avatars is the loss of epithelial integrity by multilayering of intestinal cells[59–61]. On the cellular level, epithelial deterioration of the tight honeycomb-like intercellular junctional network between EC is visualized by disruption of the septate junction marker *discs large 1* (*dlg1*)[62]. In CRC avatars expressing *>crol* and *>hZNF267*, intact hexagonal Dlg1 junction networks are significantly increased compared to control CRC avatars (Fig. 6K–M, Q). Reciprocally, *>crol-RNAi* significantly increases multilayering (Fig. 6N, Q) strengthening the idea of a tumour suppressive role for Crol and hZNF267. Epithelial deterioration results in hypotrophy of the midgut over time, which strongly reduces midgut length of CRC avatars. Additional *>crol* and *>hZNF267* expression restore midgut hypotrophy to wild-type length (Fig. 6R) and seem to correlate with multilayering and proliferation in predicting survival (Fig. 6P–R).

These functional experiments in intestinal tumour paradigms additionally support the idea of a mitotic balance controlling intestinal growth. Overall, steroidal input on Crol in ISC (Fig. 2) and EC (Fig. 5) provides evidence for an endocrine intestinal size control implicated in mating hyperplasia. Finally, we tested our hypothesis of hormonally controlled intestinal size in a mathematical model.

Mathematical modelling of endocrine relay by Crol in the control of ISC proliferation underlines complex hormonal actions on intestinal size adaptation

Our model tests whether it is mathematically plausible that these opposing trends between mitotic and anti-proliferative stimuli based on the molecular mechanisms found in this study are able to induce stable population sizes that change consistently with 20HE levels. In the supplementary material we provide all the details for the construction of the model. In addition to our current and previous data[8], we assume constant 20HE levels in VF and a higher constant 20HE level in MF[8]. Then, we test the specific hypothesis whether an 20HE increment is capable to yield a stable, larger organ by temporarily boosting

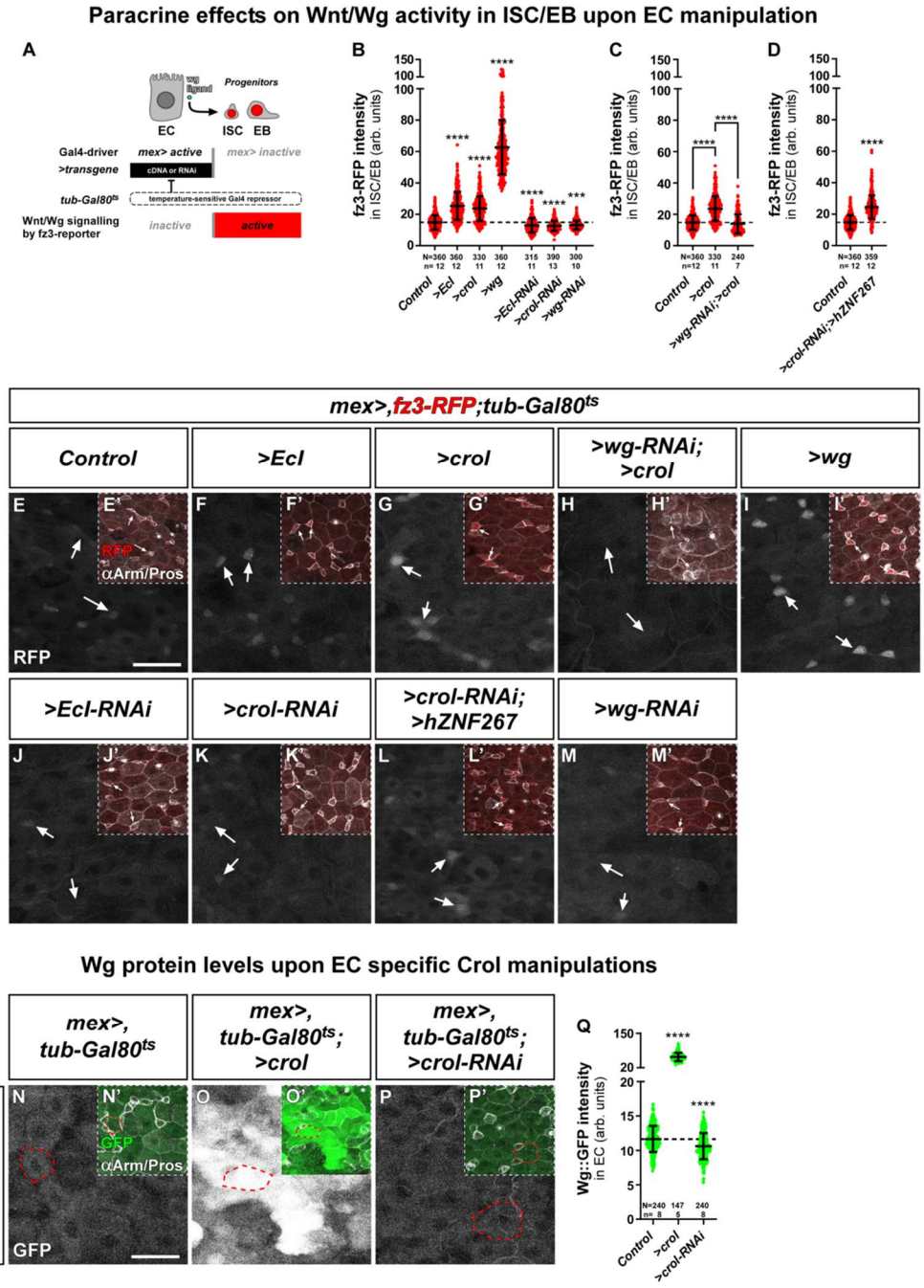

ISC mitosis, which then declines through the increment of EC numbers and the autonomous, anti-proliferative effects in ISC. Our biological findings show that downstream of mating-related 20HE stimulation, Crol autonomously (Fig. 7A, A′) and non-autonomously (Fig. 7B, B′) controls midgut size and diameter of R5 (Fig. 7A–C). In addition, we found the entire midgut increased in length and consequently cell numbers (Fig. 7C, Fig. S7F) in concordance with previous reports using cell numbers to address intestinal size[18,19,63,64].

For our model, we postulated constant hormonal input (Fig. 7D) produces equal amounts of mitogenic Wnt/Wg independent of EC numbers. In these conditions the amount of Wnt/Wg produced in a neighbourhood of an ISC decays with the increase of EC, since the

Fig. 4 | The 20HE-Crol-Wg axis in EC controls Wnt/Wg signalling activity in ISC/EB. A Schematic of the system enabling EC manipulation and simultaneous visualization of Wnt/Wg activity in ISC/EB. EC specificity of *mex-Gal4* allows manipulation of UAS-driven transgenes that are timely controlled by the ubiquitously expressed temperature sensitive Gal4 repressor (*tub-Gal80^{ts}*) and combined with the fz3-RFP reporter reflecting Wnt/Wg signalling activity in ISC/EB independent of Gal4. **B**–**D** fz3-RFP intensities in ISC/EB with (**B**) OE and KD of *EcI*, *crol* (F003414, BL41669) and *wg* (*>wg-RNAi*: $p = 0.0005$), (**C**) EC specific OE of *crol* (F003414) combined with *>wg-RNAi*, and (**D**) ectopic expression of *>hZNF267* in *crol* depleted EC (BL41669). **B**–**D** Experiments have been performed in parallel. **E-M′** Confocal images of *fz3-RFP* combined with *mex>* and *tub-Gal80^{ts}* from R5 regions of MF midguts after 24 h in (**E**–**E′**) controls, EC specific OE of (**F**–**F′**) *EcI*, (**G**–**G′**) *crol* (**H**–**H′**) with simultaneous KD of *wg*, and (**I**–**I′**) *wg*, and KD of (**J**–**J′**) *EcI*, (**K**–**K′**) *crol* (**L**–**L′**) with simultaneous expression of *>hZNF267*, and (**M**–**M′**) KD of *wg* in EC. **E**–**M** Sole fz3-RFP signal is shown in greyscale and (**E′**–**M′**) in red colour combined with αArm and αPros staining for identification of ISC/EB. Exemplary measured ISC/EB are marked by white arrows. Scale bar is 20 μm. **N**–**P′** MF midguts after 3 d with *wg::GFP* crossed to (**N**–**N′**) *mex>,tub-Gal80^{ts}* serving as control, (**O**–**O′**) combined with EC specific OE of *crol* and (**P**–**P′**) *>crol-RNAi*. **N**–**P** Sole Wg::GFP signal is shown in greyscale and (**N′**–**P′**) in green colour combined with αArm and αPros staining for identification of ISC/EB, EE and EC. Exemplary measured EC are outlined by red dashed lines. Scale bar is 20 μm. **Q** Wg::GFP levels in EC upon *mex>* driven manipulations of *crol* (F003414, BL41669). **B**–**D**, **Q** Scatter dot plots show individual values with indication of means ± SD. *N* and *n* values represent number of cells and number of biological replicas, respectively. Asterisks denote significances from multiple comparisons by Kruskal-Wallis tests (***$p < 0.001$;****$p < 0.0001$). Source data are provided as a Source Data file.

same amount of hormone per EC must be shared by a larger number of cells[65]. We call γ the net amount of hormone, E the net amount of EC and, therefore, γ/E the concentration of the hormone sensed by an EC. Generically, the concentration $c(\ell, \gamma/E)$ of Wnt/Wg-ligand decays exponentially with the distance to the source l [66,67]:

$$c(\ell, \gamma/E) = \frac{\gamma}{E} e^{-\ell\sqrt{\frac{k}{D}}} \tag{1}$$

where k is the degradation rate and D the diffusion constant of Wnt/Wg-ligand—we assume constant mapping between its concentration and 20HE concentration, with proportionality constant 1, for the sake of simplicity. Therefore, considering a section of the intestine as a 1D ring, the average amount of mitogenic Wnt/Wg-ligand reaching equidistantly scattered ISC located at position x_I will be approximately described by:

$$\approx \frac{\gamma}{E} \int_{\Omega} \left\{ e^{-|\ell - x_I|_{\rightarrow}\sqrt{\frac{k}{D}}} + e^{-|\ell - x_I|_{\leftarrow}\sqrt{\frac{k}{D}}} \right\} d\ell \tag{2}$$

where the integration runs along the whole ring of cells Ω, and the two exponential terms describe the contribution of the diffusion of Wnt/Wg-ligand either clockwise or counterclockwise from the source. The inside of the integral will decline sharply when intestinal size increases, leaving only the close neighbourhood of the ISC to effectively contribute to the Wnt/Wg levels playing an active role in their proliferation, independently of organ size. Indeed, our biological measurements show that ISC numbers remain constant after mating, thus increasing average distances between ISC upon size adaptation (Fig. S7E). Consequently, in the equations of evolution for the number of EC we have a mitotic term that is proportional to the concentration of 20HE ($\approx C\gamma/E$) and an anti-proliferative term that can be assumed to be constant or, in a more general setting, declining slower than the mitotic term as a function of the concentration (Fig. 7E). We assume the net increase of 20HE production after mating to follow a sigmoid shape (Fig. 7D). In addition, the differentiation of ISC into EC occurs in a finite time span τ. This implies that, aside from ISC and EC, we must consider a population of cells differentiating from ISC to EC. We can consider two scenarios for the inhibiting effect of the hormone: either the presence of 20HE 1/blocks the differentiation process or 2/blocks ISC proliferation. Interestingly, the predicted behaviour of the EC population is the same in these two scenarios. Overall, the equations of evolution for the number of transient cells (u) and EC (E) in case 1/ (Fig. 7F) read:

$$\frac{du}{dt} = C\frac{\gamma}{E} I - \theta u \tag{3}$$

$$\frac{dE}{dt} = \theta u - \alpha I \tag{4}$$

where I the number of ISC, α the anti-proliferative rate and $\theta = 1/\tau$ is the rate of EC production out of the population of cells coming from the proliferation of ISC transiting to EC (Fig. 7E). The key result is that incorporating the antagonistic effects of the 20HE hormone the system has a stable, fixed point for the amount of EC that grows and declines consistently with the net amount of 20HE hormone (Fig. 7F). Specifically, the stable point is found at:

$$E^{\star} = C\frac{\gamma}{\alpha}. \tag{5}$$

Interestingly, similar dynamical equations have been proposed to model the dynamics of cortisol concentration in blood for humans[68]. In the supplementary information file we provide detailed information about the construction and mathematical properties of the model.

As an example, we hypothetically explored how constant EC numbers as generated in N-LOF tumours intestines would affect ISC division dynamics. With constant EC numbers and hormone level (Fig. 7D, Fig. S7G), ISC counts in our model increase in a square-root-like manner (Fig. S7H, I) as the ISC population would provide a growing sink for mitogens such as Wg. In our experiments, block of EC generation and organ size is recapitulated in N-LOF tumours using Rapport (Fig. 6F, Fig. S7C), where upregulation of Crol/hZNF267 significantly increases ISC numbers (Fig. 6G, H, J, Fig. S7I). Our discovered interdependencies between cell population sizes, Wnt/Wg-degradation and their endocrine mitotic balance shed light on the complex endocrine involvement when tumour growth mechanisms are investigated. Together, our model is capable of capturing the emergence of a stable organ size from the antagonism of mitogenic and anti-proliferative hormonal input on ISC thresholding organ size as suggested by our functional data (Fig. 7G, G′).

Discussion

Here we identify the transcription factor *crooked legs* as coordinator of endocrine input into intestinal organ size. The discovered molecular mechanisms underline the complexity of heterologous cellular interactions: a hormonal stimulus bifurcates on stem cells and microenvironment, where it is relayed differentially into an antiproliferative and a mitogenic stimulus. This interdependent opposing crosstalk of forces balances stem cell divisions and ultimately stabilizes organ size, which is sustained by both, empirical observations and mathematical modelling.

Our novel Rapport system contributes to disentangle the underlying endocrine and local signalling organ size control mechanisms, by allowing precise genetic intervention in cell types surrounding the ISC. The independent tracing of the whole stem cell population and easy fluorophore identification of different fate choices ensures robust progeny counts in fluctuating demand situations compared to previous systems[28,46,56]. Endocrine actions on ISC are complex and involve

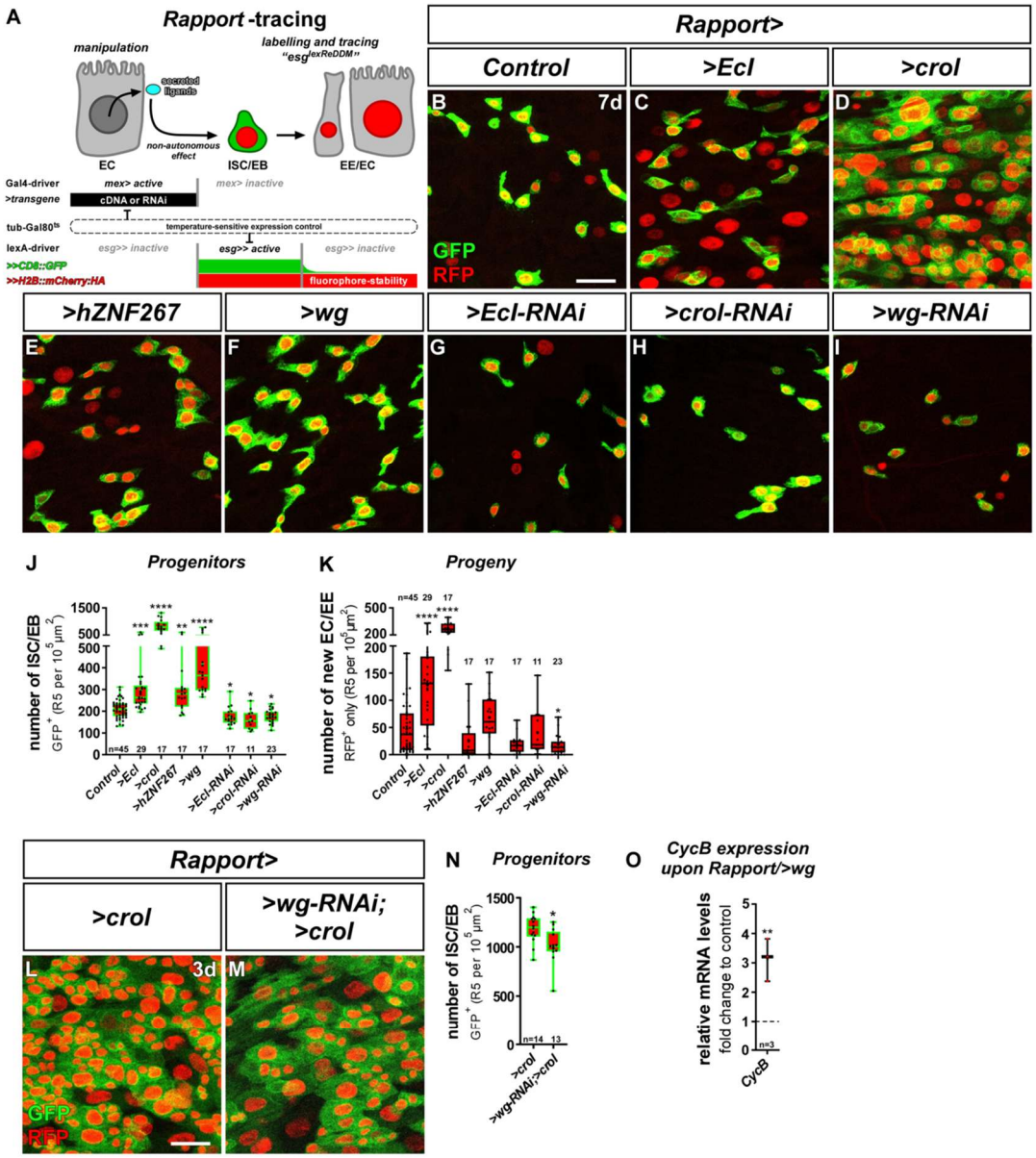

Fig. 5 | The 20HE-Crol-Wg axis in EC controls intestinal homeostasis. A Schematic of 'Repressible activity paracrine reporter' (Rapport) tracing system. Rapport consists of the EC *mex-Gal4* driver for UAS-driven transgenes like cDNAs or RNAi. Additionally, an $esg^{lexReDDM}$ system based on lexA/Aop allows Gal4/UAS independent labelling and tracing of ISC/EB by *esg-lexA* driven expression of *Aop-CD8::GFP* and *Aop-H2B::mCherry::HA* (lexA/Aop abbreviated as '>>' hereafter). Both expression systems are timely controlled by a tub-Gal80^{ts} repressor. **B**–**I** Confocal images showing R5 regions of MF midguts after 7 d of Rapport tracing in (**B**) controls, with OE of (**C**) *EcI*, (**D**) *crol* (BL58359), (**E**) *hZNF267* and (**F**) *wg*, and KD of (**G**) *EcI*, (**H**) *crol* (BL41669) and (**I**) *wg* showing GFP$^+$ and mCherry$^+$ ISC/EB and their differentiated progeny labelled by mCherry only. Scale bar is 20 µm. **J**, **K** Quantification of (**J**) progenitor cell numbers (>*EcI*:$p = 0.0003$; >*hZNF267*:$p = 0.0053$; >*EcI-RNAi*:$p = 0.0467$; >*crol-RNAi*:$p = 0.0375$; >*wg-RNAi*:$p = 0.0388$) and (**K**) their progeny (>*wg-RNAi*:$p = 0.0285$) upon EC specific manipulations using Rapport. **L**, **M** Confocal images showing R5 regions of MF midguts after 3 d of Rapport tracing with (**L**) sole OE of *crol* (F003414) and (**M**) combined with >*wg-RNAi*. (**N**) Progenitors upon EC specific OE of *crol* alone and combined with >*wg-RNAi* ($p = 0.0109$). Scale bar is 20 µm. **O** Quantitative RT-qPCR on midgut cDNA of MF with Rapport specific expression of >*wg* showing relative mRNA levels of *CycB*. **J**, **K**, **N**, **O** For Box-and-whisker plots: the center is the median, minima and maxima are 25th and 75th quartile and whiskers indicate full range of values. All individual values with 'n' representing numbers of biological replicas are shown by dots and means are indicated by '+'. Asterisks denote significances from (**J**, **K**) multiple comparison by Kruskal-Wallis tests and (**N**) unpaired two-sided *t*-test (*$p < 0.05$; **$p < 0.01$; ***$p < 0.001$; ****$p < 0.0001$). Source data are provided as a Source Data file.

Table 1 | List of Rapport-tracing variants established in our lab with indication of Gal4 driver used and the cell type/tissue with Gal4-activity

Rapport-tracing variant	Gal4-driver	Cell type/tissue with Gal4-activity
'EC-Rapport'	*mex-Gal4*	Intestinal EC
'EB-Rapport'	*klu-Gal4*	Intestinal EB
'EE-Rapport'	*Rab3-Gal4*	Intestinal EE
'ISC-Rapport'	*Dl-Gal4*	Intestinal ISC
'VM-Rapport'	*how-Gal4*	Visceral muscle (VM)
'HG-Rapport'	*byn-Gal4*	Hindgut (HG)
'CA-Rapport'	*Aug21-Gal4*	*Corpus allatum* (CA)
'hemocyte-Rapport'	*HmlΔ-Gal4*	*Hemocytes*

hormonal dosage and mating status[4,7,8], sex differences[19] and feeding[63]. Hypertrophy upon pregnancy is described in the mammalian gut[1,3] and is well-studied in reproductive organs such as the mammary epithelium where steroid hormones induce extensive remodelling and cancer susceptibility[69–71].

In gastrointestinal tumours such as CRC, epidemiological evidence about the role of steroid hormones remains controversial and ranges from favourable to detrimental[72–78]. Functional studies of both mammalian oestrogen receptors (ER) in rodents underline the complexity of oestrogen signalling in gut tumorgenicity[79,80] and reveal further complexities as pharmacological (E2/P4) and endogenous oestradiol levels differentially affect patient outcome[72,75,81]. Our functional biological and mathematical modelling data provides an initial logic to disentangle complex observations and involves the heterogeneity of tumour cell composition and its capacity to contribute to mitotic signals.

A targeted therapeutic intervention of steroid hormone signalling is supported by: (i) an overall protective tendency of ER signalling in CRC[78]. (ii) Like Crol, hZNF267 is stimulated by ER[25] and is involved in Wnt/Wg signalling (Fig. S7A)[23,24] suggesting conservation of the 20HE-Crol-Wg axis. (iii) Wnt/Wg signalling hyperactivation is central to CRC malignancy and Wnt/Wg-ligands remain indispensable for CRC growth albeit absence of APC[82]. (iv) Effectors of steroid signalling like PPARγ/Eip75B play protective roles in fly pathophysiology[4,8] and human disease[83,84].

Our findings of antagonizing autonomous and paracrine effects of Crol and hZNF267 on tumour growth (Figs. 6, 7, S7) emphasize that targeted genetic investigation is of key importance to understand how mutational heterogeneity and cell type composition differentially affect the proliferative response to hormonal input. Precise intervention and tracing methods such as Rapport open the door for untangling heterogenous findings of epidemiological and functional studies.

Methods

Genetics and fly husbandry/fly strains

The following transgenic fly stocks were used: *Gbe+Su(H)-dsRed* (T. Klein), *esg*^{ReDDM}[22], *esg*^{ReDDMCas9}[85], *klu*^{ReDDM}[34], *UAS-wg*[86], *UAS-EcI*[21], *UAS-EcI-RNAi*[21], *mex-Gal4* on II. Chromosome[44], *fz3-RFP*[40], *wg::GFP*[36], *13x LexAop2-H2B::mCherry::HA*[87], *UAS-N*^{DN} (J. Treisman), *UAS-Ras*^{G12V}, *>Apc1, Apc2, p53, Med, Pten*^{sgRNAs}[85], *hs-Flp;;actin-FRT-stop-FRT-Gal4,UAS-RFP* (A. Wodarz).

From Bloomington *Drosophila* Stock Center (BDSC): *ovo*^{D1} (BL1309), *UAS-crol* (BL56762 and BL58359), *UAS-crol-RNAi* (BL41669 and BL44643), *UAS-stg-RNAi* (BL34831), *UAS-CycB-RNAi* (BL40916), *UAS-CycB*^{gRNA}(BL80319), *UAS-hZNF267* (BL65797), *esg-lexA* (BL66632), *13xLexAop2-mCD8::GFP* (BL32205), *mex-Gal4* on X Chromosome (BL91367), *UAS-N-RNAi* (BL33616), *nos-phiC31;;attP86Fb* (BL24749), *UAS-spi* (BL63134), *UAS-nls.GFP* (BL4775).

From FlyORF, Switzerland: *UAS-crol* (F003414), *UAS-stg* (F000926).

From Vienna *Drosophila* Resource Center: *crol::GFP* (V318880), *UAS-wg-RNAi* (V104579), *UAS-y*^{gRNA} (V341666), *UAS-se*^{gRNA} (V341664).

Throughout the manuscript we use a uniform notation to distinguish between enhancer- and protein trapping. For enhancer traps we separate enhancer and reporter/transgene by '-' as in *Gbe+Su(H)-dsRed* or *UAS-wg*, whereas for protein traps we separate protein and reporter by '::' as in *wg::GFP*. Additionally, Gal4-UAS regulation is indicated by '>', and lexA-Aop by '>>'.

Food composition and fly keeping

Fly food contained 1424 g corn meal, 900 g malt extract, 800 g sugar beet syrup, 336 g dried yeast, 190 g soy fluor, 100 g agarose in 20 l H_2O. The ingredients were mixed and cooked for about one hour to reduce bioburden. After cooling down the food 90 ml propionic acid and 30 g NIPAGIN (antimycotic agent) were added, and the food was filled in small plastic vials plugged with foam. Flies were kept at 25 °C. Crosses containing a temperature sensitive Gal80^{ts} repressor were kept at 18 °C to repress Gal4 activity during development and shifted to 29 °C to start transgene expression in adult flies. Experiments distinguishing between virgin female flies and mated female flies were run on food with twice the amount of NIPAGIN to prevent the induction of tissue renewal caused by pathogenic stress upon mucous formation in the absence of larvae.

Cloning of *crol*^{gRNA} construct

Two individual guide RNAs (gRNA) targeting the coding region of genomic *crol* DNA with a distance of 603 bp were chosen using the CRISPR Optimal Target Finder[88]. Primers for amplification of these gRNAs were designed and used as descripted previously[85]: crol_gRNA_for (5′-ATAAGAAGACCTTGCAGGCCACTGCGTCGTCGCAAGCGGGTTTCAGAGCTATGCTGGAAAC-3′) and crol_gRNA_rev (5′-ATAAGAAGACCCAAACCCCGGTGTTAACTGGACCGCACCTGCACCAGCCGGGAATCGAACC-3′).

Cloning of the amplified crol^{gRNA} construct into pCFD6_noSapI was performed as descripted previously[85]. After amplification and verification of the construct, the DNA was injected into embryos of *nos-phiC31;;attP86Fb* flies for integration on the third chromosome.

Generation of Rapport-tracing

Rapport-tracing consists of '*esg*^{lexReDDM}' which is a quadruple recombinant of *esg-lexA,13xLexAop2-CD8::GFP,13xLexAop2-H2B::mCherry::HA,tub-Gal80*^{ts} on the second chromosome. Rapport can easily be combined with any Gal4-driver on the first or third chromosome enabling manipulation of other cell types or even organs and allow manipulation independent of *esg*^{lexReDDM} tracing. For our investigation of Crol we combined Rapport-tracing with an EC specific *mex-Gal4* on the third chromosome that was generated by mobilization of the *mex-Gal4* P-element in BL91367, and a *klu-Gal4* on the third chromosome for unequivocal identification of ISC. Additional Rapport-tracing variants from our lab can be found in the author response letter and Table 1.

Cloning of *lexAop-N-RNAi* construct

The *lexAop-N-RNAi* construct was generated as described previously[89]. Genomic DNA of the VALIUM20 based N-RNAi line from the Transgenic RNAi Project (Trip-3, BL33616) was isolated and added to a PCR reaction using the Q5 High-Fidelity DNA Polymerase (NEB) and the following primers: shRNA_GA_F primer (5′-GAGAACTCTGAATAGATCTGTTCTAGAAAACATCCCATAAAACATCCCATATTCA-3′) and shRNA_GA_R1 primer (5′-CTCTAGTCCTAGGTGCATATGTCCACTCTAGTA-3′)[89].

The pWALEXA20 vector[89] was digested with XbaI and NdeI prior to assembling with the amplified N-shRNA by Gibson-assembly. After verification by colony PCR and sanger sequencing constructed plasmids were amplified and injected into embryos of *nos-phiC31;;attP86Fb* flies for integration on the third chromosome.

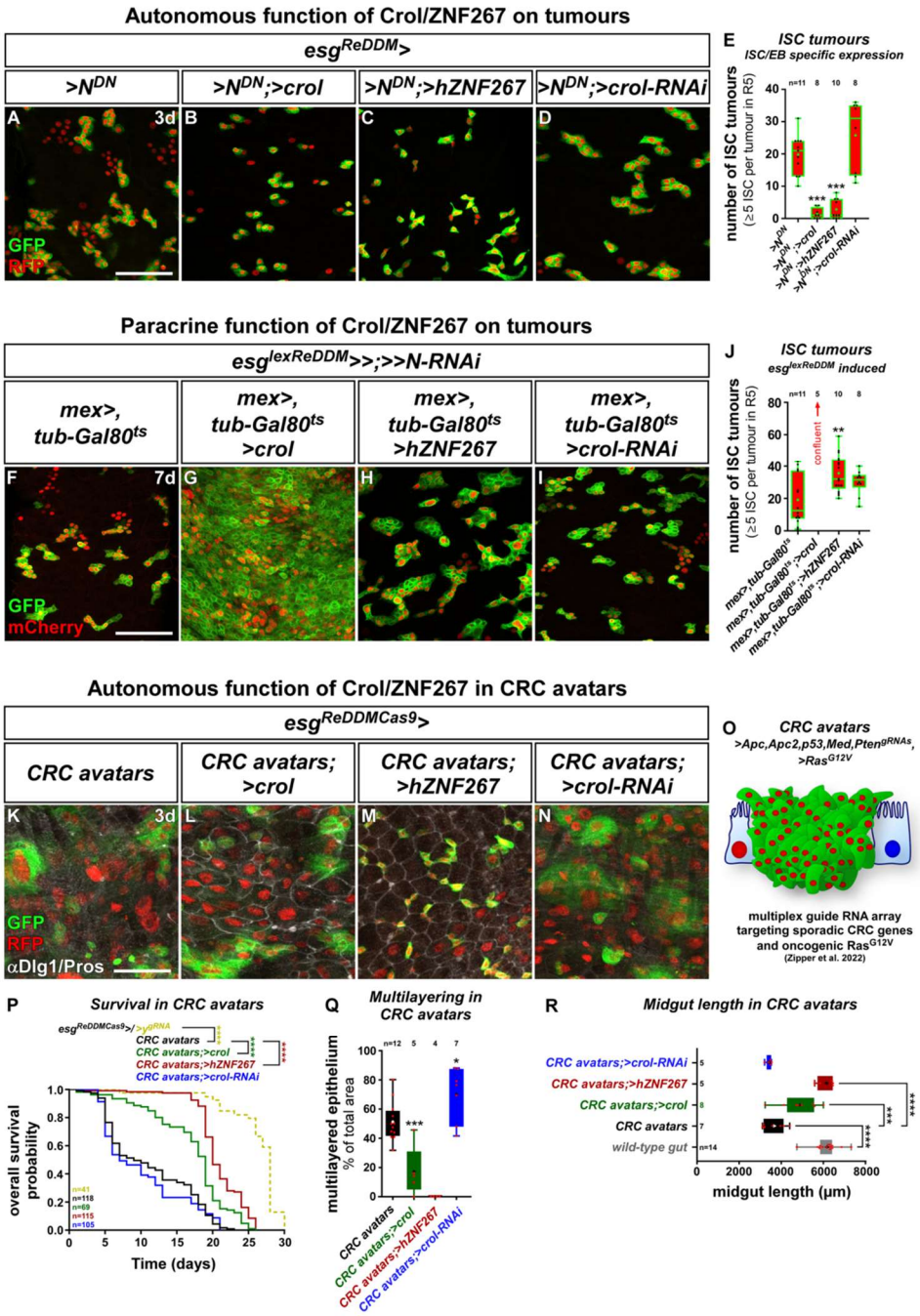

Hormone analogue treatments

RH5849 feeding experiments have been performed as described previously except for adjusted feeding durations[90]. The ecdysone agonist RH5849 (DRE-C16813000, DrEhrenstorfer) was diluted in MeOH to create a stock solution of 20 µg/µl. Then, 20 µl of this stock solution was mixed with 4 ml of reheated, liquid fly food in a fresh vial (340 µM final concentration). As a control, an equivalent volume of MeOH was added to the fly food. Flies were starved for four hours prior to RH5849 treatment to make them eat the prepared food immediately. In initial experiments we additionally added the blue dye (Erioglaucine Disodium Salt (E133) (BLD Pharmatech Ltd., Shanghai, China)) known from the so called 'Smurf assay' to the food as described previously[62,91]. The blue dye

Fig. 6 | The mitotic balance of Crol/hZNF267 is preserved in intestinal tumour models. A–D Confocal images showing R5 regions of MF midguts with esg^{ReDDM} tracing of dominant negative Notch (> N^{DN}) for 3 d in (**A**) controls, with (**B**) >*crol* (F003414), (**C**) > *hZNF267*, and (**D**) >*crol-RNAi* (BL44643). Scale bar is 50 μm. **E** Quantification of ISC tumours encompassing clusters of five or more ISC ($p = 0.0003$; $p = 0.0006$). **F–I** Confocal images showing R5 regions of MF midguts with ISC/EB specific >>*N-RNAi* using *esg-lexA* of the Rapport-tracing system for 7 d in (**F**) controls, combined with EC specific (**G**) >*crol* (F003414), (**H**) > *hZNF267*, and (**I**) >*crol-RNAi* (BL44643). Scale bar is 50 μm. **J** Quantification of ISC tumours Rapport manipulations of Crol/hZNF267 ($p = 0.0045$). **K–N** Confocal images showing R5 of MF midguts after 7 d of $esg^{ReDDMCas9}$ tracing and induction of 'CRC avatars' by multiplex guide RNA array. $esg^{ReDDMCas9}$ allows labelling and tracing of tumour cells in (**K**) controls and with tumour specific expression of (**L**) >*crol* (F003414), (**M**) > *hZNF267* and (**N**) >*crol-RNAi* (BL44643). Scale bar is 50 μm. **O** Schematic of 'CRC avatars' combined with $esg^{ReDDMCas9}$ tracing with oncogenic >Ras^{G12V} and CRISPR/Cas9 induced knockout of *Apc1,Apc2,p53,Med* and *Pten*. **P** Kaplan-Meier estimation of survival in flies with $esg^{ReDDMCas9}$ induced knockout of *yellow* (*y*) serving as 'mock'-gRNA control and CRC avatars combined with manipulations of Crol/hZNF267. Number of analyzed flies is indicated by 'n' and asterisks denote significances from Kaplan-Meier estimation (****$p < 0.0001$). (**Q**, **R**) Quantification of (**Q**) multilayered tissue encompassing percentage of area with disrupted αDlg1 staining ($p = 0.0006$; $p = 0.0205$) and (**R**) midgut length as indicator of epithelial deterioration (CRC avatars; >crol:$p = 0.0004$). **E**, **J**, **Q**, **R** For Box-and-whisker plots: the center is the median, minima and maxima are 25th and 75th quartile and whiskers indicate full range of values. All individual values with 'n' representing numbers of biological replicas are shown by dots and means are indicated by '+'. Asterisks denote significances from multiple comparisons by (**E–J**) Kruskal-Wallis tests and (**Q**, **R**) One-way ANOVA (*$p < 0.05$; **$p < 0.01$; ***$p < 0.001$; ****$p < 0.0001$). Source data are provided as a Source Data file.

allowed us to determine the food's passage time through the gut and to establish a feeding duration of 48 h for our final experiments. RH5849 treatments were performed at a temperature of 25 °C.

Flp-out clones

Flp-out clones were induced in midguts by flippase under control of a *heat-shock* promotor. Flippase expression was activated for 45 min in a 37 °C-water bath to induce positively marked clones and expression of >*EcI* and >*EcI-RNAi* within the marked clones. Guts were dissected 3 days after clone induction.

Immunohistochemistry

Guts of adult female flies were dissected in 1 × PBS and transferred into glass wells containing 4% PFA immediately after dissection. After 45 min of fixation the guts were washed once by replacing the PFA with 1 × PBS. Primary antibodies were diluted in 1 × PBS with 0.5% Triton-X and 5% normal goat serum. The incubation with primary antibodies (1:250 anti-Arm [mouse; Developmental studies Hybridoma Bank (DSHB)]; 1:200 anti-Dl [mouse; Developmental studies Hybridoma Bank (DSHB)]; 1:250 anti-Dlg1 [mouse; Developmental studies Hybridoma Bank (DSHB)]; 1:5000 anti-PH3 (Ser10), Mitosis Marker [rabbit; Sigma-Aldrich];1:250 anti-Pros [mouse; Developmental studies Hybridoma Bank (DSHB)]) was performed on an orbital shaker at 4 °C over night. The guts were washed with 1 × PBS prior to incubation with secondary antibodies (1:500 Goat anti-Mouse Alexa647 [Invitrogen]; 1:500 Goat anti-Mouse Alexa561 [Invitrogen]; 1:500 Goat anti-Rabbit Alexa647 [Invitrogen]) and DAPI (1:1000; 100 μg/ml stock solution in 0.18 M Tris pH 7.4; DAPI No. 18860, Serva, Heidelberg) for at least 1½ h at RT. After washing with 1 × PBS for a last time, the stained guts were mounted in a drop of Fluoromount-G Mounting Medium (Electron Microscopy Sciences) mixed with a drop of 1 × PBS on a microscope slide and covered with a coverslip. For squeezing of the mounted tissues, a defined weight of 28.5 g was put on top of the coverslip.

Image acquisition

After immunostaining posterior midguts were imaged using a LSM 710 confocal microscope (Carl Zeiss Microscopy GmbH, Germany) with an 40× objective. Image resolution was set to at least 3440 × 3440 pixels. About four to five confocal planes with 1 μm interval were scanned and combined into a Z-stack to image one cell layer with all different cell types.

For comparison in midgut length, diameter and total cell number of VF to MF, the entire midguts from MHB to proventriculus were imaged using a 10× objective and the tile-scan mode.

For length measurements of midguts from CRC avatars flies were imaged with an Axioplan2 microscope equipped with a PixelFly camera. Images were taken using a 5× objective and the AxioVision Rel. 4.7 software.

Quantification of cell numbers, midgut lengths, and diameters

Fiji (ImageJ 1.51 n, Wayne Rasband, National Institutes of Health, USA) was used to calculate maximum intensity images out of Z-stacks from posterior midguts. Progenitor cell numbers and numbers of progeny from esg^{ReDDM}[22] experiments were counted manually using Fiji. Numbers of DAPI positive cells in R5 were analysed semi-automatically by self-written macro for Fiji (macro available from the authors), whereas total cell numbers of entire midguts were counted manually. Midgut lengths and diameters were analysed manually in Fiji using the free-hand line tool.

Quantification of fluorescence intensities

For intensity measurements of fluorophores, posterior midguts were scanned with fixed laser/exposure time settings. Fluorescence intensities were analysed in Fiji by determining the mean intensity per area of manually selected ROI.

For quantification of Crol::GFP levels midguts were stained with antibodies targeting the ISC/EB marker Arm[31] and the EE marker Pros[30] to unequivocally distinguish the different cell types. After imaging the nuclei of the different cell types were outlined manually and mean intensities per area were determined using Fiji. 30–56 cells per cell type and gut (indicated as 'N' in figure panels) in three to four different guts (indicated as 'n' in figure panels) were measured. We also measured the total area of R5 in each group and calculated a fold change in R5 area of the tested conditions compared to the corresponding control. We multiplied the Crol::GFP intensities by the calculated fold change in R5 area thereby normalizing the intensities to take into account mating induced area changes, which lead to a dilution of actual hormone dosage reaching a single cell in a mating adapted intestine. Crol::GFP levels for crol-RNAi validation (Fig. S2I–L) are not normalized. We then compared the Crol::GFP levels between different groups by statistical analyses.

The procedures we used to measure fz3-RFP intensities were the same as described for Crol::GFP intensities except for the normalization. Fz3-RFP intensities in nulcei of $aArm^+$ ISC/EB were normalized to ISC/EB numbers. Therefore, we compared ISC/EB numbers of the tested groups and calculated the fold changes to the corresponding control. We multiplied measured fz3-RFP intensities with the calculated fold changes to compensate for dilution and degradation of Wg ligands reaching individual cells with increasing ISC/EB numbers as sink for Wg ligand.

For quantification of Wg::GFP levels midguts we also used immunostainings to unequivocally distinguish between the different cell types. After imaging we outlined 25–30 single EC per gut in R5 to define a ROI in which we measured mean intensities per area. Due to a low signal-to-noise ratio in the Wg::GFP signal we subtracted background signal from the measured Wg::GFP intensities. Therefore, we outlined ten areas per midgut within nuclei of EC where we would not

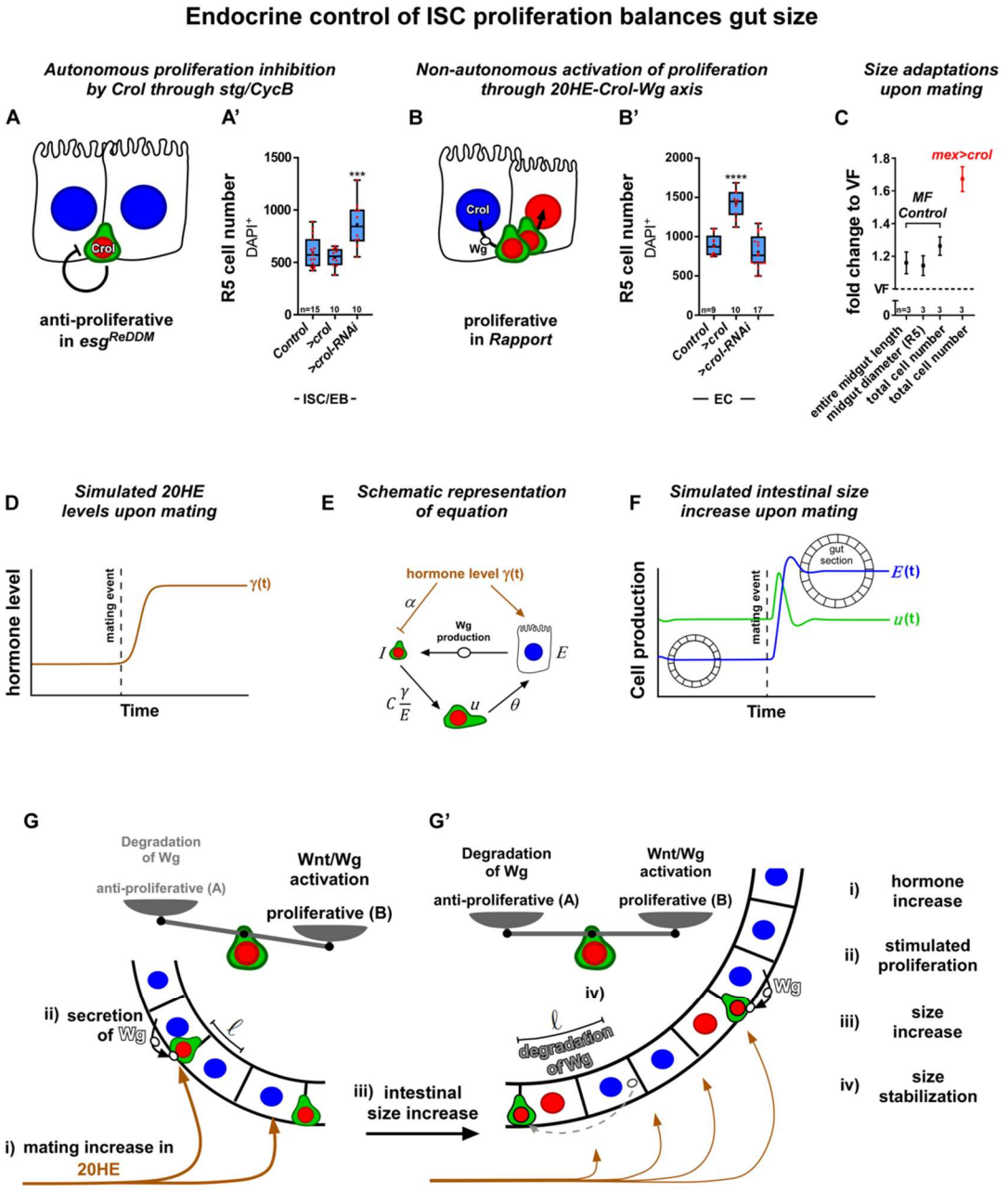

expect Wg ligands to localize. We then measured mean intensities per area within these defined ROI and calculated the average background signal for each gut. The calculated average background signal was subtracted from the individual Wg::GFP intensities we measured in EC. Resulting Wg::GFP levels of different groups were then compared by statistical analyses.

Survival assays

CRC avatar flies were grown at 18 °C and shifted to 29°C at latest 24 h after eclosion with at least ten flies per vial. Female and male flies were assayed with 34 to 118 flies for each genotype. Dead animals were counted once a day and statistical significance of survival differences determined using Kaplan-Meier log-rank survival test.

Analysis of correlation of hZNF267 and Wnt/Wg signalling components in colon adenocarcinoma

Correlating expression of hZNF267 and Wnt/Wg signalling components in colon adenocarcinoma was analyzed using the R2 Genomics analysis and visualization platform. In a single dataset analysis using the Mixed Colon Adenocarcinoma (2022-v32) from tcga we searched

Fig. 7 | Mathematical modelling of hormone level controlled intestinal size. A, B Schematics of Crol inhibiting proliferation in ISC through stg/CycB and non-autonomously activating proliferation by Wg expression in EC. **A'**–**B'** Quantification of cell numbers in R5 regions upon (**A'**) ISC/EB specific ($p = 0.0003$) and (**B'**) EC specific manipulations of *crol* (F003414, BL41669). **A'**–**B'** For Box-and-whisker plots: the center is the median, minima and maxima are 25th and 75th quartile and whiskers indicate full range of values. All individual values with 'n' representing numbers of biological replicas are shown by dots and means are indicated by '+'. Asterisks denote significances from multiple comparisons by one-way ANOVA (***$p < 0.001$; ****$p < 0.0001$). **C** MF size adaptations, shown are means ± SD of fold changes in entire midgut length, R5 diameter and total cell number of MF and EC specific >*crol* (F003414) compared to VF after 3 d of Rapport tracing. Biological replicas are indicated by 'n' values. Source data are provided as a Source Data file. **D** 20HE levels upon mating as a function of time ($y(t)$). **E** Equation visualizing the divergent effect of 20HE hormone on ISC (I) inhibiting ISC proliferation and on EC (E) stimulating Wg production and thereby production of EB (u) with C_E^Y. EB (u) are an intermediate state between ISC and EC and differentiate into EC with a rate θ. **F** A graph visualizing intestinal size increase upon mating showing functions for production of intermediate EB ($u(t)$) and EC ($E(t)$) per time with a growing gut section following the mating event. **G** Gut section with indicated mating increase in 20HE (i) reaching EC thus inducing expression of Wg ligands (ii). Wg release stimulates ISC proliferation within a distance l and thereby intestinal size increase (iii). In a growing midgut the non-autonomous Wnt/Wg activation outweighs the degradation of Wg and autonomous proliferation control. **G'** Upon an increase in EC numbers the average distance l of EC (Wg source) and the ligand receiving ISC increases. With a longer distance l Wg ligands degrade leading to a decrease in Wg concentration sensed by ISC and thereby to a decline in ISC proliferation (iv) stabilizing gut size.

Table 2 | List of primers used in real-time qPCR to investigate expression levels of *CycB* and *stg* upon oral RH5849 administration

Primer	Forward (5'–3')	Reverse (5'–3')
rp49	TGGTTTCCGGCAAGCTTCAA	TGTTGTCGATACCCTTGGGC
CycB	TTTGCAGAATCGCGGCATAAG	GTCTGTGAGCTTGAGATCCTTG
stg	GAAAACAACTGCAGCATGGATTGCA	CGACAGCTCCTCCTGGTC

for KEGG pathways that correlate with hZNF267 expression. Within the collection of Wnt/Wg signalling pathway members single genes with significant positive or negative correlation were selected for visualization in a scheme.

Alignment of Crol and hZNF267

The protein alignment of Crol and hZNF267 (Fig. S2M) has been performed with the protein sequence of CrolPA deposited at Flybase, and the protein sequence of hZNF267 isoform 1 deposited at NCBI using the CLC Main Workbench software from QIAGEN.

RNA isolation and cDNA synthesis

Freshly hatched female w^{1118} flies were collected and kept on food containing 340 µM RH5849 together with male flies. After two days at 25 °C midguts of female flies were dissected for RNA-isolation and cDNA synthesis (Fig. 2J). Adult female flies with Rapport specific overexpression of *wg* were grown at 18 °C and shifted to 29 °C for three days prior to dissection and subsequent RNA isolation and cDNA synthesis (Fig. 5O), which were performed as described previously[85].

Quantitative real-time PCR

Expression levels of *CycB* and *stg* in whole midguts of mated female flies were determined upon oral administration of RH5849 agonist (Fig. 2J) or expression of >*wg* using Rapport (Fig. 5O). Real-time qPCR was performed as described previously[85]. Relative expression levels were normalized to the house-keeping gene rp49 and calculated by ΔΔCt-Method. The primers used in real-time qPCRs are listed in Table 2.

Statistical analyses

Statistical analyses were run in GraphPad Prism 9.0. Dot plots show all individual data points with no exclusions and indication of mean plus and minus the standard deviation. Box plots show the median and the first and third quartile with mean indicated by '+' and full range of values indicated by whiskers, additionally all individual values are shown by dots. No data were excluded. For statistical comparisons we first tested all data for normal distribution using the Shapiro-Wilk test[92] and then used either unpaired two-sided *t*-test[93] for comparison of two groups with normal distribution or One-way ANOVA[94] and the two-stage step-up method of Benjamini, Krieger and Yekutieli[95] for multiple comparisons of normally distributed data[96]. For data that did not show normal distribution we used non-parametric two-sided Mann Whitney *U* test[97] for comparison of two groups and Kruskal-Wallis test[98] following two-stage step-up method of Benjamini, Krieger and Yekutieli[95] for multiple comparisons[96]. Survival curves were analyzed using Kaplan-Meier log-rank tests[99,100]. Significant differences are displayed as * for $p \le 0.05$, ** for $p \le 0.01$, *** for $p \le 0.001$ and **** for $p \le 0.0001$. Results of all statistical tests can be found in the Source Data file.

Reporting summary

Further information on research design is available in the Nature Portfolio Reporting Summary linked to this article.

Data availability

All data generated in this study are provided in the Source Data file. The expression data of Wnt/Wg signalling components in mixed colon adenocarcinoma (2022-v32, tcga) used in this study (Fig. S7A) are available in the R2 Genomics analysis and visualization platform (https://hgserver1.amc.nl/cgi-bin/r2/main.cgi) with the R2 internal identifier: ps_avgpres_tcgacoadv32a512_gencode36. Source data are provided with this paper.

References

1. Hammond, K. A. Adaptation of the maternal intestine during lactation. *J. Mammary Gland Biol. Neoplasia* **2**, 243–252 (1997).
2. Roa, J. & Tena-Sempere, M. Connecting metabolism and reproduction: roles of central energy sensors and key molecular mediators. *Mol. Cell Endocrinol.* **397**, 4–14 (2014).
3. Speakman, J. R. The physiological costs of reproduction in small mammals. *Philos. Trans. R. Soc. B: Biol. Sci.* **363**, 375–398 (2008).
4. Ahmed, S. M. H. et al. Fitness trade-offs incurred by ovary-to-gut steroid signalling in Drosophila. *Nature* **584**, 415–419 (2020).
5. Cognigni, P., Bailey, A. P. & Miguel-Aliaga, I. Enteric neurons and systemic signals couple nutritional and reproductive status with intestinal homeostasis. *Cell Metab.* **13**, 92–104 (2011).
6. Klepsatel, P. et al. Reproductive and post-reproductive life history of wild-caught Drosophila melanogaster under laboratory conditions. *J. Evol. Biol.* **26**, 1508–1520 (2013).
7. Reiff, T. et al. Endocrine remodelling of the adult intestine sustains reproduction in Drosophila. *Elife* **4**, e06930 (2015).

8. Zipper, L., Jassmann, D., Burgmer, S., Gorlich, B. & Reiff, T. Ecdysone steroid hormone remote controls intestinal stem cell fate decisions via the PPARgamma-homolog Eip75B in Drosophila. *Elife* **9**, e55795 (2020).
9. Ameku, T. & Niwa, R. Mating-induced increase in germline stem cells via the neuroendocrine system in female Drosophila. *PLoS Genet.* **12**, e1006123 (2016).
10. Harshman, L. G., Loeb, A. M. & Johnson, B. A. Ecdysteroid titers in mated and unmated Drosophila melanogaster females. *J. Insect Physiol.* **45**, 571–577 (1999).
11. Lin, G., Xu, N. & Xi, R. Paracrine Wingless signalling controls self-renewal of Drosophila intestinal stem cells. *Nature* **455**, 1119–1123 (2008).
12. Radtke, F. & Clevers, H. Self-renewal and cancer of the gut: two sides of a coin. *Science* **307**, 1904–1909 (2005).
13. D'Avino, P. P. & Thummel, C. S. crooked legs encodes a family of zinc finger proteins required for leg morphogenesis and ecdysone-regulated gene expression during Drosophila metamorphosis. *Development* **125**, 1733–1745 (1998).
14. Mitchell, N., Cranna, N., Richardson, H. & Quinn, L. The Ecdysone-inducible zinc-finger transcription factor Crol regulates Wg transcription and cell cycle progression in Drosophila. *Development* **135**, 2707–2716 (2008).
15. Mitchell, K. J. et al. Genetic analysis of Netrin genes in Drosophila: Netrins guide CNS commissural axons and peripheral motor axons. *Neuron* **17**, 203–215 (1996).
16. Dutta, D. et al. Regional cell-specific transcriptome mapping reveals regulatory complexity in the adult Drosophila Midgut. *Cell Rep.* **12**, 346–358 (2015).
17. Hung, R. J., Li, J. S. S., Liu, Y. & Perrimon, N. Defining cell types and lineage in the Drosophila midgut using single cell transcriptomics. *Curr. Opin. Insect Sci.* **47**, 12–17 (2021).
18. Hudry, B. et al. Sex differences in intestinal carbohydrate metabolism promote food intake and sperm maturation. *Cell* **178**, 901–918.e16 (2019).
19. Hudry, B., Khadayate, S. & Miguel-Aliaga, I. The sexual identity of adult intestinal stem cells controls organ size and plasticity. *Nature* **530**, 344–348 (2016).
20. Busson, D., Gans, M., Komitopoulou, K. & Masson, M. Genetic analysis of three dominant female-sterile mutations located on the X chromosome of Drosophila melanogaster. *Genetics* **105**, 309–325 (1983).
21. Okamoto, N. et al. A membrane transporter is required for steroid hormone uptake in Drosophila. *Dev. Cell* **47**, 294–305.e7 (2018).
22. Antonello, Z. A., Reiff, T., Ballesta-Illan, E. & Dominguez, M. Robust intestinal homeostasis relies on cellular plasticity in enteroblasts mediated by miR-8-Escargot switch. *EMBO J.* **34**, 2025–2041 (2015).
23. Schnabl, B., Valletta, D., Kirovski, G. & Hellerbrand, C. Zinc finger protein 267 is up-regulated in hepatocellular carcinoma and promotes tumor cell proliferation and migration. *Exp. Mol. Pathol.* **91**, 695–701 (2011).
24. Yang, H. et al. Knockdown of zinc finger protein 267 suppresses diffuse large B-cell lymphoma progression, metastasis, and cancer stem cell properties. *Bioengineered* **13**, 1686–1701 (2022).
25. Stossi, F. et al. Transcriptional profiling of estrogen-regulated gene expression via estrogen receptor (ER) alpha or ERbeta in human osteosarcoma cells: distinct and common target genes for these receptors. *Endocrinology* **145**, 3473–3486 (2004).
26. Li, T. R. & White, K. P. Tissue-specific gene expression and ecdysone-regulated genomic networks in Drosophila. *Dev. Cell* **5**, 59–72 (2003).
27. Mitchell, N. C. et al. The Ecdysone receptor constrains wingless expression to pattern cell cycle across the Drosophila wing margin in a Cyclin B-dependent manner. *BMC Dev. Biol.* **13**, 28 (2013).
28. Patel, P. H., Dutta, D. & Edgar, B. A. Niche appropriation by Drosophila intestinal stem cell tumours. *Nat. Cell Biol.* **17**, 1182–1192 (2015).
29. Zhang, P. et al. An SH3PX1-dependent endocytosis-autophagy network restrains intestinal stem cell proliferation by counteracting EGFR-ERK signaling. *Dev. Cell* **49**, 574–589.e5 (2019).
30. Micchelli, C. A. & Perrimon, N. Evidence that stem cells reside in the adult Drosophila midgut epithelium. *Nature* **439**, 475–479 (2006).
31. Ohlstein, B. & Spradling, A. The adult Drosophila posterior midgut is maintained by pluripotent stem cells. *Nature* **439**, 470–474 (2006).
32. Ohlstein, B. & Spradling, A. Multipotent Drosophila intestinal stem cells specify daughter cell fates by differential notch signaling. *Science* **315**, 988–992 (2007).
33. Korzelius, J. et al. The WT1-like transcription factor Klumpfuss maintains lineage commitment of enterocyte progenitors in the Drosophila intestine. *Nat. Commun.* **10**, 4123 (2019).
34. Reiff, T. et al. Notch and EGFR regulate apoptosis in progenitor cells to ensure gut homeostasis in Drosophila. *EMBO J.* **38**, e101346 (2019).
35. Kaspar, M., Schneider, M., Chia, W. & Klein, T. Klumpfuss is involved in the determination of sensory organ precursors in Drosophila. *Dev. Biol.* **324**, 177–191 (2008).
36. Port, F., Chen, H. M., Lee, T. & Bullock, S. L. Optimized CRISPR/Cas tools for efficient germline and somatic genome engineering in Drosophila. *Proc. Natl Acad. Sci. USA* **111**, E2967–E2976 (2014).
37. Takashima, S., Mkrtchyan, M., Younossi-Hartenstein, A., Merriam, J. R. & Hartenstein, V. The behaviour of Drosophila adult hindgut stem cells is controlled by Wnt and Hh signalling. *Nature* **454**, 651–655 (2008).
38. Bartscherer, K., Pelte, N., Ingelfinger, D. & Boutros, M. Secretion of Wnt ligands requires Evi, a conserved transmembrane protein. *Cell* **125**, 523–533 (2006).
39. Bänziger, C. et al. Wntless, a conserved membrane protein dedicated to the secretion of Wnt proteins from signaling cells. *Cell* **125**, 509–522 (2006).
40. Olson, E. R. et al. Yan, an ETS-domain transcription factor, negatively modulates the Wingless pathway in the Drosophila eye. *EMBO Rep.* **12**, 1047–1054 (2011).
41. Tian, A. et al. Intestinal stem cell overproliferation resulting from inactivation of the APC tumor suppressor requires the transcription cofactors Earthbound and Erect wing. *PLoS Genet* **13**, e1006870 (2017).
42. Fang, H., Martinez-Arias, A. & de Navascués, J. Autocrine and paracrine Wingless signalling in the Drosophila midgut by both continuous gradient and asynchronous bursts of wingless expression *F1000Research* **5**, 317 (2016).
43. Cordero, J. B., Stefanatos, R. K., Scopelliti, A., Vidal, M. & Sansom, O. J. Inducible progenitor-derived Wingless regulates adult midgut regeneration in Drosophila. *EMBO J.* **31**, 3901–3917 (2012).
44. Phillips, M. D. & Thomas, C. M. Brush border spectrin is required for early endosome recycling in Drosophila. *J. Cell Sci.* **119**, 1361–1370 (2006).
45. Yagi, R., Mayer, F. & Basler, K. Refined LexA transactivators and their use in combination with the Drosophila Gal4 system. *Proc. Natl Acad. Sci. USA* **107**, 16166–16171 (2010).
46. Liang, J., Balachandra, S., Ngo, S. & O'Brien, L. E. Feedback regulation of steady-state epithelial turnover and organ size. *Nature* **548**, 588–591 (2017).
47. Chen, T.-A. et al. Canonical Wnt signaling promotes formation of somatic permeability barrier for proper germ cell differentiation. *Front. Cell Dev. Biol.* **10**, 877047 (2022).
48. Shtutman, M. et al. The cyclin D1 gene is a target of the beta-catenin/LEF-1 pathway. *Proc. Natl Acad. Sci. USA* **96**, 5522–5527 (1999).

49. Barker, N. et al. Crypt stem cells as the cells-of-origin of intestinal cancer. *Nature* **457**, 608–611 (2009).
50. Jin, Y. et al. EGFR/Ras signaling controls Drosophila intestinal stem cell proliferation via capicua-regulated genes. *PLOS Genet.* **11**, e1005634 (2015).
51. Vermeulen, L. et al. Wnt activity defines colon cancer stem cells and is regulated by the microenvironment. *Nat. Cell Biol.* **12**, 468–476 (2010).
52. Hanahan, D. & Weinberg, R. A. Hallmarks of cancer: the next generation. *Cell* **144**, 646–674 (2011).
53. Patel, S., Alam, A., Pant, R. & Chattopadhyay, S. Wnt signaling and its significance within the tumor microenvironment: novel therapeutic insights. *Front. Immunol.* **10**, 2872 (2019).
54. McAllister, S. S. & Weinberg, R. A. The tumour-induced systemic environment as a critical regulator of cancer progression and metastasis. *Nat. Cell Biol.* **16**, 717–727 (2014).
55. Hanahan, D. Hallmarks of cancer: new dimensions. *Cancer Discov.* **12**, 31–46 (2022).
56. Ngo, S., Liang, J., Su, Y. H. & O'Brien, L. E. Disruption of EGF feedback by intestinal tumors and neighboring cells in Drosophila. *Curr. Biol.* **30**, 1537–1546.e3 (2020).
57. Zipper, L., Batchu, S., Kaya, N. H., Antonello, Z. A. & Reiff, T. The MicroRNA miR-277 controls physiology and pathology of the adult Drosophila midgut by regulating the expression of fatty acid beta-oxidation-related genes in intestinal stem cells. *Metabolites* **12**, 315 (2022).
58. Hanahan, D. & Weinberg, R. A. The hallmarks of cancer. *Cell* **100**, 57–70 (2000).
59. Bangi, E., Murgia, C., Teague, A. G., Sansom, O. J. & Cagan, R. L. Functional exploration of colorectal cancer genomes using Drosophila. *Nat. Commun.* **7**, 13615 (2016).
60. Martorell, O. et al. Conserved mechanisms of tumorigenesis in the Drosophila adult midgut. *PLoS ONE* **9**, e88413 (2014).
61. Zhai, Z. et al. Accumulation of differentiating intestinal stem cell progenies drives tumorigenesis. *Nat. Commun.* **6**, 10219 (2015).
62. Hodge, R. A. et al. The septate junction component bark beetle is required for Drosophila intestinal barrier function and homeostasis. *iScience* **26**, 106901 (2023).
63. O'Brien, L. E., Soliman, S. S., Li, X. & Bilder, D. Altered modes of stem cell division drive adaptive intestinal growth. *Cell* **147**, 603–614 (2011).
64. Christensen, C. F., Laurichesse, Q., Loudhaief, R., Colombani, J. & Andersen, D. S. Drosophila activins adapt gut size to food intake and promote regenerative growth. *Nat. Commun.* **15**, 273 (2024).
65. Dubois, L., Lecourtois, M., Alexandre, C., Hirst, E. & Vincent, J. P. Regulated endocytic routing modulates wingless signaling in Drosophila embryos. *Cell* **105**, 613–624 (2001).
66. Berg, H. C. *Random Walks in Biology*, (Princeton University Press, 1993).
67. Wartlick, O., Kicheva, A. & González-Gaitán, M. Morphogen gradient formation. *Cold Spring Harb. Perspect. Biol.* **1**, a001255 (2009).
68. Alon, U. *Systems Medicine: Physiological Circuits and the Dynamics of Disease 1st edn* (Chapman and Hall/CRC, 2023).
69. Joshi, P. A., Di Grappa, M. A. & Khokha, R. Active allies: hormones, stem cells and the niche in adult mammopoiesis. *Trends Endocrinol. Metab.* **23**, 299–309 (2012).
70. Russo, J. & Russo, I. H. The role of estrogen in the initiation of breast cancer. *J. Steroid Biochem. Mol. Biol.* **102**, 89–96 (2006).
71. Yager, J. D. & Davidson, N. E. Estrogen carcinogenesis in breast cancer. *N. Engl. J. Med.* **354**, 270–282 (2006).
72. Barzi, A., Lenz, A. M., Labonte, M. J. & Lenz, H. J. Molecular pathways: estrogen pathway in colorectal cancer. *Clin. Cancer Res.* **19**, 5842–5848 (2013).
73. Chlebowski, R. T. et al. Estrogen plus progestin and colorectal cancer in postmenopausal women. *N. Engl. J. Med.* **350**, 991–1004 (2004).
74. Foster, P. A. Oestrogen and colorectal cancer: mechanisms and controversies. *Int. J. Colorectal Dis.* **28**, 737–749 (2013).
75. Manson, J. E. et al. Menopausal hormone therapy and long-term all-cause and cause-specific mortality: the Women's Health Initiative randomized trials. *JAMA* **318**, 927–938 (2017).
76. Nie, X., Xie, R. & Tuo, B. Effects of Estrogen on the gastrointestinal tract. *Dig. Dis. Sci.* **63**, 583–596 (2018).
77. Simon, M. S. et al. Estrogen plus progestin and colorectal cancer incidence and mortality. *J. Clin. Oncol.* **30**, 3983–3990 (2012).
78. Nakhostin, L., Stadler, A. & Stute, P. Impact of menopausal hormone therapy on colorectal cancer risk-A systematic review. *Clin. Endocrinol.* **95**, 390–397 (2021).
79. Campbell-Thompson, M., Lynch, I. J. & Bhardwaj, B. Expression of estrogen receptor (ER) subtypes and ERbeta isoforms in colon cancer. *Cancer Res.* **61**, 632–640 (2001).
80. Hoff, M. B., Chang, W. W. & Mak, K. M. Effect of estrogen on cell proliferation in colonic mucosa of the mouse. *Virchows Arch. B Cell Pathol. Incl. Mol. Pathol.* **35**, 263–273 (1981).
81. Charlton, B. M. et al. Oral contraceptive use and colorectal cancer in the Nurses' Health Study I and II. *Cancer Epidemiol. Biomark. Prev.* **24**, 1214–1221 (2015).
82. Voloshanenko, O. et al. Wnt secretion is required to maintain high levels of Wnt activity in colon cancer cells. *Nat. Commun.* **4**, 2610 (2013).
83. Lecarpentier, Y., Claes, V., Vallée, A. & Hébert, J. L. Interactions between PPAR gamma and the canonical Wnt/Beta-Catenin pathway in type 2 diabetes and colon cancer. *PPAR Res.* **2017**, 5879090 (2017).
84. Sabatino, L. et al. Emerging role of the beta-catenin-PPARgamma axis in the pathogenesis of colorectal cancer. *World J. Gastroenterol.* **20**, 7137–7151 (2014).
85. Zipper, L., Batchu, S., Kaya, N. H., Antonello, Z. A. & Reiff, T. The MicroRNA miR-277 controls physiology and pathology of the adult drosophila midgut by regulating the expression of fatty acid β-oxidation-related genes in intestinal stem cells. *Metabolites* **12**, 315 (2022).
86. Klein, T. & Arias, A. M. Different spatial and temporal interactions between Notch, wingless,and vestigial specify proximal and distal pattern elements of the wing in Drosophila. *Dev. Biol.* **194**, 196–212 (1998).
87. Sherer, L. M. et al. Octopamine neuron dependent aggression requires dVGLUT from dual-transmitting neurons. *PLoS Genet.* **16**, e1008609 (2020).
88. Gratz, S. J. et al. Highly specific and efficient CRISPR/Cas9-catalyzed homology-directed repair in Drosophila. *Genetics* **196**, 961–971 (2014).
89. Chang, K. R. et al. Transgenic Drosophila lines for LexA-dependent gene and growth regulation. *G3* **12**, jkac018 (2022).
90. Zipper, L., Jassmann, D., Burgmer, S., Görlich, B. & Reiff, T. Ecdysone steroid hormone remote controls intestinal stem cell fate decisions via the PPARγ-homolog Eip75B in Drosophila. *Elife* **9**, e55795 (2020).
91. Rera, M. et al. Modulation of longevity and tissue homeostasis by the Drosophila PGC-1 homolog. *Cell Metab.* **14**, 623–634 (2011).
92. Shapiro, S. S. & Wilk, M. B. An analysis of variance test for normality (complete samples)†. *Biometrika* **52**, 591–611 (1965).
93. Student. The Probable Error of a Mean. *Biometrika* **6**, 1–25 (1908).
94. Ostertagova, E. & Ostertag, O. Methodology and application of oneway ANOVA. *Am. J. Mech. Eng.* **1**, 256–261 (2013).

95. Benjamini, Y., Krieger, A. M. & Yekutieli, D. Adaptive linear step-up procedures that control the false discovery rate. *Biometrika* **93**, 491–507 (2006).
96. Nayak, B. K. & Hazra, A. How to choose the right statistical test? *Indian J. Ophthalmol.* **59**, 85–86 (2011).
97. Mann, H. B. & Whitney, D. R. On a test of whether one of two random variables is stochastically larger than the other. *Ann. Math. Stat.* **18**, 50–60 (1947).
98. Kruskal, W. H. & Wallis, W. A. Use of ranks in one-criterion variance analysis. *J. Am. Stat. Assoc.* **47**, 583–621 (1952).
99. Mantel, N. Evaluation of survival data and two new rank order statistics arising in its consideration. *Cancer Chemother. Rep.* **50**, 163–170 (1966).
100. Harrington, D. Linear rank tests in survival analysis. In *Encyclopedia of Biostatistics*. (eds Armitage, P. & Colton, T.) 1–10 (Wiley, 2005).

Acknowledgements

The authors thank the Vienna Drosophila RNAi Center (VDRC) and the Bloomington Drosophila Stock Center (NIHP400D018537) as well as Thomas Klein and Andreas Wodarz for reagents. We also thank the Center for Advanced Imaging (CAi) at Heinrich Heine University (DFG INST 208/539-1 FUGG) for imaging training and facilities. In addition, we are grateful to Reiff laboratory members for comments and feedback on experiments and the manuscript. TR and LZ are supported by the Deutsche Forschungsgemeinschaft (DFG-Sachbeihilfe RE 3453/2–1), the Wilhelm Sander-Stiftung (2018.145.1) and the Deutsche Krebshilfe (70115333). BCM wants to acknowledge the support of the field of excellence "Complexity of Life, Basic Research and Innovation" of the University of Graz.

Author contributions

LZ, BCM, and TR designed the research. LZ conducted all biological experiments and BCM performed the mathematical modelling. LZ and TR analysed biological data, TR supervised the project, and all authors contributed to writing the manuscript.

Funding

Open Access funding enabled and organized by Projekt DEAL.

Competing interests

The authors declare no competing interests.

Additional information

Supplementary information The online version contains supplementary material available at https://doi.org/10.1038/s41467-024-55664-2.

Correspondence and requests for materials should be addressed to Tobias Reiff.

Peer review information *Nature Communications* thanks Jaakko Mattila, and the other, anonymous, reviewer(s) for their contribution to the peer review of this work. A peer review file is available.

Supplemental figures

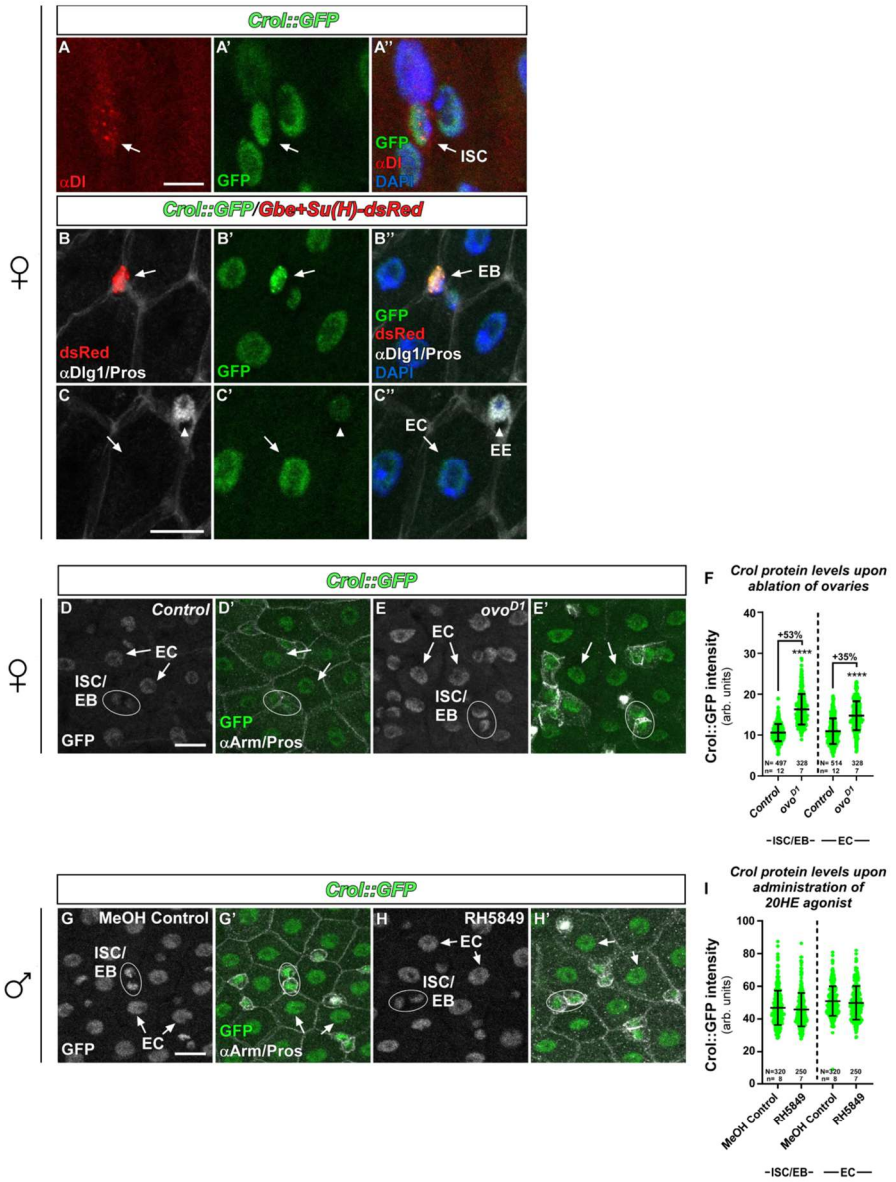

Fig.S1: Crol is expressed in the adult *Drosophila* midgut
(A-A'') Confocal images of Crol::GFP in adult midguts of MF showing localization of Crol in nuclei of ISC positive for antibody staining targeting the ISC marker Delta (αDl) and marked with white arrows. Scale bar is 5µm. (B-C'') Confocal images of Crol::GFP combined with the EB marker Gbe+Su(H)-dsRed showing Crol localization in (B-B'') dsRed positive EB marked by white arrows, and (C-C'') in epithelial EC (white arrows) stained with αDlg1 and EE (white arrowheads) stained by αPros. Scale bar is 10µm. (D-E') Confocal images showing Crol::GFP in R5 regions of mated female midguts in (D-D') w^{1118} controls compared to (E-E') heterozygous ovo^{D1} mutants. (D-E) Sole Crol::GFP signal is shown in greyscale and (D'-E') in green colour combined with antibody staining targeting Arm and Pros for identification of ISC/EB, EC and EE. Duplets of ISC/EB are outlined by white ellipses and EC are marked with white arrows. Scale bar is 10µm. (F) Quantification of Crol::GFP intensities in ISC/EB and EC in control MF compared to heterozygous ovo^{D1} mutant MF. (G-H') Confocal images showing Crol::GFP in R5 regions of adult midguts of (G-G') male flies fed with MeOH (MeOH Control) and (H-H') males fed with the 20HE agonist RH5849. (G-H) Sole Crol::GFP signal is shown in greyscale and (G'-H') in green colour combined with antibody staining targeting Arm and Pros for identification of ISC/EB, EC and EE. Duplets of ISC/EB are outlined by white ellipses and EC are marked with white arrows. Scale bar is 10µm. (I) Quantification of Crol::GFP intensities in ISC/EB and EC in males fed with MeOH compared to males fed with RH5849. (F,I) Scatter dot plots show individual values with indication of means ± SD. N and n values represent number of cells and number of biological replicas respectively. Asterisks denote significances from comparisons by two-sided Mann Whitney U tests (****p<0.0001). Source data are provided as a Source Data file.

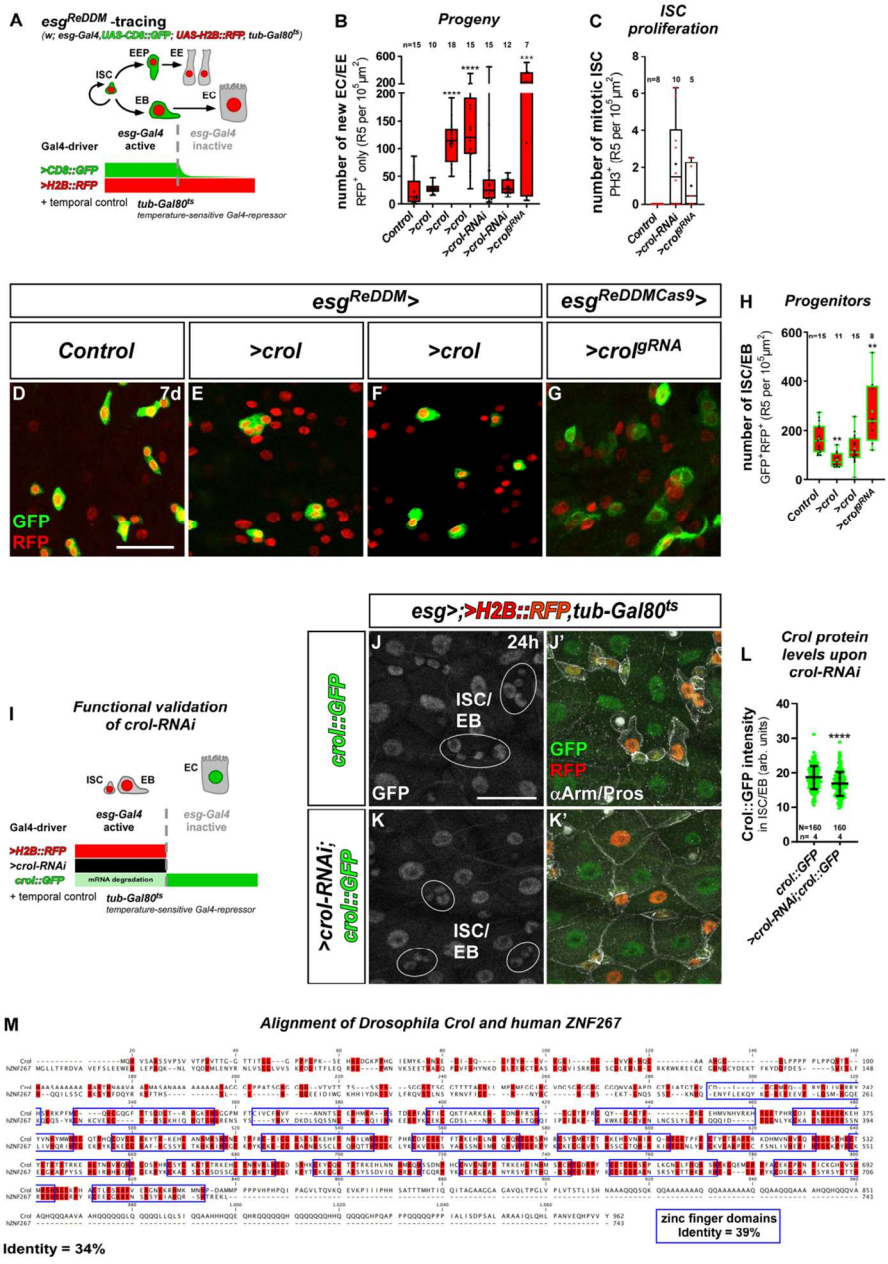
A
esgReDDM -tracing
(w; esg-Gal4,UAS-CD8::GFP; UAS-H2B::RFP, tub-Gal80ts)
EEP
EE
ISC
EB
EC
esg-Gal4 active
esg-Gal4 inactive
Gal4-driver
>CD8::GFP
>H2B::RFP
+ temporal control
tub-Gal80ts
temperature-sensitive Gal4-repressor
B
Progeny
number of new EC/EE
RFP+ only (R5 per 10^5 µm^2)
n=15 10 18 15 15 12 7
Control
>crol
>crol
>crol-RNAi
>crol-RNAi
>crolgRNA
C
ISC proliferation
number of mitotic ISC
PH3+ (R5 per 10^5 µm^2)
n=8 10 5
esgReDDM>
esgReDDMCas9>
Control
>crol
>crol
>crolgRNA
D
7d
E
F
G
GFP
RFP
H
Progenitors
number of ISC/EB
GFP+RFP+ (R5 per 10^5 µm^2)
n=15 11 15 8
I
Functional validation of crol-RNAi
ISC
EB
EC
esg-Gal4 active
esg-Gal4 inactive
Gal4-driver
>H2B::RFP
>crol-RNAi
crol::GFP
mRNA degradation
+ temporal control
tub-Gal80ts
temperature-sensitive Gal4-repressor
esg>;>H2B::RFP,tub-Gal80ts
crol::GFP
>crol-RNAi; crol::GFP
J
24h
ISC/ EB
GFP
J'
GFP
RFP
αArm/Pros
K
ISC/ EB
K'
L
Crol protein levels upon crol-RNAi
Crol::GFP intensity
in ISC/EB (arb. units)
N=160 160
n= 4 4
crol::GFP
>crol-RNAi;crol::GFP
M
Alignment of Drosophila Crol and human ZNF267
zinc finger domains
Identity = 39%
Identity = 34%

Fig.S2: Crol controls ISC proliferation
(A) In *esg^{ReDDM}* tracing *esg-Gal4* double marks ISC/EB driving expression of *>CD8::GFP* (membrane, green) and *>H2B::RFP* (nuclei, red). Upon differentiation new EC/EE lose CD8::GFP, whereas nuclear H2B::RFP persists due to its long half-life. Transgene expression is timely controlled by an ubiquitously expressed Gal80^{ts} repressor (*tub-Gal80^{ts}*). (B-C) Quantification of (B) progeny (*>crol^{gRNA}*:p=0.0004) and (C) PH3^{+} mitotic active ISC upon *crol* manipulations using *esg^{ReDDM}* (B: F003414,BL58359,BL56762,BL41669,BL44643, C: BL41669). (D-G) Confocal images showing R5 regions of MF after 7d of *esg^{ReDDM}* tracing in (D) controls, (E-F) with *>crol* (BL58359,BL56762) and (G) CRISPR/Cas9 induced knockout of *crol* by *esg^{ReDDMCas9}* driven expression of guideRNAs targeting *crol* (*>crol^{gRNA}*). Scale bar is 50µm. (H) Quantification of progenitor cell numbers upon *crol* manipulations using *esg^{ReDDM}* (BL58359:p=0.0048, BL56762, *>crol^{gRNA}*:p=0.0012). (B-C,H) For Box-and-whisker plots: the center is the median, minima and maxima are 25th and 75th quartile and whiskers indicate full range of values. Individual values with 'n' representing biological replicas are shown by dots and means are indicated by '+'. Asterisks denote significances from multiple comparisons by (B) Kruskal-Wallis test and (H) One-way ANOVA (**p<0.01;***p<0.001;****p<0.0001). (I) Schematic for functional validation of *>crol-RNAi* and *crol::GFP* transgenes. *esg-Gal4* drives expression of *>H2B::RFP* and *>crol-RNAi* inducing degradation of Crol::GFP. (J-K') Confocal images showing Crol::GFP combined with *esg >H2B::RFP* In R5 regions of MF midguts after shifting for 24h in (J-J') controls and (K-K') with *>crol-RNAi* (BL41669). (J-K) Sole Crol::GFP signal in greyscale and (J'-K') combined with H2B::RFP signal and αArm/αPros staining for identification of different cell types. Duplets of ISC/EB are outlined by white ellipses. Scale bar is 20µm. (L) Crol::GFP levels in controls compared to *>crol-RNAi* (BL41669). Scatter dot plots show individual values with indication of means ± SD. N and n values represent number of cells and number of biological replicas respectively. Asterisks denote significances from unpaired two-sided t-test (****p<0.0001). Source data are provided as a Source Data file. (M) Alignment of *Drosophila* Crol and the human orthologue ZNF267 (hZNF267) indicating zinc finger domains with an identity of 39%, overall identity is 34%.

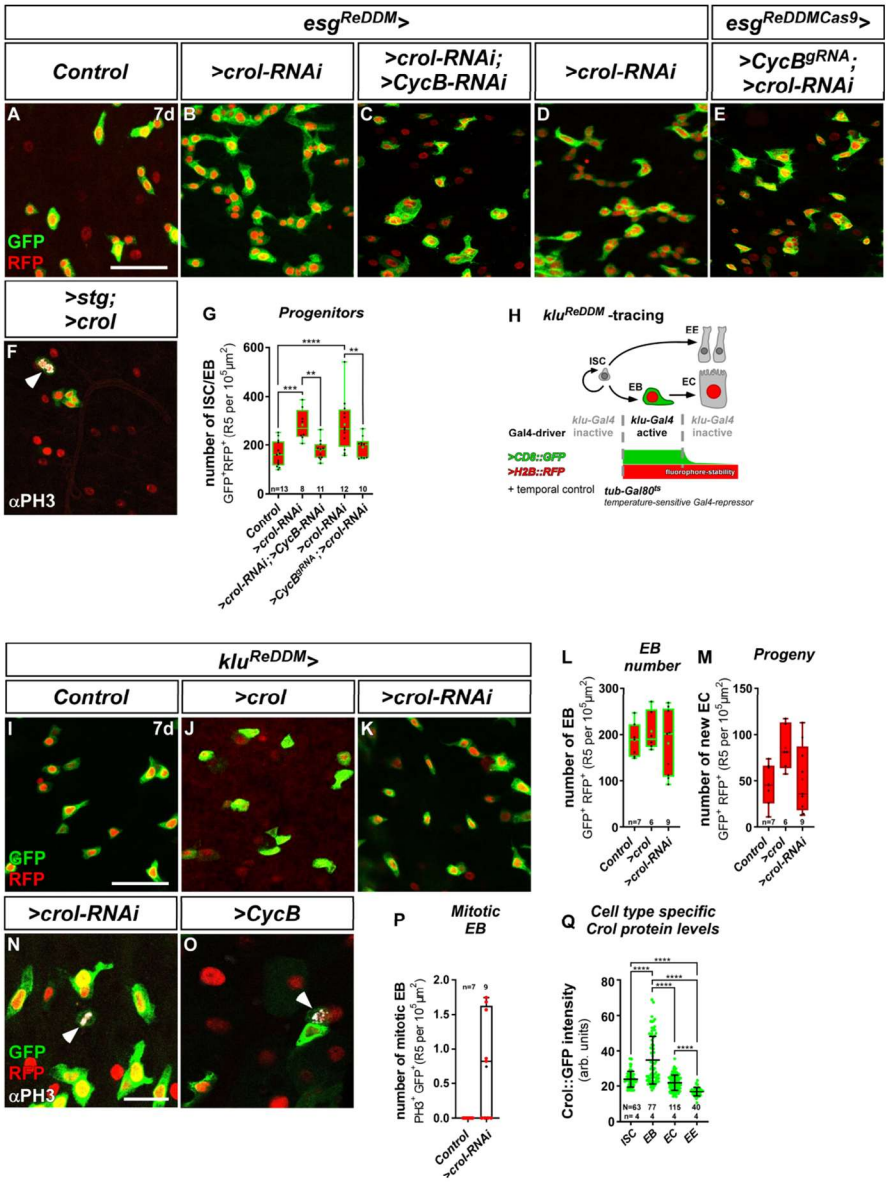
esg^ReDDM>
esg^ReDDMCas9>
Control
>crol-RNAi
>crol-RNAi; >CycB-RNAi
>crol-RNAi
>CycB^gRNA; >crol-RNAi
A 7d
B
C
D
E
GFP
RFP
>stg; >crol
F
αPH3
G Progenitors
number of ISC/EB
GFP+ RFP+ (R5 per 10^5 µm^2)
n=13 8 11 12 10
Control
>crol-RNAi
>crol-RNAi; >CycB-RNAi
>crol-RNAi
>CycB^gRNA; >crol-RNAi
H klu^ReDDM -tracing
EE
ISC
EB
EC
klu-Gal4 inactive
klu-Gal4 active
klu-Gal4 inactive
Gal4-driver
>CD8::GFP
>H2B::RFP
+ temporal control
fluorophore-stability
tub-Gal80^ts
temperature-sensitive Gal4-repressor
klu^ReDDM>
Control
>crol
>crol-RNAi
I 7d
J
K
GFP
RFP
L EB number
number of EB
GFP+ RFP+ (R5 per 10^5µm^2)
n=7 6 9
Control
>crol
>crol-RNAi
M Progeny
number of new EC
GFP+ RFP+ (R5 per 10^5µm^2)
n=7 6 9
Control
>crol
>crol-RNAi
>crol-RNAi
>CycB
N
O
GFP
RFP
αPH3
P Mitotic EB
number of mitotic EB
PH3+ GFP+ (R5 per 10^5 µm^2)
n=7 9
Control
>crol-RNAi
Q Cell type specific Crol protein levels
Crol::GFP intensity
(arb. units)
N=63 77 115 40
n= 4 4 4 4
ISC
EB
EC
EE

Fig.S3: Crol controls proliferation in ISC and EB by regulating CycB
(A-F) Confocal images showing R5 regions of adult female midguts after 7d of *esg*^{ReDDM} tracing in (A) controls, (B) upon expression of *>crol-RNAi* (BL41669) (C) combined with *>CycB-RNAi*, and (D) *>crol-RNAi* (BL44643) (E) combined with *>CycB*^{gRNA}, and (F) simultaneous expression of *>stg* and *>crol* (F003414) stained with an antibody targeting PH3. Scale bar is 50µm. (G) Progenitor cell numbers in combined depletions of *crol* and *CycB* using *esg*^{ReDDM} (p=0.0002;p=0.0015;p=0.0019). (H) In *klu*^{ReDDM} tracing *klu-Gal4* double marks EB driving expression of *>CD8::GFP* (membrane, green) and *>H2B::RFP* (nuclei, red). Upon differentiation new EC lose the CD8::GFP, whereas nuclear H2B::RFP persists due to its long half-life enabling tracing of EB progeny. ISC and EE are not labelled/traced by fluorophores. Transgene expression is timely controlled by an ubiquitously expressed Gal80^{ts} repressor (*tub-Gal80*^{ts}). (I-K) Confocal images showing R5 regions of MF midguts after 7d of *klu*^{ReDDM} tracing in (I) controls, (J) driving expression of *>crol* (F003414) and (K) *>crol-RNAi* (BL41669). Scale bar is 50µm. (L-M) Quantification of (L) EB numbers and (M) progeny of *klu*^{ReDDM} specific *crol* manipulations. (N-O) Confocal images showing R5 regions of female midguts after *klu*^{ReDDM} tracing and (N) expression of *>crol-RNAi* (BL41669) and (O) *>CycB*. White arrowheads point to PH3^{+} EB marked by GFP and RFP. Scale bar is 20µm. (P) Quantification of mitotic active PH3^{+} EB upon specific expression of *>crol-RNAi.* (G,L-M,P) For Box-and-whisker plots: the center is the median, minima and maxima are 25th and 75th quartile and whiskers indicate full range of values. Individual values with 'n' representing biological replicas are shown by dots and means are indicated by '+'. Asterisks denote significances from multiple comparisons by (G) One-way ANOVA and (L-M,P) Kruskal-Wallis tests (**p<0.01;***p<0.001;****p<0.0001). (Q) Crol::GFP intensities within different cell types in R5 regions of adult female midguts. Scatter dot plots show individual values with indication of means ± SD. N and n values represent number of cells and number of biological replicas respectively. Asterisks denote significances from multiple comparisons by Kruskal-Wallis test (****p<0.0001). Source data are provided as a Source Data file.

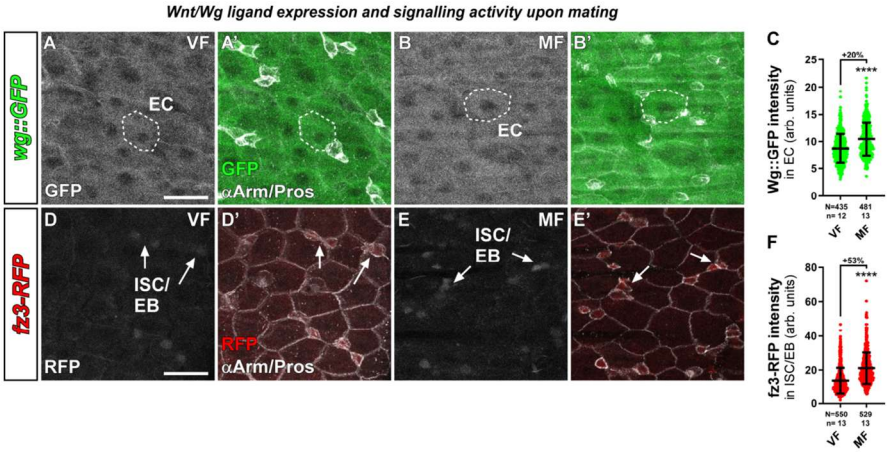

Fig.S4: Wnt/Wg activity in ISC/EB responds to mating dependent 20HE release

(A-B') Confocal images showing Wg::GFP in R5 regions of adult midguts of (A-A') VF and (B-B') MF. (A-B) Sole Wg::GFP signal is shown in greyscale and (A'-B') in green colour combined with αArm and αPros staining for identification of different cell types. Exemplary measured EC are outlined by white dashed lines. Scale bar is 20µm. (C) Quantification of Wg::GFP intensities in EC upon mating. (D-E') Confocal images showing fz3-RFP in R5 regions of adult midguts of (D-D') VF and (E-E') MF. (D-E) Sole fz3-RFP signal is shown in greyscale and (D'-E') in red colour combined with αArm and αPros staining for identification of different cell types. Exemplary measured ISC/EB are marked by white arrows. (F) Quantification of fz3-RFP intensities in ISC/EB upon mating. (C,F) Scatter dot plots show individual values with indication of means ± SD. N and n values represent number of cells and number of biological replicas respectively. Asterisks denote significances from two-sided Mann Whitney U tests (****p<0.0001). Fold changes are shown in percentages. Source data are provided as a Source Data file.

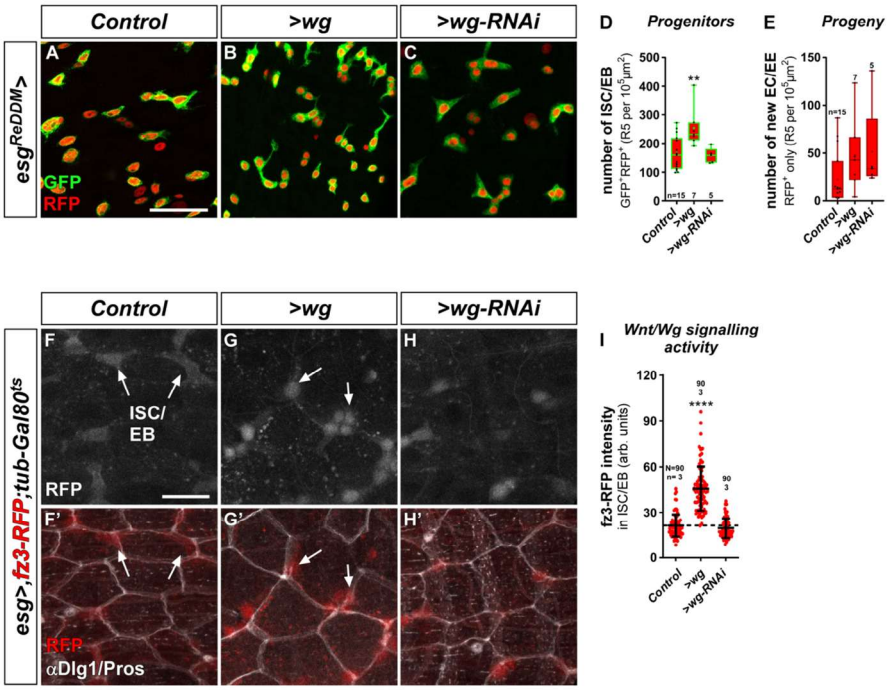

Fig.S5: Wg depletion in ISC/EB is not altering Wnt/Wg signalling activity

(A-C) Confocal images showing R5 regions of adult female midguts after seven days of *esg*^{ReDDM} tracing in (A) controls, upon (B) OE, and (C) KD of *wg*. Scale bar is 50µm. (D-E) Quantification of (D) progenitor cell numbers (p=0.0068) and (E) progeny upon ISC/EB specific manipulations of *wg.* For Box-and-whisker plots: the center is the median, minima and maxima are 25th and 75th quartile and whiskers indicate full range of values. Individual values with 'n' representing biological replicas are shown by dots and means are indicated by '+'. Asterisks denote significances from multiple comparisons by Kruskal-Wallis tests (**p<0.01). (F-H') Confocal images showing fz3-RFP signal in R5 regions of adult female midguts combined with *esg-Gal4* in (F-F') controls, (G-G') driving expression of *>wg* and (H-H') *>wg-RNAi*. (F-H) Sole fz3-RFP signal is shown in greyscale and (F'-H') in red colour combined with αDlg1 and αPros staining for identification of different cell types. Exemplary measured ISC/EB are marked by white arrows. (I) Quantification of fz3-RFP levels in ISC/EB upon *esg-Gal4* specific *>wg* and *>wg-RNAi.* Scatter dot plots show individual values with indication of means ± SD. N and n values represent number of cells and number of biological replicas respectively. Asterisks denote significances from two-sided Mann Whitney U test (****p<0.0001). Source data are provided as a Source Data file.

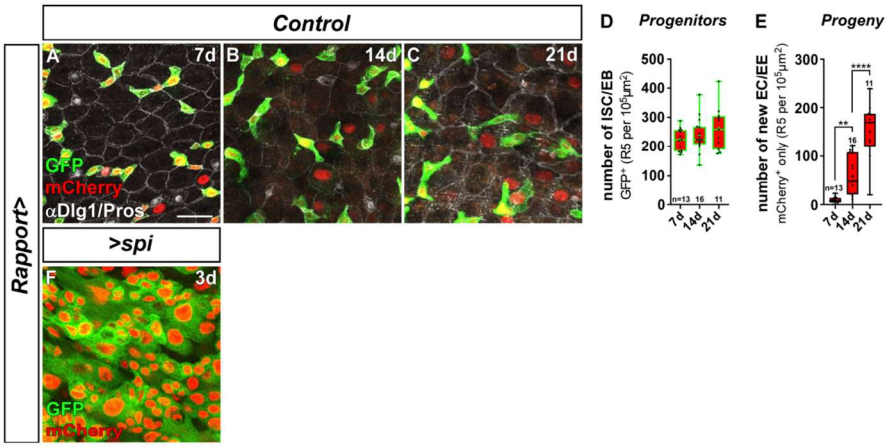

Fig.S6: Rapport tracing shows incremental tissue renewal over three weeks
(A-C) Confocal images showing Rapport tracing in R5 regions of adult female control midguts after (A) seven (7d), (B) 14 (14d), and (C) 21 days (21d) of tracing. ISC/EB are double labelled by GFP and mCherry, whereas their progeny are labelled by mCherry only. EC and EE are additionally marked by αDlg1 and αPros staining. Scale bar is 20µm. (D-E) Quantifications of (D) progenitor cell numbers and (E) progeny (p=0.0023) in control midguts upon seven, 14 and 21 days (7d, 14d, 21d) of tracing. For Box-and-whisker plots: the center is the median, minima and maxima are 25th and 75th quartile and whiskers indicate full range of values. Individual values with 'n' representing biological replicas are shown by dots and means are indicated by '+'. Asterisks denote significances from multiple comparisons by One-way ANOVA (**p<0.01;****p<0.0001). (F) Confocal image of Rapport driven expression of *UAS-spitz* (*>spi*) in the R5 region of an adult female midgut after three days (3d) of tracing. Source data are provided as a Source Data file.

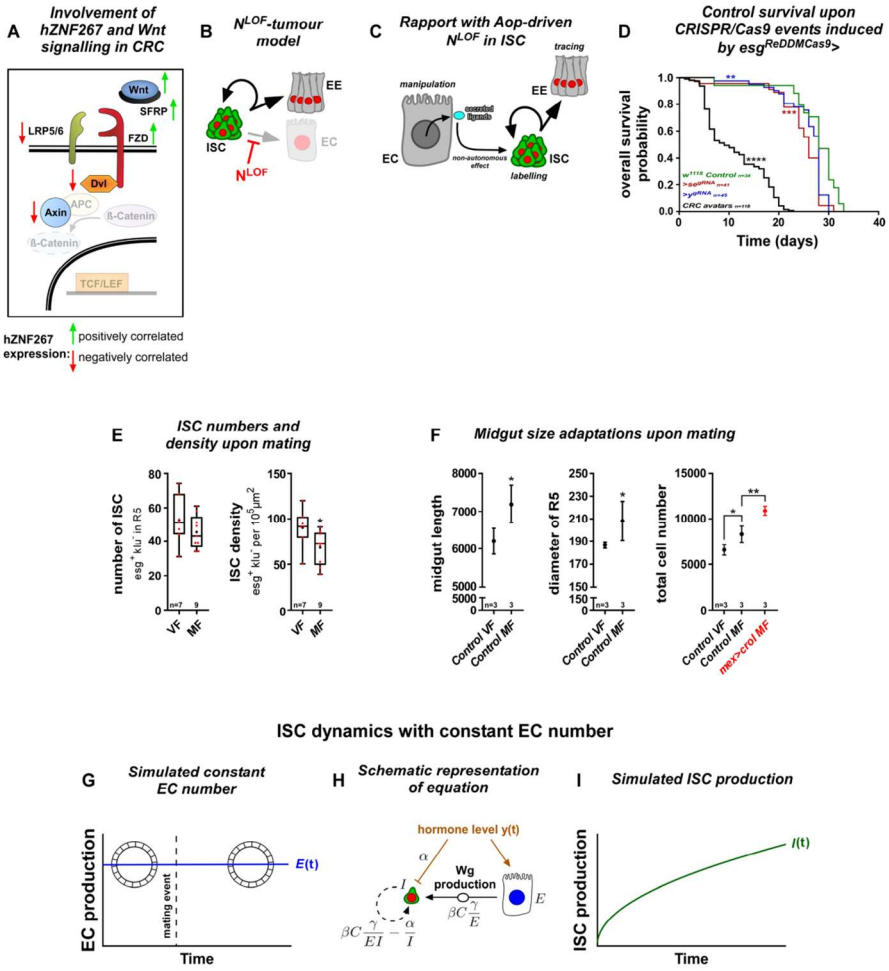
A
Involvement of hZNF267 and Wnt signalling in CRC
Wnt
SFRP
LRP5/6
FZD
Dvl
APC
Axin
ß-Catenin
ß-Catenin
TCF/LEF
hZNF267 expression:
positively correlated
negatively correlated
B
N^LOF-tumour model
EE
ISC
EC
N^LOF
C
Rapport with Aop-driven N^LOF in ISC
tracing
manipulation
EE
EC
ISC
non-autonomous effect
labelling
D
Control survival upon CRISPR/Cas9 events induced by esg^ReDDMCas9>
overall survival probability
Time (days)
E
ISC numbers and density upon mating
number of ISC
esg+ klu- in R5
ISC density
esg+ klu- per 10^5 µm^2
VF
MF
F
Midgut size adaptations upon mating
midgut length
diameter of R5
total cell number
Control VF
Control MF
mex>ctrol MF
ISC dynamics with constant EC number
G
Simulated constant EC number
EC production
E(t)
mating event
Time
H
Schematic representation of equation
hormone level y(t)
Wg production
I
Simulated ISC production
ISC production
I(t)
Time

Fig.S7: Additional data for tumour models and mathematical modelling
(A) Schematic of Wnt/Wg signalling pathway in humans. Marked are pathway components that positively (green arrows) and negatively (red arrows) correlate with enhanced hZNF267 expression in CRC. (B) Schematic of the N^{LOF} tumour model blocking EC differentiation thereby inducing the formation of ISC and EE tumours. (C) Schematic of *Rapport* combined with N^{LOF} by expression of *Aop-N-RNAi*. (D) Kaplan-Meier estimation of survival in $esg^{ReDDMCas9}$ w^{1118} controls and induced knockout of *yellow* (*y,* p=0.0017) and *sepia* (*se,* p=0.0001) serving as 'mock'-gRNA controls compared to CRC avatars. Number of analyzed flies is indicated by 'n' and asterisks denote significances from Kaplan-Meier estimation (**p<0.01;***p<0.001;****p<0.0001). (E) Quantification of ISC numbers and density (p=0.0459) upon mating in adult female midguts with combined expression of *esg>>CD8::GFP* and *klu>H2B::RFP* enabling identification ISC and EB. ISC numbers (absolute numbers, left) in R5 and ISC (ISC per area, right). For Box-and-whisker plots: the center is the median, minima and maxima are 25th and 75th quartile and whiskers indicate full range of values. Individual values with 'n' representing biological replicas are shown by dots and means are indicated by '+'. (F) Quantification of midgut size adaptations (p=0.0462;p=0.0156;p=0.0211;p=0.0031) upon mating in female flies of *Rapport* controls and expression of *>crol* (F003414). Midgut size adaptations encompassing entire midgut length (left), diameter of R5 (centre) and total cell number of entire midguts (right). Graphs show means ± SD. Number of biological replicas is indicated by 'n' values and asterisks denote significances from comparisons by (F,G: left and center) unpaired two-sided t-tests and multiple comparison by (E,G: right) One-way ANOVA (*p<0.05;**p<0.01). Source data are provided as a Source Data file. (H-J) Schematics of ISC dynamics with constant EC number depicted by (H) a function $E(t)$ visualizing constant EC number and intestinal size depicted by gut sections, (I) Schematic representation of equation visualizing the divergent effect of 20HE hormone on ISC (I) and EC (E) showing that ISC proliferation increases with $\beta c \frac{\gamma}{EI} - \frac{\alpha}{I}$, and (J) a function $I(t)$showing ISC proliferation over time.

Supplemental material for the mathematical model

Introduction

We construct i) a mean-field equation for the number of EC to demonstrate that the opposing roles of 20HE hormone lead to a stable population of EC and that the increase in hormone production projects into an increase of organ size. ii) a mean-field system of equations demonstrating the above claims considering a more realistic scenario where the differentiation process from ISC to EC is not happening instantaneously, thereby incorporating a transient state cell population, and iii) a mean field equation for the number of ISC in the case where differentiation is blocked, to qualitatively predict the evolution of the amount of ISC in this pathological scenario. We consider gradient diffusion and degradation of Wg ligands. In all cases, we assume that number of EC is a proxy for organ size.

For the first case, we consider the following scenario:

- 20HE activates the production of Wg in EC which, in turn, activates the production of EC from proliferation and differentiation of ISC. The production of Wg (and thus, of EC) depends on the hormone concentration (amount of hormone/cell number).
- 20HE inhibits the production of EC from differentiation of ISC at a constant rate α.

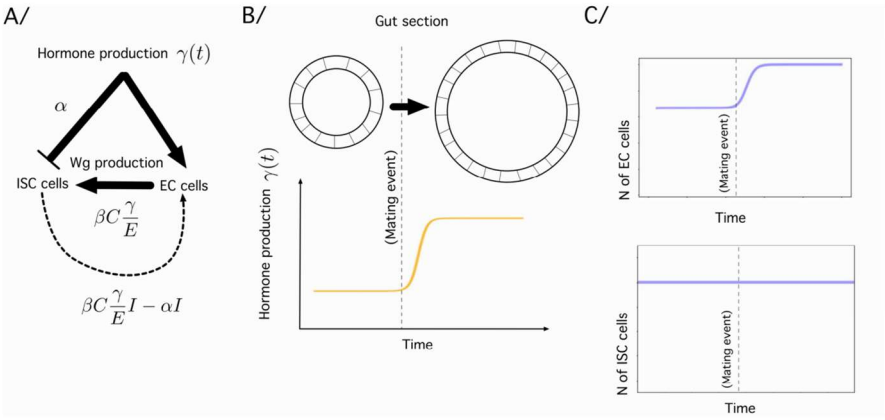

Fig.S8: **Equation showing stable population size of EC upon increased hormone levels**

A/ Construction of the dynamical equations B/ After a mating event there is an increase of midgut size (up) due to the increase in hormone production (down). C/ Evolution of the number of EC under the time evolution of the hormone production described in B/ (up). The curve is obtained integrating equation (6) with parameter γ(t) as defined in equation (1). The population of ISC remains nevertheless constant (bottom).

In Fig.S8 we provide a schematic way to understand the construction of the dynamical equations. In Fig.S9 we provide a schematic explanation of the involved terms.

Wg production and gradient

Production of Hormone

The net production of hormone γ is a function of time. At t_M a mating event triggers a sudden growth. The sudden increase of γ after a mating event can be qualitatively described by a sigmoid:

$$\gamma(t) = a\left(1 + \frac{b}{1+ce^{-(t-t_M)}}\right), \quad (1)$$

being $a, b, c > 0$ constants tuning the intensity of the hormone production. This function is plotted in orange in Fig.S8B/, down. The concentration of the hormone will be evaluated as dependent of the total amount of EC, E sharing the amount of hormone γ, i.e.:

$$\frac{\gamma}{E}.$$

Production of Wg from hormone levels

The presence of the hormone triggers the generation of Wg by EC. The amount of EC (E) will consequently represent the size of the organ, as the tissue is an epithelial (2D) tissue embedded in a cylindric geometry. We call $c(0, \gamma/E)$ the concentration of Wg at the surface of EC (E). Since the hormone levels are assumed to be constant in space, $c(0, \gamma/E)$ is assumed to be the same for all EC. We assume $c(0, \gamma/E)$ to be a monotonously growing function of γ/E. For the sake of simplicity, we will consider the dependency to be linear with proportionality constant $= 1$:

$$c(0, \gamma/E) = \frac{\gamma}{E}. \quad (2)$$

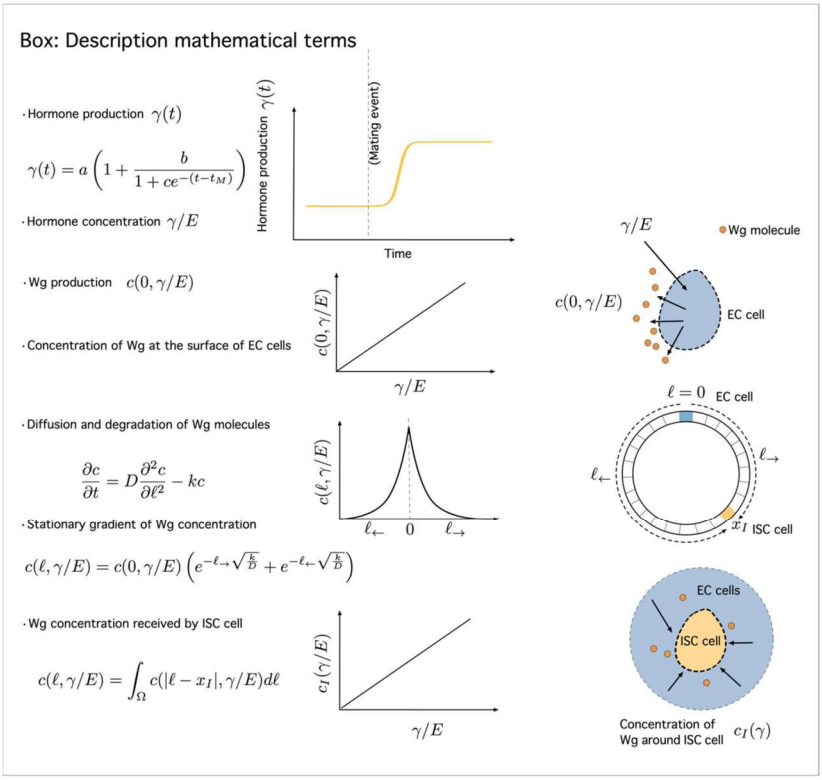

Fig.S9: **Description of the mathematical terms.**

Diffusion and degradation of Wg

We consider a section of the intestine as made of a 1D ring of cells. These cells can be either EC or ISC. Each EC occupies a fraction $\Delta\ell$ of the ring, and we approach the production of Wg with certain hormone concentration levels γ/E as:

$$\sim c(0, E/\gamma)\Delta\ell.$$

Assuming $\Delta\ell$ sufficiently small when compared with the size of the whole organ, one can consider that there is a continuum of EC with some "holes" filled by ISC. We call the set of points in the ring corresponding to EC cells Ω. Consequently, the number of EC, will be given by:

$$E = \int_\Omega d\ell\,; d\ell = Rd\theta,$$

where R is the radius of the ring, computed in units of cell diameter. Each point of Ω will produce an amount of Wg $\sim c(0, E/\gamma)d\ell$. Wg molecules will diffuse through the 1D ring with diffusion constant D and will degrade at rate k. The contribution of a single EC of the

ring to the total amount of Wg that diffuses along the ring can be grasped by the following diffusion equation with degradation [1,2]:

$$\frac{\partial c}{\partial t} = D\frac{\partial^2 c}{\partial \ell^2} - kc.$$

At the steady state, the above diffusive process will define a gradient of concentration of Wg that decays exponentially with the distance to the source ℓ:

$$c(\ell, \gamma/E) = c(0, \gamma/E)e^{-\ell\sqrt{\frac{k}{D}}}. \quad (3)$$

Since we are considering a ring, we have to take into account that the diffusion process runs in two directions from the source, clockwise and counterclockwise –see Fig.S9. Therefore, the Wg concentration at point ℓ must consider the two directions from the source:

$$c(\ell, \gamma/E) = c(\ell_{\rightarrow}, \gamma/E) + c(\ell_{\leftarrow}, \gamma/E),$$

where, by convention, $\ell_{\rightarrow}$ is the distance between the source and ℓ, computed clockwise (i.e.: $\ell_{\rightarrow} = \ell$); and $\ell_{\leftarrow}$ is the distance from the source and ℓ, computed counterclockwise (i.e.: $x_{\leftarrow} = 2\pi R - \ell$, where R is the radius of the ring).

Assumption: We consider that contributions to the concentration of Wg at distances beyond $2\pi R$ (the molecule traversed the whole ring already once since it departed from the source) are negligible.

Dynamical equations of the cell numbers

Concentration of Wg sensed by ISC

In the continuum approximation, at each point $\ell \in \Omega$ there will be a production of hormone $c(0, \gamma/E)$, as they are occupied by EC. The concentration of Wg at at the location of a given ISC, c_I, will be approximated by:

$$c_I(\gamma/E) = \int_{\Omega} \left\{c(|\ell - x_I|_{\rightarrow}, \gamma/E) + c(|\ell - x_I|_{\leftarrow}, \gamma/E)\right\} d\ell,$$

where x_I is the location of the ISC within the ring. According to the formal expression of $c(\ell, \gamma/E)$ given in equation (3), the above integral can be factorized as:

$$\int_{\Omega} \{\ldots\} d\ell = c(0, \gamma/E) \int_{\Omega} \left\{e^{-(|\ell - x_I|_{\rightarrow})\sqrt{\frac{k}{D}}} + e^{-(|\ell - x_I|_{\leftarrow})\sqrt{\frac{k}{D}}}\right\} d\ell.$$

Interestingly, given the symmetry of the system, the above integral is constant for all ISC of the system and does not directly depend on E/γ. So, we define the constant C as:

$$C(\Omega) = \int_{\Omega} \left\{e^{-(|\ell - x_I|_{\rightarrow})\sqrt{\frac{k}{D}}} + e^{-(|\ell - x_I|_{\leftarrow})\sqrt{\frac{k}{D}}}\right\} d\ell,$$

leading, after considering the value of $c(0, \gamma/E)$ as defined in equation (2), to the following general form:

$$c_I(\gamma/E) = C(\Omega)\frac{\gamma}{E}.$$

We observe that we still have a dependency of c_I on Ω which, in turn, may depend on c_I. However, the effect of this coupling can be assumed negligible, as we detail in the following assumption.

Assumption: Due to the exponential decay of the concentration of Wg with the distance to the source, we consider that only a finite neighbourhood of EC surrounding the ISC will effectively contribute to $c_I(\gamma/E)$. In consequence, the size of Ω becomes irrelevant for the computation of c_I, as the distant EC will have a negligible effect in the concentration of Wg sensed by the ISC. Therefore, we can neglect the dependency on Ω of $C(\Omega)$:

$$C(\Omega) \Rightarrow C,$$

thereby behaving as a constant that depends only on the degradation rate k and the diffusion constant D which do not change upon changes on γ or E. In consequence, from equation (2):

$$c_I(\gamma/E) = C\frac{\gamma}{E}. \tag{4}$$

Dynamical equations

Collecting the above facts, and assuming that the production of EC by ISC is proportional to the amount of Wg they sense, we have a time evolution of EC with a proliferative term that reads:

$$\beta C\frac{\gamma}{E}I, \tag{5}$$

where I is the amount of ISC and β is a parameter that describes the strength of hormone abundance. In the main text, we set $\beta = 1$, for the sake of simplicity, as the qualitative behaviour is not affected. At the same time, the production of EC is inhibited directly by the presence of the hormone at constant rate α. Therefore, the (mean-field) equation governing the evolution of EC numbers is:

$$\frac{dE}{dt} = \beta C\frac{\gamma}{E}I - \alpha I. \tag{6}$$

Considering fast equilibration and, in consequence, decoupling of time scales, one can find the only equilibrium point of the above system at:

$$E^* = \beta C\frac{\gamma}{\alpha}. \tag{7}$$

The above fixed point is stable, as:

$$\frac{d}{dE}\left(\beta C\frac{\gamma}{E}I - \alpha I\right)\Big|_{E^*} < 0.$$

As expected:

$$\gamma(t + \Delta t) > \gamma(t) \Rightarrow E(t + \Delta t) > E(t).$$

We therefore have qualitatively proven that the combined inhibition and indirect activation of ISC proliferation proposed by our experimental data lead to a stable organ size that changes consistently with the abundance of 20HE hormone.

Non-instantaneous differentiation from ISC to EC

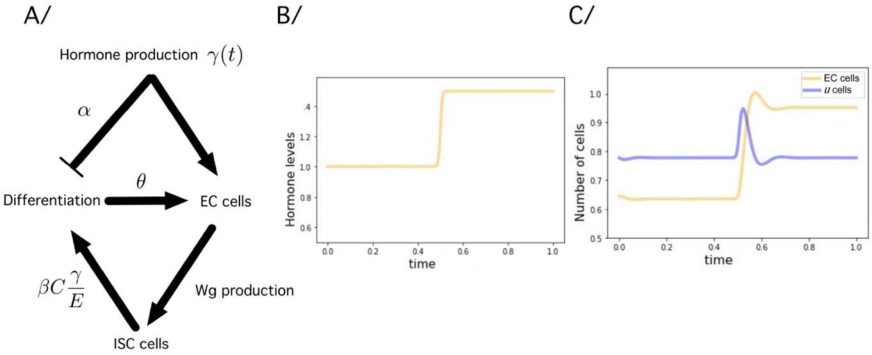

Fig.S10: **Equation showing stable population size of EC upon increased hormone levels including cells in an intermediate state**

A/ schematics of the mechanism where the transition between ISC → EC is not immediate, taking an average duration τ. Cells in process of differentiation are described by the variable u. The rates are shown by the arrows representing the transitions. According to equation (8) θ = 1/τ. The schema depicts the situation described by equations (9) and (10), i.e., case 1/. B/ A sigmoid-like pulse describing a sudden increase of 20HE hormone of 1/2 at t = 0.5. C/ Effect on the EC population and cells in transient state (u). We observe a peak in cell numbers resulting from proliferation of ISC after the increase of 20HE hormone which declines as cells are acquiring a differentiated EC identity. As predicted, the amount of EC increases with the hormone concentrations, whereas the amount of cells in transit (u) from ISC to EC goes back to its original amount despite the hormone levels increase. Integration parameters: C=10, I=10, inhibition parameter α=0.35, rate of differentiation of EC θ=0.1. Initial conditions for the integration: $u(0)$=35, $E(0)$=29.

One may consider a more realistic scenario where the differentiation from ISC into EC is not instantaneous. The natural question arises whether this affects the dynamics described so far. Here we consider that from mitosis of ISC to the full differentiation into an EC, there is a time span τ where the cell is in an intermediate state u. For this second case, we assume the following two scenarios:

- 20HE activates the production of Wg in EC which, in turn, activates the production of u cells from proliferation of ISC
- In the absence of direct inhibition of differentiation into EC, u cells last, in average, a time span τ transiting from ISC to EC
- Case 1/ 20HE inhibits the production of EC from differentiation of u cells at constant rate α

  Case 2/ 20HE inhibits the production of u cells from ISC at constant rate α

Remark: Since u cells require a finite time τ for transiting towards differentiated EC, we assume that the rate θ at which EC are produced out of u cells is:

$$\theta \approx \frac{1}{\tau}. \qquad (8)$$

In Fig.S10 we provide a scheme on how the dynamics is enriched by introducing a finite time τ in the process of transition form ISC to EC. We will see that, for a large range of parameters, the dynamics is just delayed —thereby making it more realistic— but remains qualitatively the same.

Let us call $u(t)$ the population of cells in the transit from ISC to EC at time t. Now we have, aside of ISC, two interdependent populations of cells: EC and u cells. The equations for case 1/ now read:

$$\frac{du}{dt} = \beta C \frac{\gamma}{E} I - \theta u \quad (9)$$

$$\frac{dE}{dt} = \theta u - \alpha I. \quad (10)$$

If we rewrite explicitly the above equations in terms of the lifetime τ of u cells, using equation (8) we are led to:

$$\begin{aligned} \frac{du}{dt} &= \beta C \frac{\gamma}{E} I - \frac{u}{\tau} \\ \frac{dE}{dt} &= \frac{u}{\tau} - \alpha I. \end{aligned}$$

The fixed point of the dynamical system defined by equations (9) and (10) is:

$$\begin{aligned} u^\star &= \frac{\alpha I}{\theta} \\ E^\star &= \beta C \frac{\gamma}{\alpha}. \end{aligned}$$

We observe that the predicted amount of EC is independent of the time τ needed for transiting from ISC to EC. In consequence, it remains invariant with respect to the previous simplified model.

The above approach assumed that the inhibition is happening at the level of differentiation. If one assumes case 2/, i.e., that the inhibition takes place at the level of proliferation, we are led to:

$$\frac{du}{dt} = \beta C \frac{\gamma}{E} I - \theta u - \alpha I \quad (11)$$

$$\frac{dE}{dt} = \theta u. \quad (12)$$

We notice that the dynamical system defined by equations (11) and (12) is obtained by just moving the term $-\alpha I$ to the first equation of the dynamical system defined by equations (9) and (10). Similar equations have been derived for the regulation of cortisol hormone levels [3]. The fixed point now reads:

$$\begin{aligned} u^\star &= 0 \\ E^\star &= \beta C \frac{\gamma}{\alpha}, \end{aligned}$$

i.e., the amount of EC remains the same, whereas cells in the intermediate state only appear temporarily as burst upon increases of the hormone. When the hormone levels stabilize, all newly produced cells end the differentiation process and become EC.

It remains to check the stability properties of the fixed points. To that end, we have to compute the Jacobian matrix at the fixed point and, since it is a 2D system, it is enough to check the signs of the trace and the determiner. Let us define $f(u,E) = \beta C \frac{\gamma}{E} I - \theta u$ and $g(u,E) = \theta u - \alpha I$. The Jacobian matrix of this 2D dynamical system is:

$$J = \begin{pmatrix} \frac{\partial f}{\partial u} & \frac{\partial f}{\partial E} \\ \frac{\partial g}{\partial u} & \frac{\partial g}{\partial E} \end{pmatrix} = \begin{pmatrix} -\theta & -\beta C \frac{\gamma}{E^2} I \\ \theta & 0 \end{pmatrix}.$$

It turns out that, if we define $f(u,E) = \beta C \frac{\gamma}{E} I - \theta u - \alpha I$ and $g(u,E) = \theta u$ the Jacobian matrix is the same. We now check the signs of the trace and the determiner at the fixed point:

$$\boldsymbol{tr}\begin{pmatrix} -\theta & -\beta C \frac{\gamma}{E^{\star 2}} I \\ \theta & 0 \end{pmatrix} < 0, \begin{vmatrix} -\theta & -\beta C \frac{\gamma}{E^{\star 2}} I \\ \theta & 0 \end{vmatrix} > 0,$$

a result easy to check because all the involved constants are positive. Given this combination of signs, $\boldsymbol{tr}(J) < 0$ and $|J| > 0$ we conclude that the fixed point is stable [4].

Observations on the generality of the results

The above computations have been performed by assuming that i) $c(0, \gamma/E)$ is a linear growing function of γ/E, ii) that the proliferative term in the dynamical equation (6) is linear as well with I –see equation (5)– and iii) that the inhibitory term α is constant and does not depend on γ/E.

The choice of linear and constant functions has been performed for the sake of simplicity. Let us briefly comment on the generality of the main result, namely, the existence of a stable fix point in E that shifts monotonously with γ/E as described in equation (7). We observe that the same qualitative results could be achieved by considering both dependencies described in i) and ii) just monotonously increasing functions, not necessarily linear.

The case of the inhibitory term α, commented in iii) can be as well generalized. Let us assume that $\alpha = \alpha(\gamma/E)$ and a generalized proliferation term $f(\gamma/E)$. Now, equation (6) reads:

$$\frac{dE}{dt} = If\left(\frac{\gamma}{E}\right) - I\alpha\left(\frac{\gamma}{E}\right).$$

In this context, what we require is that both the inhibitory term $\alpha(\gamma/E)$ and the proliferative term $f(\gamma/E)$ are, positive, non-decreasing functions with γ/E and that there exists a E^* by which:

$$f\left(\frac{\gamma}{E^*}\right) = \alpha\left(\frac{\gamma}{E^*}\right),$$

i.e., that there is a cross-over between the proliferative and inhibitory terms. In addition, we require that, if $E < E^*$, then:

$$f\left(\frac{\gamma}{E^*}\right) > \alpha\left(\frac{\gamma}{E^*}\right),$$

and that, if $E > E^*$, then:

$$f\left(\frac{\gamma}{E^*}\right) < \alpha\left(\frac{\gamma}{E^*}\right).$$

With these general properties, it follows naturally that:

$$\frac{d}{dE}\left(If\left(\frac{\gamma}{E}\right) - I\alpha\left(\frac{\gamma}{E}\right)\right)\Big|_{E^*} < 0,$$

and, therefore, that the fixed point is stable.

Blocking of cell differentiation: ISC Proliferation

In the previous modelling we considered that the amount of ISC is constant, since the division of an ISC leads to one ISC and one differentiated EC. Using the same line of reasoning, now we consider the case where such differentiation is blocked in a way that a division of a single ISC creates other two ISC. In this setting, the amount of EC will remain constant and the amount of ISC will eventually grow in time. Explicitly, we have that:

- 20HE inhibits the proliferation of ISC at rate α/ISC
- 20HE activates the production of Wg in the existing EC which, in turn, activates the production of ISC from proliferation of already existing ISC. The production of Wg depends on the hormone concentration (amount of hormone/cell number).

Note that, since the relative volume of ISC is negligible when compared to the volume of the EC, we can safely assume that the volume of the organ remains constant. As we did before, in Fig.S11A-B we provide a schematic way to understand the construction of the dynamic equations for this case.

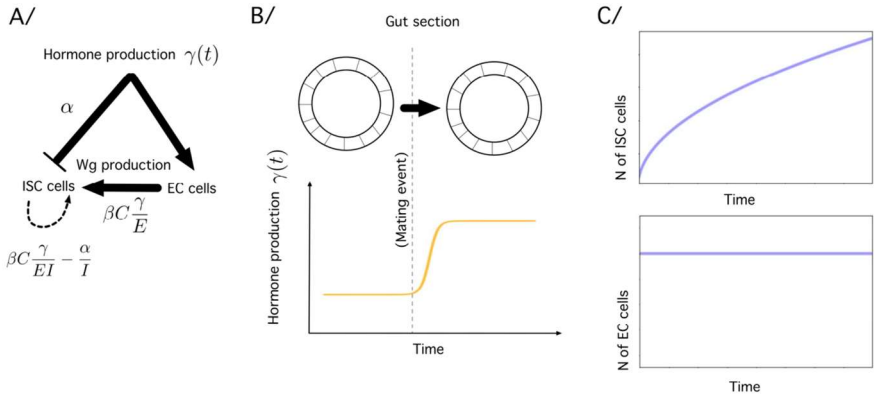

Fig.S11: Equation showing ISC numbers upon increased hormone levels and blocked EC differentiation

A/ Construction of the dynamical equations for the blocking of differentiation. B/ Contrary to the previous case, after a mating event there is no increase in midgut size (up) due to the increase of the hormone production (down), since the volume occupied by the ISC is negligible compared to the volume occupied by the EC. C/ (up) Evolution of ISC numbers when differentiation is blocked under constant hormone production, showing a square-root-like evolution in time. (bottom) the block of differentiation maintains a constant amount of EC.

Since both the amount of hormone and the amount of EC are constant, so will be the proliferative strength given by the amount of Wg. There is a positive constant K, that can be inferred from equation (5) as:

$$K \equiv \beta C \frac{\gamma}{E}.$$

This proliferative strength provided by the hormone level is assumed to be proportional to the Wg ligand produced by the EC, and will be shared by all the ISC. The same will happen with the inhibitor term, α. In consequence, the evolution of ISC number upon blocking of differentiation into EC will be given by:

$$\frac{dI}{dt} = \frac{K}{I} - \frac{\alpha}{I}.$$

As soon as $K > \alpha$, we expect to observe an unbounded growth of EC number–recall that here we are not considering other phenomena that could play a role! Indeed, considering that at $t = 0$ we have I_0 ISC, we expect to observe:

$$I(t) = \sqrt{2}\sqrt{(K-\alpha)t + I_0}.$$

Qualitatively, one expects, therefore:

$$I(t) \propto \sqrt{t}.$$

In Fig.S11C we have an example of this kind of growth.

References

[1] Berg, H. C. (1993) *Random walks in biology* Princeton University Press, Princeton

[2] Wartlick, O., Kicheva, A., González-Gaitán, M. (2009) Morphogen gradient formation. Cold Spring Harb. Perspect. Biol. 1(3):a001255

[3] Alon, U. (2024) *Systems Medicine. Physiological Circuits and the Dynamics of Disease* CRC Press (Boca Raton: FL)

[4] Strogatz, S. *Nonlinear Dynamics and Chaos : with Applications to Physics, Biology, Chemistry, and Engineering* Westview press (Boulder:CO)

3 General Discussion

Female reproduction is energetically costly and relies on a proportional size-increase of the maternal intestine to complement higher energy demands (Hammond, 1997; Speakman, 2008). The *Drosophila* midgut, with its comparable cellular composition and functionality to the mammalian small intestine, serves as an excellent model for studying the role of endocrine signals in pregnancy-induced intestinal re-sizing. Prior to this work pregnancy-related physiological adaptations of the intestine in *Drosophila* have already been described and shown to be induced by endocrine JH (Reiff *et al.*, 2015). Another potential driver of pregnancy-related intestinal adaptations is the functional oestrogen orthologue 20HE, which is already known to regulate reproduction and mating-induced metabolic adaptations in females. But if 20HE also has a role in regulating intestinal size adaptations upon mating remained unknown.

This work shows that increases in 20HE levels upon mating are not restricted to ovaries, but are also detected in circulating haemolymph, which suggest a role for 20HE in inter-organ signalling (Paper I Figure 2). In fact, 20HE drives differentiation of adult midgut precursors into EC via its downstream effector and Peroxisome proliferator-activated receptor gamma (hPPARγ)-homologue Eip75B-A/C to ensure an expansion of the absorptive epithelium upon higher energy demands during egg production (Paper I Figure 3, Fig.4). Human hPPARγ regulates adaptations of lipid metabolism in pregnant women (Rodriguez-Cuenca *et al*, 2012; Vivas *et al*, 2016; Waite *et al*, 2000) and was shown to induce differentiation in colon cancer cell lines (Cesario *et al*, 2006; Shimizu & Moriwaki, 2008; Yamazaki *et al*, 2007; Yoshizumi *et al*, 2004). In the *Drosophila* midgut, activation of 20HE signalling enhances lipid uptake in EC (Paper I Figure 2-figure supplement 1), and in line with the differentiation-promoting effect of hPPARγ in colon cancer cell lines, treatment with the hPPARγ agonist Pioglitazone similarly drives EB towards EC fate (Paper I Figure 4). The observed induction of EC differentiation via systemic 20HE signalling through Eip75B-A/C complements the previously described proliferation stimulation regulated by endocrine JH (Reiff *et al.*, 2015). 20HE and JH act synergistically to drive intestinal adaptations upon mating, with the JH mediator Kr-h1 promoting ISC proliferation and the 20HE effector Eip75B-A/C enhancing differentiation into epithelial EC (Paper I Figure 5, Fig.4).

Besides its physiological functions in adipocyte differentiation (Rosen *et al*, 1999) loss-of-function mutations in hPPARγ are associated with CRC (Sarraf *et al*, 1999). This work shows, that increased levels of the hPPARγ homologue Eip75B-A/C or treatment with the agonist Pioglitazone prevent tumour formation in a benign N-tumour model by inducing differentiation of N deficient ISC into postmitotic, epithelial EC (Paper I Figure 6, Figure 6-figure supplement 1, Figure 7, Figure 7-figure supplement 1).

Simultaneous with this thesis Ahmed et al. also investigated the impact of ovary-derived 20HE in physiological adaptations of the *Drosophila* midgut. Consistent with the findings of this thesis, they demonstrated that mating, along with genetic or pharmacologic activation of 20HE signalling, stimulates ISC mitosis and intestinal growth through the downstream targets Broad, Eip75B, and Hormone Receptor 3 (Ahmed *et al*, 2020).

In addition, this thesis unravels Crol as another factor linking systemic 20HE signalling with local signalling pathways in the adult *Drosophila* midgut. Developmental studies in wing imaginal discs already showed that Crol links systemic 20HE with local Wnt/Wg signalling and the cell cycle regulator and CDC25-orthologue Stg (D'Avino & Thummel, 1998; Mitchell *et al.*, 2008; Mitchell *et al.*, 2013). Given the shown role of 20HE signalling in adult midgut adaptations upon mating and the previously discovered regulation of Crol by 20HE, a function of Crol in physiological intestinal adaptations was suggested.

The data presented in the included Paper III show that Crol protein levels within the adult *Drosophila* midgut cells are regulated by 20HE signalling activity (Paper III Figure 1, FigureS1). Whereas this regulation of Crol by 20HE is comparable in different intestinal cell types, the paper aimed at separately investigating the functions of Crol in undifferentiated ISC/EB and epithelial EC. To investigate Crol's role in ISC/EB, the established esg^{ReDDM} system was used. Whereas the novel Rapport system was developed to investigate the non-autonomous regulation of ISC behaviour by Crol within EC. Rapport is a binary expression system that enables labelling of ISC and tracing of their progeny with simultaneous and independent manipulation of EC.

The results show that Crol inhibits ISC proliferation by autonomously repressing the cell cycle regulators Stg and Cyclin-B (CycB) (Paper III Figure 2, FigureS2, FigureS3, Fig.4). In contrast to the antiproliferative role in ISC, Crol stimulates expression and secretion of

mitogenic Wg ligand in EC, which in turn non-autonomously induces ISC mitosis (Paper III Figure 4, Figure 5, Fig.4). These opposing roles of Crol in different cell types are also observed in intestinal tumours. Using the established N-tumour model (Patel *et al*, 2015) as well as novel CRC avatars (Paper II), this thesis demonstrates that Crol plays a protective role within the tumour by suppressing tumour formation, thereby mitigating midgut hypotrophy and enhancing survival in CRC avatar flies (Paper II, Paper III Figure 6). Similarly, as observed in physiological conditions, Crol has an opposite function within the EC surrounding the tumours. When expressed in EC as part of the tumour microenvironment Crol boosts tumour formation and growth (Paper III Figure 6). Analysis of the human Crol ortholog hZNF267 reveals similar findings regarding its distinct roles in ISC/EB and EC (Paper III Figure 2, Figure 4, Figure 5), as well as its involvement in intestinal tumours and their microenvironment (Paper III Figure 6). One hallmark of cancer cells is the intra-tumour heterogeneity defined by distinct cell populations within the same tumours. The newly established Rapport-tracing system allows to manipulate the distinct cell populations within a tumour or its microenvironment while simultaneously tracing its progeny as shown for the analysis of Crol/hZNF267 in this thesis (Paper III Figure 6).

Besides the local events that were shown to be regulated by Crol, Paper III also explores the resulting global effects analysing whole organ size of female intestines. During this thesis Ahmed et al. 2020 also demonstrated that female intestinal size in *Drosophila* is regulated by 20HE signalling (Ahmed *et al.*, 2020). However, a potential role for Crol and the molecular mechanisms stabilizing intestinal size after growth remained unknown. Advancing the understanding of pregnancy-related intestinal re-sizing is of particular interest as it would allow to prevent or treat postpartum weight retention which comes along with increased risks of developing metabolic disorders like diabetes or certain types of cancer (Haslam & James, 2005; James *et al.*, 2004). Indeed, female intestinal size is increased upon ISC/EB specific knockdown of Crol and upon EC specific overexpression of Crol (Paper III Figure 7, Figure S7) once more underlining the opposing roles of Crol in controlling ISC mitosis (Fig.4). In addition to the non-autonomous stimulation of ISC mitosis by the 20HE-Crol-Wg axis in EC, Eip75B induces differentiation into epithelial EC (Paper I Figure 3, Figure 3–figure supplement 2) to yield a larger organ thus ensuring increased nutrient uptake to match higher energy demands (Fig.4). Finally, mathematical

modelling demonstrates that the opposing roles of Crol likely balance and stabilize intestinal size during growth, depending on 20HE levels.

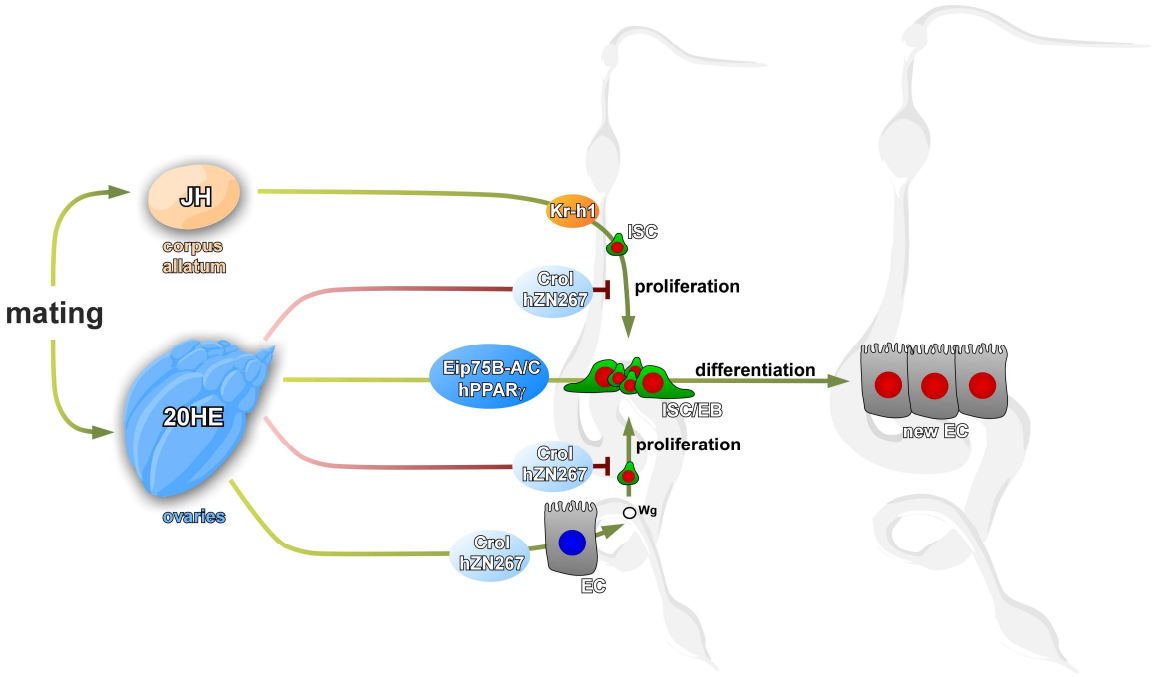

Fig.4: Graphical summary depicting the roles of endocrine JH and 20HE in mating-induced physiological adaptations of the *Drosophila* midgut.

Upon mating synthesis of JH in the corpus allatum and synthesis of 20HE in ovaries is induced. Both hormones are released into the circulating haemolymph and reach remote organs such as the midgut. Within the midgut JH induces proliferation in ISC via its target Kr-h1 increasing the number of midgut progenitor cells (ISC/EB). In EC, 20HE, through its target Crol/hZNF267, induces the expression and release of mitogenic Wg ligand, enhancing ISC proliferation in a non-autonomous manner. Downstream of 20HE, Eip75B-A/C/hPPARγ induces differentiation of the generated ISC/EB into new EC. Together these molecular mechanisms increase the number of epithelial cells and sequentially the size of the female *Drosophila* midgut in response to mating (green arrows). On the other hand, Crol/hZNF267 autonomously inhibits ISC proliferation downstream of 20HE, thereby antagonizing the growth stimulating mechanisms and balancing intestinal size (red lines).

The mechanisms described here represent an example of inter-organ communication involving a steroid hormone which ensures adaptations of the female body to changes in metabolic demands during the production of offspring. Upon mating increased levels of 20HE/oestrogen secreted from the ovaries act on remote organs like the intestine to

control size adaptations and thereby nutrient uptake. This work shows how a single endocrine signal is translated into different autonomous and paracrine outputs in the remote intestine, thereby differentially affecting ISC proliferation in both physiology and pathology. This bifurcation of a sole hormonal stimulus into different signals gives further insights into the complexity of tissue size regulations. Understanding the molecular mechanisms that control pregnancy induced re-sizing of the intestine could also help to further unravel the processes that generally control organ sizes. Especially the mechanism of a sole systemic signal inducing organ growth and conversely also stalling further growth after reaching an adequate size is of particular interest. The opposing effects of 20HE and its downstream factor Crol in different cell types will also pave the way for untangling the controversial role of steroidal oestrogens on CRC development and progression.

4 Summary

Inter-organ communication is an important mechanism that evolved with the transition from unicellular to multicellular organisms and is crucial throughout development and during adaptations to external conditions. The generation of offspring relies on several adaptations of the mother's body to ensure proper development of the offspring. These adaptations are orchestrated by steroid hormones like oestrogens and include a size increase of the absorptive epithelium in the intestine to fit higher energy demands. Hormone-mediated intestinal re-sizing during pregnancy has already been shown in mice as well as the invertebrate model organism *Drosophila melanogaster*, but the detailed mechanisms which coordinate intestinal size adaptations remained unknown.

This thesis shows a role for the steroid hormone 20 hydroxy ecdysone (20HE) in re-sizing of the female *Drosophila* intestine. Two effectors, Ecdysone-induced protein 75B (Eip75B) and Crooked legs (Crol), have been identified that function downstream of systemic 20HE to locally control intestinal stem cell (ISC) behaviour. Upon mating and increased circulating 20HE levels Eip75B induces differentiation of ISC into epithelial enterocytes (EC) to ensure increased nutrient uptake. Crol and its human ortholog hZNF267 were shown to differentially affect ISC behaviour depending on the cell type. Within ISC, Crol/hZNF267 has an antiproliferative role by repressing cell cycle regulators String (Stg) and Cyclin-B (CycB). In EC, Crol/hZNF267 non-autonomously promotes ISC proliferation by inducing expression and secretion of mitogenic Wingless (Wg) ligand. Mathematical modelling proved the plausibility that these opposing roles of Crol on ISC behaviour can induce a stable intestinal size which depends on 20HE levels. In different tumour models Eip75B induces differentiation of tumour stem cells into postmitotic EC, whereas Crol/hZNF267 prevents tumour formation within the tumour cells and non-autonomously fuels tumour growth when expressed in surrounding EC.

Together, the findings presented in this thesis describe an example of inter-organ communication involving a steroid hormone which is translated into different outputs with opposing effects on ISC behaviour. These local outputs ensure adaptations of the female intestine to changes in metabolic demands during the production of offspring and advance the understanding of mechanisms controlling organ size.

5 Zusammenfassung

Die Kommunikation zwischen Organen ist ein Prozess, welcher sich gleichzeitig mit dem Übergang von Einzellern zu Mehrzellern entwickelt hat. Diese Art von Kommunikation ist in der Entwicklung essenziell, und auch während der Anpassung adulter Organismen an äußere Einflüsse. Anpassungen des weiblichen Körpers finden zum Beispiel während der Schwangerschaft statt, um die richtige Entwicklung der Nachkommen zu gewährleisten. Diese von Steroidhormonen gesteuerten Anpassungen umfassen eine Vergrößerung des Darms zur Erhöhung der Nährstoffaufnahme. Derartige Größenanpassungen des Darms konnten schon in Mäusen und *Drosophila melanogaster* gezeigt werden, Details über die kontrollierenden Mechanismen blieben dabei jedoch unbekannt.

In dieser Arbeit wurde der Einfluss des Steroidhormons 20 Hydroxyecdyson (20HE) auf die Größenanpassung des Darms in weiblichen *Drosophila* untersucht. Identifiziert und charakterisiert wurden zwei Faktoren, Ecdysone-induced protein 75B (Eip75B) und Crooked legs (Crol), welche abhängig von 20HE das Verhalten von intestinalen Stammzellen (ISC) kontrollieren. Erhöhte 20HE Vorkommen nach der Verpaarung induzieren durch Eip75B die Differenzierung von Vorläuferzellen zu epithelialen Enterozyten (EC). Für Crol und das humane Ortholog hZNF267 konnten unterschiedliche Effekte auf das ISC-Verhalten gezeigt werden. In ISC inhibiert Crol die Zellzyklus-Regulatoren String (Stg) und Cyclin-B (CycB) und somit die ISC-Proliferation. In EC stimuliert Crol nicht-autonom die ISC-Proliferation durch Induktion des mitogenen Wingless (Wg) Liganden. Ein mathematisches Modell konnte zeigen, dass die unterschiedlichen Effekte von Crol auf die ISC eine stabile Organgröße des Darms abhängig von der 20HE Konzentration induzieren können. Auch in Tumor-Modellen induziert Eip75B die Differenzierung von Tumor-Stammzellen in postmitotische EC, während Crol/hZNF267 in Tumor-Stammzellen die Entstehung von Tumoren verhindert und andererseits nicht-autonom das Tumorwachstum fördert.

Zusammengefasst zeigen die hier dargestellten Ergebnisse ein Beispiel für die Kommunikation zwischen Organen. Ein Steroidhormon wird in lokale Signale übersetzt, die das ISC-Verhalten unterschiedlich beeinflussen, um somit die Größenanpassung des weiblichen Darms während der Erzeugung von Nachkommen zu steuern.

6 References

Ables ET, Bois KE, Garcia CA, Drummond-Barbosa D (2015) Ecdysone response gene E78 controls ovarian germline stem cell niche formation and follicle survival in *Drosophila*. *Developmental biology* 400: 33-42

Ables ET, Drummond-Barbosa D (2010) The steroid hormone ecdysone functions with intrinsic chromatin remodeling factors to control female germline stem cells in *Drosophila*. *Cell Stem Cell* 7: 581-592

Ahmed SMH, Maldera JA, Krunic D, Paiva-Silva GO, Penalva C, Teleman AA, Edgar BA (2020) Fitness trade-offs incurred by ovary-to-gut steroid signalling in *Drosophila*. *Nature* 584: 415-419

Ameku T, Niwa R (2016) Mating-Induced Increase in Germline Stem Cells via the Neuroendocrine System in Female *Drosophila*. *PLoS genetics* 12: e1006123

Antonello ZA, Reiff T, Ballesta-Illan E, Dominguez M (2015) Robust intestinal homeostasis relies on cellular plasticity in enteroblasts mediated by miR-8-Escargot switch. *The EMBO journal* 34: 2025-2041

Aranda A, Pascual A (2001) Nuclear hormone receptors and gene expression. *Physiol Rev* 81: 1269-1304

Bailey CJ, Ahmed-Sorour H (1980) Role of ovarian hormones in the long-term control of glucose homeostasis. *Diabetologia* 19: 475-481

Bangi E, Ang C, Smibert P, Uzilov AV, Teague AG, Antipin Y, Chen R, Hecht C, Gruszczynski N, Yon WJ *et al* (2019) A personalized platform identifies trametinib plus zoledronate for a patient with KRAS-mutant metastatic colorectal cancer. *Sci Adv* 5: eaav6528

Bangi E, Murgia C, Teague AG, Sansom OJ, Cagan RL (2016) Functional exploration of colorectal cancer genomes using *Drosophila*. *Nature communications* 7: 13615

Banjac I, Maimets M, Tsang IHC, Dioli M, Hansen SL, Krizic K, Bressan RB, Lövkvist C, Jensen KB (2025) Fate mapping in mouse demonstrates early secretory differentiation directly from Lgr5+ intestinal stem cells. *Developmental cell*

Cairnie AB, Bentley RE (1967) Cell proliferation studies in the intestinal epithelium of the rat: Hyperplasia during lactation. *Experimental cell research* 46: 428-440

Calle EE, Miracle-McMahill HL, Thun MJ, Heath CW, Jr. (1995) Estrogen Replacement Therapy and Risk of Fatal Colon Cancer in a Prospective Cohort of Postmenopausal Women. *JNCI: Journal of the National Cancer Institute* 87: 517-523

Carney GE, Bender M (2000) The *Drosophila* ecdysone receptor (EcR) Gene Is Required Maternally for Normal Oogenesis. *Genetics* 154: 1203-1211

Casirola DM, Ferraris RP (2003) Role of the small intestine in postpartum weight retention in mice2. *The American Journal of Clinical Nutrition* 78: 1178-1187

Cesario RM, Stone J, Yen W-C, Bissonnette RP, Lamph WW (2006) Differentiation and growth inhibition mediated via the RXR:PPARγ heterodimer in colon cancer. *Cancer Letters* 240: 225-233

Chen J, Xu N, Wang C, Huang P, Huang H, Jin Z, Yu Z, Cai T, Jiao R, Xi R (2018) Transient Scute activation via a self-stimulatory loop directs enteroendocrine cell pair specification from self-renewing intestinal stem cells. *Nature cell biology* 20: 152-161

Chute CG, Willett WC, Culditz GA, Stampfer MJ, Rosner B, Speizer FE (1991) A Prospective Study of Reproductive History and Exogenous Estrogens on the Risk of Colorectal Cancer in Women. *Epidemiology* 2: 201-207

Clarke ND, Berg JM (1998) Zinc Fingers in *Caenorhabditis elegans*: Finding Families and Probing Pathways. *Science (New York, NY)* 282: 2018-2022

Cordero JB, Stefanatos RK, Myant K, Vidal M, Sansom OJ (2012a) Non-autonomous crosstalk between the Jak/Stat and Egfr pathways mediates *Apc1*-driven intestinal stem cell hyperplasia in the *Drosophila* adult midgut. *Development (Cambridge, England)* 139: 4524-4535

Cordero JB, Stefanatos RK, Scopelliti A, Vidal M, Sansom OJ (2012b) Inducible progenitor-derived Wingless regulates adult midgut regeneration in *Drosophila*. *The EMBO journal* 31: 3901-3917

Costrini NV, Kalkhoff RK (1971) Relative effects of pregnancy, estradiol, and progesterone on plasma insulin and pancreatic islet insulin secretion. *The Journal of Clinical Investigation* 50: 992-999

D'Avino PP, Thummel CS (1998) crooked legs encodes a family of zinc finger proteins required for leg morphogenesis and ecdysone-regulated gene expression during *Drosophila* metamorphosis. *Development (Cambridge, England)* 125: 1733-1745

de Verdier MG, London S (1992) Reproductive factors, exogenous female hormones, and colorectal cancer by subsite. *Cancer Causes & Control* 3: 355-360

Della Torre S, Benedusi V, Fontana R, Maggi A (2014) Energy metabolism and fertility: a balance preserved for female health. *Nat Rev Endocrinol* 10: 13-23

Fevr T, Robine S, Louvard D, Huelsken J (2007) Wnt/β-Catenin Is Essential for Intestinal Homeostasis and Maintenance of Intestinal Stem Cells. *Molecular and Cellular Biology* 27: 7551-7559

Flatt T, Tu M-P, Tatar M (2005) Hormonal pleiotropy and the juvenile hormone regulation of Drosophila development and life history. *BioEssays* 27: 999-1010

Fraumeni JF, Jr., Lloyd JW, Smith EM, Wagoner JK (1969) Cancer mortality among nuns: role of marital status in etiology of neoplastic disease in women. *J Natl Cancer Inst* 42: 455-468

Fungfuang W, Terada M, Komatsu N, Moon C, Saito TR (2013) Effects of estrogen on food intake, serum leptin levels and leptin mRNA expression in adipose tissue of female rats. *lar* 29: 168-173

Gilbert LI, Warren JT (2005) A Molecular Genetic Approach to the Biosynthesis of the Insect Steroid Molting Hormone. In: *Vitamins & Hormones*, pp. 31-57. Academic Press:

Groden J, Thliveris A, Samowitz W, Carlson M, Gelbert L, Albertsen H, Joslyn G, Stevens J, Spirio L, Robertson M *et al* (1991) Identification and characterization of the familial adenomatous polyposis coli gene. *Cell* 66: 589-600

Hammond KA (1997) Adaptation of the Maternal Intestine During Lactation. *Journal of Mammary Gland Biology and Neoplasia* 2: 243-252

Haslam DW, James WPT (2005) Obesity. *The Lancet* 366: 1197-1209

Hendifar A, Yang D, Lenz F, Lurje G, Pohl A, Lenz C, Ning Y, Zhang W, Lenz HJ (2009) Gender disparities in metastatic colorectal cancer survival. *Clin Cancer Res* 15: 6391-6397

Huang X, Warren JT, Gilbert LI (2008) New players in the regulation of ecdysone biosynthesis. *Journal of Genetics and Genomics* 35: 1-10

Hytten FE (1991) Weight gain in pregnancy. *Clinical physiology in obstetrics*

James WPT, Jackson-Leach R, Mhurchu CN, Kalamara E, Shayeghi M, Rigby NJ, Nishida C, Rodgers A (2004) Overweight and obesity (high body mass index). *Comparative quantification of health risks: global and regional burden of disease attributable to selected major risk factors* 1: 497-596

Jinek M, Chylinski K, Fonfara I, Hauer M, Doudna JA, Charpentier E (2012) A Programmable Dual-RNA–Guided DNA Endonuclease in Adaptive Bacterial Immunity. *Science (New York, NY)* 337: 816-821

König A, Yatsenko AS, Weiss M, Shcherbata HR (2011) Ecdysteroids affect *Drosophila* ovarian stem cell niche formation and early germline differentiation. *The EMBO journal* 30: 1549-1562

Kozlova T, Thummel CS (2000) Steroid Regulation of Postembryonic Development and Reproduction in *Drosophila*. *Trends in Endocrinology & Metabolism* 11: 276-280

Krausova M, Korinek V (2014) Wnt signaling in adult intestinal stem cells and cancer. *Cellular Signalling* 26: 570-579

Kretzschmar K, Clevers H (2017) Wnt/β-catenin signaling in adult mammalian epithelial stem cells. *Developmental biology* 428: 273-282

Kushiro T, Nambara E, McCourt P (2003) Hormone evolution: The key to signalling. *Nature* 422: 122-122

Laudet V, Markov G, V. (2018) Evolution of Hormonal Mechanisms. In: *Encyclopedia of Endocrine Diseases, Second Edition*,

Lin G, Xu N, Xi R (2008) Paracrine Wingless signalling controls self-renewal of *Drosophila* intestinal stem cells. *Nature* 455: 1119-1123

Martinez E, Givel F, Wahli W (1991) A common ancestor DNA motif for invertebrate and vertebrate hormone response elements. *The EMBO journal* 10: 263-268

Martorell O, Merlos-Suarez A, Campbell K, Barriga FM, Christov CP, Miguel-Aliaga I, Batlle E, Casanova J, Casali A (2014) Conserved mechanisms of tumorigenesis in the *Drosophila* adult midgut. *PloS one* 9: e88413

McMichael AJ, Potter JD (1980) Reproduction, endogenous and exogenous sex hormones, and colon cancer: a review and hypothesis. *J Natl Cancer Inst* 65: 1201-1207

Micchelli CA, Perrimon N (2006) Evidence that stem cells reside in the adult *Drosophila* midgut epithelium. *Nature* 439: 475-479

Mitchell N, Cranna N, Richardson H, Quinn L (2008) The Ecdysone-inducible zinc-finger transcription factor Crol regulates Wg transcription and cell cycle progression in *Drosophila*. *Development (Cambridge, England)* 135: 2707-2716

Mitchell NC, Lin JI, Zaytseva O, Cranna N, Lee A, Quinn LM (2013) The Ecdysone receptor constrains wingless expression to pattern cell cycle across the *Drosophila* wing margin in a Cyclin B-dependent manner. *BMC developmental biology* 13: 28

Morris LX, Spradling AC (2012) Steroid signaling within *Drosophila* ovarian epithelial cells sex-specifically modulates early germ cell development and meiotic entry. *PloS one* 7: e46109

Moya J, Phillips L, Sanford J, Wooton M, Gregg A, Schuda L (2014) A review of physiological and behavioral changes during pregnancy and lactation: Potential exposure factors and data gaps. *Journal of Exposure Science & Environmental Epidemiology* 24: 449-458

Muzny DM, Bainbridge MN, Chang K, Dinh HH, Drummond JA, Fowler G, Kovar CL, Lewis LR, Morgan MB, Newsham IF *et al* (2012) Comprehensive molecular characterization of human colon and rectal cancer. *Nature* 487: 330-337

Oberdörster E, Clay MA, Cottam DM, Wilmot FA, McLachlan JA, Milner MJ (2001) Common phytochemicals are ecdysteroid agonists and antagonists: a possible evolutionary link between vertebrate and invertebrate steroid hormones. *J Steroid Biochem Mol Biol* 77: 229-238

Ohlstein B, Spradling A (2006) The adult *Drosophila* posterior midgut is maintained by pluripotent stem cells. *Nature* 439: 470-474

Ohlstein B, Spradling A (2007) Multipotent *Drosophila* intestinal stem cells specify daughter cell fates by differential notch signaling. *Science (New York, NY)* 315: 988-992

Patel PH, Dutta D, Edgar BA (2015) Niche appropriation by Drosophila intestinal stem cell tumours. *Nature cell biology* 17: 1182-1192

Port F, Bullock SL (2016) Augmenting CRISPR applications in *Drosophila* with tRNA-flanked sgRNAs. *Nature methods* 13: 852-854

Port F, Chen HM, Lee T, Bullock SL (2014) Optimized CRISPR/Cas tools for efficient germline and somatic genome engineering in Drosophila. *Proceedings of the National Academy of Sciences of the United States of America* 111: E2967-2976

Port F, Muschalik N, Bullock SL (2015) Systematic Evaluation of *Drosophila* CRISPR Tools Reveals Safe and Robust Alternatives to Autonomous Gene Drives in Basic Research. *G3 (Bethesda)* 5: 1493-1502

Reiff T, Jacobson J, Cognigni P, Antonello Z, Ballesta E, Tan KJ, Yew JY, Dominguez M, Miguel-Aliaga I (2015) Endocrine remodelling of the adult intestine sustains reproduction in *Drosophila*. *eLife* 4: e06930

Riddiford LM (1993) Hormones and *Drosophila* development. *The development of Drosophila melanogaster* 2: 899-939

Riddiford LM (1994) Cellular and Molecular Actions of Juvenile Hormone I. General Considerations and Premetamorphic Actions. In: *Advances in Insect Physiology*, Evans P.D. (ed.) pp. 213-274. Academic Press:

Rodriguez-Cuenca S, Carobbio S, Velagapudi VR, Barbarroja N, Moreno-Navarrete JM, Tinahones FJ, Fernandez-Real JM, Orešič M, Vidal-Puig A (2012) Peroxisome Proliferator-Activated Receptor γ-Dependent Regulation of Lipolytic Nodes and Metabolic Flexibility. *Molecular and Cellular Biology* 32: 1555-1565

Rosen ED, Sarraf P, Troy AE, Bradwin G, Moore K, Milstone DS, Spiegelman BM, Mortensen RM (1999) PPAR gamma is required for the differentiation of adipose tissue in vivo and in vitro. *Mol Cell* 4: 611-617

Sarraf P, Mueller E, Smith WM, Wright HM, Kum JB, Aaltonen LA, de la Chapelle A, Spiegelman BM, Eng C (1999) Loss-of-Function Mutations in PPARγ Associated with Human Colon Cancer. *Molecular Cell* 3: 799-804

Schepers A, Clevers H (2012) Wnt Signaling, Stem Cells, and Cancer of the Gastrointestinal Tract. *Cold Spring Harbor Perspectives in Biology* 4

Scholl TO, Hediger ML, Schall JI, Ances IG, Smith WK (1995) Gestational Weight Gain, Pregnancy Outcome, and Postpartum Weight Retention. *Obstetrics & Gynecology* 86

Shimizu M, Moriwaki H (2008) Synergistic Effects of PPARγ Ligands and Retinoids in Cancer Treatment. *PPAR Research* 2008: 181047

Sieber MH, Spradling AC (2015) Steroid Signaling Establishes a Female Metabolic State and Regulates SREBP to Control Oocyte Lipid Accumulation. *Current biology : CB* 25: 993-1004

Siegel R, Jemal A (2011) Colorectal cancer facts & Figures, 2011–2013. *Atlanta, GA: American Cancer Society*

Siegel RL, Miller KD, Fedewa SA, Ahnen DJ, Meester RGS, Barzi A, Jemal A (2017) Colorectal cancer statistics, 2017. *CA: A Cancer Journal for Clinicians* 67: 177-193

Singh SR, Aggarwal P, Hou SX (2019) Cancer Stem Cells and Stem Cell Tumors in *Drosophila*. *Advances in experimental medicine and biology* 1167: 175-190

Soldin OP, Guo T, Weiderpass E, Tractenberg RE, Hilakivi-Clarke L, Soldin SJ (2005) Steroid hormone levels in pregnancy and 1 year postpartum using isotope dilution tandem mass spectrometry. *Fertil Steril* 84: 701-710

Speakman JR (2008) The physiological costs of reproduction in small mammals. *Philosophical Transactions of the Royal Society B: Biological Sciences* 363: 375-398

Stelmańska E, Sucajtys-Szulc E (2014) Enhanced food intake by progesterone-treated female rats is related to changes in neuropeptide genes expression in hypothalamus. *Endokrynologia Polska* 65: 46-56

Tiano JP, Mauvais-Jarvis F (2012) Importance of oestrogen receptors to preserve functional β-cell mass in diabetes. *Nature Reviews Endocrinology* 8: 342-351

Truman JW, Riddiford LM (2002) Endocrine Insights into the Evolution of Metamorphosis in Insects. *Annual Review of Entomology* 47: 467-500

Uryu O, Ameku T, Niwa R (2015) Recent progress in understanding the role of ecdysteroids in adult insects: Germline development and circadian clock in the fruit fly *Drosophila melanogaster*. *Zoological Letters* 1: 32

van Es JH, Haegebarth A, Kujala P, Itzkovitz S, Koo B-K, Boj SF, Korving J, van den Born M, van Oudenaarden A, Robine S *et al* (2012) A Critical Role for the Wnt Effector Tcf4 in Adult Intestinal Homeostatic Self-Renewal. *Molecular and Cellular Biology* 32: 1918-1927

Vivas Y, Díez-Hochleitner M, Izquierdo-Lahuerta A, Corrales P, Horrillo D, Velasco I, Martínez-García C, Campbell M, Sevillano J, Ricote M *et al* (2016) Peroxisome Proliferator-Activated Receptor γ 2 Modulates Late-Pregnancy Homeostatic Metabolic Adaptations. *Molecular Medicine* 22: 724-736

Waite LL, Person EC, Zhou Y, Lim K-H, Scanlan TS, Taylor RN (2000) Placental Peroxisome Proliferator-Activated Receptor-γ Is Up-Regulated by Pregnancy Serum1. *The Journal of Clinical Endocrinology & Metabolism* 85: 3808-3814

Weiss NS, Daling JR, Chow WH (1981) Incidence of cancer of the large bowel in women in relation to reproductive and hormonal factors. *J Natl Cancer Inst* 67: 57-60

Weyant MJ, Carothers AM, Mahmoud NN, Bradlow HL, Remotti H, Bilinski RT, Bertagnolli MM (2001) Reciprocal expression of ERalpha and ERbeta is associated with estrogen-mediated modulation of intestinal tumorigenesis. *Cancer research* 61: 2547-2551

Wood LD, Parsons DW, Jones S, Lin J, Sjöblom T, Leary RJ, Shen D, Boca SM, Barber T, Ptak J *et al* (2007) The Genomic Landscapes of Human Breast and Colorectal Cancers. *Science (New York, NY)* 318: 1108-1113

Wu AH, Paganini-Hill A, Ross RK, Henderson BE (1987) Alcohol, physical activity and other risk factors for colorectal cancer: A prospective study. *British Journal of Cancer* 55: 687-694

Xiu M, Wang Y, Yang D, Zhang X, Dai Y, Liu Y, Lin X, Li B, He J (2022) Using Drosophila melanogaster as a suitable platform for drug discovery from natural products in inflammatory bowel disease. *Front Pharmacol* 13: 1072715

Yamazaki K, Shimizu M, Okuno M, Matsushima-Nishiwaki R, Kanemura N, Araki H, Tsurumi H, Kojima S, Weinstein IB, Moriwaki H (2007) Synergistic effects of RXRα and PPARγ ligands to inhibit growth in human colon cancer cells—phosphorylated RXRα is a critical target for colon cancer management. *Gut* 56: 1557-1563

Yoshizumi T, Ohta T, Ninomiya I, Terada I, Fushida S, Fujimura T, Nishimura G, Shimizu K, Yi S, Miwa K (2004) Thiazolidinedione, a peroxisome proliferator-activated receptor-gamma ligand, inhibits growth and metastasis of HT-29 human colon cancer cells through differentiation-promoting effects. *Int J Oncol* 25: 631-639

7 List of Abbreviations

20HE	20 hydroxy ecdysone
Apc	Adenomatous polyposis coli
CDC25	Cell division cycle 25C
CRC	colorectal cancer
CRISPR/Cas9	Clustered Regularly Interspaced Short Palindromic Repeats/ CRISPR-associated protein 9
Crol	Crooked legs
CycB	Cyclin-B
EB	enteroblast(s)
EC	enterocyte(s)
EE	enteroendocrine cell(s)
Eip75B	Ecdysone-induced protein 75B
esg	escargot
$Gal80^{ts}$	temperature sensitive Gal80 repressor
Gce	Germ cell-expressed bHLH-PAS
GFP	green fluorescent protein
GSC	germline stem cells
ISC	intestinal stem cell(s)
JH	juvenile hormone
Kr-h1	Kr transcription factor homolog 1
Med	Medea
Met	Methoprene tolerant
P53	Tumor protein p53
PC	paneth cells
hPPARγ	human Proliferator-activated receptor gamma
Pten	Phosphatase and tensin homolog
Rapport	Repressible activity paracrine reporter
Ras^{G12V}	oncogenic version of *Drosophila* Ras85D with aminoacid substitution G to V at position 12
ReDDM	Repressible Dual Differential stability cell Marker
RFP	red fluorescent protein
SP	sex peptide
SRBP	sterol regulatory element-binding proteins
Stg	String
TA cells	transit amplifying cells
tub-	tub-promotor
UAS	upstream activating sequence
Wg	Wingless
hZNF267	human Zinc finger protein 267

8 Acknowledgements

First, I would like to thank Dr. Tobias Reiff for the opportunity to do my thesis in his lab and to work on several very interesting topics. Furthermore, I want to thank Dr. Tobias Reiff for sparking my interest for *Drosophila* since the beginning of my MSc, and his support throughout the years including a lot of scientific discussions, but also motivation during challenging phases.

I would like to thank Prof. Dr. Thomas Klein and Prof. Dr. Hermann Aberle for being part of the thesis committee and co-supervising this work. Furthermore, I want to thank both for the opportunity to present the progress of my work in the Notch-club and for giving me constructive feedback and suggestions.

Many thanks go out to Prof. Dr. Bernat Corominas-Murtra, Dr. Zeus Andrea Antonello, Sai Batchu and the former members of the Reiff Lab who were involved in writing the presented papers. Their work substantially contributed to the shown scientific findings.

I would like to thank Stefan for generating transgenic flies that were crucial for many experiments and for sustaining essential laboratory processes together with Andre, Irina, Gisela and Mehmet.

Finally, I want to thank my family and especially my boyfriend Peter for always having my back.

9 Eidesstattliche Erklärung

Ich, Frau Lisa Zipper, versichere an Eides Statt, dass die Dissertation von mir selbständig und ohne unzulässige fremde Hilfe unter Beachtung der „Grundsätze zur Sicherung guter wissenschaftlicher Praxis an der Heinrich-Heine-Universität Düsseldorf“ erstellt worden ist. Diese Dissertation hat noch keiner anderen Fakultät zur Prüfung vorgelegen.

Düsseldorf, August 2025 Lisa Zipper